



COLORFUL PACKAGES

Fluorescent proteins in
complex coacervate core micelles

Antsje Nolles

Colorful packages
Fluorescent proteins in
complex coacervate core micelles

Antsje Nolles

Thesis committee

Promotor

Prof. Dr W. J. H. van Berkel
Personal chair at the Laboratory of Biochemistry
Wageningen University & Research

Co-promotors

Dr J. W. Borst
Assistant professor, Laboratory of Biochemistry
Wageningen University & Research

Dr J. M. Kleijn
Assistant professor, Physical Chemistry and Soft Matter
Wageningen University & Research

Other members

Prof. Dr R. M. Boom, Wageningen University & Research
Prof. Dr D. Wöll, RWTH Aachen University, Germany
Dr I. K. Voets, Eindhoven University of Technology
Dr M. A. Hink, University of Amsterdam

This research was conducted under the auspices of the Graduate School VLAG (Advanced studies in Food Technology, Agrobiotechnology, Nutrition and Health Sciences).

Colorful packages
Fluorescent proteins in
complex coacervate core micelles

Antsje Nolles

Thesis

submitted in fulfillment of the requirements for the degree of doctor
at Wageningen University
by the authority of the Rector Magnificus,
Prof. Dr A. P. J. Mol,
in the presence of the
Thesis Committee appointed by the Academic Board
to be defended in public
on Wednesday 14 February 2018
at 1.30 p.m. in the Aula.

Antsje Nolles
Colorful packages:
Fluorescent proteins in complex coacervate core micelles,
176 pages.

PhD thesis, Wageningen University, Wageningen, the Netherlands (2018)
With references, with summaries in English, Dutch, and Frisian

ISBN 978-94-6343-722-6
DOI <https://doi.org/10.18174/426138>

Contents

List of abbreviations	p. 7
List of symbols	p. 8
Chapter 1	p. 13
<i>Introduction</i>	
Chapter 2	p. 31
<i>Encapsulation of GFP in complex coacervate core micelles</i>	
Chapter 3	p. 53
<i>Encapsulation into complex coacervate core micelles promotes EGFP dimerization</i>	
Chapter 4	p. 81
<i>Colorful packages: Encapsulation of fluorescent proteins in complex coacervate core micelles</i>	
Chapter 5	p. 119
<i>FRET reveals formation and exchange dynamics of protein-containing complex coacervate core micelles</i>	
Chapter 6	p. 143
<i>General discussion</i>	
Chapter 7	p. 155
<i>English summary</i>	
<i>Nederlandse samenvatting</i>	
<i>Fryske gearfetting</i>	
About the author	p. 169
<i>Dankwoord</i>	
<i>Curriculum Vitae</i>	
<i>List of publications</i>	
<i>Overview of completed training activities</i>	

List of abbreviations

General

<i>anFP</i>	Anthozoa fluorescent protein
<i>avFP</i>	<i>Aequorea victoria</i> fluorescent protein
BSA	bovine serum albumin
C3M	complex coacervate core micelle
CD	circular dichroism
CMC	critical micelle concentration
DLS	dynamic light scattering
DQ	degree of quaternization
ESPT	excited-state proton transfer
FCS	fluorescence correlation spectroscopy
FP	fluorescent protein
FRET	Förster resonance energy transfer
P128	P2MVP ₁₂₈ - <i>b</i> -PEO ₄₇₇
P2MVP- <i>b</i> -PEO	poly(2-methyl-vinyl-pyridinium)- <i>b</i> -poly(ethylene-oxide)
P41	P2MVP ₄₁ - <i>b</i> -PEO ₁₂₈
PDB	protein data bank
PDI	polydispersity index
PMC	preferred micellar composition
TRFA	time-resolved fluorescence anisotropy

Fluorescent proteins

SBFP2	strongly enhanced blue fluorescent protein 2
ECFP	enhanced cyan fluorescent protein
mTurquoise2	monomeric turquoise fluorescent protein 2
GFP	green fluorescent protein
wtGFP	wild-type green fluorescent protein
EGFP	enhanced green fluorescent protein
mEGFP	monomeric enhanced green fluorescent protein
darkGFP	non-fluorescent enhanced green fluorescent protein
EYFP	enhanced yellow fluorescent protein
SYFP2	strongly enhanced yellow fluorescent protein 2
mKO2	monomeric Kusabira orange fluorescent protein 2
TagRFP	tag red fluorescent protein
mCherry	monomeric cherry fluorescent protein

Amino acids

Ala	A	alanine
Arg	R	arginine
Asn	N	asparagine
Asp	D	aspartic acid
Cys	C	cysteine
Gln	Q	glutamine
Glu	E	glutamic acid
Gly	G	glycine
His	H	histidine
Ile	I	isoleucine
Leu	L	leucine
Lys	K	lysine
Met	M	methionine
Phe	F	phenylalanine
Pro	P	proline
Ser	S	serine
Thr	T	threonin
Trp	W	tryptophan
Tyr	T	tyrosine
Val	V	valine

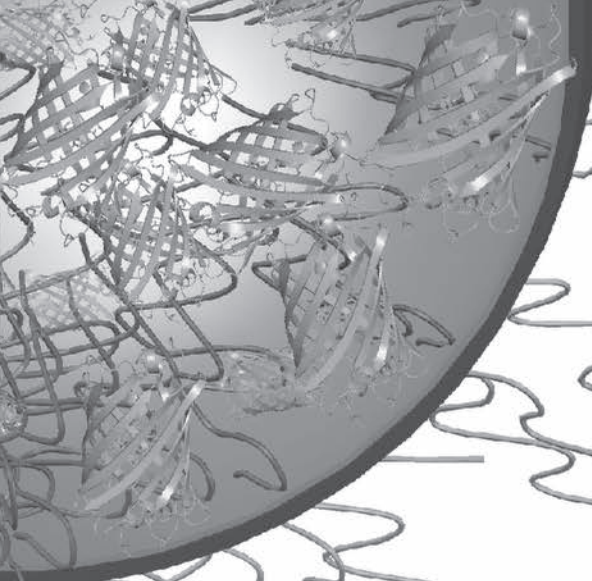
List of symbols

α	amplitude of lifetime
β	amplitude of correlation time
Γ	decay rate
ε	molar extinction coefficient
η	viscosity
θ	angle
κ^2	dipole orientation factor
λ	wavelength
τ_{dif}	diffusion time
τ_f	fluorescence lifetime
ϕ	rotational/transfer correlation time
Φ	quantum yield
ω_{xy}	equatorial radii of the confocal volume
ω_z	axial radius of the confocal volume

a	structural parameter of the confocal volume
c_+, c_-	concentration of charged compound
CpM	counts per second per molecule
CpS	counts per second
D	diffusion coefficient
E	FRET efficiency
F	FRET ratio
F^+	composition based on charge
F_i	fraction of species i
F_{trip}	fraction of molecules in the triplet state
ΔG	Gibbs energy
i	species
I	ionic strength
I	scattered/fluorescence light intensity
J	spectral overlap integral
k	kinetic coefficient
K	salt stability constant
k_B	Boltzmann constant
K_D	dissociation constant
k_t	transfer rate constant
M_n	number average molecular weight
M_w	molecular weight
n	refractive index
n_+, n_-	total concentration of charged groups
N	number of fluorescent particles
N_+, N_-	number of charged groups
pI	isoelectric point
pK_a	acid dissociation constant
r	reaction rate
R	gas constant
R	distance
R_0	Förster distance
R_b	hydrodynamic radius
t	time
T	absolute temperature
T_{trip}	time of a molecule in the triplet state

Stille wateren hebben diepe gronden





Chapter 1

Introduction

This thesis describes the encapsulation and properties of fluorescent proteins (FPs) in complex coacervate core micelles (C3Ms). In this introductory chapter, we first describe some basic properties of polyelectrolytes and the history of complex coacervation. Next, we give an overview what is known about C3Ms, and then turn into the world of protein encapsulation. Finally, before describing the outline of the work, we summarize the history and properties of fluorescent proteins, and the biophysical techniques applied in this thesis.

1.1. Polyelectrolytes

Polymers are molecules composed of multiple repeating structural units, *i.e.* monomers, which are generally connected by covalent chemical bonds. Polymers are found in nature (for example DNA and proteins) or in man-made products (for example plastics and tires). A homopolymer is composed of only one type of monomer, while a copolymer consists of different types of monomers. A protein is an example of a copolymer, as it consists of different amino acid residues. A polymer that contains monomers with electrolyte groups is called a polyelectrolyte. In the case of a 'weak' polyelectrolyte, it carries ionizable (acid and/or base) groups and their net charge and charge sign are dependent on the pH of the solution. Hence, their degree of ionization is non-fixed and they are partially charged (for example proteins). A 'strong' polyelectrolyte bears ionic groups and is fully charged in solution (for example poly(2-methyl-vinyl-pyridinium-iodide)). If a polyelectrolyte bears only positive charges it is called a polycation and if it bears only negative charges the term polyanion applies (Figure 1.1).

1.2. Complex coacervation

Complex coacervation is the liquid-liquid phase separation of a mixture of two oppositely charged polyelectrolytes in water (Figure 1.1). The resulting macroscopic two-phase system contains a dilute polymer-poor solution phase separated from a dense polymer-rich phase. Bungenberg de Jong and Kruyt first described this phenomenon in 1929.^{1,2} They observed that sometimes solid precipitates were formed, while in other cases they found so-called coacervates, *i.e.*, viscous polymer-rich phases in which the polyelectrolytes remained charged and hydrated. Only after more than half a century these coacervate systems were further investigated in the groups of Kabanov, Kataoka, and Cohen Stuart.³⁻⁶ For the polymer-rich phases different terms are used, such as inter-polyelectrolyte complexes (IPEC) and polyion complexes (PIC).^{3,4,7}

In solution, polyelectrolytes are surrounded by counterions: a polycation is accompanied by negatively charged small ions and a polyanion by positively charged small ions (Figure 1.1). When polycations and polyanions are mixed under the right conditions, complex coacervates are formed due to electrostatic interactions between the polyelectrolytes, especially due to coulombic attraction and entropic counterion release.⁸⁻¹⁰ Consequently, the formation and stability of the coacervates are significantly influenced by pH and ionic strength (salt), since these parameters determine the charge density on the polyions, the degree of screening of the charges and the entropy gain from counter ion release. The effect of these parameters highly

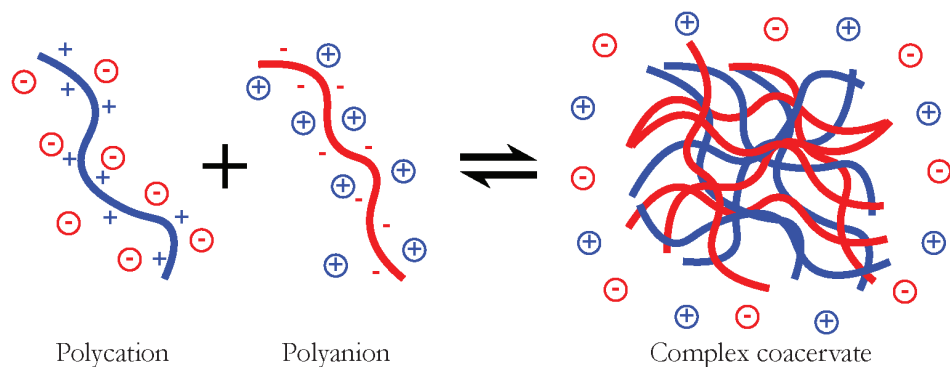


Figure 1.1. Schematic representation of the formation of a complex coacervate: in an aqueous mixture of polyanions and polycations, the polyelectrolytes attract each other and form a separate phase, expelling their counter ions in the process. The coacervate phase still contains a significant amount of water.⁸

depends on the chain length (up to sufficiently long chain lengths), chemical structure and nature (weak or strong) of the polyelectrolyte.^{8,11,12} As a result, the critical salt concentration (CSC), which is the salt concentration above which no complex coacervates are formed, varies from a few tens of mM to several M depending on the specific polyelectrolyte pair. For example, for the combination of a weakly charged protein (gelatin) and a weakly charged polysaccharide (acacia) the critical salt concentration is about 30 - 50 mM (with an optimum coacervation at pH 4),¹³ while for a pair of strongly charged polyelectrolytes it can amount to 1.25 M.¹⁴

1.3. Complex coacervate core micelles (C3Ms)

When one of the oppositely charged polyelectrolytes in a complex coacervate is replaced by a neutral-ionic diblock copolymer, micelles are formed. The neutral water-soluble block forms a solubilizing corona around the polyelectrolyte complex, which creates a microscopic phase in the core (Figure 1.2). These structures are known as complex coacervate core micelles (C3Ms, used throughout this thesis)^{5,10}, block ionomer complexes (BICs)⁴, polyion complex (PIC) micelles³, and inter-polyelectrolyte complex (IPEC) micelles¹⁵.

The formation of C3Ms is driven by the same electrostatic interactions as the formation of macroscopic complex coacervate phases. Therefore, formation and stability of C3Ms is also dependent on pH and salt concentration. A balance between these attractive interactions and entropic penalties opposing association determine the size of C3Ms. These latter penalties involve stretching of the polymer blocks in the corona as a result of the dense packing of monomers, the stretching of the core blocks due to their connection with the blocks in the corona, and the interfacial tension of the core-corona interface.¹⁶

Furthermore, the formation of C3Ms depends on the ratio of the concentration of positive charges and negative charges on the polyelectrolytes and on the concentration of the polymers. Generally, the highest concentration of C3Ms is obtained at or near stoichiometric

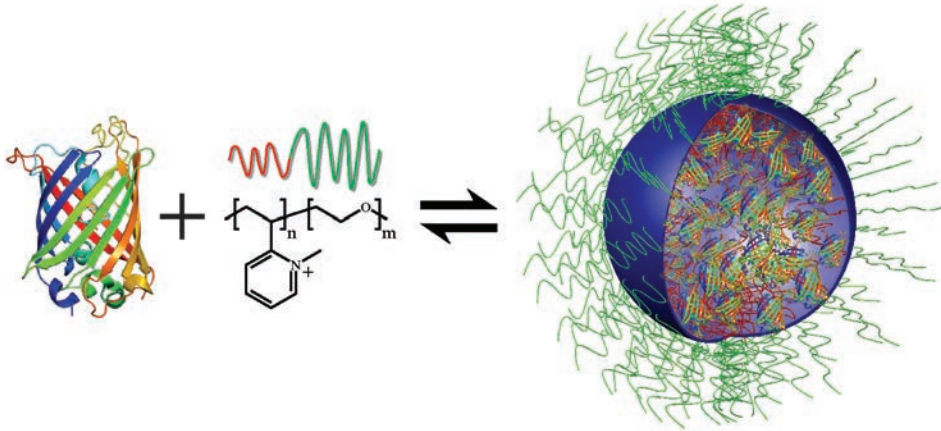


Figure 1.2. Schematic representation of the formation of a complex coacervate core micelle (C3M) from a fluorescent protein and the diblock copolymer P2MVP_n-*b*-PEO_m.

charge ratio, depending also on the chemistry of the polyelectrolytes. This optimal concentration corresponds to the preferred micellar composition (PMC). The concentration of polymers at which the first micelles are formed is called the critical micelle concentration (CMC), usually defined at the PMC, below this concentration no micelles are formed. If the ionic strength is increased, the CMC shift to higher values, reflecting the loss of stability of the complex coacervate core.^{14,17,18} Just like for the complex coacervates, beyond the CSC all micelles are disintegrated.

1.4. Protein encapsulation

Proteins are the building blocks of life and all living organisms depend on their existence. Proteins are the most common biomacromolecules found in cells and consist of a chain originating from a variation of 20 different amino acids. These amino acids have various properties, *e.g.*, some dislike water (hydrophobic) and some like water (hydrophilic) of which some are (electrically) charged. The amino acids are covalently attached to one another to make a polypeptide chain. Further modification and folding of this polypeptide chain creates a fully functional protein. The different properties of the amino acid side chains and their order on the polypeptide chain determine the structure and function of a fully folded protein. Proteins are responsible for nearly every task in a cell: proteins give a cell its shape and firmness (*e.g.*, collagen), they are responsible for the communication in and between cells (*e.g.*, hormones), protect the body (*e.g.*, antibodies) and catalyze biochemical reactions (*e.g.*, enzymes).

Proteins are used in many applications, for example in food formulations, as therapeutic agents, or in enzymatic conversion processes in industry. For all these applications, it might be beneficial to protect proteins from their environment to preserve their function. For example, therapeutic proteins that are administered in the body need to be protected against gastric or other body fluids, or the immune system. Therefore, it is important to find strategies to protect proteins in such a way that they maintain their key features and can be used at will.

Several methods have been developed to protect proteins of interest in an appropriate manner. A very popular method in biocatalysis concerns protein immobilization on a solid support.¹⁹ Such an approach may improve the operational stability and re-use of the biocatalyst, together with simplified downstream processing.²⁰ Another widely used strategy to protect proteins concerns bioconjugation. An example of this is the attachment of linear poly(ethylene-glycol) chains (PEGylation) to proteins, which increases the solubility and shields the protein.^{21,22} PEGylation is a well-established and widely employed technique in the pharmaceutical industry.

A third approach to protect proteins concerns procedures that are based on entrapment or encapsulation. Entrapment may occur in hydrogels, and is sometimes combined with protein cross-linking.²³⁻²⁷ Protein encapsulation on the other hand, includes the application of wrapping nanoparticles such as liposomes, polymersomes, virus capsids, or micelles.²⁷⁻²⁹ Here, we further focus on the properties of protein-containing polymeric micelles.

Protein-containing polymeric micelles are a co-assembly of proteins and polymers, which can have either hydrophobic and/or hydrophilic properties. Major limitations of using hydrophobic polymers for protein-containing micelles are the harsh preparation conditions often involving organic solvents and the lack of permeability for hydrophilic solutes.³⁰⁻³² Protein containers built up from hydrophilic polymers overcome these issues and thus are very promising structures for protection, stabilization, sustained biological activity and controlled delivery.^{12,33} Hydrophilic protein-containing micelles (C3Ms) are simple to prepare, are small enough to remain in solution, evade the uptake by macrophages, can passively accumulate in tumors, contain a core that can accommodate some cargo, and - as is shown in this thesis - many protein molecules can be incorporated into one micelle.^{27,34-36} The micellar core provides a relatively water-rich environment, thereby shielding the protein molecules from the outer solution while protein structure and functionality are preserved.

In this thesis, we have studied the properties of fluorescent proteins in C3Ms. For the encapsulation of these proteins, we make use of a cationic-neutral diblock copolymer, *i.e.*, poly(2-methyl-vinyl-pyridinium)_n-*b*-poly(ethylene-oxide)_m (P2MVP_n-*b*-PEO_m, Figure 1.2). This block copolymer has been used before for the encapsulation of α -lactalbumin³⁷ and lipase^{38,39}. Next to that, PEO is a hydrophilic block that is highly hydrated, soluble, low toxic, and low immunogenic, so it is a very suitable block for nanoparticles in biological media.^{4,40,41}

Although application of protein-containing C3Ms has great potential, it should be noted that these structures may disintegrate depending on salt concentration and pH, since their formation is based on electrostatic interactions between the protein molecules and the charged blocks of the diblock copolymers. In addition, dilution of the C3M solution below the CMC results into disintegration of the micelles. In this research, we aimed for a better understanding of the properties of protein-containing C3Ms. For this, we made use of green fluorescent protein (GFP) and a number of related proteins. These proteins were selected, because we argued that they might be very useful for obtaining insight into their encapsulation efficiency and exchange dynamics, while also providing valuable additional information about the formation, composition and stability of the C3Ms.

1.5. Fluorescent proteins

In this thesis, different members of the fluorescent protein (FP) family have been encapsulated into C3Ms. This allowed the application of various fluorescence spectroscopic methods to characterize C3M formation and their dynamic behavior without labeling the protein or polymer with fluorescent dyes.

The history of FPs has started in the early 1960s with the identification of the greenish glow of the *Aequorea victoria* jellyfish by Osamu Shimomura (Figure 1.3A).⁴² The chemiluminescent protein aequorin was the first to be isolated and purified, but it was found to emit blue light instead of green. Further investigation revealed, that the extracts of the jellyfish contained another protein that ‘exhibited a very bright, greenish fluorescence’ under ultraviolet (UV) light illumination. It was identified as a companion protein of aequorin, which absorbed the excited state energy from aequorin and emitted green light. This companion protein is now widely known as GFP. Several colored variants have been generated by mutagenesis of the original GFP gene (Figures 1.3E and 1.3F). The cyan (CFP) and yellow (YFP) variants of GFP are often used as FRET (Förster resonance energy transfer) pair in protein interaction studies.^{43,44}

In 1999, the bright fluorescent colors of many Anthozoa species were investigated further. This led to the cloning of the first six FPs homologous of GFP and to the discovery of more FPs in different Anthozoa species.^{49,50} While the most common found color is green, other hues were also observed. The FPs emitting at longer wavelengths are of special interest, because mutagenesis of GFP yielded FP color variants with emission maxima that

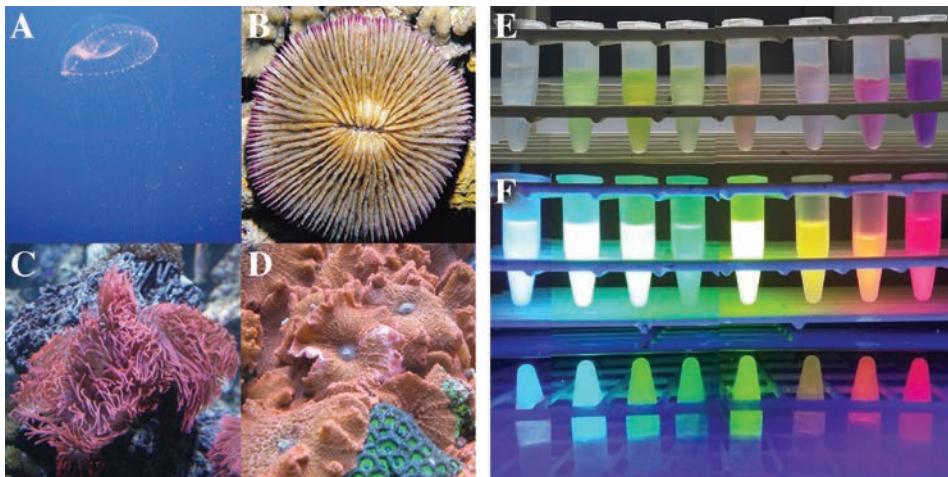


Figure 1.3. Fluorescent proteins used in this study and their organisms of origin. Organisms in which fluorescent proteins have been found from which mutants are used in this thesis: (A) *Aequorea victoria*, (B) *Fungia concinna*, (C) *Entacmeae quadricolor*, and (D) *Discosoma sp.*⁴⁵⁻⁴⁸ Range of the used fluorescent proteins under (E) normal and (F) UV illumination, from left to right: SBFP2 (blue FP), mTurquoise2 (cyan FP), EGFP (green FP), SYFP2 (yellow FP), mKO2 (orange FP), TagRFP (red FP), and mCherry (red FP).

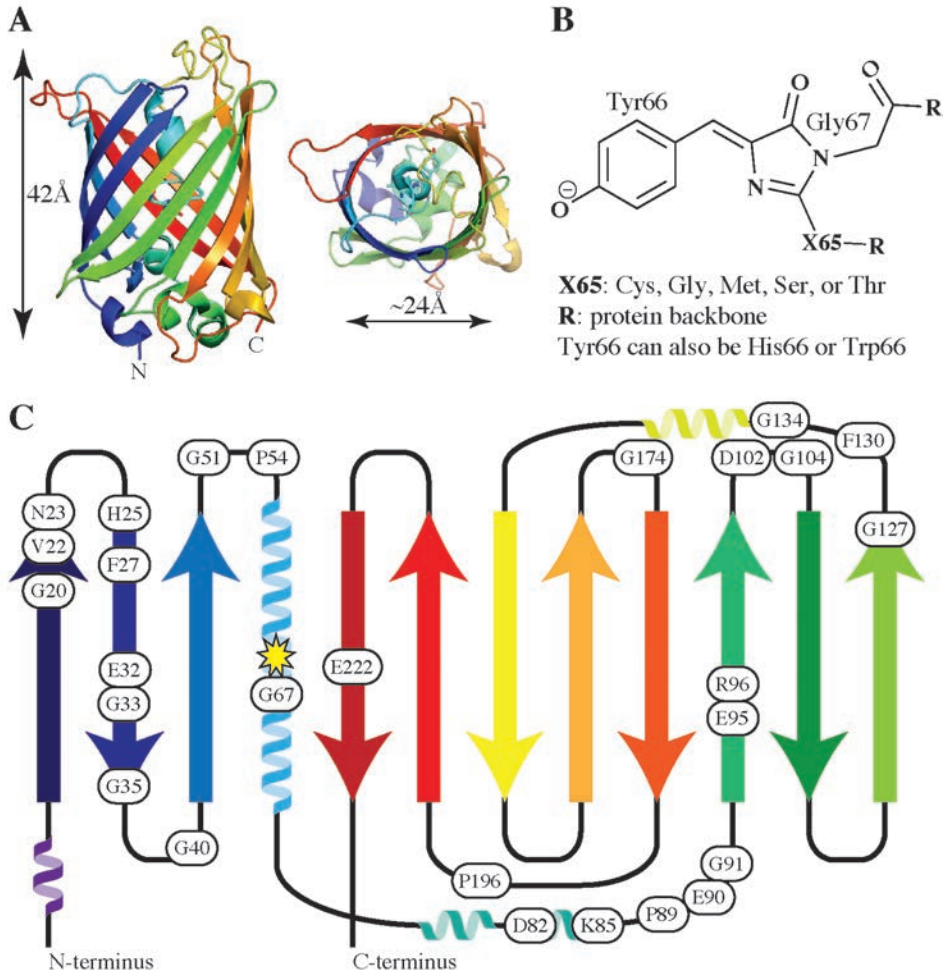
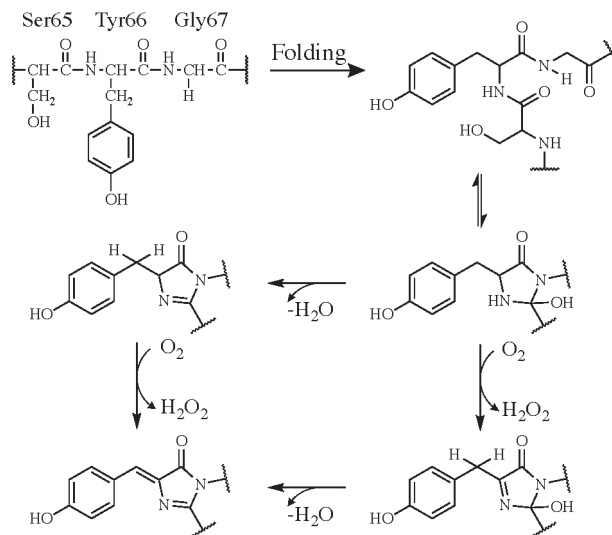


Figure 1.4. Structure of a fluorescent protein and its chromophore. (A) FP 11-stranded β -barrel architecture and approximate dimensions in two different orientations (PDB entry 4EUL⁵⁵). (B) General chromophore structure of a FP from the three adjacent amino acid residues 65, 66, and 67 (according to GFP numbering). (C) Conserved amino acid residues shown on a topological layout of the peptide structure colored according to the structure in A. β -Sheets are depicted as arrows pointing towards the C-terminus, α -helices are depicted as coils, and the chromophore is depicted as star.

range from blue to yellow.⁵¹ In this thesis, variants of FPs found in *Discosoma sp.*, *Entacmeae quadricolor*, and *Fungia concinna* are used (Figures 1.3B to 1.3D), next to GFP variants from *Aequorea victoria*.⁵²⁻⁵⁴ These FPs cover the whole visible spectrum (Figures 1.3E and 1.3F).

All fluorescent proteins are relatively small (~ 27 kDa) and share the same β -barrel fold with a height of 42 Å and a diameter of about 24 Å (Figure 1.4A).^{58,59} The β -barrel is constructed from 11 β -strands that wrap around a single central helix (Figure 1.4C). The central helix contains three adjacent amino acid residues, at positions 65, 66, and 67, that together form the chromophore (Figure 1.4B).^{60,61} The folding of the protein into a cylindrical



Scheme 1.1. Chromophore maturation of fluorescent proteins occurs via a sequence of cyclization, dehydration, and oxidation reactions. The sequence of events in the last two steps in this reaction is still under debate.^{56,57}

structure drives the formation of the mature chromophore via a cyclization, dehydration, and oxidation reaction without the assistance of an external factor (Scheme 1.1). The actual sequence of events in the last two steps of this reaction is still under debate.^{56,57} For the coral FPs, an additional oxidation step takes place to form an acylimine linkage with the polypeptide backbone, which extends the π -conjugation system resulting in considerably red-shifted excitation and emissions wavelengths.^{56,62}

Not only the chromophore impacts the fluorescence characteristics of a fluorescent protein, but also the microenvironment of the chromophore plays a pivotal role.^{63,64} In the *cis*-configuration of the chromophore the conjugated rings exist in a nearly co-planar orientation. This orientation and its rigidity are maintained through an extensive hydrogen-bonding network, formed by neighboring amino acid residues.

Amongst all FPs, several amino acids are conserved (Figure 1.4C). Only the most important conserved residues in the chromophore environment will be discussed here (according to GFP numbering). Gly67, which is part of the chromophore, is the most essential amino acid residue for the formation of the chromophore; without it the chromophore is not formed. The conserved arginine residue, Arg96, functions as an electrostatic catalyst driving the cyclization reaction. In the mature, native structure of a FP, Arg96 forms a hydrogen bond with the chromophore and the positive charge of Arg96 stabilizes the enolate intermediate of the chromophore.⁶⁵ On the other side of the chromophore Glu222 acts as a base catalyst, thereby facilitating the dehydrogenation step, which leads to conjugation of the rings. Furthermore, Glu222 is involved in the hydrogen-bonding network in wild type GFP (wtGFP). This amino acid residue stabilizes the neutral form of the chromophore via the phenolic oxygen of the chromophore, water molecules, and the Ser205 residue. Glu222 is

in the same network involved in the excited-state proton transfer in wtGFP.⁶⁴ In other FPs, Glu222 is differently orientated, thereby disrupting the hydrogen-bond network and amongst others causing the stabilization of the anionic form of the chromophore (Figure 1.4B).^{64,66}

1.6. Techniques used to investigate fluorescent protein-containing C3Ms

We perceive the world around us as colored, because almost every object interacts with light rays in four basic ways: specular reflection (reflection in one direction), diffuse reflection (reflection in more than one direction), refraction, and absorption. Different objects have different characteristics regarding the interaction with light rays, not only on the macroscale, but also on the microscale. For example, the dominant way of nanoparticles is diffuse reflection and of proteins it is absorption. The techniques used in this thesis are based on these dominant ways of the interaction with light.

1.6.1. Absorption and fluorescence

In physics, absorption of light is defined as the uptake of the energy of a photon by atoms or molecules, typically by excitation of electrons. The absorption spectrum is molecule dependent, because the energy levels of the electron orbitals have varying distances among molecules (Figure 1.5).^{67,68} After excitation of an electron, it goes back to the ground state. This can occur directly via internal conversion in which the energy is converted to heat and absorbed by the environment. With fluorescence, the electron initially goes back to the lowest excited state via internal conversion, but subsequently falls back to the ground state via emission of a photon, which has less energy, corresponding to a higher wavelength, than was required to excite the electron.

The electronic states of a molecule can alter through changes in the environment, for example in proteins by changes in amino acid residues near the chromophore. For instance, protonation of a hydroxyl-group causes a change in the electron density distribution over the molecule, which in turn can cause differences in the absorption and fluorescence emission spectra. In FPs the fluorescent chromophore is located in the center of the β -barrel (Figure 1.4A), which protects the chromophore from the bulk solution. Changes in the absorption and fluorescence properties of FPs are mainly related to the direct surroundings of the chromophore in the center of the β -barrel. The absorption and fluorescence properties of FPs and its deviations can be detected using absorption and fluorescence spectroscopy.

1.6.2. Dynamic light scattering

Dynamic light scattering (DLS) makes use of the diffuse reflection, or Rayleigh scattering, of particles.⁷⁰ A laser beam is directed to a solution with the particles of interest and provided that the particles do not absorb the laser light, it is reflected in all directions. A detector is located at a certain angle to the sample relative to the incident laser beam (Figure 1.6A). With DLS the Brownian motions of the particles are detected. Due to these random particle movements, the detected reflected light fluctuates in intensity. These fluctuations

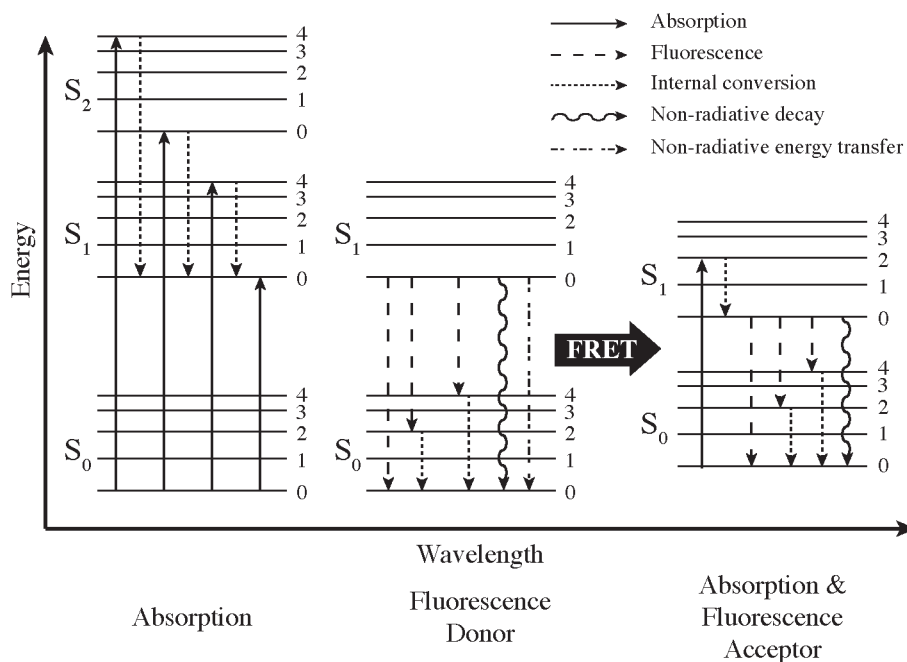


Figure 1.5. Jablonski diagram featuring different energy levels within a molecule where electrons can be found complemented with the Förster resonance energy transfer (FRET) process between donor and acceptor.⁶⁷⁻⁶⁹ This diagram illustrates a singlet ground (S_0), first (S_1) and second (S_2) electronic state. The multiple lines in each electronic state represent a number of vibrational energy levels (0–4). The arrows indicate the transitions of an electron between the different states and levels. *Absorption:* Light of a specific wavelength interacts with an electron in the ground state (S_0) and causes its excitation to a higher-energy level (S_2 or S_1): the lower the wavelength, the more energy it contains so the electron can be excited to a higher energy level, *i.e.*, S_2 rather than S_1 . *Fluorescence donor:* Excited states are short-lived, so an excited electron has several ways to release its energy: through radiationless transitions or fluorescence. There are various types of radiationless transitions, of which only internal conversion, non-radiative decay and non-radiative energy transfer are indicated here. *Absorption & fluorescence acceptor:* A special transition is the non-radiative energy transfer, which can only occur if donor and acceptor meet the requirements for Förster resonance energy transfer (FRET). If they do, the acceptor molecule is excited and can emit a photon at a higher wavelength.

can be auto-correlated from which the diffusion coefficients of the particles in solution can be retrieved. Subsequently, via the Stokes-Einstein relation, the radii of the particles can be calculated. Since Rayleigh scattering varies strongly with particle radius (6th power dependency), contaminating particles (*e.g.*, dust) or aggregates can mask the signal of the nanoparticles when performing DLS.

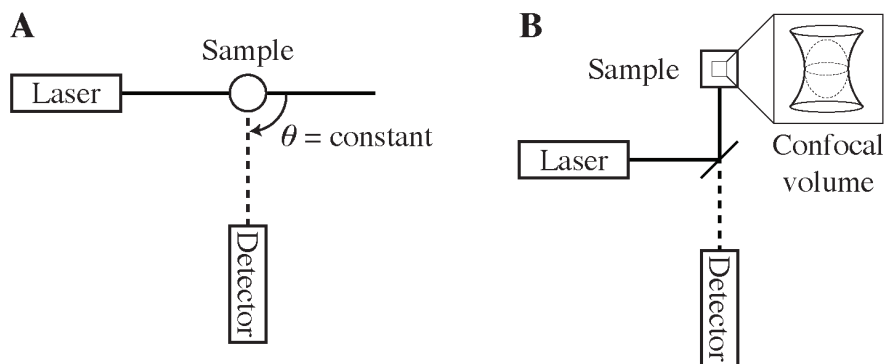


Figure 1.6. Schematic representation of (A) a dynamic light scattering (DLS) and (B) a fluorescence correlation spectroscopy (FCS) setup.

1.6.3. Fluorescence correlation spectroscopy

Another technique with which particle size can be determined is fluorescence correlation spectroscopy (FCS), which is based on monitoring fluctuations in the fluorescence intensity from the Brownian motion of fluorescent molecules or particles.⁷¹⁻⁷³ The fluctuations are also auto-correlated, from which again the diffusion coefficient of the particles is obtained and their radii are calculated using the Stokes-Einstein relation. FCS is solely detecting the fluorescence of the molecules, so the intensity signal cannot be disturbed by dust. Next to that, the setup of FCS makes it possible to determine the volume in which the particles are detected, *i.e.*, the confocal volume (Figure 1.6B). This yields the amount of particles on average in the confocal volume during an FCS run, which can be related to the concentration of the particles in solution. This is why FCS is a technique that works at or near single molecule detection.

1.6.4. Circular dichroism

A special form of absorption is used by the circular dichroism (CD) technique, which involves the difference in absorption between left- and right-handed circular polarized light. CD occurs when a molecule contains one or more chiral light-absorbing groups. The technique is mostly used to study the secondary structure of proteins, because these structures have distinct CD spectra in the far-UV. Since proteins contain different amounts of secondary structures, their far-UV CD spectra are specific per protein. In this research, we have used CD also to monitor changes of the FP chromophore, as this can specifically be detected in the visible region of the electromagnetic spectrum.

1.6.5. Förster resonance energy transfer

If a fluorescent molecule (donor) is close enough to another fluorescent molecule (acceptor), the donor cannot only emit a photon, but also transfer its excited state energy to the acceptor (Figure 1.5). This process is called Förster or fluorescence resonance energy transfer (FRET).^{69,74,75} For FRET, several prerequisites must be fulfilled: (1) donor and

acceptor should be in close proximity of each other, *i.e.*, closer than 10 nm, (2) the donor emission spectrum should overlap with the absorption spectrum of the acceptor (spectral overlap), (3) the dipole moments of donor and acceptor are oriented relative to each other in a manner that allows FRET. FRET mostly occurs between two different types of molecules, in which the donor is excited at higher wavelengths than the acceptor. If FRET occurs, this will result in emission by the acceptor after excitation of the donor and thus the emission spectrum of the acceptor is detected; the emission of the donor is partly or completely reduced. The efficiency of the FRET process strongly depends on the distance between donor and acceptor, following a 6th power dependency. Therefore, FRET can be used to accurately determine the distance between donor and acceptor. In this thesis, we determined the distance between the proteins within C3Ms. FRET can be measured in various ways, by fluorescence intensity based methods or fluorescence lifetime analysis. The first methods monitor the decrease of the fluorescence intensity of the donor and the increase of acceptor fluorescence (sensitized emission). The latter methodology will be explained in more detail in the next section.

1.6.6. Fluorescence lifetime analysis

Using fluorescence lifetime analysis for the detection of FRET, one compares the fluorescence lifetime of a donor alone with the donor fluorescence lifetime in the presence of acceptor molecules. The reduction of donor fluorescence lifetime upon interaction is a measure of the FRET efficiency. In most cases hetero-FRET is used, wherein donor and acceptor are molecules with different spectral characteristics. However, if donor and acceptor are the same type of molecule, one speaks of homo-FRET. For homo-FRET the same prerequisites hold as for hetero-FRET, so homo-FRET is only possible if the excitation and emission spectra of one molecule show some spectral overlap. In the case of homo-FRET there is no difference visible between the spectra with or without FRET, because donor and acceptor are similar. So, homo-FRET is not spectrally determinable and an alternative technique is needed to detect it, which is time-resolved fluorescence anisotropy (TRFA).⁷⁶ This technique is used in this thesis. In TRFA linearly polarized light is applied and it detects the degree of fluorescence polarization in time. In general, if molecules do not move, only molecules with their excitation dipole moment in the same plane as the polarized light get excited, and subsequently the emitted light is polarized within a particular range of angles to the applied light. Further depolarization of the incident light occurs through rotation of the molecule due to Brownian motion. However, if molecules are close together and FRET can occur, another depolarization source is available. With TRFA an anisotropy decay curve is obtained, which can be fitted with the decay time, residual anisotropy and rotational correlation time. Comparing the correlation times from proteins free in solution with proteins present in C3Ms is an indication to the degree of homo-FRET of proteins in C3Ms.

1.7. Outline of this thesis

The focus of this thesis is the characterization of fluorescent protein-containing C3Ms with respect to their composition, formation, stability and protein exchange. In addition, the spectral and structural properties of the FPs in the C3Ms have been investigated.

In **Chapter 2** we start with encapsulation of enhanced green fluorescent protein (EGFP) in C3Ms using a cationic-neutral diblock copolymer of two different lengths: P2MVP₄₁-*b*-PEO₂₀₅ and P2MVP₁₂₈-*b*-PEO₄₇₇. C3Ms formed with these two block copolymers were investigated with DLS and FCS. First, with both techniques the PMC was determined for both complexes. Next, with FCS the CMCs were determined and the amount of GFP molecules per C3M could be calculated. To determine this latter property, a non-fluorescent variant of GFP (darkGFP) was mixed in different ratios with EGFP. For both diblock copolymers similar results were found for the PMC, CMC, and the number of GFP molecules per C3M. We did, however, not observe a linear increase with the fluorescent GFP content per C3M. In addition, it was found that the fluorescence spectra of free and encapsulated EGFP have different spectral properties. These findings were further investigated in Chapter 3.

In **Chapter 3** we explain the difference in spectral properties between free and encapsulated EGFP, as was found in Chapter 2. For this, we compared encapsulation of EGFP with the diblock copolymer P2MVP₄₁-*b*-PEO₂₀₅ with that of mEGFP, a monomeric variant of EGFP. The spectroscopic features of both encapsulated EGFP molecules were investigated with absorption, steady-state fluorescence spectroscopy, CD, and TRFA. The results show that absorption, fluorescence properties, and circular dichroism characteristics of mEGFP are affected to a much lesser extent than for EGFP. TRFA experiments revealed the occurrence of homo-FRET of mEGFP and EGFP in C3Ms, with significantly larger transfer correlation times in case of EGFP. These findings indicate that EGFP dimerizes in the densely packed C3Ms, whereas encapsulated mEGFP is distributed homogeneous in the micellar core.

A systematic study was performed in **Chapter 4** on the encapsulation of seven FPs with the diblock copolymers P2MVP₄₁-*b*-PEO₂₀₅ and P2MVP₁₂₈-*b*-PEO₄₇₇. The FPs, obtained from different species, were selected to cover the whole visible spectrum. Remarkable differences in packaging densities and structural properties were observed between FPs derived from *Aequorea victoria* GFP and FPs derived from the Anthozoa class species.

Formation and dynamics of C3Ms were revealed in **Chapter 5** using FRET. The combination of mTurquoise2 and SYFP2 was used as FRET pair and they were encapsulated in C3Ms with P2MVP₁₂₈-*b*-PEO₄₇₇. Additionally, SBFP2 was used as an invisible protein substitute. FRET was observed in C3Ms and therefore kinetics of micellization, protein exchange between preformed C3Ms, and salt stability of C3Ms could be measured. Based on the experiments and a proposed model, we estimated the overall Gibbs energy of C3M formation.

The main insights obtained from the research described in this thesis are discussed in **Chapter 6**, as well as their implications for possible application in biotechnology and pharmaceuticals and directions for future research.

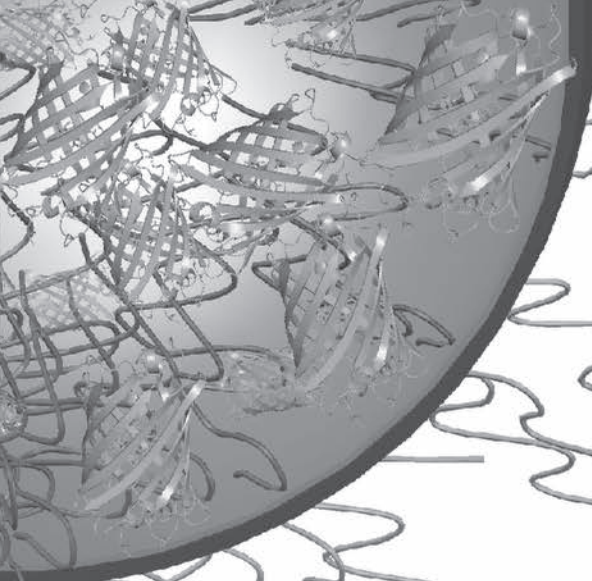
References

1. Bungenberg de Jong, H. G.; Kruyt, H. R., Coacervation. *Proc. K. Ned. Akad. Wet.* **1929**, *32*, 849-856.
2. Bungenberg de Jong, H. G.; Kruyt, H. R., Koazervation. *Kolloid-Z.* **1930**, *50*, 39-48.
3. Harada, A.; Kataoka, K., Formation of polyion complex micelles in an aqueous milieu from a pair of oppositely-charged block-copolymers with poly(ethylene glycol) segments. *Macromolecules* **1995**, *28*, (15), 5294-5299.
4. Kabanov, A. V.; Bronich, T. K.; Kabanov, V. A.; Yu, K.; Eisenberg, A., Soluble stoichiometric complexes from poly(N-ethyl-4-vinylpyridinium) cations and poly(ethylene oxide)-block-polymethacrylate anions. *Macromolecules* **1996**, *29*, (21), 6797-6802.
5. Cohen Stuart, M. A.; Besseling, N. A. M.; Fokkink, R. G., Formation of micelles with complex coacervate cores. *Langmuir* **1998**, *14*, (24), 6846-6849.
6. Kabanov, A. V.; Vinogradov, S. V.; Suzdaltseva, Y. G.; Alakhov, V. Y., Water-soluble block polycations as carriers for oligonucleotide delivery. *Bioconjugate Chem.* **1995**, *6*, (6), 639-643.
7. Pergushov, D. V.; Muller, A. H.; Schacher, F. H., Micellar interpolyelectrolyte complexes. *Chem. Soc. Rev.* **2012**, *41*, (21), 6888-6901.
8. van der Gucht, J.; Spruijt, E.; Lemmers, M.; Cohen Stuart, M. A., Polyelectrolyte complexes: bulk phases and colloidal systems. *J. Colloid Interface Sci.* **2011**, *361*, (2), 407-422.
9. Overbeek, J. T.; Voorn, M. J., Phase separation in polyelectrolyte solutions; theory of complex coacervation. *J. Cell. Physiol.* **1957**, *49*, 7-26.
10. Voets, I. K.; de Keizer, A.; Cohen Stuart, M. A., Complex coacervate core micelles. *Adv. Colloid Interface Sci.* **2009**, *147-148*, 300-318.
11. Spruijt, E.; Westphal, A. H.; Borst, J. W.; Cohen Stuart, M. A.; van der Gucht, J., Binodal compositions of polyelectrolyte complexes. *Macromolecules* **2010**, *43*, (15), 6476-6484.
12. Blocher, W. C.; Perry, S. L., Complex coacervate-based materials for biomedicine. *WIREs Nanomed. Nanobiotechnol.* **2017**, *9*, (4).
13. Burgess, D. J.; Carless, J. E., Microelectrophoretic studies of gelatin and acacia for the prediction of complex coacervation. *J. Colloid Interface Sci.* **1984**, *98*, (1), 1-8.
14. Spruijt, E.; Sprakel, J.; Cohen Stuart, M. A.; van der Gucht, J., Interfacial tension between a complex coacervate phase and its coexisting aqueous phase. *Soft Matter* **2010**, *6*, (1), 172-178.
15. Gohy, J. F.; Varshney, S. K.; Antoun, S.; Jérôme, R., Water-soluble complexes formed by sodium poly(4-styrenesulfonate) and a poly(2-vinylpyridinium)-block-poly(ethyleneoxide) copolymer. *Macromolecules* **2000**, *33*, (25), 9298-9305.
16. Voets, I. K., Electrostatically driven assembly of polyelectrolytes. In *Fluorescence Studies of Polymer Containing Systems*, Procházka, K., Ed. 2016; Vol. 16, pp 65-89.
17. Wang, J.; de Keizer, A.; Fokkink, R.; Yan, Y.; Cohen Stuart, M. A.; van der Gucht, J., Complex coacervate core micelles from iron-based coordination polymers. *J. Phys. Chem. B* **2010**, *114*, (25), 8313-8319.
18. Yan, Y.; de Keizer, A.; Cohen Stuart, M. A.; Drechsler, M.; Besseling, N. A., Stability of complex coacervate core micelles containing metal coordination polymer. *J. Phys. Chem. B* **2008**, *112*, (35), 10908-10914.
19. Przybysz, A.; Volmer, A. A.; Westphal, A. H.; van Berkel, W. J., Bifunctional immobilization of a hyperthermostable endo-beta-1,3-glucanase. *Appl. Microbiol. Biotechnol.* **2014**, *98*, (3), 1155-1163.
20. Sheldon, R. A.; van Pelt, S., Enzyme immobilisation in biocatalysis: why, what and how. *Chem. Soc. Rev.* **2013**, *42*, (15), 6223-6235.
21. Nischan, N.; Hackenberger, C. P., Site-specific PEGylation of proteins: recent developments. *J. Org. Chem.* **2014**, *79*, (22), 10727-10733.
22. Zarafshani, Z.; Obata, T.; Lutz, J. F., Smart PEGylation of trypsin. *Biomacromolecules* **2010**, *11*, (8), 2130-2135.
23. Lindhoud, S.; Claessens, M. M., Accumulation of small protein molecules in a macroscopic complex coacervate. *Soft Matter* **2016**, *12*, (2), 408-413.
24. Zhang, X.; Malhotra, S.; Molina, M.; Haag, R., Micro- and nanogels with labile crosslinks - from synthesis to biomedical applications. *Chem. Soc. Rev.* **2015**, *44*, (7), 1948-1973.
25. Wu, C.; Botzcher, C.; Haag, R., Enzymatically crosslinked dendritic polyglycerol nanogels for encapsulation of catalytically active proteins. *Soft Matter* **2015**, *11*, (5), 972-980.
26. Hennink, W. E.; van Nostrum, C. F., Novel crosslinking methods to design hydrogels. *Adv. Drug Deliv. Rev.* **2012**, *64*, 223-236.

27. Zhao, F.; Yao, D.; Guo, R.; Deng, L.; Dong, A.; Zhang, J., Composites of polymer hydrogels and nanoparticulate systems for biomedical and pharmaceutical applications. *Nanomaterials* **2015**, *5*, (4), 2054-2130.
28. Fu, A.; Tang, R.; Hardie, J.; Farkas, M. E.; Rotello, V. M., Promises and pitfalls of intracellular delivery of proteins. *Bioconjugate Chem.* **2014**, *25*, (9), 1602-1608.
29. Minter, S. D., *Enzyme stabilization and immobilization*. Humana Press: New York, NY, USA, 2017.
30. Swaminathan, J.; Ehrhardt, C., Liposomal delivery of proteins and peptides. *Expert Opin. Drug Deliv.* **2012**, *9*, (12), 1489-1503.
31. Chaize, B.; Colletier, J. P.; Winterhalter, M.; Fournier, D., Encapsulation of enzymes in liposomes: high encapsulation efficiency and control of substrate permeability. *Artif. Cells, Blood Substitutes, Biotechnol.* **2004**, *32*, (1), 67-75.
32. Pisal, D. S.; Kosloski, M. P.; Balu-Iyer, S. V., Delivery of therapeutic proteins. *J. Pharm. Sci.* **2010**, *99*, (6), 2557-2575.
33. Lee, Y.; Kataoka, K., Biosignal-sensitive polyion complex micelles for the delivery of biopharmaceuticals. *Soft Matter* **2009**, *5*, (20), 3810-3817.
34. Cabral, H.; Kataoka, K., Progress of drug-loaded polymeric micelles into clinical studies. *J. Control. Release* **2014**, *190*, 465-476.
35. Black, K. A.; Priftis, D.; Perry, S. L.; Yip, J.; Byun, W. Y.; Tirrell, M., Protein encapsulation via polypeptide complex coacervation. *ACS Macro Lett.* **2014**, *3*, (10), 1088-1091.
36. Kataoka, K.; Harada, A.; Nagasaki, Y., Block copolymer micelles for drug delivery: design, characterization and biological significance. *Adv. Drug Deliv. Rev.* **2001**, *47*, (1), 113-131.
37. Lindhoud, S.; Norde, W.; Cohen Stuart, M. A., Reversibility and relaxation behavior of polyelectrolyte complex micelle formation. *J. Phys. Chem. B* **2009**, *113*, (16), 5431-5439.
38. Lindhoud, S.; de Vries, R.; Schweins, R.; Cohen Stuart, M. A.; Norde, W., Salt-induced release of lipase from polyelectrolyte complex micelles. *Soft Matter* **2009**, *5*, (1), 242-250.
39. Lindhoud, S.; Norde, W.; Cohen Stuart, M. A., Effects of polyelectrolyte complex micelles and their components on the enzymatic activity of lipase. *Langmuir* **2010**, *26*, (12), 9802-9808.
40. Kwon, G. S.; Kataoka, K., Block-copolymer micelles as long-circulating drug vehicles. *Adv. Drug Deliv. Rev.* **1995**, *16*, (2-3), 295-309.
41. Riess, G., Micellization of block copolymers. *Prog. Polym. Sci.* **2003**, *28*, (7), 1107-1170.
42. Shimomura, O.; Johnson, F. H.; Saiga, Y., Extraction, purification and properties of aequorin, a bioluminescent protein from the luminous hydromedusa, *Aequorea*. *J. Cell. Comp. Physiol.* **1962**, *59*, 223-239.
43. Bajar, B. T.; Wang, E. S.; Zhang, S.; Lin, M. Z.; Chu, J., A guide to fluorescent protein FRET pairs. *Sensors (Basel)* **2016**, *16*, (9).
44. Piston, D. W.; Kremers, G. J., Fluorescent protein FRET: the good, the bad and the ugly. *Trends Biochem. Sci.* **2007**, *32*, (9), 407-414.
45. G, J., Crystal Jelly (*Aequorea victoria*), Monterey Bay Aquarium, Monterey, California, USA. In Wikimedia Commons, 2013.
46. Veron, C., *Fungia concinna* in Great Barrier Reef, Australia, a small polyp. In Australian Institute of Marine Science, 2000.
47. Хомелка, *Entacmaea quadricolor* in tropicarium-oceanarium Budapest. In Wikimedia Commons, 2013.
48. Kevmin, A group of *Discosoma* sp individuals colonizing a head of *Zoanthus* sp at the Seattle aquarium. In Wikimedia Commons, 2009.
49. Matz, M. V.; Fradkov, A. F.; Labas, Y. A.; Savitsky, A. P.; Zaraisky, A. G.; Markelov, M. L.; Lukyanov, S. A., Fluorescent proteins from nonbioluminescent *Anthozoa* species. *Nat. Biotechnol.* **1999**, *17*, (10), 969-973.
50. Matz, M. V.; Lukyanov, K. A.; Lukyanov, S. A., Family of the green fluorescent protein: journey to the end of the rainbow. *Bioessays* **2002**, *24*, (10), 953-959.
51. Tsien, R. Y., The green fluorescent protein. *Annu. Rev. Biochem.* **1998**, *67*, 509-544.
52. Shaner, N. C.; Campbell, R. E.; Steinbach, P. A.; Giepmans, B. N.; Palmer, A. E.; Tsien, R. Y., Improved monomeric red, orange and yellow fluorescent proteins derived from *Discosoma* sp. red fluorescent protein. *Nat. Biotechnol.* **2004**, *22*, (12), 1567-1572.
53. Merzlyak, E. M.; Goedhart, J.; Scherbo, D.; Bulina, M. E.; Shcheglov, A. S.; Fradkov, A. F.; Gaintzeva, A.; Lukyanov, K. A.; Lukyanov, S.; Gadella, T. W. J.; Chudakov, D. M., Bright monomeric red fluorescent protein with an extended fluorescence lifetime. *Nat. Methods* **2007**, *4*, (7), 555-557.
54. Karasawa, S.; Araki, T.; Nagai, T.; Mizuno, H.; Miyawaki, A., Cyan-emitting and orange-emitting fluorescent proteins as a donor/acceptor pair for fluorescence resonance energy transfer. *Biochem. J.* **2004**, *381*, (Pt 1), 307-312.

55. Arpino, J. A.; Rizkallah, P. J.; Jones, D. D., Crystal structure of enhanced green fluorescent protein to 1.35 Å resolution reveals alternative conformations for Glu222. *PLoS One* **2012**, 7, (10), e47132.
56. Craggs, T. D., Green fluorescent protein: structure, folding and chromophore maturation. *Chem. Soc. Rev.* **2009**, 38, (10), 2865-2875.
57. Ma, Y.; Sun, Q.; Smith, S. C., The mechanism of oxidation in chromophore maturation of wild-type green fluorescent protein: a theoretical study. *Phys. Chem. Chem. Phys.* **2017**, 19, (20), 12942-12952.
58. Yang, F.; Moss, L. G.; Phillips, G. N. J., The molecular structure of green fluorescent protein. *Nat. Biotechnol.* **1996**, 14, (10), 1246-1251.
59. Ormö, M.; Cubitt, A. B.; Kallio, K.; Gross, L. A.; Tsien, R. Y.; Remington, S. J., Crystal structure of the *Aequorea victoria* green fluorescent protein. *Science* **1996**, 273, (5280), 1392-1395.
60. Cody, C. W.; Prasher, D. C.; Westler, W. M.; Prendergast, F. G.; Ward, W. W., Chemical structure of the hexapeptide chromophore of the *Aequorea* green-fluorescent protein. *Biochemistry* **1993**, 32, (5), 1212-1218.
61. Brejc, K.; Sixma, T. K.; Kitts, P. A.; Kain, S. R.; Tsien, R. Y.; Ormö, M.; Remington, S. J., Structural basis for dual excitation and photoisomerization of the *Aequorea victoria* green fluorescent protein. *Proc. Natl. Acad. Sci. U. S. A.* **1997**, 94, (6), 2306-2311.
62. Subach, F. V.; Verkhusha, V. V., Chromophore transformations in red fluorescent proteins. *Chem. Rev.* **2012**, 112, (7), 4308-4327.
63. Ganim, Z.; Rief, M., Mechanically switching single-molecule fluorescence of GFP by unfolding and refolding. *Proc. Natl. Acad. Sci.* **2017**, 114, (42), 11052-11056.
64. Svendsen, A.; Kiefer, H. V.; Pedersen, H. B.; Bochenkova, A. V.; Andersen, L. H., Origin of the intrinsic fluorescence of the green fluorescent protein. *J. Am. Chem. Soc.* **2017**, 139, (25), 8766-8771.
65. Sniegowski, J. A.; Lappe, J. W.; Patel, H. N.; Huffman, H. A.; Wachter, R. M., Base catalysis of chromophore formation in Arg96 and Glu222 variants of green fluorescent protein. *J. Biol. Chem.* **2005**, 280, (28), 26248-26255.
66. Elsliger, M. A.; Wachter, R. M.; Hanson, G. T.; Kallio, K.; Remington, S. J., Structural and spectral response of green fluorescent protein variants to changes in pH. *Biochemistry* **1999**, 38, (17), 5296-5301.
67. Jiskoot, W.; Visser, A. J. W. G.; Herron, J. N.; Sutter, M., Fluorescence spectroscopy. *Methods for structural analysis of protein pharmaceuticals* **2005**, 1, 27-82.
68. Valeur, B., Fluorescence polarization. Emission anisotropy. *Molecular Fluorescence: Principles and Applications* **2002**, 125-154.
69. Förster, T., Zwischenmolekulare energiewanderung und fluoreszenz. *Ann. Phys.* **1948**, 437, 55-75.
70. Berne, B. J.; Pecora, R., *Dynamic light scattering with application to chemistry, biology and physics*. Courier Dover: New York, NY, USA, 1976.
71. Rigler, R.; Elson, E. S., *Fluorescence correlation spectroscopy: theory and applications*. Springer Science & Business Media: 2001; Vol. 65.
72. Schwille, P.; Haustein, E., *Fluorescence correlation spectroscopy: a tutorial for the biophysics textbook online*. Biophysical Society, Rockville, MD: 2002.
73. Hink, M. A.; Borst, J. W.; Visser, A. J. W. G., Fluorescence correlation spectroscopy of GFP fusion proteins in living plant cells. *Methods Enzymol.* **2003**, 361, 93-112.
74. Stryer, L., Fluorescence energy transfer as a spectroscopic ruler. *Annu. Rev. Biochem.* **1978**, 47, 819-846.
75. Stryer, L.; Haugland, R. P., Energy transfer: a spectroscopic ruler. *Proc. Natl. Acad. Sci.* **1967**, 58, (2), 719-726.
76. Gautier, I.; Tramier, M.; Durieux, C.; Coppey, J.; Pansu, R. B.; Nicolas, J. C.; Kemnitz, K.; Coppey-Moisan, M., Homo-FRET microscopy in living cells to measure monomer-dimer transition of GFP-tagged proteins. *Biophys. J.* **2001**, 80, (6), 3000-3008.





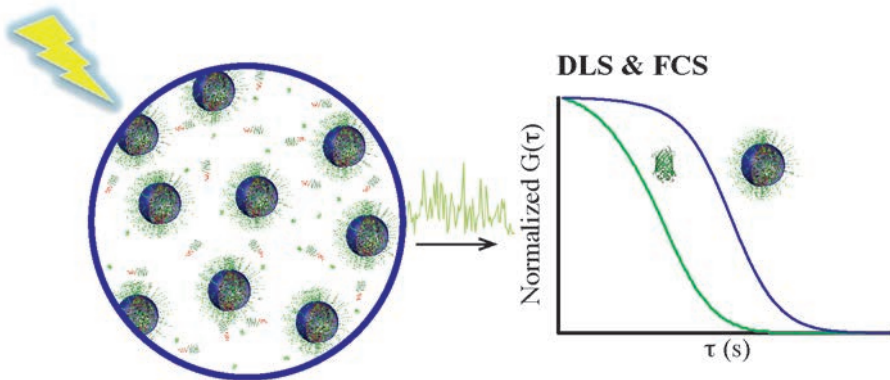
Chapter 2

Encapsulation of GFP in complex coacervate core micelles

Published as: A. Nolles, A. H. Westphal, J. A. de Hoop,
R. G. Fokkink, J. M. Kleijn, W. J. H. van Berkel, and J. W. Borst,
Biomacromolecules, **2015**, 16, 1542-1549.

Abstract

Protein encapsulation with polymers has a high potential for drug delivery, enzyme protection and stabilization. Formation of such structures can be achieved by the use of polyelectrolytes to generate so-called complex coacervate core micelles (C3Ms). Here, encapsulation of enhanced green fluorescent protein (EGFP) was investigated using a cationic-neutral diblock copolymer of two different sizes: poly(2-methyl-vinyl-pyridinium)₄₁-*b*-poly(ethylene-oxide)₂₀₅ and poly(2-methyl-vinyl-pyridinium)₁₂₈-*b*-poly(ethylene-oxide)₄₇₇. Dynamic light scattering and fluorescence correlation spectroscopy (FCS) revealed a preferred micellar composition (PMC) with a positive charge composition of 0.65 for both diblock copolymers and micellar hydrodynamic radii of approximately 34 nm. FCS data show that at the PMC, C3Ms are formed above 100 nM EGFP, independent of polymer length. Mixtures of EGFP and non-fluorescent GFP were used to quantify the amount of GFP molecules per C3M, resulting in approximately 450 GFPs encapsulated per micelle. This study shows that FCS can be successfully applied for the characterization of protein-containing C3Ms.



2.1. Introduction

Micellar protein-polyelectrolyte complexes are unique soluble structures that can be used for biomedical and biological applications.¹ Such complexes, further defined as complex coacervate core micelles (C3Ms), have great potential to protect, stabilize, enhance biological activity, and control delivery of the encapsulated protein.²⁻⁴ C3Ms are co-assemblies of a charged-neutral diblock copolymer with a counter-charged polyelectrolyte or protein. A core-shell structure is formed in aqueous solutions of which the shell consists of neutral soluble chains. The formation is electrostatically driven and, therefore, by default, responsive to ionic strength and, in the case of weak polyelectrolytes and proteins, also to pH.⁵

Investigation of protein-polyelectrolyte complexes started already in the 1950s with bovine serum albumin (BSA).⁶ Morawetz and co-workers⁶ successfully separated BSA from oxyhemoglobin by incubation with polymethacrylic acid, thereby keeping BSA in its native state after complexation. Research on protein encapsulation using C3Ms has been performed mainly on BSA and lysozyme using dynamic light scattering (DLS).^{7,8} The overall aim of our work is to determine the potential of polyelectrolyte micellar complexes as packaging and delivery systems for proteins in food and pharmaceutical applications. In this study, we use enhanced green fluorescent protein (EGFP), fluorescence correlation spectroscopy (FCS) and DLS to characterize in detail protein-loaded structures and the processes of their formation and disintegration.

EGFP is widely applied in biological studies because of its high stability and unique fluorescence properties.⁹⁻¹¹ EGFP has been previously used for encapsulation in AOT (sodium bis(2-ethylhexyl)sulfosuccinate) reversed micelles as pH-indicator¹² and in virus particles as an inclusion molecule.¹³

DLS can be used to determine the size distribution profile of micelles,¹⁴ but does not provide direct information on the number of protein molecules that has been incorporated.¹⁵ FCS is a selective and sensitive technique that can measure single molecules; it can be used to measure diluted samples up to the nanomolar range and to investigate diffusion-controlled processes in biological and colloidal systems on the micro- to millisecond time scale.¹⁶⁻²⁰ FCS has already been used to determine micelle diffusion coefficients,^{21,22} the relative amount of encapsulated dye molecules,²³ and the critical micelle concentration (CMC) of micellar systems.²⁴

In this study, EGFP (27 kDa, pI = 5.6) has been encapsulated at pH 9 using the polymer poly(2-methyl-vinyl-pyridinium)_n-*b*-poly(ethylene-oxide)_m (P2MVP_n-*b*-PEO_m)^{25,26} of two different sizes: P2MVP₄₁-*b*-PEO₂₀₅ and P2MVP₁₂₈-*b*-PEO₄₇₇. P2MVP_n-*b*-PEO_m is a diblock copolymer consisting of a cationic block and a neutral water-soluble block (Figure 2.1). Using DLS and FCS, the preferred micellar composition (PMC) was determined, *i.e.*, the solution composition at which the maximum number of micelles are formed, which is dependent on the amount of charge on the polymer relative to the total amount of charged groups of polymer and protein. Moreover, FCS allowed determining the critical micelle concentration (CMC) and quantifying the amount of GFP molecules per C3M.

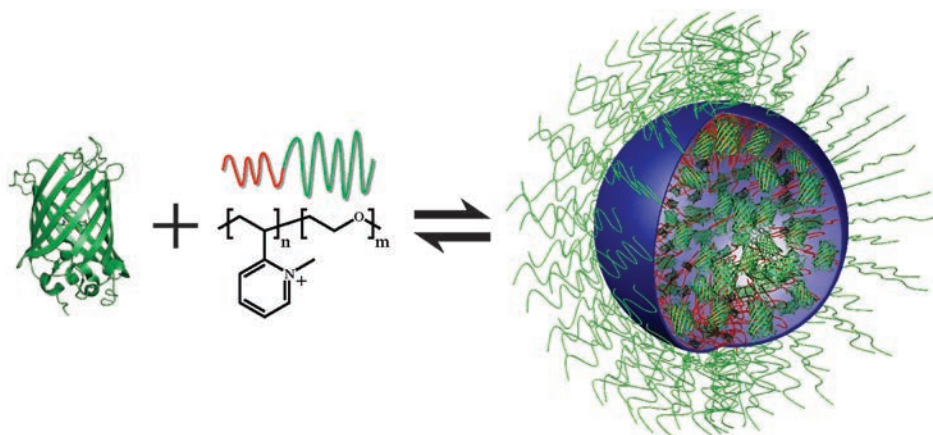


Figure 2.1. Schematic representation of a complex coacervate core micelle (C3M) formed from EGFP and poly(2-methyl-vinyl-pyridinium)_n-b-poly(ethylene-oxide)_m.

2.2. Experimental section

2.2.1. Materials

Complex coacervate core micelles were prepared in aqueous solution from enhanced green fluorescent protein (EGFP), which is an ampholyte with pH-dependent charges, and poly(2-methyl-vinyl-pyridinium)-*b*-poly(ethylene-oxide) (P2MVP-*b*-PEO), a cationic-neutral diblock copolymer with pH-independent charges. Two polymers with different chain lengths were used. P2VP₄₁-*b*-PEO₂₀₅ (Polymer Source *Inc.*, $M_w/M_n = 1.05$, $M_n = 13.3$ kg/mol) and P2VP₁₂₈-*b*-PEO₄₇₇ (Polymer Source *Inc.*, $M_w/M_n = 1.10$, $M_n = 34.5$ kg/mol) were quaternized with iodomethane (99%, Sigma-Aldrich), according to a procedure described elsewhere.²⁵ For P2MVP₄₁-*b*-PEO₂₀₅ ($M_n = 19.1$ kg/mol) and for P2MVP₁₂₈-*b*-PEO₄₇₇ ($M_n = 50.7$ kg/mol) a final degree of quaternization (DQ) of approximately 80% and 87% was obtained, respectively. All other chemicals were from commercial sources and of the purest grade available.

2.2.2. Protein production

EGFP ($M_w = 26.9$ kDa) was cloned into the pTYB11 vector (New England Biolabs, Impact vector system²⁷⁻²⁹) and expressed in *Escherichia coli* BL21 cells. Induction of EGFP expression was performed at 20°C for correct chromophore formation. The purification of EGFP was performed following the protocol in the manual of New England Biolabs, Impact vector system.²⁹ On column cleavage of EGFP from the chitin binding domain was performed by overnight incubation of the bound fusion protein in 50 mM β-mercaptoethanol and 50 mM dithiothreitol in 25 mM HEPES buffer (25 mM HEPES, 2 M NaCl, pH 8.5). The eluted protein sample was collected and the buffer was exchanged into 10 mM borate buffer (pH 9.0) using an ultrafiltration unit (Amicon) with a 10-kDa cut-off PES-membrane (Millipore). Aliquots of 32 μM EGFP were stored at -80°C.

Non-fluorescent EGFP (henceforth denoted as darkGFP, $M_w = 26.8$ kDa) was obtained by mutating the three amino acids TYG, forming the chromophore in EGFP, into GGG.^{30,31} The primer used to change the DNA sequence coding for the corresponding amino acids was 5'-GCA CTG CAC GCC GCC TCC CAG GGT GGT C and used in a PCR strategy for site-directed mutagenesis.³² DarkGFP was produced, purified and stored (30 μM aliquots) as described for EGFP. Protein concentrations

were determined using BCA protein assay (Pierce™) or using an absorption measurement at 488 nm for EGFP ($\epsilon_{\text{EGFP}} = 56 \text{ mM}^{-1} \text{ cm}^{-1}$).

2.2.3. Sample preparation

Stock solutions of P2MVP₄₁-*b*-PEO₂₀₅ (51 μM) and P2MVP₁₂₈-*b*-PEO₄₇₇ (50 μM) were prepared by dissolving the polymers in 10 mM borate buffer (pH 9.0). All solutions were filtered through 0.20 μm poly(ether-sulfone) membrane syringe filters (Advanced Microdevices Pvt. Ltd.). Encapsulation of EGFP with polymers was achieved by first diluting the EGFP stock solution (or mixtures of EGFP and darkGFP) in 10 mM borate buffer (pH 9.0) to the desired concentration, followed by addition of the polymer. After mixing, samples were stored at room temperature for 24 h before measurements. Angle-dependent static light scattering (SLS) experiments to determine the structure factor of the C3Ms indicated that the micelles are spherical objects. For each sample, DLS measurements involved collection of 10 light scattering intensity fluctuation traces, and in FCS measurements, five fluorescence intensity fluctuation traces of 30 s each were collected.

2.2.4. Dynamic light scattering

Dynamic light scattering (DLS) measurements were performed on an ALV instrument equipped with a 22 mW Uniphase Model 1145P HeNe-laser operating at 632.8 nm, and an ALV/Dual High QE APD Detector Unit with a fiber splitting device for two detectors connected to an external ALV7004 Multiple Tau Digital Correlator (ALV-Laser Vertriebsgesellschaft m-b.H.). The detection angle, θ , was set at 90°.

The intensity autocorrelation functions

$$G_2(\tau) = \frac{\langle I(t) \times I(t+\tau) \rangle}{\langle I(t) \rangle^2} \quad (2.1)$$

were analyzed using the inverse Laplace transformation.³³ In the above equation, I is the intensity of the scattered light. For non-interacting monodisperse spherical particles, the field autocorrelation function $G_1(\tau)$ is an exponentially decaying function dependent on the correlation decay rate Γ , diffusion coefficient D of the particles, and the wave vector q :

$$G_1(q, \tau) = e^{-\Gamma\tau}, \quad \Gamma = q^2 D \quad \text{and} \quad q = \frac{4\pi n}{\lambda_0} \sin\left(\frac{\theta}{2}\right) \quad (2.2)$$

Here, λ_0 is the used wavelength, n is the refractive index of the medium and θ is the detection angle. In the case of a polydisperse system, the overall decay of the function $G_1(\tau)$ can be written as a weight-average of all possible decays:

$$G_1(\tau) = \lim_{n \rightarrow \infty} \frac{1}{n} \sum_{i=1}^n w_i(\Gamma_i) e^{-\Gamma_i \tau} \quad (2.3)$$

where $w_i(\Gamma_i)$ is a weighting function determined by the size and the amount of particles in size range i . The hydrodynamic radii of the scattering particles, R_h , were calculated using the Stokes-Einstein relation for spherical particles:

$$R_h = \frac{k_B T}{6\pi\eta D} \quad (2.4)$$

where k_B is the Boltzmann constant, T is the absolute temperature and η is the viscosity of the solvent. The polydispersity of the mixtures can be calculated or a polydispersity index of a peak can be determined. The latter is done in this paper according to the relation:

$$\text{PDI} = \left(\frac{\text{width}}{\text{radius}} \right)^2 \quad (2.5)$$

where the width is at half height of the peak of interest in the particle size distribution and the radius is at the maximum of that same peak. Results from DLS composition experiments are plotted as a function of the composition F^+ , defined by

$$F^+ = \frac{[n_+]}{[n_+] + [n_-]} \quad (2.6)$$

where $[n_+] = c_+N_+$ and refers to the total concentration of positively charged groups on the polymers and $[n_-] = c_-N_-$ is the total concentration of negatively charged groups on the protein molecules. The number of charged groups on the diblock copolymers (N_+), taking the DQ into account, is +33.1 for P2MVP₄₁-*b*-PEO₂₀₅ and +112.0 for P2MVP₁₂₈-*b*-PEO₄₇₇, to calculate $[n_+]$. The net charge of EGFP as a function of pH was calculated using the software package PROPKA 3.1^{34,35} (see Figure S2.1). At pH 9.0, the charge of the native protein (N_-) is -9.72, which is used to calculate $[n_-]$ for EGFP and darkGFP as well.

2.2.4.1. Preferred micellar composition

For determination of the preferred micellar composition (PMC) at pH 9.0, solutions of different polymer/protein compositions were prepared wherein the number of charged groups of protein and polymer was kept constant. In this experiment, $F^+ = 0$ corresponds to a 12.5 μM EGFP solution and $F^+ = 1$ corresponds to a 3.32 μM P2MVP₄₁-*b*-PEO₂₀₅ or a 1.06 μM P2MVP₁₂₈-*b*-PEO₄₇₇ solution, respectively.

2.2.4.2. DLS data analysis

DLS autocorrelation curves were generated from 10 individual intensity traces and averaged. The inverse Laplace transformation of the average $G_2(\tau)$, performed by CONTIN software (AfterALV 1.0d, Dullware), was used to analyze the size distributions of the C3Ms.³³

2.2.5. Fluorescence correlation spectroscopy

Fluorescence correlation spectroscopy (FCS) was performed on a Leica TCS SP5 X system equipped with a 63x 1.20 NA water immersion objective and a super continuum laser, which emits a continuous spectrum from 470 to 670 nm. EGFP was excited by selecting the 488 nm laser line at a pulsed frequency of 40 MHz. Fluorescence was collected through a size-adjustable pinhole, set at 70 μm , and filtered using a 495-525 nm spectral filter. Fluorescence was recorded via the internal hybrid detector, which was coupled to a PicoHarp 300 TCSPC module (PicoQuant).

The basic principles of FCS have been previously described and reviewed.^{36,37} The observed fluorescence intensity emerging from a confocal spot can be described as a constant average fluorescence intensity I with a time-dependent part $I(t)$. When this fluorescence intensity at time t is correlated with the intensity at time $t + \tau$, an autocorrelation function $G(t)$ can be described as follows:

$$G(t) = \frac{\langle I(t) \times I(t + \tau) \rangle}{\langle I(t) \rangle^2} = \frac{\langle I \rangle^2 + \langle \Delta I(t) \times \Delta I(t + \tau) \rangle}{\langle I \rangle^2} \quad (2.7)$$

Generally, fluctuations in the fluorescence intensity are caused by diffusion of molecules in and out of the confocal volume. Other processes, however, can also contribute to these fluctuations, like triplet state behavior of the fluorophore, resulting in a signal in the short time range (μs) of the autocorrelation curve. The equation used to fit translational diffusion data, including triplet state,³⁸ is as follows:

$$G(t) = 1 + \frac{1}{\langle N \rangle} \left(1 + \frac{F_{trip}}{1 - F_{trip}} \cdot e^{-t/T_{trip}} \right) \cdot \sum_{i=1}^n \frac{F_i}{(1 + t/\tau_{diff,i}) \cdot \sqrt{1 + (\omega_{xy}/\omega_z)^2 \cdot t/\tau_{diff,i}}} \quad (2.8)$$

where $\langle N \rangle$ represents the average number of fluorescent particles, N , in the spot. The exponential term describes the triplet state behavior of the molecule, in which F_{trip} is the fraction of molecules in the triplet state and T_{trip} is the average time a molecule resides in the triplet state. The last part of the equation describes the diffusion behavior of the molecules, where F_i is the fraction of species i , $\tau_{diff,i}$ is the diffusion time of species i , and ω_{xy} and ω_z are the equatorial and axial radii of the detection volume, respectively. The diffusion constant D_i of species i is directly related to the observed diffusion time $\tau_{diff,i}$ according to the following equation:

$$D_i = \frac{\omega_{xy}^2}{4 \cdot \tau_{diff,i}} \quad (2.9)$$

The value of ω_{xy}^2 can be obtained by calibration with a solution of a fluorophore with a known diffusion constant. The hydrodynamic radius (R_h) of freely diffusing EGFP and of the C3Ms in which the EGFP molecules are trapped was calculated using the Stokes-Einstein relation for spherical particles (Equation 2.4).

Rhodamine 110 ($D = 4.3 \times 10^{-10} \text{ m}^2 \text{ s}^{-1}$) was used to calibrate the confocal volume of the setup. A diffusion time of 18 μs and a structural parameter (a , expressed as (ω_z/ω_{xy})) between 5 and 10 was obtained, resulting in a confocal volume of approximately 0.2 fL. Measurements were performed in 8-well chamber slides from Nunc™ Lab-Tek™ (Thermo Fisher Scientific).

2.2.5.1. Preferred micellar composition

For determination of the PMC, 500 μL solutions with different polymer/protein compositions were prepared. The EGFP concentration was kept constant at 5 μM for each composition. Stock solutions of P2MVP_{41-b-PEO₂₀₅} and P2MVP_{128-b-PEO₄₇₇} were used for the desired values of F^+ . Measurements were performed at a laser power of 0.32 μW .

2.2.5.2. Critical micelle concentration

For the critical micelle concentration (CMC) determination, 300 μL solutions were prepared at the PMC in 10 mM borate buffer (pH 9.0). The most concentrated solutions contained 5 μM EGFP with 2.75 μM P2MVP_{41-b-PEO₂₀₅} and 5 μM EGFP with 0.70 μM P2MVP_{128-b-PEO₄₇₇}. The other samples were obtained by making a dilution series from the concentrated solution. The samples were measured at a laser power of 0.32 μW .

2.2.5.3. Number of protein molecules per C3M

For the determination of the number of GFP molecules per C3M, 250 μL solutions were prepared at the PMC with 5 μM GFP and 2.75 μM P2MVP_{41-b-PEO₂₀₅} and 5 μM GFP with 0.70 μM P2MVP_{128-b-PEO₄₇₇} in 10 mM borate buffer (pH 9.0). Encapsulation with different EGFP/darkGFP ratios was used for quantification purposes. After mixing, samples were stored at room temperature for 24 h before measurements. Free EGFP and C3Ms were measured at a laser power of 2.3 μW .

2.2.5.4. FCS data analysis

For the FCS data analysis, the FFS-data processor version 2.3 (Scientific Software Technologies Software Centre) was used.³⁷ Equation 2.8 was used to fit the autocorrelation functions $G(t)$ to obtain, $\tau_{diff,i}$ and the fractions belonging to $\tau_{diff,i}$. Fractions were determined by fixing the diffusion times for the PMC determination at 76.5 μs for free EGFP, 1412 μs for C3Ms with P2MVP_{41-b-PEO₂₀₅}, and

1460 μs for C3Ms with P2MVP₄₁-*b*-PEO₂₀₅. For the CMC determination diffusion times were fixed at 80.0 μs for free EGFP, 1400 μs for C3Ms with P2MVP₄₁-*b*-PEO₂₀₅, and 1680 μs for C3Ms with P2MVP₁₂₈-*b*-PEO₄₇₇. The diffusion times were not fixed at the same values for the two types of experiments, because the experimental settings and conditions were slightly different. With Equations 2.3 and 2.9 the hydrodynamic radii of EGFP and the C3Ms were calculated.

2.2.6. Fluorescence spectra of free and encapsulated EGFP

Fluorescence spectra were measured on a Varian Cary Eclipse spectrophotometer. Excitation and emission slits were set to a bandwidth of 5 nm. Spectra were taken at a PMT voltage of 500 V. Samples with concentrations of 5 μM of free EGFP and 5 μM EGFP in C3Ms at the PMCs were measured. For the excitation spectra, emission was set at 540 nm and excitation was recorded between 300 and 530 nm, each sample was scanned five times and averaged. For the emission spectra, excitation was set at 480 nm and fluorescence emission was recorded between 485 and 600 nm.

2.3. Results

Encapsulation of EGFP was investigated using DLS and FCS. Figures 2.2A and 2.2B show examples of experimental and fitted autocorrelation curves for free EGFP (green lines) and C3Ms containing EGFP (blue lines), based on the detected scattered light intensities (DLS, inset Figure 2.2A), and on the detected fluorescence intensity fluctuations (FCS, inset Figure 2.2B), respectively. The corresponding autocorrelation curves were calculated based on the same mathematical function (Equation 2.1) and by using applicable models for both techniques typical diffusion constants of EGFP and C3Ms containing EGFP were calculated. For DLS, the distributions of radii for free EGFP and C3Ms containing EGFP are plotted (Figure 2.2C). From these diffusion constants obtained, using the Stokes-Einstein relation (Equation 2.4), a hydrodynamic radius (R_h) of 2.20 ± 0.58 nm is found for free EGFP, while for C3Ms containing EGFP an R_h of 37.6 ± 0.6 nm is found (right bars in Figure 2.2D).

Analysis of FCS autocorrelation curves reveals an additional parameter compared to DLS: the average number of fluorescent particles in the confocal volume (N indicated in Figure 2.2B and corresponding results in Figure 2.2E). Similar to DLS, the diffusion constants were converted to hydrodynamic radii (Equation 2.4) and comparable values for the hydrodynamic radii were found: for free EGFP $R_h = 1.98 \pm 0.04$ nm and for C3Ms containing EGFP $R_h = 35.2 \pm 2.5$ nm (left bars in Figure 2.2D).

2.3.1. Preferred micellar composition; DLS

DLS composition experiments were carried out by keeping the total number of charged groups on the polymers and proteins constant at different compositions F^+ (Equation 2.6). We here present the results for P2MVP₄₁-*b*-PEO₂₀₅, the results for P2MVP₁₂₈-*b*-PEO₄₇₇ can be found in the Supplementary information. The light scattering intensities, hydrodynamic radii, and polydispersity indices (PDI) as function of the composition F^+ for EGFP with both polymers are shown in Figures 2.3 and S2.2. Encapsulation of EGFP with these two polymers results in a maximum scattered light intensity at an F^+ composition of 0.65 ± 0.03 (Figures 2.3A and S2.2A). At this composition we also observe a low value for the PDIs

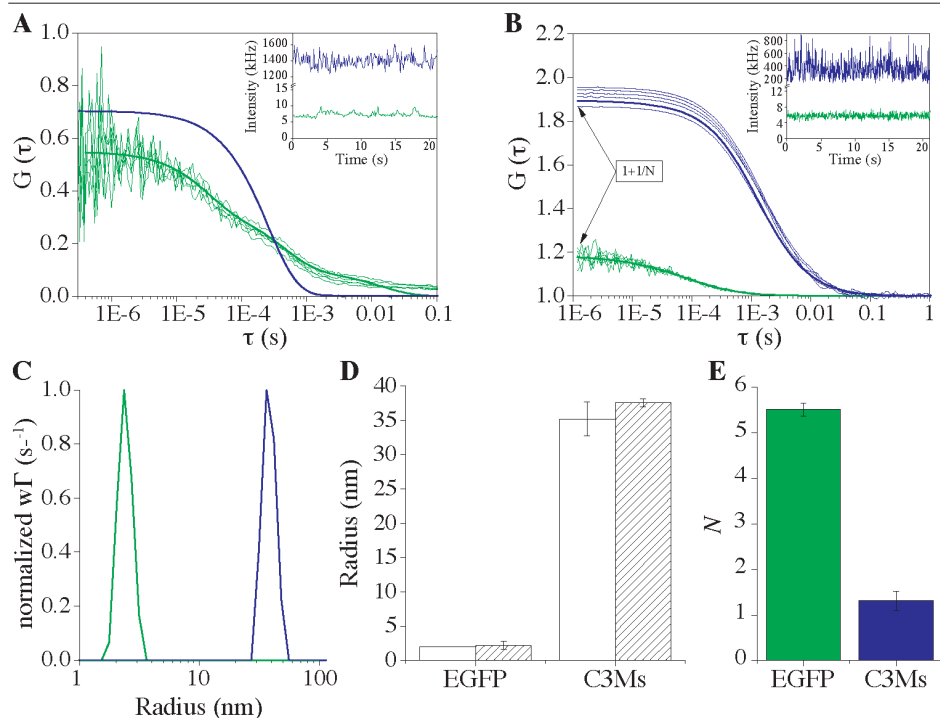


Figure 2.2. Autocorrelation curves for free EGFP (green lines) and C3Ms containing EGFP (blue lines) measured by (A) dynamic light scattering (DLS) and (B) fluorescence correlation spectroscopy (FCS), insets show the detected scattered light intensities and the detected fluorescence intensities, respectively. (C) Size distribution of free EGFP (green line) and C3Ms containing EGFP (blue line) determined by DLS. For comparison, we have plotted normalized data. (D) Hydrodynamic radii of free EGFP and C3Ms containing EGFP determined by FCS (left empty bars) and DLS (right dashed bars); $n = 3$. (E) Average number of particles (N) in the confocal volume calculated for 50 nM EGFP in solution and for 5 μ M C3Ms containing EGFP determined by FCS of three independent experiments.

(Figures 2.3C and S2.2C), indicating relatively monodisperse samples. The radii of the formed C3Ms are constant over a large range of compositions ($0.1 < F^+ < 0.8$), resulting in C3Ms of approximately 33 nm (Figures 2.3B and S2.2B). These results indicate that similar sized C3Ms are formed at relatively low concentrations of one of the components, either of the polymer ($F^+ = 0.1$) or of the protein ($F^+ = 0.9$) and that the maximum amount of C3Ms is reached around $F^+ = 0.65$, denoted as PMC.

2.3.2. Preferred micellar composition; FCS

DLS experiments revealed encapsulation of EGFP in micellar structures. FCS was employed to investigate structural properties of C3Ms based on fluorescence detection. EGFP was mixed with P2MVP₄₁-*b*-PEO₂₀₅ or P2MVP₁₂₈-*b*-PEO₄₇₇ at different compositions, while keeping the concentration of EGFP constant. Figures 2.4 and S2.3 show that the number of fluorescent particles (N) diminishes strongly when F^+ increases, because encapsulation of EGFP in C3Ms lowers the amount of EGFP free in solution. To gain insight at which

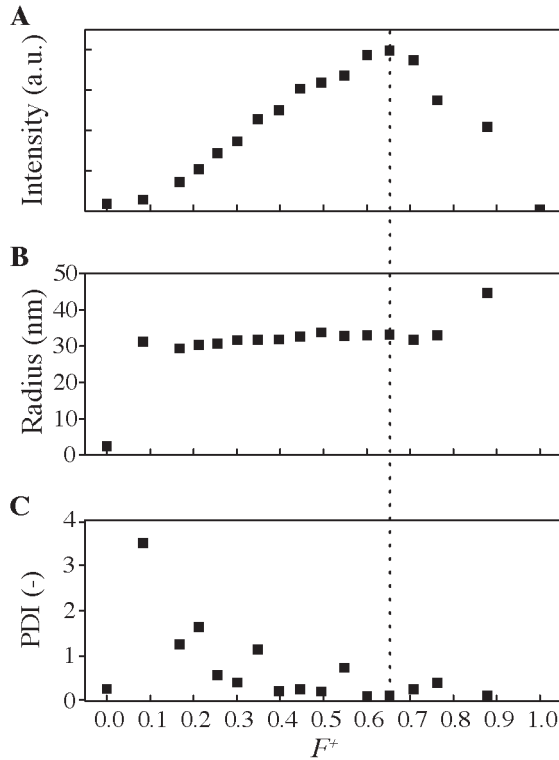


Figure 2.3. DLS composition experiment of EGFP and P2MVP₄₁-*b*-PEO₂₀₅ wherein the number of charged groups of protein and polymer was kept constant: (A) scattered intensity *versus* composition, (B) hydrodynamic radius *versus* composition, and (C) polydispersity index (PDI) *versus* composition. The dotted line indicates the preferred micellar composition.

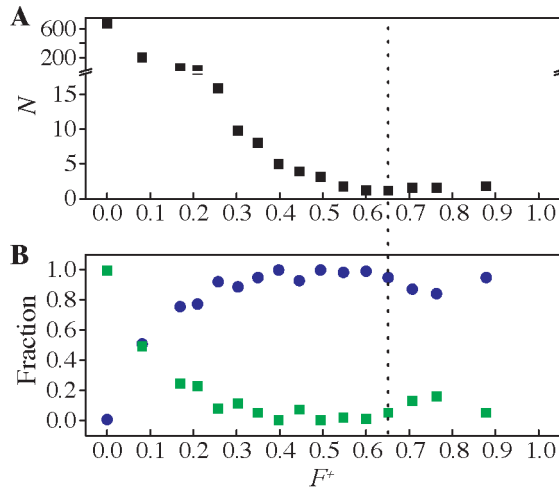


Figure 2.4. FCS composition experiment of EGFP and P2MVP₄₁-*b*-PEO₂₀₅ wherein the concentration of EGFP was kept constant: (A) number of fluorescent particles (N) *versus* composition and (B) fraction of free EGFP (green squares) and fraction of C3Ms (blue dots) belonging to a radius of 2.20 nm and 39.8 nm, respectively, *versus* composition. The dotted line indicates the preferred micellar composition.

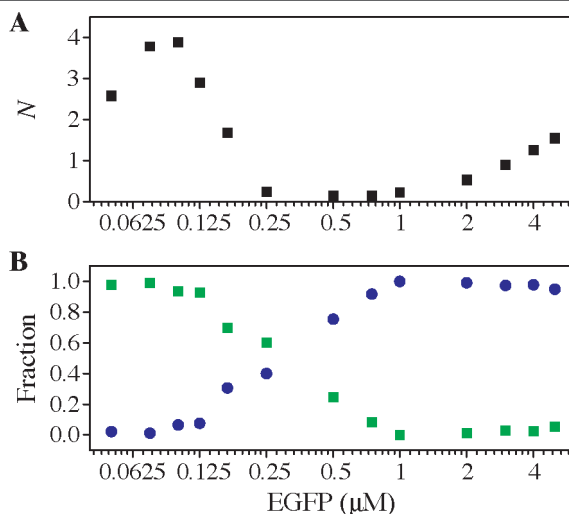


Figure 2.5. Critical micelle concentration determination of C3Ms composed of EGFP and P2MVP₄₁-*b*-PEO₂₀₅ at the PMC, measured by FCS: (A) number of fluorescent particles (N) versus EGFP concentration and (B) fractions of free EGFP (green squares) and C3Ms (blue dots) corresponding to a radius of 2.20 nm and 34.3 nm, respectively, versus EGFP concentration.

composition C3Ms are formed, the fractions of free EGFP and that of C3Ms were determined. Figures 2.4B and S2.3B show that C3Ms are present over a large range of compositions ($0.1 < F^+ < 0.8$). Comparable with DLS, C3Ms are formed at relative low concentrations of one of the components, either of the polymer ($F^+ = 0.1$) or of the protein ($F^+ = 0.9$). The PMC, as determined from the composition at which the minimum for N is reached, is $F^+ = 0.65$ for EGFP with both polymers (Figures 2.4 and S2.3).

2.3.3. Critical micelle concentration

Formation of C3Ms is dependent on several factors like ionic strength, pH, choice of polymer and concentrations of polymer and protein. A major advantage of using FCS is that fluorescent particles can be detected at very low concentrations (nM range), which allowed us to estimate the critical micelle concentration (CMC). The concentration at which the first micellar structures are detected, we define as the CMC. Figures 2.5 and S2.4 show the results of the CMC determination at the PMC; the ionic strength was kept constant by using buffer for the dilution. In these figures, the number of fluorescent particles (N) and the fractions of free EGFP and C3Ms containing EGFP are plotted versus the EGFP concentration. In Figures 2.5B and S2.4B it is shown that the fraction of C3Ms decreases below a concentration of 1 μM EGFP and is zero below a concentration of 100 nM EGFP. This, together with the rise in the number of fluorescent particles (Figures 2.5A and S2.4A), suggests the disintegration of C3Ms and the appearance of free EGFP. The leveling off of the fractions above 1 μM EGFP together with the increase of the number of fluorescent particles, suggests an increase in the amount of C3Ms proportional to the EGFP concentration. The C3Ms already appear above a concentration of 100 nM EGFP with P2MVP₄₁-*b*-PEO₂₀₅ as well as with P2MVP₁₂₈-*b*-PEO₄₇₇, which we define as the CMC.

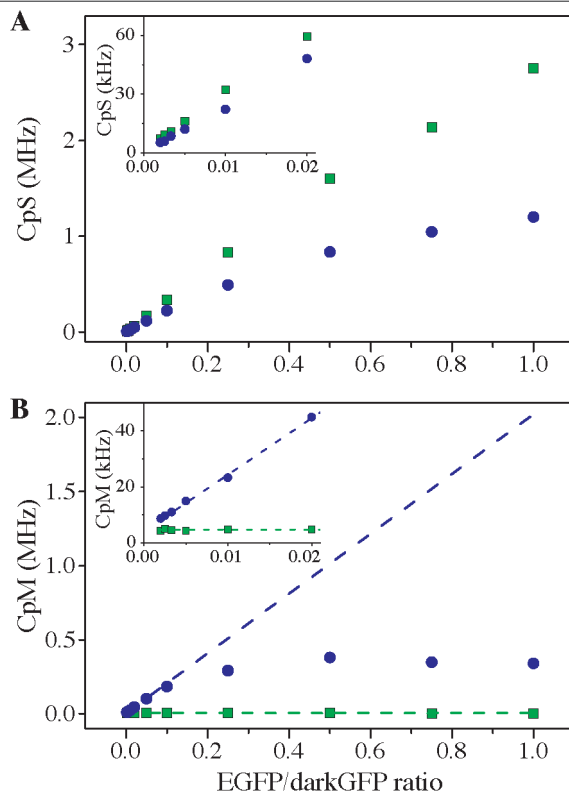


Figure 2.6. (A) Counts per second (CpS) and (B) Counts per second per molecule (CpM) *versus* EGFP/darkGFP ratio for free EGFP (green squares) and EGFP present in C3Ms (blue dots) with P2MVP₄₁-*b*-PEO₂₀₅. The lines represent the fit to the data between 0.005 < EGFP/darkGFP ratio < 0.02 for determination of the number of GFPs present per C3M. Insets are magnifications of the lowest EGFP/darkGFP ratios.

2.3.4. Number of GFPs per C3M

FCS detects bursts of photons from fluorescent particles passing through the detection volume. The fluorescence intensity of these bursts can be used to quantify the amount of EGFP encapsulated in C3Ms by relating the photon counts of free EGFP to the photon counts of C3Ms containing EGFP. FCS analysis revealed a value for N of ~ 550 for $5 \mu\text{M}$ EGFP free in solution ($N = 5.5$ for 50 nM EGFP free in solution, Figure 2.2E) whereas encapsulation of $5 \mu\text{M}$ EGFP in C3Ms using P2MVP₄₁-*b*-PEO₂₀₅ resulted in $N = 1.3$. This suggests that about 420 EGFP molecules are encapsulated in one C3M. The counts per second per molecule (CpM) of free EGFP in a typical experiment was 0.0045 MHz , which means that a CpM in the order of 1.9 MHz would be expected for the C3Ms. However, a CpM of only 0.45 MHz was found (Figure 2.6B). This discrepancy led us to perform measurements on samples containing both fluorescent GFP (EGFP) and non-fluorescent GFP (darkGFP) mixed in different ratios. Figures 2.6 and S2.5 show the data obtained from samples containing only EGFP (green squares) and from C3Ms (blue dots) with different ratios of EGFP/darkGFP. The counts per second (CpS) for free EGFP in solution

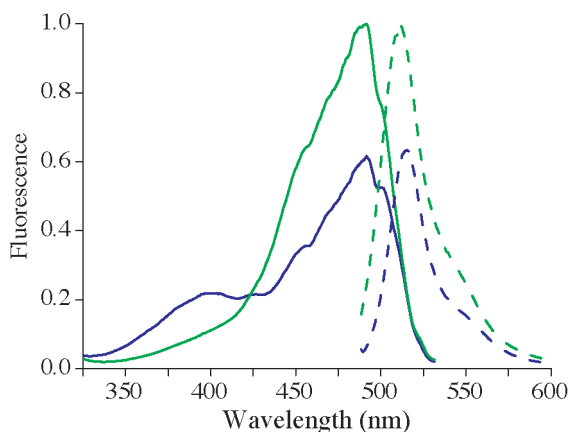


Figure 2.7. Excitation (solid lines) and emission (dashed lines) spectra for free EGFP (green lines) and EGFP encapsulated in C3Ms (blue lines) using diblock polymer P2MVP₄₁-*b*-PEO₂₀₅. For recording the excitation spectra, the emission wavelength was set at 540 nm. Fluorescence emission spectra were recorded between 490 and 600 nm upon 480 nm excitation. Spectra are normalized to the spectra of free EGFP.

shows a linear relationship up to a ratio of 0.5 and starts to deviate slightly at higher ratios (Figures 2.6A and S2.5A). However, if EGFP is encapsulated in C3Ms, linearity starts to deviate already at an EGFP/darkGFP ratio of 0.1 (Figures 2.6A and S2.5A). In Figures 2.6B and S2.5B the calculated CpM are plotted versus the EGFP/darkGFP ratio. The CpM is almost constant for EGFP in solution independent of the ratio. However, the counts per C3M, which should increase linearly with the EGFP/darkGFP ratio, show a downward deflection at higher EGFP/darkGFP ratio.

The observed non-linearity is mainly caused by a change of the excitation spectrum of EGFP when encapsulated in C3Ms. In Figure 2.7 the excitation and emission spectra are shown for 5 μ M EGFP and 5 μ M EGFP inside the C3Ms. Clearly visible from these spectra is the decrease of excitation of EGFP at 488 nm upon encapsulation. Consequently, a loss of approximately 40% of the fluorescence emission at 510 nm is found.

To estimate the number of GFP molecules in the C3Ms, the deviation in fluorescence intensity was by-passed by determining the slope of the line in Figure 2.6B at low EGFP/darkGFP ratios, in the range of $0.005 < \text{EGFP/darkGFP ratio} < 0.02$. Extrapolation of this line to a ratio of 1 yields a CpM of 2 MHz per C3M (Figure 2.6B), with 0.0045 MHz per EGFP, resulting in about 450 GFP molecules together with 132 P2MVP₄₁-*b*-PEO₂₀₅ polymers encapsulated per C3M. The CpM is 2.4 MHz per C3M for EGFP with P2MVP₁₂₈-*b*-PEO₄₇₇ (Figure S2.5B), resulting in about 530 GFP molecules together with 46 P2MVP₁₂₈-*b*-PEO₄₇₇ polymers encapsulated per C3M. For both systems this means that the C3Ms have a weight of approximately 70 MDa with a water content of 84%.

2.4. Discussion

We have demonstrated that GFP can be encapsulated in micellar structures with two differently sized P2MVP-*b*-PEO polymers. With these two diblock copolymers C3Ms of similar size are formed. This is probably due to the similar size ratios of the neutral and charged blocks, which is 0.20 for P2MVP₄₁-*b*-PEO₂₀₅ and 0.27 for P2MVP₁₂₈-*b*-PEO₄₇₇. Addition of a relatively small amount of protein or polymer to a concentrated polymer or protein solution, respectively, already leads to formation of C3Ms. In the range $0.1 < F^+ < 0.9$ the radius of the micelles is constant, about 33 nm (Figures 2.3B and S2.2B). This is remarkable, since for other systems generally at both sides of the PMC smaller polyelectrolyte complexes are found.^{2,3,7,16} This was for example the case in the study of Lindhoud *et al.* (2009) on encapsulation of α -lactalbumin using P2MVP₄₁-*b*-PEO₂₀₅ polymers.²⁵ Although α -lactalbumin has almost the same net charge as EGFP (-8 at pH 7), a negatively charged homopolymer PAA₁₃₉ was included for generating C3Ms. In contrast to our data, the radius of the formed protein-polyelectrolyte complexes showed a gradual increase from $F^+ = 1$ with a maximum at the PMC ($F^+ = 0.48$).

For our system we found a PMC around $F^+ = 0.65$, whereas one may expect a PMC at a stoichiometric charge ratio, *i.e.*, at $F^+ = 0.5$. This deviation can be caused by two factors. Firstly, EGFP may adapt its charge in the C3Ms: in response to the positive potential of the cationic block of the polymer, the protein may release some of its protons and obtains a higher negative charge.³⁹ Secondly, complex formation is likely not purely electrostatically driven, but other forces like hydrophobic interactions may also play a role.

FCS has already been used for monitoring formation of micelles²⁴ and dye-containing polymeric nanocontainers²³, but to the best of our knowledge not yet for studying the encapsulation of proteins in C3Ms. This study shows that FCS is an appropriate method to investigate the formation of C3Ms. FCS has some advantages compared to DLS. Firstly, FCS can be applied at much lower concentrations than is required for DLS measurements, which allowed us to determine the critical concentration at which C3Ms are formed. Furthermore, FCS is a quantitative method that allows obtaining the number of fluorescent particles in the detection volume. However, extracting quantitative information from FCS data can be hampered if large differences in brightness are present, which is observed in our case for free EGFP in solution compared to EGFP encapsulated in C3Ms. As a consequence, the amount of free EGFP in a solution containing C3Ms may be underestimated. We observed a discrepancy and a non-linearity of CpM in relation to the number of total photon counts, which is mainly caused by the change in the environment of the chromophore of EGFP when encapsulated. This change leads to reduction in excitation at 488 nm and a decline of approximately 40% in fluorescence emission. The loss in fluorescence intensity can be partly due to homo-FRET between EGFP molecules in a C3M. Skakun and coworkers³⁸ have demonstrated in an FCS brightness analysis that a dimer of EGFP does not have a double brightness value compared to monomeric GFP, instead a loss of about 15% in fluorescence intensity was observed. Next to that, the excitation spectrum of EGFP in C3Ms showed an additional band at 400 nm (Figure 2.7). The cause of this phenomenon can be protonation of Tyr66.¹⁰

We found that each C3M contains approximately 450 GFP molecules for the C3Ms containing P2MVP₄₁-*b*-PEO₂₀₅. One may wonder if such a high amount of molecules fits into the core of a micelle. A rough calculation, assuming a radius of 30 nm for the core of the micelle and of 2.3 nm for the protein, shows that the core volume is in the order of 2000 times that of the protein volume. Therefore, incorporation of several hundreds of GFP molecules in micelles is feasible.

2.5. Conclusion

In this study we show efficient encapsulation of GFP with two sizes of P2MVP-*b*-PEO diblock copolymer in C3Ms. Encapsulation was investigated with both DLS and FCS, and the results are very similar: the hydrodynamic radius of the C3Ms is about 33 nm and they form already at low protein/polymer and polymer/protein ratios. The PMC lies at $F^+ \approx 0.65$. In addition, FCS enabled us to determine the lowest concentration of GFP at which C3Ms are formed, which amounts to approximately 100 nM GFP at the PMC. Compared to free EGFP, encapsulated EGFP showed a loss in fluorescence intensity due to changes in the excitation and emission spectra. Determination of the number of protein molecules per micelle could be achieved by mixing fluorescent with non-fluorescent GFP molecules. The amount of GFP molecules encapsulated is approximately 450 per C3M using P2MVP₄₁-*b*-PEO₂₀₅.

Acknowledgments

Financial support from the Graduate School VLAG (Wageningen, The Netherlands) is gratefully acknowledged. The FCS experiments were performed on a multimode confocal microscope supported by a NWO Middelgroot investment grant (721.011.004; Jan Willem Borst). Victor V. Skakun from the Department of Systems Analysis and Computer Simulation, Belarusian State University, Minsk, Belarus and Mark A. Hink from the Department of Molecular Cytology van Leeuwenhoek Centre for Advanced Microscopy, University of Amsterdam, Amsterdam, Netherlands are acknowledged for their support in the FCS experiments.

References

- Kayitmazer, A. B.; Seeman, D.; Minsky, B. B.; Dubin, P. L.; Xu, Y. S., Protein-polyelectrolyte interactions. *Soft Matter* **2013**, *9*, (9), 2553-2583.
- Lindhoud, S.; de Vries, R.; Schweins, R.; Cohen Stuart, M. A.; Norde, W., Salt-induced release of lipase from polyelectrolyte complex micelles. *Soft Matter* **2009**, *5*, (1), 242-250.
- Lindhoud, S.; Norde, W.; Cohen Stuart, M. A., Effects of polyelectrolyte complex micelles and their components on the enzymatic activity of lipase. *Langmuir* **2010**, *26*, (12), 9802-9808.
- Harada, A.; Kataoka, K., Supramolecular assemblies of block copolymers in aqueous media as nanocontainers relevant to biological applications. *Prog. Polym. Sci.* **2006**, *31*, (11), 949-982.
- Voets, I. K.; de Keizer, A.; de Waard, P.; Frederik, P. M.; Bomans, P. H.; Schmalz, H.; Walther, A.; King, S. M.; Leermakers, F. A.; Cohen Stuart, M. A., Double-faced micelles from water-soluble polymers. *Angew. Chem. Int. Ed. Engl.* **2006**, *45*, (40), 6673-6676.
- Morawetz, H.; Hughes, W. L., The interaction of proteins with synthetic polyelectrolytes. 1. Complexing of bovine serum albumin. *J. Phys. Chem.* **1952**, *56*, (1), 64-69.
- Lindhoud, S.; Voorhaar, L.; de Vries, R.; Schweins, R.; Cohen Stuart, M. A.; Norde, W., Salt-induced disintegration of lysozyme-containing polyelectrolyte complex micelles. *Langmuir* **2009**, *25*, (19), 11425-11430.
- Kayitmazer, A. B.; Strand, S. P.; Tribet, C.; Jaeger, W.; Dubin, P. L., Effect of polyelectrolyte structure on protein-polyelectrolyte coacervates: coacervates of bovine serum albumin with poly(diallyldimethylammonium chloride) versus chitosan. *Biomacromolecules* **2007**, *8*, (11), 3568-3577.
- Tsien, R. Y., The green fluorescent protein. *Annu. Rev. Biochem.* **1998**, *67*, 509-544.
- Haupts, U.; Maiti, S.; Schwille, P.; Webb, W. W., Dynamics of fluorescence fluctuations in green fluorescent protein observed by fluorescence correlation spectroscopy. *Proc. Natl. Acad. Sci. U. S. A.* **1998**, *95*, (23), 13573-13578.
- Arpino, J. A.; Rizkallah, P. J.; Jones, D. D., Crystal structure of enhanced green fluorescent protein to 1.35 Å resolution reveals alternative conformations for Glu222. *PLoS One* **2012**, *7*, (10), e47132.
- Uskova, M. A.; Borst, J. W.; Hink, M. A.; van Hoek, A.; Schots, A.; Klyachko, N. L.; Visser, A. J., Fluorescence dynamics of green fluorescent protein in AOT reversed micelles. In *Biophys. Chem.*, 2000; Vol. 87, pp 73-84.
- Minten, I. J.; Nolte, R. J. M.; Cornelissen, J. J. L. M., Complex assembly behavior during the encapsulation of green fluorescent protein analogs in virus derived protein capsules. *Macromol. Biosci.* **2010**, *10*, (5), 539-545.
- Voets, I. K.; de Keizer, A.; Cohen Stuart, M. A., Complex coacervate core micelles. *Adv. Colloid Interface Sci.* **2009**, 147-148, 300-318.
- Berne, B. J.; Pecora, R., *Dynamic light scattering with application to chemistry, biology and physics*. Courier Dover, New York: 1976.
- Spruijt, E.; Westphal, A. H.; Borst, J. W.; Cohen Stuart, M. A.; van der Gucht, J., Binodal compositions of polyelectrolyte complexes. *Macromolecules* **2010**, *43*, (15), 6476-6484.
- Hink, M. A.; Griep, R. A.; Borst, J. W.; van Hoek, A.; Eppink, M. H. M.; Schots, A.; Visser, A. J. W. G., Structural dynamics of green fluorescent protein alone and fused with a single chain Fv protein. *J. Biol. Chem.* **2000**, *275*, (23), 17556-17560.
- Bourouina, N.; Cohen Stuart, M. A.; Kleijn, J. M., Complex coacervate core micelles as diffusional nanopores. *Soft Matter* **2014**, *10*, (2), 320-331.
- Garcia-Saez, A. J.; Schwille, P., Fluorescence correlation spectroscopy for the study of membrane dynamics and protein/lipid interactions. *Methods* **2008**, *46*, (2), 116-122.
- van den Berg, P. A.; Widengren, J.; Hink, M. A.; Rigler, R.; Visser, A. J., Fluorescence correlation spectroscopy of flavins and flavoenzymes: photochemical and photophysical aspects. *Spectrochim. Acta, Part A* **2001**, *57*, (11), 2135-2144.
- Luschinetz, F.; Dosche, C., Determination of micelle diffusion coefficients with fluorescence correlation spectroscopy (FCS). *J. Colloid Interface Sci.* **2009**, *338*, (1), 312-315.
- Humpolickova, J.; Prochazka, K.; Hof, M.; Tuzar, Z.; Spirkova, M., Fluorescence correlation spectroscopy using octadecylrhodamine B as a specific micelle-binding fluorescent tag; Light scattering and tapping mode atomic force microscopy studies of amphiphilic water-soluble block copolymer micelles. *Langmuir* **2003**, *19*, (10), 4111-4119.
- Rigler, P.; Meier, W., Encapsulation of fluorescent molecules by functionalized polymeric nanocontainers: investigation by confocal fluorescence imaging and fluorescence correlation spectroscopy. *J. Am. Chem. Soc.* **2006**, *128*, (1), 367-373.

24. Bonn , T. B.; L dtke, K.; Jordan, R.;  t p nek, P.; Papadakis, C. M., Aggregation behavior of amphiphilic poly(2-alkyl-2-oxazoline) diblock copolymers in aqueous solution studied by fluorescence correlation spectroscopy. *Colloid Polym. Sci.* **2004**, *282*, (12), 1425-1425.
25. Lindhoud, S.; Norde, W.; Cohen Stuart, M. A., Reversibility and relaxation behavior of polyelectrolyte complex micelle formation. *J. Phys. Chem. B* **2009**, *113*, (16), 5431-5439.
26. Wang, J.; Velders, A. H.; Gianolio, E.; Aime, S.; Vergeldt, F. J.; Van As, H.; Yan, Y.; Drechsler, M.; de Keizer, A.; Cohen Stuart, M. A.; van der Gucht, J., Controlled mixing of lanthanide(III) ions in coacervate core micelles. *Chem. Commun.* **2013**, *49*, (36), 3736-3738.
27. Xu, M. Q.; Paulus, H.; Chong, S., Fusions to self-splicing inteins for protein purification. *Methods Enzymol.* **2000**, *326*, 376-418.
28. Evans, T. C., Jr.; Xu, M. Q., Intein-mediated protein ligation: harnessing nature's escape artists. *Biopolymers* **1999**, *51*, (5), 333-342.
29. Chong, S.; Mersha, F. B.; Comb, D. G.; Scott, M. E.; Landry, D.; Vence, L. M.; Perler, F. B.; Benner, J.; Kucera, R. B.; Hirvonen, C. A.; Pelletier, J. J.; Paulus, H.; Xu, M. Q., Single-column purification of free recombinant proteins using a self-cleavable affinity tag derived from a protein splicing element. *Gene* **1997**, *192*, (2), 271-281.
30. Barondeau, D. P.; Putnam, C. D.; Kassmann, C. J.; Tainer, J. A.; Getzoff, E. D., Mechanism and energetics of green fluorescent protein chromophore synthesis revealed by trapped intermediate structures. *Proc. Natl. Acad. Sci. U. S. A.* **2003**, *100*, (21), 12111-12116.
31. Barondeau, D. P.; Kassmann, C. J.; Tainer, J. A.; Getzoff, E. D., Understanding GFP chromophore biosynthesis: controlling backbone cyclization and modifying post-translational chemistry. *Biochemistry* **2005**, *44*, (6), 1960-1970.
32. Sawano, A.; Miyawaki, A., Directed evolution of green fluorescent protein by a new versatile PCR strategy for site-directed and semi-random mutagenesis. *Nucleic Acids Res.* **2000**, *28*, (16), E78.
33. Provencher, S. W., Contin - a general-purpose constrained regularization program for inverting noisy linear algebraic and integral-equations. *Comput. Phys. Commun.* **1982**, *27*, (3), 229-242.
34. Rostkowski, M.; Olsson, M. H. M.; Sondergaard, C. R.; Jensen, J. H., Graphical analysis of pH-dependent properties of proteins predicted using PROPKA. *BMC Struct. Biol.* **2011**, *11*, 6.
35. Olsson, M. H.; Sondergaard, C. R.; Rostkowski, M.; Jensen, J. H., PROPKA3: Consistent treatment of internal and surface residues in empirical pKa predictions. *J. Chem. Theory Comput.* **2011**, *7*, (2), 525-537.
36. Magde, D.; Elson, E. L.; Webb, W. W., Fluorescence correlation spectroscopy. II. An experimental realization. *Biopolymers* **1974**, *13*, (1), 29-61.
37. Skakun, V. V.; Hink, M. A.; Digris, A. V.; Engel, R.; Novikov, E. G.; Apanasovich, V. V.; Visser, A. J. W. G., Global analysis of fluorescence fluctuation data. *Eur. Biophys. J.* **2005**, *34*, (4), 323-334.
38. Skakun, V. V.; Engel, R.; Digris, A. V.; Borst, J. W.; Visser, A. J. W. G., Global analysis of autocorrelation functions and photon counting distributions. *Front. Biosci., Elite Ed.* **2011**, *3*, 489-505.
39. de Vos, W. M.; Leermakers, F. A.; de Keizer, A.; Cohen Stuart, M. A.; Kleijn, J. M., Field theoretical analysis of driving forces for the uptake of proteins by like-charged polyelectrolyte brushes: effects of charge regulation and patchiness. *Langmuir* **2010**, *26*, (1), 249-259.

Supplementary information

S2.1. Charges of EGFP

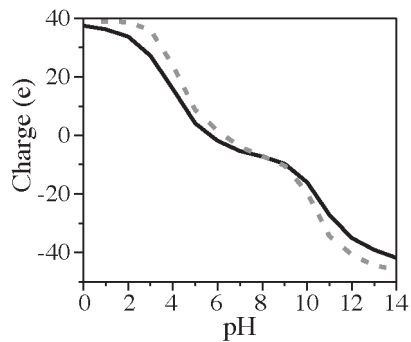


Figure S2.1. Number of charges calculated on folded (black solid line) and unfolded EGFP (gray dashed line) as a function of pH using the software package PROPKA 3.1^{34,35}.



S2.2. Results of C₃M_s with EGFP and P2MVP₁₂₈-*b*-PEO₄₇₇

S2.2.1. Preferred micellar composition; DLS

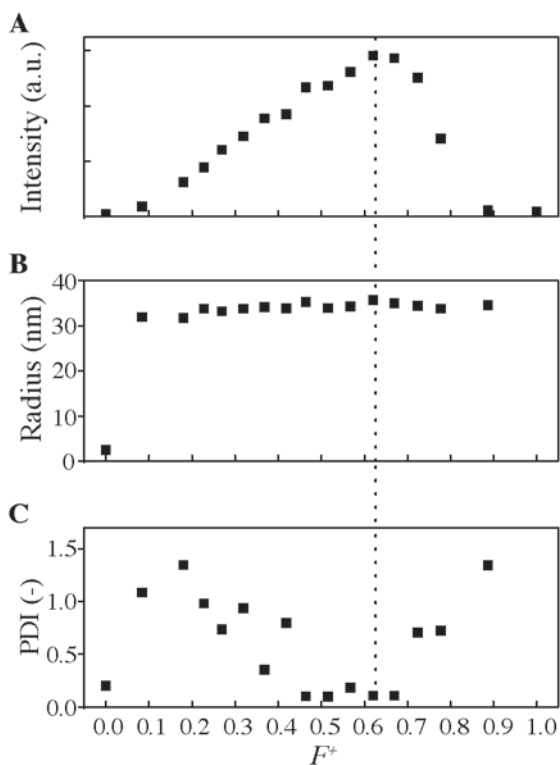


Figure S2.2. DLS composition experiment of EGFP and P2MVP₁₂₈-*b*-PEO₄₇₇ wherein the number of charged groups of protein and polymer was kept constant: (A) scattered intensity *versus* composition, (B) hydrodynamic radius *versus* composition, and (C) polydispersity index (PDI) *versus* composition. The dotted line indicates the preferred micellar composition.

S2.2.2. Preferred micellar composition; FCS

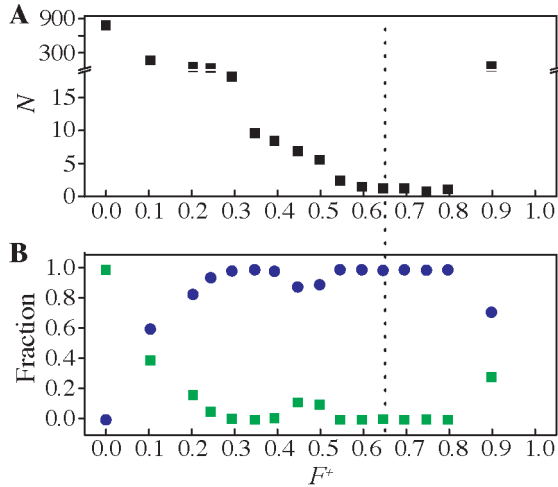


Figure S2.3. FCS composition experiment of EGFP and P2MVP₁₂₈-*b*-PEO₄₇₇ wherein the concentration of EGFP was kept constant: (A) number of fluorescent particles (N) *versus* composition and (B) fraction of free EGFP (green squares) and fraction of C3Ms (blue dots) belonging to a radius of 2.20 nm and 41.7 nm, respectively, *versus* composition. The dotted line indicates the preferred micellar composition.

S2.2.3. Critical micelle concentration

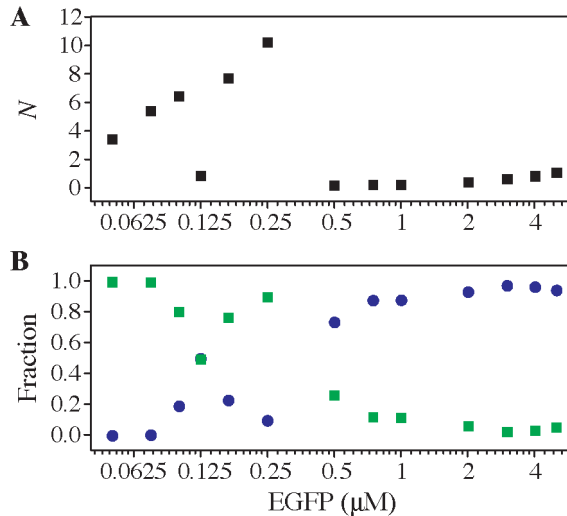


Figure S2.4. Critical micelle concentration determination of C3Ms composed of EGFP and P2MVP₁₂₈-*b*-PEO₄₇₇ at the PMC, measured by FCS: (A) number of fluorescent particles (N) *versus* EGFP concentration and (B) fractions of free EGFP (green squares) and C3Ms (blue dots) corresponding to a radius of 1.97 nm and 41.2 nm, respectively, *versus* EGFP concentration. For a more suitable presentation of the data a log₂ scale was used.

S2.2.4. Number of GFPs per C3M

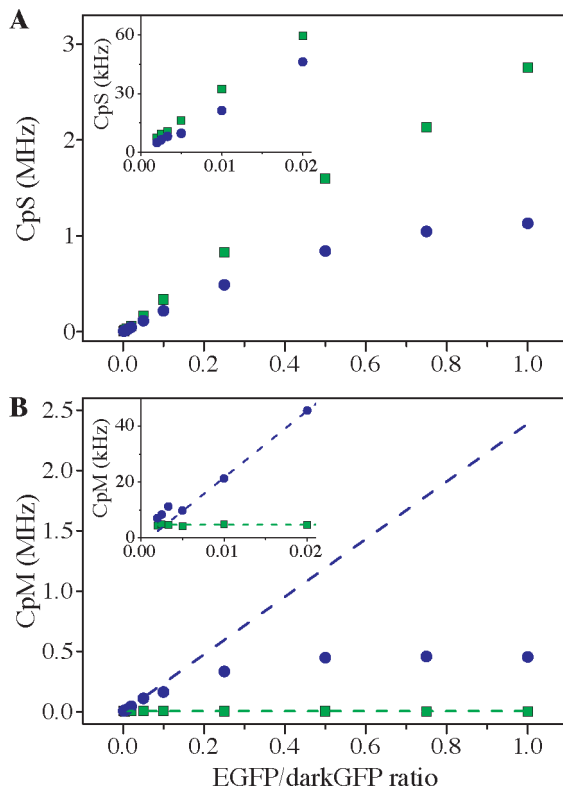
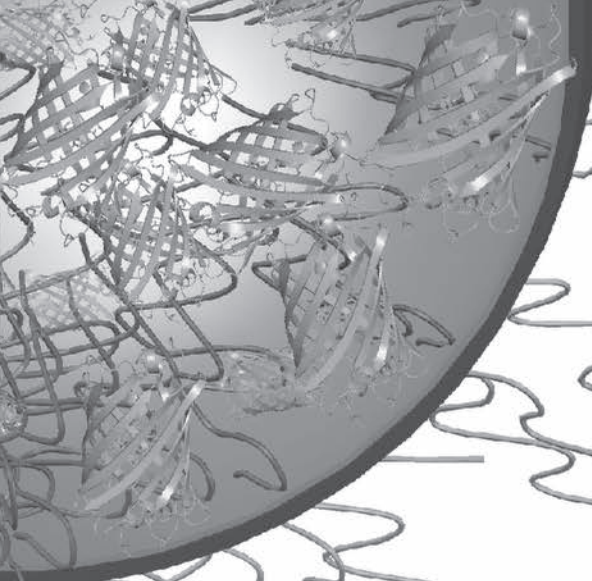


Figure S2.5. (A) Counts per second (CpS) and (B) Counts per second per molecule (CpM) *versus* EGFP/darkGFP ratio for free EGFP (green squares) and EGFP present in C3Ms (blue dots) with P2MVP₁₂₈-*b*-PEO₄₇₇. The lines represent the fit to the data between 0.005 < EGFP/darkGFP ratio < 0.02 for determination of the number of GFPs present per C3M. Insets are magnifications of the lowest EGFP/darkGFP ratios.



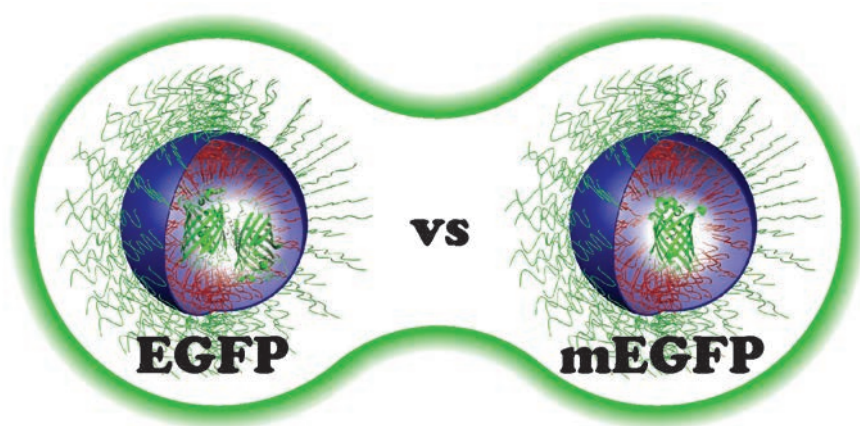
Chapter 3

Encapsulation into complex coacervate core micelles promotes EGFP dimerization

Published as: A. Nolles, N. J. E. van Dongen, A. H. Westphal,
A. J. W. G. Visser, J. M. Kleijn, W. J. H. van Berkel, and
J. W. Borst, *Phys. Chem. Chem. Phys.*, **2017**, 19, 11380-11389.

Abstract

Complex coacervate core micelles (C3Ms) are colloidal structures useful for encapsulation of biomacromolecules. We previously demonstrated that enhanced green fluorescent protein (EGFP) can be encapsulated into C3Ms using the diblock copolymer poly(2-methyl-vinyl-pyridinium)₄₁-*b*-poly(ethylene-oxide)₂₀₅. This packaging resulted in deviating spectroscopic features of the encapsulated EGFP molecules. Here we show that for the monomeric EGFP variant (mEGFP) micellar encapsulation affects the absorption and fluorescence properties to a much lesser extent, and that changes in circular dichroism characteristics are specific for encapsulated EGFP. Time-resolved fluorescence anisotropy experiments of the encapsulated (m)EGFP proteins established the occurrence of homo-FRET (Förster resonance energy transfer) with larger transfer correlation times in case of EGFP. Together, these findings support that EGFP dimerizes whereas mEGFP mainly remains a monomer in the densely packed C3Ms. We propose that dimerization of encapsulated EGFP causes a reorientation of Glu222, resulting in a pK_a shift of the chromophore, which is fully reversible after release of EGFP from the C3Ms at high ionic strength.



3.1. Introduction

The co-assembly of a neutral-ionic diblock copolymer with oppositely charged biopolymers, such as proteins, results in complex coacervate core micelles (C3Ms).¹⁻³ The formation of these C3Ms is electrostatically driven, therefore responsive to ionic strength and in the case of proteins also responsive to pH.¹ Encapsulation of proteins can be useful for protection or stabilization purposes and can be applied for controlled delivery, making these systems beneficial for food and biomedical applications.^{4,5} In some protein encapsulation studies, enhanced green fluorescent protein (EGFP) has been used as a model protein.^{3,6} EGFP is a remarkable stable protein, which is used for many applications in biochemistry and cell biology^{7,8}, such as fluorescent tag for visualizing proteins of interest in living organisms.⁹⁻¹¹

Previously, we have shown that encapsulation of EGFP can be accomplished using a positively charged diblock copolymer.³ At pH 9, EGFP has about 11 negative unit charges, which is sufficient to form complex coacervate core micelles (C3Ms) with the diblock copolymer poly(2-methyl-vinyl-pyridinium)_n-*b*-poly(ethylene-oxide)_m (P2MVP_n-*b*-PEO_m). C3Ms were prepared with two different lengths of diblock copolymer (P2MVP₄₁-*b*-PEO₂₀₅ and P2MVP₁₂₈-*b*-PEO₄₇₇) and the formation and quantification of EGFP encapsulation was studied using spectroscopic techniques. With the use of fluorescence correlation spectroscopy (FCS), we determined that a single C3M contains about 450 protein molecules.³ Furthermore, spectral analysis revealed that encapsulated EGFP displays a change in the absorption spectrum compared to that of EGFP free in solution, resulting in different fluorescence properties. We proposed that this effect could be due to either protonation of the EGFP chromophore or homo-FRET (Förster resonance energy transfer between fluorophores having identical spectra) between packed EGFP molecules.³ In the present study, we elucidate the molecular basis of the spectral and structural changes of EGFP upon tight packing in C3Ms.

EGFP is comprised of 238 amino acid residues, which fold into an eleven-stranded β -barrel with a length of 4.2 nm and a diameter of 2.4 nm (Figure 3.1A).^{12,13} In the middle of the barrel a single central helix is located with three amino acid residues, creating the chromophore, which is physically isolated from the solution.⁷ The fluorescent moiety of EGFP is formed by cyclization, dehydration and oxidation of residues Thr65, Tyr66, and Gly67 initially present in the helix, resulting in the *para*-hydroxybenzylidene-imidazolidinone chromophore (Figure 3.1B).¹⁴ The chromophore of EGFP is present in the anionic form, leading to an absorption maximum at 488 nm and an emission maximum at 507 nm.^{15,16}

The crystal structure of wild-type GFP (wtGFP) revealed a dimeric configuration comprised of two quite regular β -barrels (Figure S3.1).¹² The core of the dimer interface consists of a hydrophobic patch formed by the side chains of Ala206, Leu221, and Phe223 (Figure 3.1C). This dimer interface can cause false positives in interaction studies between fluorescently labeled proteins at high protein concentrations.^{17,18} To suppress dimerization of fluorescent proteins, Zacharias *et al.*, (2002) replaced the apolar alanine at position 206 with a positively charged lysine (A206K, Figure 3.1D).¹⁸ This replacement increases the dimer

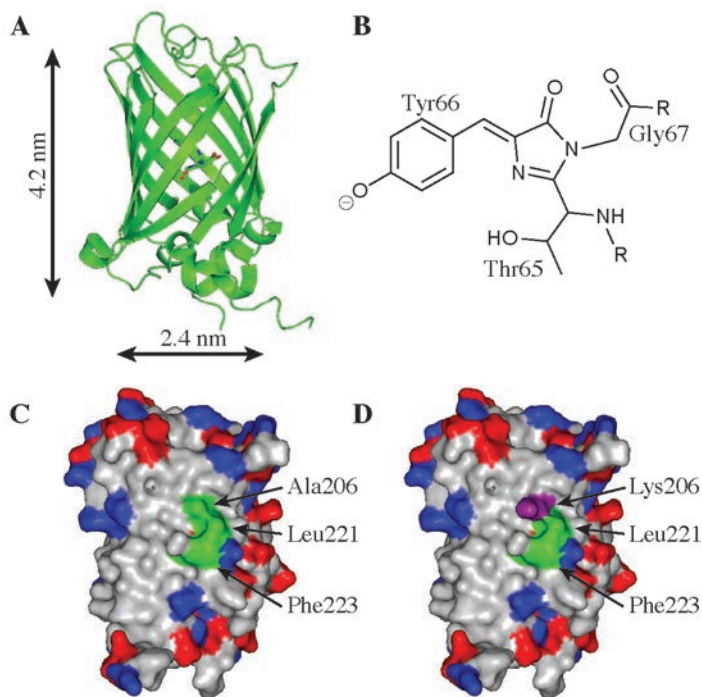


Figure 3.1. Structural characteristics of EGFP and mEGFP. (A) The β -barrel architecture of (m)EGFP and its dimensions, based on crystal structure PDB entry 4EUL.¹⁹ (B) The chromophore of EGFP and mEGFP formed by cyclization of Thr65, Tyr66, and Gly67. The solvent accessible surface areas of (C) EGFP and (D) mEGFP projecting the dimerization interface. For C and D, neutral amino acid residues are shown in gray; positively charged residues in blue; negatively charged residues in red; Ala206, Leu221, and Phe223 in green; and Lys206 in purple. Images were created with PyMOL (Schrödinger, LLC).

dissociation constant from 0.11 mM for EGFP to approximately 74 mM for its monomeric variant, mEGFP.

In this work, we investigate the molecular basis of the fluorescence properties of encapsulated EGFP. For this, both EGFP and mEGFP were incorporated in C3Ms with the use of P2MVP₄₁-*b*-PEO₂₀₅. Application of spectral analysis, circular dichroism (CD), and time-resolved fluorescence anisotropy (TRFA) revealed that encapsulation of the two EGFP variants results in high packaging densities, but with noticeable differences in spectral properties.

3.2. Experimental section

3.2.1. Materials

Poly(2-vinyl-pyridinium)₄₁-*b*-poly(ethylene-oxide)₂₀₅ (Polymer Source Inc., Canada, $M_w/M_n = 1.05$, $M_n = 13.3$ kg/mol) was quaternized with iodomethane (99%, Sigma-Aldrich) to poly(2-methyl-vinyl-pyridinium-iodide)₄₁-*b*-poly(ethylene-oxide)₂₀₅ (P2MVP₄₁-*b*-PEO₂₀₅), according to the procedure described elsewhere.³ For P2MVP₄₁-*b*-PEO₂₀₅ ($M_n = 18.6$ kg/mol), a final degree of quaternization of approximately 80% was obtained. A stock solution of P2MVP₄₁-*b*-PEO₂₀₅ (51 μ M) was prepared by dissolving the polymer in 10 mM borate buffer (pH 9.0) and stored at -20°C . All solutions were filtered through 0.20 μ m poly(ether-sulfone) membrane syringe filters (Advanced Microdevices Pvt. Ltd.). All chemicals were from commercial sources and of the purest grade available.

3.2.2. Protein production

The EGFP gene was cloned in the bacterial expression vector pTYB12 (New England Biolabs Inc.) to generate an EGFP fusion with a chitin-binding domain (CBD) and an intein.²⁰⁻²² The cDNAs of mEGFP and SBFP2 (strongly enhanced blue fluorescent protein) in pRSETb vectors were kindly provided by Dr. Joachim Goedhart, University of Amsterdam.²³ Pre-cultures of 5 mL (grown overnight) inoculated with plasmid containing *E. coli* BL21 cells were transferred to 2 L Erlenmeyer flasks, containing 500 mL LB medium and 100 μ g/mL ampicillin. Cells were grown at 37°C with a shaking rate of 200 rpm until an optical density of ~ 0.5 at 600 nm was reached. For EGFP protein production, cells were induced with 120 μ g/mL IPTG at 20°C for 18 h. For mEGFP and SBFP2 protein production, cells were left to grow at 20°C for 42 h (no IPTG was added, because the promoter of the used pRSETb vector is leaky). For all three proteins, cells were harvested by centrifugation (10 000 g at 4°C for 25 min) and stored at -20°C until further use.

The purification of EGFP was performed according to the protocol described before.³ The purification of mEGFP and SBFP2 was as follows: *E. coli* cells obtained after culturing were resuspended in 20 mM potassium phosphate (pH 7.4) containing 300 mM NaCl, 0.1 mg/mL DNaseI, 1 mM MgCl₂ and an EDTA-free Complete Protease Inhibitor Cocktail tablet (Roche Diagnostics GmbH). Cells were lysed by passing them three times through a pre-cooled French Press cell (SLM Aminco Instruments) at 10 000 psi. Cell lysate was centrifuged at 40 000 g at 4°C for 45 min. An Äkta explorer FPLC system (GE Healthcare Life Sciences) was used for further chromatography steps. The soluble fraction was loaded on a Ni-NTA (16 x 75 mm) column (Qiagen), pre-equilibrated in 20 mM potassium phosphate, 300 mM NaCl, pH 7.4. After washing, bound protein was eluted with 125 mM imidazole in 20 mM potassium phosphate, 300 mM NaCl, pH 7.4. Fractions containing fluorescent proteins were pooled, Ni²⁺ ions were chelated with 1 mM EDTA, and the protein solution was concentrated using an Amicon ultrafiltration unit with a 10 kDa cut-off PES-membrane (Merck Millipore). The proteins were further purified on a Superdex 75 26/600 column (GE Healthcare Life Sciences) equilibrated with 10 mM borate buffer (pH 9.0) and 150 mM NaCl. Pure mEGFP and SBFP2 fractions were pooled, concentrated, and stored in 10 mM borate buffer (pH 9.0) at -20°C .

Protein concentrations were determined with a Pierce BCA protein assay (Pierce Biotechnology), using bovine serum albumin as reference. The purity of the fluorescent proteins was checked by SDS-PAGE.

3.2.3. C₃M preparation

Encapsulation of EGFP, mEGFP and SBFP2 with P2MVP₄₁-*b*-PEO₂₀₅ was achieved by first diluting the protein stock solutions (31.0 μM EGFP, 14.8 μM mEGFP, 35.5 μM SBFP2) in 10 mM borate buffer (pH 9.0) to the desired concentration, followed by addition of polymer solution.

3.2.4. Absorption and fluorescence spectral analysis

Absorption spectra were recorded on a Hewlett Packard 8453 diode array spectrophotometer in 10 mM borate buffer (pH 9.0) at 20°C. Spectrophotometer settings were controlled using the UV-Visible ChemStation software package (Hewlett Packard). Samples with concentrations of 2.4 μM EGFP or 2.4 μM mEGFP were measured free in buffered solution, as well as encapsulated at their preferred micellar composition (PMC).

Fluorescence excitation and emission spectra were measured using a Cary Eclipse spectrofluorimeter (Varian Inc.). Excitation and emission slits were set to yield bandwidths of 5 nm. All measurements were performed at 20°C. Samples with concentrations of 1 μM EGFP or 1 μM mEGFP were measured free in buffered solution and encapsulated at their respective PMCs.

For the pH-dependent measurements, a master buffer was used consisting of 20 mM sodium phosphate, 20 mM citric acid, 10 mM glycine, and 150 mM NaCl adjusted to the desired pH by additions of 1 M NaOH. Samples with concentrations of 1 μM EGFP or 1 μM mEGFP at pH 5.2, 7.1, 9.0, and 10.0 were measured.

3.2.5. Circular dichroism

Circular dichroism (CD) experiments were performed on a JASCO J-715 spectropolarimeter with a Jasco PTC 348 WI temperature controller set at 20°C. The far-UV CD spectra (195 - 260 nm) were obtained of samples in a 0.3 mL quartz cuvette with a path length of 1 mm. Thirty spectra, each recorded with a resolution of 1 nm, a scan speed of 50 nm/min and a response time of 1 s, were accumulated and averaged. The visible-near-UV CD spectra (300 - 600 nm) were obtained of samples in a 1 cm path length quartz cuvette with black side walls (volume 0.4 mL). Twenty spectra, each with a resolution of 1 nm, a scan speed of 50 nm/min and a response time of 1 s, were collected and averaged. The simultaneously collected high tension (HT) signal of the (m)EGFP chromophore was converted to absorbance using the Spectra Manager for Windows 95/NT Spectra Analysis (Version 1.53.02).

Far-UV CD spectra of 2.4 μM EGFP or 2.4 μM mEGFP were recorded free in buffered solution and encapsulated at their respective PMC. For the visible-near-UV CD spectra, samples of 10 μM EGFP or 10 μM mEGFP were measured free in buffered solution and encapsulated at their respective PMC. For the different experiments buffer blank spectra, obtained at identical conditions, were subtracted.

3.2.6. Time-resolved fluorescence anisotropy

Fluorescence anisotropy decay measurements were performed as described by Borst *et al.*²⁴ In short, fluorescence anisotropy decay measurements were carried out using a mode-lock continuous laser for excitation and time-correlated single photon counting (TCSPC) as detection technique. The mode-locked laser was a titanium:sapphire laser (Coherent Inc., model Mira 900-D in fs mode), tuned to 960 nm. A pulse picker was used (APE GmbH, model Pulse Select) for decreasing the repetition rate

of excitation pulses to 3.8×10^6 pulses per second. The output of the pulse picker was directed towards a frequency doubler (Inrad Inc., model 5-050, Ultrafast Harmonic Generation System). For excitation, maximum pulse energy was at sub-pJ level, with a pulse duration of about 0.2 ps at a wavelength of 480 nm. The fluorescence emission was detected at a wavelength of 512.2 ± 5 nm selected with a Schott interference filter. Samples were measured in 1 mL quartz cuvettes with a path length of 1 cm. The time-resolved fluorescence anisotropy (TRFA) Data Processing Package (Scientific Software Technologies Centre) was used for data analysis.²⁵

First, the total fluorescence decay was analyzed, which consists of a sum of discrete exponentials with lifetimes τ_i and amplitudes α_i . These parameters were retrieved from fitting the total fluorescence $I(t)$ ($I(t) = I_{\parallel}(t) + 2 I_{\perp}(t)$) to the function:

$$I(t) = E(t) \otimes \sum_{i=1}^N \alpha_i e^{-t/\tau_i} \quad (3.1)$$

$E(t)$ is the instrumental response function and \otimes denotes a convolution product. After obtaining the optimal time-resolved fluorescence decay function with major fluorescence lifetimes (τ_i) of (m)EGFP free in solution and encapsulated in C3Ms, the analysis of the TRFA could be carried out. The model function to which the experimental bi-exponential anisotropy decay of encapsulated (m)EGFP, $r(t)$, should be fitted is:

$$r(t) = \beta_1 \exp(-t/\phi_1) + \beta_2 \exp(-t/\phi_2) \quad (3.2)$$

ϕ_1 is a short correlation time arising from reversible energy transfer between the chromophores (this is called the transfer correlation time), ϕ_2 is the rotational correlation time of the micelle, and β_1 and β_2 are their respective amplitudes.

To investigate the effect of homo-FRET between (m)EGFP molecules, C3Ms with different ratios of (m)EGFP and SBFP2 were prepared. Samples containing 1 μM of total protein with different percentages of EGFP or mEGFP (varying from 10% up to 50%) and SBFP2 were encapsulated with P2MVP₄₁-*b*-PEO₂₀₅ at their respective PMCs. The (m)EGFP was selectively excited at 480 nm, because SBFP2 does not exhibit significant absorption at this wavelength.

3.3. Results

3.3.1. Spectral properties of encapsulated EGFP and mEGFP

Measurements on encapsulated proteins in C3Ms are commonly performed at the preferred micellar composition (PMC), which is the optimal ratio between protein and polymer for the formation of C3Ms.^{2,3} The PMC is expressed as $F^+ = [n_+]/([n_+] + [n_-])$ with $[n_+]$ and $[n_-]$ the total concentration of positively charged groups on the polymers and the net concentration of negative charges on the protein, respectively. To determine the PMC, DLS composition experiments were carried out for mEGFP with the diblock copolymer P2MVP₄₁-*b*-PEO₂₀₅ (see Section S3.2 and Figure S3.2A). The PMC for mEGFP was determined at an F^+ value of 0.70 ± 0.05 , with an average radius of 29.9 ± 0.3 nm for the C3Ms, which is in good agreement with the PMC found for EGFP ($F^+_{\text{EGFP}} = 0.65 \pm 0.03$).³

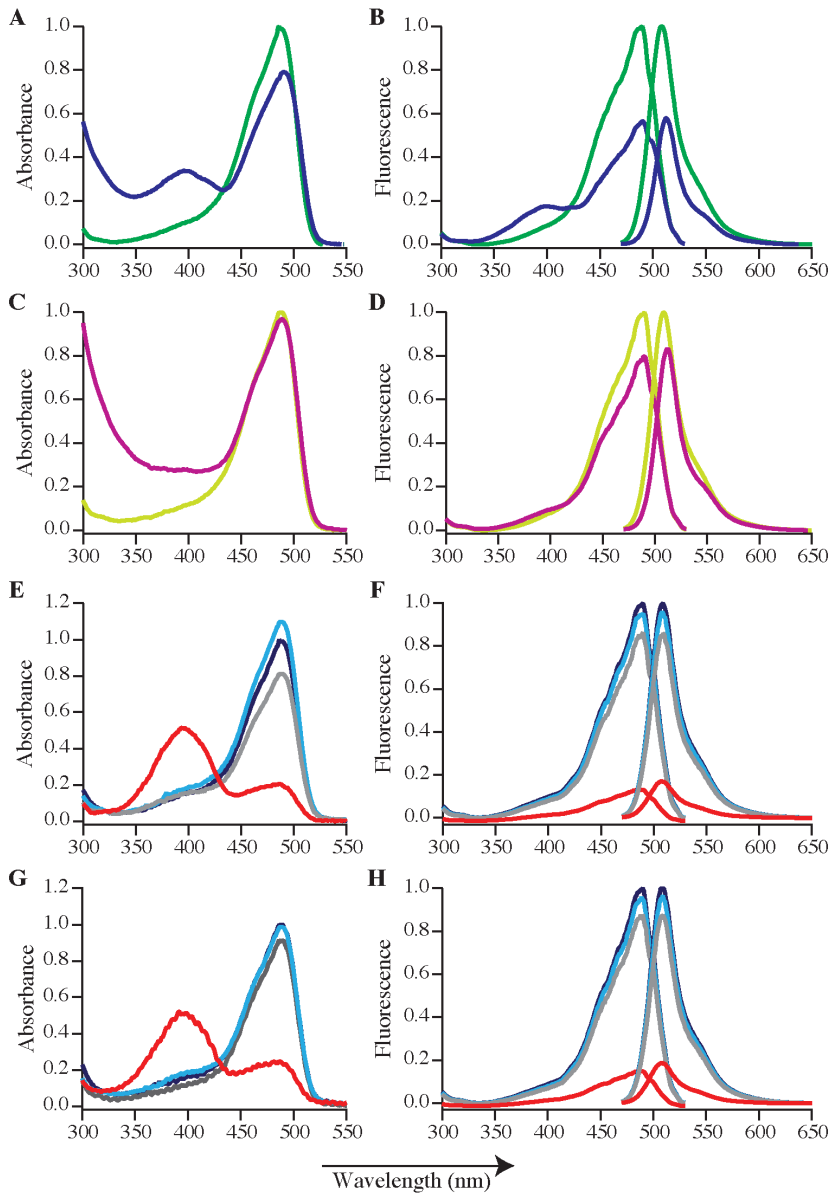


Figure 3.2. Spectral properties of EGFP and mEGFP free in solution and encapsulated in C₃Ms. (A) Absorption spectra and (B) fluorescence excitation and emission spectra of free (green lines) and encapsulated EGFP (blue lines). (C) Absorption spectra and (D) fluorescence excitation and emission spectra of free (green lines) and encapsulated mEGFP (purple lines). (E) Absorption spectra and (F) fluorescence excitation and emission spectra of EGFP in solution as a function of pH. (G) Absorption spectra and (H) fluorescence excitation and emission spectra of mEGFP in solution as a function of pH. For E to G the lines are colored according to: pH 10.0, dark blue; pH 9.0, light blue; pH 7.1, gray; and pH 5.2, red. Spectra are normalized to the spectra of (m)EGFP free in solution (A to D) and of (m)EGFP at pH 10.0 (E and F).

Next, we recorded absorption and fluorescence spectra of EGFP and mEGFP free in solution as well as encapsulated in C3Ms at their respective PMCs (Figure 3.2). Free EGFP and mEGFP displayed absorption and fluorescence excitation maxima at 490 nm and the corresponding fluorescence emission spectra showed maxima at 509 nm (Figures 3.2A to 3.2D). The absorption and fluorescence properties for encapsulated EGFP and mEGFP clearly deviated from those of the proteins free in solution. Encapsulated EGFP showed an additional absorption peak at 395 nm, which is in agreement with previous data³. The corresponding peak was much lower in the respective spectra of encapsulated mEGFP (Figures 3.2A and 3.2C). Upon excitation at 460 nm, the fluorescence emission spectra for both encapsulated proteins displayed a narrower and slightly shifted profile with a less intense maximum at 512 nm compared to that of both free proteins (Figures 3.2B and 3.2D). Moreover, excitation of encapsulated EGFP at 390 nm led to a strong fluorescence emission with a spectrum similar to the one recorded for 490 nm excitation (Figures 3.2B and S3.3).

To investigate the spectral properties of EGFP after release from C3Ms, we disintegrated the C3Ms by addition of NaCl (with a final concentration of 0.1 M). The resulting spectra of the released EGFP perfectly matched the spectra of EGFP free in solution (Figure S3.4), proving that the spectral changes, and therefore the structural adjustments, of EGFP as a result of encapsulation, are fully reversible. The absorption and excitation spectra of encapsulated EGFP showed an additional peak at 395 nm, which resembles the absorption peak at 395 nm of wtGFP and GFP S65T at low pH.^{7,16} This peak is attributed to protonation of the phenolate of Tyr66 in the chromophore. To investigate whether protonation of the chromophore can also take place in EGFP and mEGFP, pH titrations were performed on the free proteins (Figures 3.2E to 3.2H). Such titrations were not performed on encapsulated proteins, because the interactions in the C3Ms are electrostatically driven and responsive to pH due to the pH-dependent charges of the proteins. For EGFP and mEGFP, lowering the pH resulted in a decrease in fluorescence excitation and emission (Figures 3.2F and 3.2H). The absorption spectra of both proteins showed a decrease at 490 nm upon lowering of the pH, while at pH 5.2 an extra absorption peak at 395 nm was observed (Figures 3.2E and 3.2G), which is similar to GFP S65T at low pH.²⁶ This means that the chromophores of EGFP and mEGFP become protonated at lower pH values. The main difference between the free proteins at pH 5.2 and the encapsulated EGFP is that for encapsulated EGFP the absorption peak at 395 nm is also visible in the fluorescence excitation spectrum (Figure 3.2B). In other words, the protonated chromophore of free EGFP at pH 5.2 is non-fluorescent (Figures 3.2E and 3.2F), while for encapsulated EGFP absorption at 395 nm leads to a fluorescence signal (Figures 3.2A, 3.2B, and S3.3). In wtGFP, absorption at 395 nm also leads to fluorescence, so the chromophore in encapsulated EGFP should resemble wtGFP's chromophore and its environment rather than that of GFP S65T at low pH.^{16,27}

3.3.2. Structural characteristics of the β -barrel and the chromophore

The proposed protonation of the chromophore of encapsulated EGFP is not a result of a change in pH, because the bulk pH is kept constant at pH 9. Instead, protonation might result from a change in protein structure. To investigate whether (m)EGFP encapsulation affects its

secondary structure, circular dichroism (CD) experiments were performed. Figures 3.3A and 3.3B show the far-UV CD spectra of EGFP and mEGFP free in solution and encapsulated in C3Ms. For all cases, a negative mean residue ellipticity near 219 nm in the far-UV CD spectra was observed, which points to a high content of β -sheet in these proteins, in line with previous observations (Figure 3.1A).^{19,28} However, comparison of the CD spectra of (m)EGFP in solution with that of encapsulated proteins shows a different zero crossing, suggesting a change in the β -barrel structure of both proteins upon encapsulation.

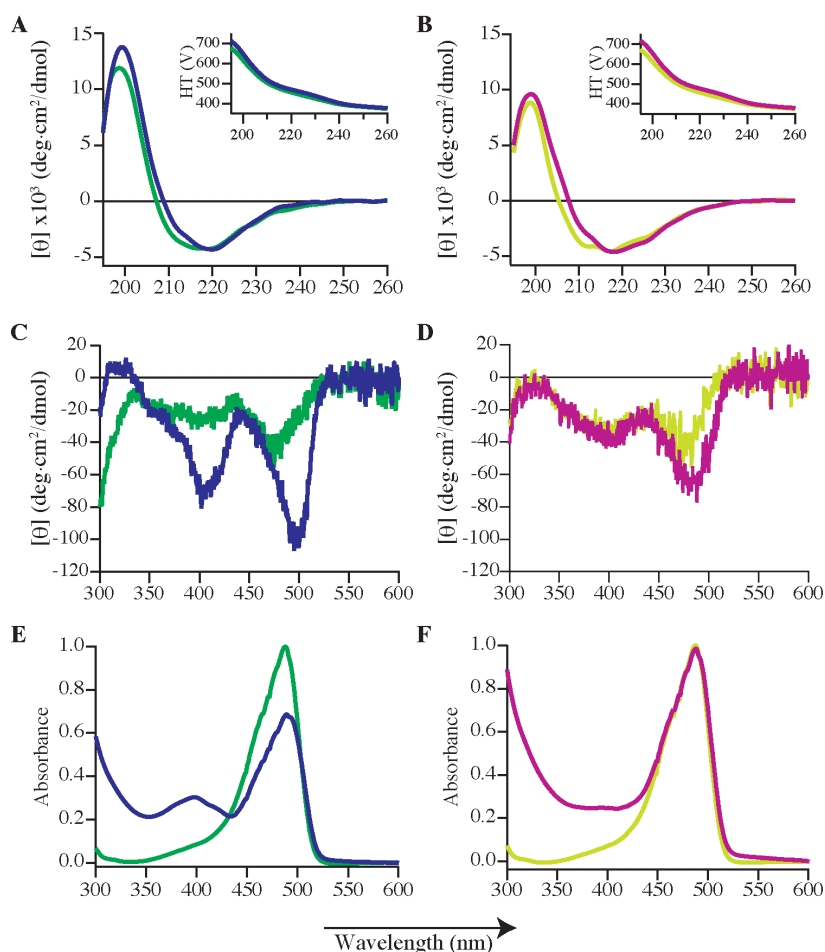


Figure 3.3. CD and absorption spectra of (m)EGFP free in solution (green lines) and (m)EGFP encapsulated in C3Ms (blue and purple lines). Far-UV CD spectra of (A) EGFP and (B) mEGFP, insets show the corresponding high tension (HT) signals. Visible-near-UV CD spectra of (C) EGFP and (D) mEGFP. Normalized absorption spectra (converted from the HT signal) of the visible-near-UV CD measurement of (E) EGFP and (F) mEGFP are shown (normalization was performed to the spectra of (m)EGFP free in solution).

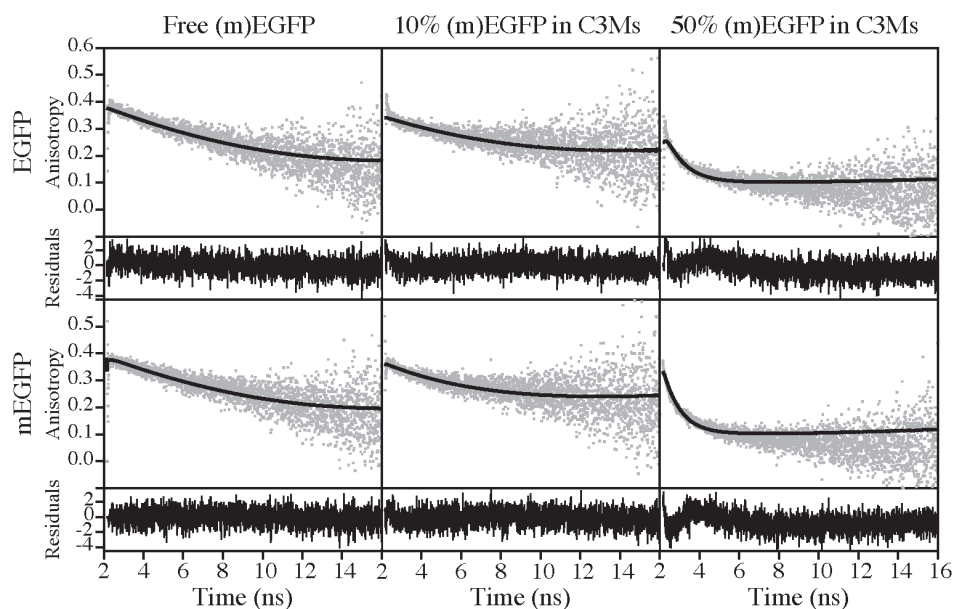


Figure 3.4. Experimental (gray dots) and fitted (black lines) fluorescence anisotropy decay curves of EGFP (top) and mEGFP (bottom), free in solution and of mixed (m)EGFP/SBFP2 C3Ms at 10% and 50%. The corresponding anisotropy parameters are listed in Table 3.1.

Table 3.1 Anisotropy decay parameters for free EGFP and mEGFP (rotational correlation times) and for C3Ms with different (m)EGFP/SBFP2 ratios (transfer correlation times). Values in parentheses are the 67% confidence limits.

Sample	β_1	ϕ_1 (ns)	β_{inf}
EGFP ^a	0.375 (0.375 - 0.380)	12.7 (12.6 - 12.9)	
10% EGFP in C3Ms	0.209 (0.200 - 0.211)	8.6 (7.6 - 14.4)	0.133 (0.132 - 0.133)
20% EGFP in C3Ms	0.192 (0.186 - 0.194)	3.6 (3.5 - 3.9)	0.127 (0.126 - 0.127)
30% EGFP in C3Ms	0.160 (0.156 - 0.163)	1.67 (1.58 - 1.83)	0.142 (0.142 - 0.143)
40% EGFP in C3Ms	0.180 (0.175 - 0.182)	1.23 (1.20 - 1.36)	0.114 (0.113 - 0.114)
50% EGFP in C3Ms	0.201 (0.198 - 0.206)	0.94 (0.87 - 0.97)	0.097 (0.096 - 0.097)
mEGFP ^a	0.384 (0.383 - 0.385)	13.5 (13.4 - 13.6)	
10% mEGFP in C3Ms	0.162 (0.152 - 0.173)	5.1 (4.4 - 5.8)	0.198 (0.198 - 0.199)
20% mEGFP in C3Ms	0.200 (0.192 - 0.200)	3.2 (3.2 - 3.7)	0.135 (0.133 - 0.135)
30% mEGFP in C3Ms	0.231 (0.192 - 0.232)	1.24 (1.18 - 1.25)	0.137 (0.132 - 0.137)
40% mEGFP in C3Ms	0.238 (0.213 - 0.238)	0.85 (0.84 - 1.21)	0.120 (0.118 - 0.121)
50% mEGFP in C3Ms	0.238 (0.238 - 0.251)	0.81 (0.80 - 1.03)	0.096 (0.094 - 0.097)

^avalues are obtained with Equation 3.2.

The orientational freedom of the proteins in the C3Ms can be revealed by recording the visible-near-UV CD spectra of the (m)EGFP chromophore. For both free and encapsulated proteins these spectra show two dichroic bands with a negative Cotton effect (Figures 3.3C and 3.3D). In all cases, these two dichroic bands coincide with the absorption bands (Figures 3.2E and 3.2G) of the protonated chromophore (state A: absorption 395 nm, CD ca. 397 nm) and the deprotonated chromophore (state B: absorption 488 nm, CD ca. 474 nm). In agreement with previous observations, the dichroic bands are visible only at high concentrations of the chromophore.²⁸ Although the absorption band arising from state A has hardly oscillator strength for both free proteins (Figures 3.3E and 3.3F), its rotational strength is significant (Figures 3.3C and 3.3D). For mEGFP, the rotational strength patterns of free and encapsulated protein are similar (Figure 3.3D). The rotational strength pattern for the encapsulated EGFP molecules, however, has evidently increased in magnitude and is slightly shifted compared to free EGFP (Figure 3.3C). Both states of the chromophore have an increased rotational strength for the encapsulated protein compared to the free EGFP, while this is not seen in the corresponding absorption spectra (Figure 3.3E). The change in rotational strength in the case of EGFP suggests less molecular orientational freedom of the chromophores upon encapsulation.

3.3.3. Quantitative analysis of homo-FRET in C3Ms

The above results suggest that encapsulation of (m)EGFP molecules brings them in close proximity, which might lead to excited-state energy transfer upon excitation, *i.e.*, Förster resonance energy transfer (FRET). If FRET occurs between identical fluorophores, it is referred to as homo-FRET.²⁹ We utilized time-resolved fluorescence anisotropy (TRFA) to determine energy transfer between packed (m)EGFP molecules in C3Ms. First, fluorescence lifetimes of (m)EGFP in solution and encapsulated in C3Ms were obtained. For EGFP and mEGFP in solution, fluorescence lifetimes of $\tau_f = 2.7$ and 2.6 ns were found, respectively. For both proteins, encapsulation resulted in a slight decrease of the fluorescence lifetimes: EGFP and mEGFP decreased to $\tau_f = 2.4$ and 2.3 ns, respectively.

TRFA can detect changes in the orientation of a fluorophore, reflecting the rotation of the molecule, which is characterized by a single rotational correlation time. For freely diffusing EGFP and mEGFP we obtained rotational correlation times of 12.7 and 13.5 ns, respectively, which is in good agreement with other studies.³⁰⁻³³ We used increasing ratios of (m)EGFP/SBFP2 in C3Ms to determine whether homo-FRET occurs between (m)EGFP molecules. The increasing probability of (m)EGFP molecules to get in close proximity of each other is expected to result in increased homo-FRET. SBFP2 was used as a dark (m)EGFP substitute, because this protein has a similar charge distribution as the (m)EGFP proteins, has a similar value for its PMC ($F_{SBFP2}^+ = 0.70 \pm 0.05$, Figure S3.2B) and does not absorb and emit light at the used wavelengths.

FCS and DLS revealed C3Ms with a hydrodynamic radius (R_h) of about 35 nm.³ Such a particle has a theoretical rotational correlation time, ϕ_2 in Equation 3.2, of 44 μ s, which is much longer than the detection window of 20 ns used in the current TRFA measurements.

Therefore, the second exponential term in Equation 3.2, reflecting overall micellar rotation, becomes equal to 1 and this equation then becomes:

$$r(t) = \beta_1 \exp(-t/\phi_1) + \beta_{\text{inf}} \quad (3.3)$$

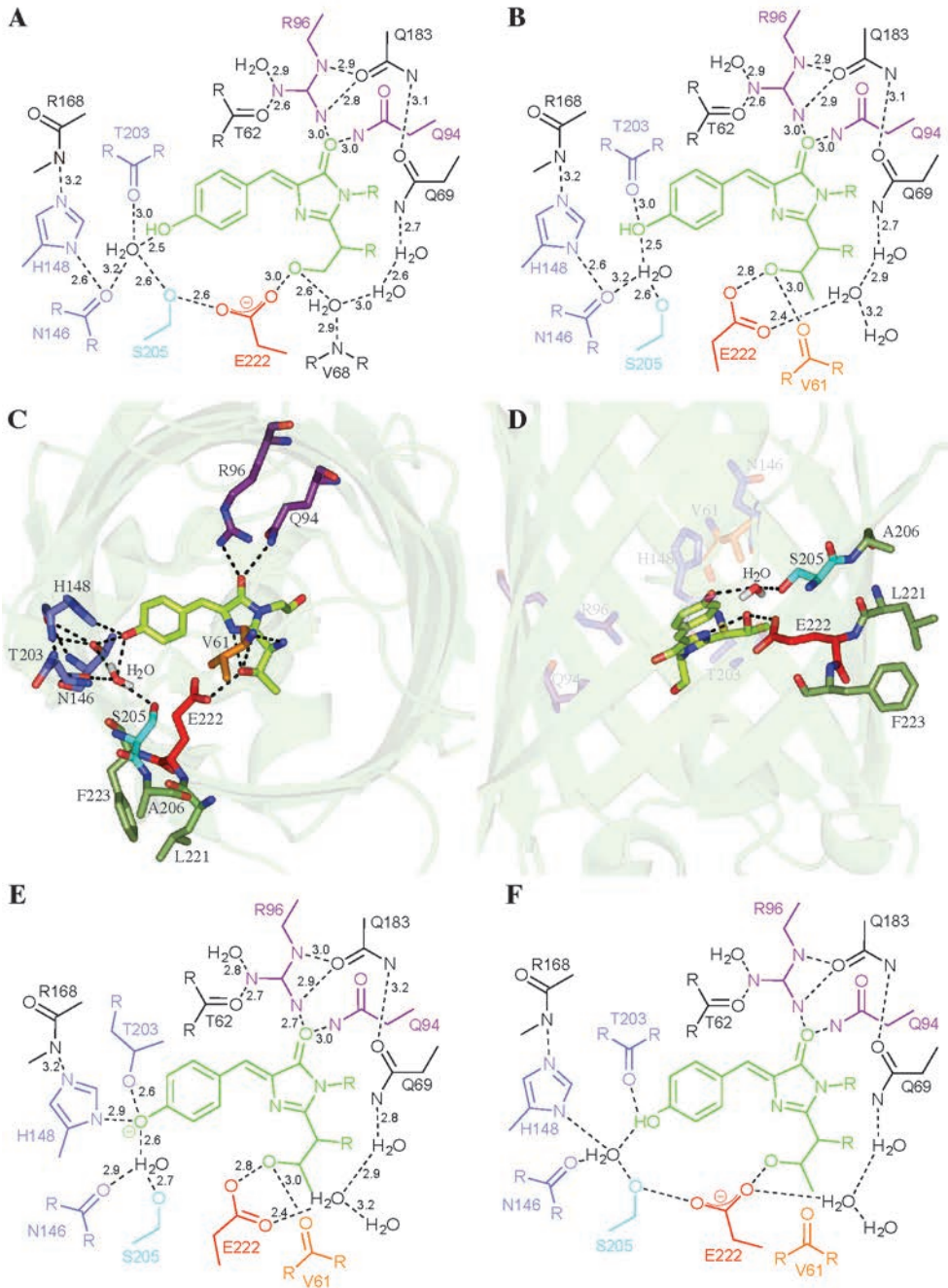
in which the amplitude β_2 has been replaced by the constant anisotropy term β_{inf} . The TRFA data of the encapsulated proteins were fitted to Equation 3.3 resulting in a transfer correlation time (ϕ_1) instead of a rotational correlation time. Experimental and fitted fluorescence anisotropy decay curves are presented in Figure 3.4 and the corresponding parameters are listed in Table 3.1. For both free proteins a clear one exponential curve is shown in Figure 3.4, which is evidently related to one rotational correlation time (Table 3.1). The samples with 10% (m)EGFP in C3Ms show a faster depolarization than both free proteins, but half of the signal is still present after 16 ns. However, for the samples with 50% (m)EGFP in C3Ms, most of the signal is already lost after 2 - 4 ns, which corresponds to a fast transfer correlation time (Table 3.1). So, encapsulation of the proteins with increasing ratios of (m)EGFP/SBFP2 resulted in decreased transfer correlation times (from approximately 8.6 to 0.8 ns). Interestingly, C3Ms with increasing mEGFP/SBFP2 ratios gave lower ϕ_1 values than similar C3Ms composed of EGFP/SBFP2, pointing at a larger distance between the EGFP moieties (dimers) than between the mEGFP moieties (monomers) that are involved in homo-FRET or at different distributions of encapsulated EGFP and mEGFP molecules.

3.4. Discussion

In this study, we encapsulated EGFP in C3Ms and showed that small perturbations of the protein structure cause spectral changes (Figures 3.2 and 3.3)³, which have been observed before with the self-assembly of EGFP-poly(*N*-isopropylacrylamide) conjugates.^{34,35} In both cases, tight packing of EGFP results in the appearance of a secondary absorbance peak at 395 nm. To better understand the molecular nature of this phenomenon, we compared the encapsulation of EGFP with its monomeric variant, mEGFP. This latter variant has the A206K mutation in the hydrophobic patch of EGFP, which significantly diminishes dimerization of mEGFP molecules.¹⁸

We show in Figures 3.2E and 3.2F that the chromophore of (m)EGFP can be protonated at pH 5.2, leading to an absorbance at 395 nm, which is a non-fluorescent species. Encapsulation of EGFP in C3Ms also shows an absorbance at 395 nm, but the protein still displays a clear

Figure 3.5 (next page). Schematic diagrams and crystal structures showing the immediate chromophore environment of (E)GFP variants. Chromophore environment of (A) wtGFP and (B) the S65T variant at pH 4.6. (C) Representation of the chromophore environment inside the β -barrel of EGFP to the three amino acid residues involved in dimerization. (D) Conformation of the three amino acid residues (A206, L221, and F223) involved in dimerization relative to the chromophore environment. (C) and (D) are based on PDB entry 4EUL.¹⁹ Schematic diagrams of (E) state B of the chromophore and its environment in EGFP and (F) the proposed state of the chromophore and its environment in encapsulated EGFP. For (A), (B), (E), and (F): proposed hydrogen bonds are shown with dashed lines; protonation state is assigned for the chromophore only, the rest of the hydrogens are not indicated; colors correspond with the structures shown in (C) and (D). The diagrams shown in (A), (B), and (E) are based on diagrams of Brejc²⁷ and Elsliger¹⁶.



fluorescence signal (Figures 3.2A, 3.2B, and S3.3). The absorbance and excitation peak at 395 nm is the primary peak observed in wtGFP.^{7,17,36} In wtGFP, excitation at 395 nm leads to an excited-state proton transfer (ESPT) from the hydroxyl group of Tyr66 to the connecting hydrogen bond network (Figure 3.5A), allowing fluorescence emission around 505 nm.³⁷ The critical proton acceptor for this ESPT has been suggested to be Glu222 on the basis of crystal structures and ¹³C NMR.^{15,27} The crystal structure of GFP S65T at pH 4.6 reveals a different orientation of Glu222 compared to wtGFP (Figure 3.5B).^{16,38} Through this reorientation of Glu222, the internal proton transfer network is interrupted, which leads to the non-fluorescent form of the protonated chromophore. Relating this to the encapsulated EGFP suggests that only protonation of the chromophore is not enough to explain the excitation peak at 395 nm and that also a reorientation of Glu222 should take place.

Reorientation of just an amino acid residue is not easily accomplished in EGFP, and therefore it is more likely that upon encapsulation a structural change occurs in the chromophore environment or the entire protein. With the far-UV CD spectra of encapsulated (m)EGFP a shifted zero crossing was observed (Figure 3.3A and 3.3B), pointing to a minor modification in the β -barrel of both protein variants. Next to that, the visible-near-UV CD spectrum of encapsulated EGFP showed a clear increase in magnitude for both dichroic bands compared to that of free EGFP (Figure 3.3C). This suggests that the chromophores of the EGFP molecules encapsulated in C3Ms have a restricted molecular orientational freedom, possibly caused by dimerization of the protein molecules. In contrast, the chromophores of encapsulated mEGFP show only minor differences in CD signal compared to that of free mEGFP (Figure 3.3D), suggesting that these protein molecules are randomly oriented.

Dimerization of EGFP might be stimulated by a high concentration of proteins in the C3Ms. Previously, we estimated the number of protein molecules per C3M to be about 450, while the micelles have a radius of 35 nm; this results in an EGFP concentration of about 5 - 10 mM.³ The dissociation constant (K_D) of EGFP is 0.11 mM, which would mean that 93% of the EGFP molecules are present as dimers in the C3Ms, under the assumption that the K_D of EGFP is similar in C3Ms as in solution (see Section S3.4).¹⁸ For mEGFP, the dissociation constant is much higher ($K_D = 74$ mM), which would imply that in the C3Ms only 18% of this protein variant is in the dimeric form.

The high concentration of (m)EGFP inside C3Ms was confirmed by the TRFA data reported in the present work, which showed tight packing of the proteins inside C3Ms. Free EGFP and mEGFP show rotational correlation times of 12.5 and 13.6 ns, respectively, whereas encapsulation of these proteins in C3Ms clearly led to lower transfer correlation times (superimposed on a constant anisotropy (β_{int})). The transfer correlation times can be explained by homo-FRET between (m)EGFP molecules in the micelles (Figure 3.4 and Table 3.1). However, EGFP dimers have a quite high orientation factor ($\kappa^2 = 1.86$, Section S3.5), which will not give rise to significant depolarization of fluorescence, thus EGFP homo-FRET within a dimer will not be observed with TRFA. Therefore, the observed transfer correlation time must arise from homo-FRET between EGFP dimers. The concentration of (m)EGFP moieties in the core of the C3Ms involved in homo-FRET

is lower for EGFP (mainly present as dimers) than for mEGFP (mainly monomers), so the average distance between dimers is larger than the distance between monomers. Since the transfer correlation time is related to the average distance between chromophores involved in FRET (Section S3.5), this explains the slightly slower depolarization observed for encapsulated EGFP than for encapsulated mEGFP (Table 3.1).

In summary, we conclude that the observed spectral changes (absorption, fluorescence and CD spectra) upon encapsulation of EGFP can be explained by the difference in the dimerization interface of EGFP and mEGFP. The dimerization interface of EGFP (Ala206, Leu221, and Phe223) is in direct contact with the chromophore environment (Figures 3.5C, 3.5D and 3.5E) and two of these surface residues are directly connected to Glu222 (Leu221 and Phe223, Figure 3.5D). We propose that dimerization of EGFP in C3Ms causes a conformational change of Glu222, resulting in stabilization of the protonated form of the chromophore. The proton of the phenolic moiety of Tyr66 is accepted by the carboxylate of Glu222 through an internal proton transfer network in state A in encapsulated EGFP (Figure 3.5F), just like in wtGFP (Figure 3.5A).³⁹ In addition, it is proposed that the configuration of Thr203 is different in the A and B states of EGFP.²⁷ In the B state, the hydroxyl group of Thr203 points towards the chromophore (Figure 3.5E), stabilizing the phenolate status of Tyr66, which is not the case in state A, where the side chain of Thr203 is flipped (Figure 3.5B). With the stabilization of the protonated chromophore and the presence of the internal proton transfer network, ESPT can take place, which results in a decrease in absorption at 490 nm and an increase in absorption at 395 nm.

Micelles composed of polyelectrolyte complexes are very promising structures for protein protection, stabilization, sustained biological activity and controlled delivery. They are spontaneously formed by mixing protein solutions with oppositely charged diblock copolymer solutions and are small enough to remain in solution. The PEO corona shields protein molecules from the bulk solution while protein structure and functionality are preserved and any immune response is reduced. The core of C3Ms has a high loading capacity: hundreds of protein molecules can be incorporated into one micelle.³ This high loading capacity is beneficial if administrated for controlled delivery, because it reduces the quantity of micelles required. Furthermore, the core of C3Ms provides a relatively water-rich environment.⁴⁰ This leads to easy diffusion of small molecular substrates and cofactors to the core of the micelles, which makes C3Ms a nano-reactor if enzymes are encapsulated. Small changes in protein structure, as we observed for encapsulated EGFP, may be the cause for the observed changes in the activity of certain enzymes; for lipase and lysozyme for example, an increase in activity upon encapsulation has been found.^{41,42} For controlled delivery, however, such local structural changes are probably not relevant, since our measurements show that the effects of encapsulation on the structure of EGFP are completely reversible.

Finally, it is worthy to note that C3Ms are of interest for potential applications in protein design. Generating dynamic nanocontainers, with high protein load, can be used to investigate the folding and interaction properties of a wide range of engineered proteins.

3.5. Conclusion

By comparison of the encapsulation of EGFP and mEGFP in C3Ms, we elucidated the origin of the spectral changes, which were previously observed for encapsulated EGFP. Making use of homo-FRET measurements, we confirmed tight packing of EGFP and mEGFP in C3Ms. Due to a strongly different association tendency, EGFP dimerizes in the micelles, whereas mEGFP mainly remains a monomer. Dimerization of EGFP results in a preferred stacking of the protein molecules, perturbing the local chromophore environment. This perturbation results in a pK_a shift, which we propose is caused by a reorientation of Glu222. Due to the pK_a shift, the absorption and excitation spectra of encapsulated EGFP show an additional band at 395 nm, which disappears after the release of EGFP from the C3Ms by increasing the ionic strength. This research shows that tight packing of proteins in polyelectrolyte micelles can lead to local structural changes, which might cause a disturbance of the bioactivity or functionality if enzymes or proteins are encapsulated. However, in the case of EGFP these changes proved to be fully reversible.

Acknowledgments

We thank Dr. Joachim Goedhart (University of Amsterdam, Amsterdam, The Netherlands) for providing us with pRSETb vectors containing mEGFP and SBFP2 and Dr. Arjen Bader (Wageningen University & Research, Wageningen, The Netherlands) for technical assistance. Financial support from The Graduate School VLAG (Wageningen, The Netherlands) is gratefully acknowledged.

References

1. Voets, I. K.; de Keizer, A.; Cohen Stuart, M. A., Complex coacervate core micelles. *Adv. Colloid Interface Sci.* **2009**, 147-148, 300-318.
2. Lindhoud, S.; Norde, W.; Cohen Stuart, M. A., Reversibility and relaxation behavior of polyelectrolyte complex micelle formation. *J. Phys. Chem. B* **2009**, 113, (16), 5431-5439.
3. Nolles, A.; Westphal, A. H.; de Hoop, J. A.; Fokkink, R. G.; Kleijn, J. M.; van Berkel, W. J. H.; Borst, J. W., Encapsulation of GFP in complex coacervate core micelles. *Biomacromolecules* **2015**, 16, (5), 1542-1549.
4. Blocher, W. C.; Perry, S. L., Complex coacervate-based materials for biomedicine. *WIREs Nanomed. Nanobiotechnol.* **2017**, 9, (4).
5. Harada, A.; Kataoka, K., Supramolecular assemblies of block copolymers in aqueous media as nanocontainers relevant to biological applications. *Prog. Polym. Sci.* **2006**, 31, (11), 949-982.
6. Minten, I. J.; Nolte, R. J. M.; Cornelissen, J. J. L. M., Complex assembly behavior during the encapsulation of green fluorescent protein analogs in virus derived protein capsules. *Macromol. Biosci.* **2010**, 10, (5), 539-545.
7. Tsien, R. Y., The green fluorescent protein. *Annu. Rev. Biochem.* **1998**, 67, 509-544.
8. Zimmer, M., Green fluorescent protein (GFP): applications, structure, and related photophysical behavior. *Chem. Rev.* **2002**, 102, (3), 759-781.
9. Lippincott-Schwartz, J.; Patterson, G. H., Development and use of fluorescent protein markers in living cells. *Science* **2003**, 300, (5616), 87-91.
10. Bücherl, C. A.; Bader, A.; Westphal, A. H.; Lapternok, S. P.; Borst, J. W., FRET-FLIM applications in plant systems. *Protoplasma* **2014**, 251, (2), 383-394.
11. Hoffman, R. M., Use of fluorescent proteins and color-coded imaging to visualize cancer cells with different genetic properties. *Cancer Metastasis Rev.* **2016**, 35, (1), 5-19.
12. Yang, F.; Moss, L. G.; Phillips, G. N. J., The molecular structure of green fluorescent protein. *Nat. Biotechnol.* **1996**, 14, (10), 1246-1251.
13. Ormö, M.; Cubitt, A. B.; Kallio, K.; Gross, L. A.; Tsien, R. Y.; Remington, S. J., Crystal structure of the *Aequorea victoria* green fluorescent protein. *Science* **1996**, 273, (5280), 1392-1395.
14. Cody, C. W.; Prasher, D. C.; Westler, W. M.; Prendergast, F. G.; Ward, W. W., Chemical structure of the hexapeptide chromophore of the *Aequorea* green-fluorescent protein. *Biochemistry* **1993**, 32, (5), 1212-1218.
15. Oltrogge, L. M.; Wang, Q.; Boxer, S. G., Ground-state proton transfer kinetics in green fluorescent protein. *Biochemistry* **2014**, 53, (37), 5947-5957.
16. Elsliger, M. A.; Wachter, R. M.; Hanson, G. T.; Kallio, K.; Remington, S. J., Structural and spectral response of green fluorescent protein variants to changes in pH. *Biochemistry* **1999**, 38, (17), 5296-5301.
17. Ward, W. W.; Prentice, H. J.; Roth, A. F.; Cody, C. W.; Reeves, S. C., Spectral perturbations of the *Aequorea* green-fluorescent protein. *Photochem. Photobiol.* **1982**, 35, (6), 803-808.
18. Zacharias, D. A.; Violin, J. D.; Newton, A. C.; Tsien, R. Y., Partitioning of lipid-modified monomeric GFPs into membrane microdomains of live cells. *Science* **2002**, 296, (5569), 913-916.
19. Arpino, J. A.; Rizkallah, P. J.; Jones, D. D., Crystal structure of enhanced green fluorescent protein to 1.35 Å resolution reveals alternative conformations for Glu222. *PLoS One* **2012**, 7, (10), e47132.
20. Chong, S.; Mersha, F. B.; Comb, D. G.; Scott, M. E.; Landry, D.; Vence, L. M.; Perler, F. B.; Benner, J.; Kucera, R. B.; Hirvonen, C. A.; Pelletier, J. J.; Paulus, H.; Xu, M. Q., Single-column purification of free recombinant proteins using a self-cleavable affinity tag derived from a protein splicing element. *Gene* **1997**, 192, (2), 271-281.
21. Evans, T. C., Jr.; Xu, M. Q., Intein-mediated protein ligation: harnessing nature's escape artists. *Biopolymers* **1999**, 51, (5), 333-342.
22. Xu, M. Q.; Paulus, H.; Chong, S., Fusions to self-splicing inteins for protein purification. *Methods Enzymol.* **2000**, 326, 376-418.
23. Kremers, G. J.; Goedhart, J.; van den Heuvel, D. J.; Gerritsen, H. C.; Gadella, T. W. J., Improved green and blue fluorescent proteins for expression in bacteria and mammalian cells. *Biochemistry* **2007**, 46, (12), 3775-3783.
24. Borst, J. W.; Hink, M. A.; van Hoek, A.; Visser, A. J. W. G., Effects of refractive index and viscosity on fluorescence and anisotropy decays of enhanced cyan and yellow fluorescent proteins. *J. Fluoresc.* **2005**, 15, (2), 153-160.
25. Digris, A. V.; Novikov, E. G.; Skakun, V. V.; Apanasovich, V. V., Global analysis of time-resolved fluorescence data. *Methods Mol. Biol.* **2014**, 1076, 257-277.

26. Kneen, M.; Farinas, J.; Li, Y.; Verkman, A. S., Green fluorescent protein as a noninvasive intracellular pH indicator. *Biophys. J.* **1998**, *74*, (3), 1591-1599.
27. Brejc, K.; Sixma, T. K.; Kitts, P. A.; Kain, S. R.; Tsien, R. Y.; Ormö, M.; Remington, S. J., Structural basis for dual excitation and photoisomerization of the *Aequorea victoria* green fluorescent protein. *Proc. Natl. Acad. Sci. U. S. A.* **1997**, *94*, (6), 2306-2311.
28. Visser, N. V.; Hink, M. A.; Borst, J. W.; van der Krogt, G. N. M.; Visser, A. J. W. G., Circular dichroism spectroscopy of fluorescent proteins. *FEBS Lett.* **2002**, *521*, (1-3), 31-35.
29. Vogel, S. S.; Thaler, C.; Blank, P. S.; Koushik, S. V., Time resolved fluorescence anisotropy. *FLIM Microsc. Biol. Med.* **2009**, *1*, 245-288.
30. Hink, M. A.; Griep, R. A.; Borst, J. W.; van Hoek, A.; Eppink, M. H. M.; Schots, A.; Visser, A. J. W. G., Structural dynamics of green fluorescent protein alone and fused with a single chain Fv protein. *J. Biol. Chem.* **2000**, *275*, (23), 17556-17560.
31. Suhlring, K.; Davis, D. M.; Phillips, D., The influence of solvent viscosity on the fluorescence decay and time-resolved anisotropy of green fluorescent protein. *J. Fluoresc.* **2002**, *12*, (1), 91-95.
32. Borst, J. W.; Visser, A. J. W. G., Fluorescence lifetime imaging microscopy in life sciences. *Meas. Sci. Technol.* **2010**, *21*, (10), 102002.
33. Visser, A. J. W. G.; Westphal, A. H.; Skakun, V. V.; Borst, J. W., GFP as potential cellular viscosimeter. *Methods Appl. Fluoresc.* **2016**, *4*, (3), 035002.
34. Lam, C. N.; Kim, M.; Thomas, C. S.; Chang, D.; Sanoja, G. E.; Okwara, C. U.; Olsen, B. D., The nature of protein interactions governing globular protein-polymer block copolymer self-assembly. *Biomacromolecules* **2014**, *15*, (4), 1248-1258.
35. Lam, C. N.; Yao, H.; Olsen, B. D., The effect of protein electrostatic interactions on globular protein-polymer block copolymer self-assembly. *Biomacromolecules* **2016**, *17*, (9), 2820-2829.
36. Haupts, U.; Maiti, S.; Schwille, P.; Webb, W. W., Dynamics of fluorescence fluctuations in green fluorescent protein observed by fluorescence correlation spectroscopy. *Proc. Natl. Acad. Sci. U. S. A.* **1998**, *95*, (23), 13573-13578.
37. Chattoraj, M.; King, B. A.; Bublitz, G. U.; Boxer, S. G., Ultra-fast excited state dynamics in green fluorescent protein: multiple states and proton transfer. *Proc. Natl. Acad. Sci. U. S. A.* **1996**, *93*, (16), 8362-8367.
38. Stoner-Ma, D.; Jaye, A. A.; Matousek, P.; Towrie, M.; Meech, S. R.; Tonge, P. J., Observation of excited-state proton transfer in green fluorescent protein using ultrafast vibrational spectroscopy. *J. Am. Chem. Soc.* **2005**, *127*, (9), 2864-2865.
39. Nifosi, R.; Tozzini, V., Molecular dynamics simulations of enhanced green fluorescent proteins: effects of F64L, S65T and T203Y mutations on the ground-state proton equilibria. *Proteins* **2003**, *51*, (3), 378-389.
40. Lindhoud, S.; de Vries, R.; Schweins, R.; Cohen Stuart, M. A.; Norde, W., Salt-induced release of lipase from polyelectrolyte complex micelles. *Soft Matter* **2009**, *5*, (1), 242-250.
41. Lindhoud, S.; Norde, W.; Cohen Stuart, M. A., Effects of polyelectrolyte complex micelles and their components on the enzymatic activity of lipase. *Langmuir* **2010**, *26*, (12), 9802-9808.
42. Harada, A.; Kataoka, K., Pronounced activity of enzymes through the incorporation into the core of polyion complex micelles made from charged block copolymers. *J. Control. Release* **2001**, *72*, (1-3), 85-91.
43. Rostkowski, M.; Olsson, M. H. M.; Sondergaard, C. R.; Jensen, J. H., Graphical analysis of pH-dependent properties of proteins predicted using PROPKA. *BMC Struct. Biol.* **2011**, *11*, 6.
44. Olsson, M. H.; Sondergaard, C. R.; Rostkowski, M.; Jensen, J. H., PROPKA3: Consistent treatment of internal and surface residues in empirical pKa predictions. *J. Chem. Theory Comput.* **2011**, *7*, (2), 525-537.
45. Provencher, S. W., Contin - a general-purpose constrained regularization program for inverting noisy linear algebraic and integral-equations. *Comput. Phys. Commun.* **1982**, *27*, (3), 229-242.
46. Suhlring, K.; Siegel, J.; Phillips, D.; French, P. M. W.; Lévêque-Fort, S.; Webb, S. E. D.; Davis, D. M., Imaging the environment of green fluorescent protein. *Biophys. J.* **2002**, *83*, (6), 3589-3595.
47. Suhlring, K.; Davis, D. M.; Petrasek, Z.; Siegel, J.; Phillips, D., Influence of the refractive index on EGFP fluorescence lifetimes in mixtures of water and glycerol. *Proc. S. P. I. E.* **2001**, *4259*, 92-101.
48. Malikova, N. P.; Visser, N. V.; van Hoek, A.; Skakun, V. V.; Vysotski, E. S.; Lee, J.; Visser, A. J. W. G., Green-fluorescent protein from the bioluminescent jellyfish *Clytia gregharia* is an obligate dimer and does not form a stable complex with the Ca(2+)-discharged photoprotein clytin. *Biochemistry* **2011**, *50*, (20), 4232-4241.
49. Steinberg, I. Z., Long-range nonradiative transfer of electronic excitation energy in proteins and polypeptides. *Annu. Rev. Biochem.* **1971**, *40*, 83-114.

50. Pletneva, N. V.; Pletnev, S. V.; Bogdanov, A. M.; Goryacheva, E. A.; Artemyev, I. V.; Suslova, E. A.; Arkhipova, S. F.; Pletnev, V. Z., Spatial structure of dimeric a genetically engineered variant of green fluorescent protein EGFP-K162Q in the P6(1) crystal space group. *Russ. J. Bioorg. Chem.* **2014**, 40, (4), 383-389.
51. Ansbacher, T.; Srivastava, H. K.; Stein, T.; Baer, R.; Merx, M.; Shurki, A., Calculation of transition dipole moment in fluorescent proteins-towards efficient energy transfer. *Phys. Chem. Chem. Phys.* **2012**, 14, (12), 4109-4117.

Supplementary information

S3.1. Ribbon diagram of the structure of wtGFP dimer

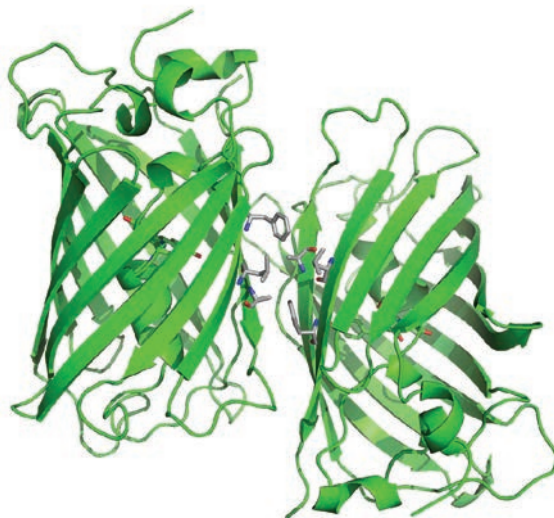


Figure S3.1. Ribbon diagram of the structure of wtGFP dimer. The side chains of the hydrophobic residues that are involved in dimerization (Ala206, Leu221, Phe223) are shown in gray. Cartoon based on the crystal structure of the wtGFP dimer (PDB entry 1GFL).¹²

S3.2. PMC determination of mEGFP and SBFP2

Dynamic light scattering (DLS) measurements were performed on an ALV instrument equipped with a 300 mW Cobolt Samba-300 DPSS laser operating at 660 nm and 100 mW, and static and dynamic enhancer fiber optics for an ALV/HIGH QE APD single photon detector connected to an ALV5000/60X0 External Correlator (ALV-Laser Vertriebsgesellschaft m-b.H.). The detection angle, θ , was set at 90° . For determination of the preferred micellar composition (PMC), 500 μL solutions with different polymer/protein compositions were prepared. The protein concentration was kept constant at 1 μM for each composition and the amount of P2MVP₄₁-*b*-PEO₂₀₅ was varied to obtain the desired values of F^{T+} : $F^{T+} = [n_+]/([n_+] + [n_-])$ where $[n_+] = c_+ N_+$ refers to the total concentration of positively charged groups on the polymer and $[n_-] = c_- N_-$ refers to the total concentration of negatively charged groups on the protein molecules. The number of charged groups on the diblock copolymer (N_+) taking the degree of quaternization into account, is +33.1 for P2MVP₄₁-*b*-PEO₂₀₅, which is used to calculate $[n_+]$. The net charge of the proteins as a function of pH was calculated using the software package PROPKA 3.1.^{43,44} The charge of the native proteins at pH 9 (N_-) is -9.87 for mEGFP and -8.96 for SBFP2, which are used to calculate $[n_-]$.

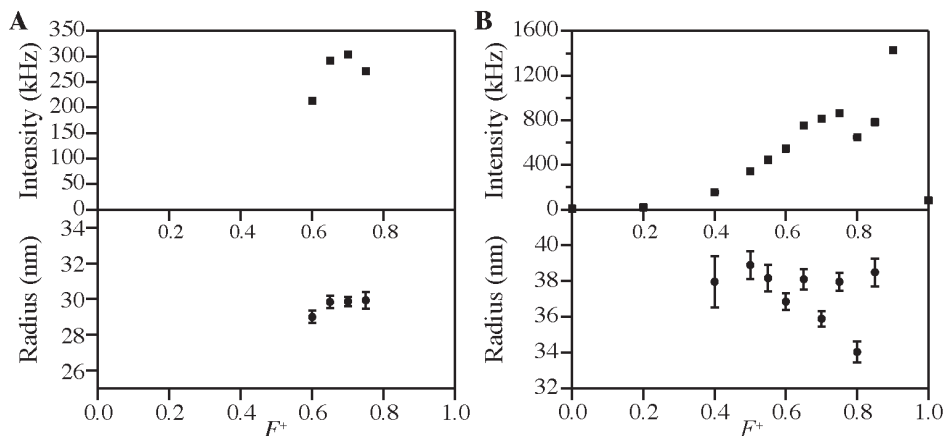


Figure S3.2 DLS composition experiments to determine the PMC of mEGFP and SBFP2 with P2MVP₄₁-*b*-PEO₂₀₅. Scattered intensity *versus* composition and hydrodynamic radius *versus* composition of (A) mEGFP with P2MVP₄₁-*b*-PEO₂₀₅ and (B) SBFP2 with P2MVP₄₁-*b*-PEO₂₀₅. Error bars show the standard deviation of ten scans of one experiment.

DLS autocorrelation curves were generated from 10 individual intensity traces and averaged. The inverse Laplace transformation of the average $G_2(\tau) \left(G_2(\tau) = \langle I(t) \times I(t+\tau) \rangle / \langle I(t) \rangle^2 \right)$ performed by CONTIN software (AfterALV 1.0d, Dullware Inc.), was used to analyze the size distributions of the samples of encapsulated mEGFP and SBFP2 (Figure S3.2).^{3,45}

S3.3. Additional spectral analysis of EGFP

Excitation and emission spectra of 1 μ M EGFP free in solution and encapsulated in C3Ms at its PMC were measured using a Cary Eclipse spectrofluorimeter (Varian Inc.). All measurements were performed at 20°C. To measure the fluorescence of state A of the encapsulated EGFP's chromophore, the two samples were excited at 390 nm and their emission spectra were recorded from 400 to 650 nm (Figure S3.3).

To see whether the fluorescence properties of EGFP remain the same before and after encapsulation, we measured the two samples before and after addition of NaCl (after 1 hour) with a final concentration of 0.1 M (Figure S3.4), with the NaCl concentration to be high enough to disintegrate the C3Ms.

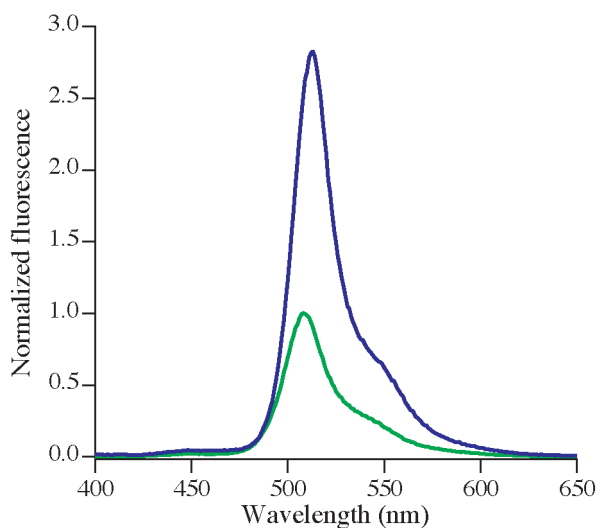


Figure S3.3. Normalized emission spectra of EGFP in solution (green curves) and of EGFP encapsulated in C3Ms (blue curves) after excitation at 390 nm. Spectra are normalized to the spectra of EGFP in solution.

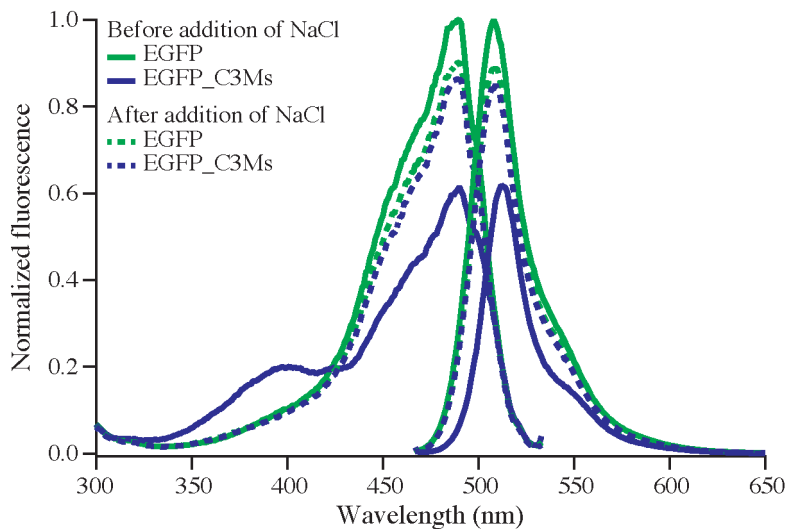


Figure S3.4. Normalized excitation and emission spectra of EGFP in solution (green curves) and of EGFP encapsulated in C3Ms (blue curves) before (solid line) and after (dotted line) addition of NaCl with a final concentration of 0.1 M. Spectra are normalized to the spectra of EGFP free in solution before addition of NaCl.

S3.4. Calculation of the percentage of (m)EGFP dimers present in C3Ms

The dissociation constant (K_D) of EGFP is 0.11 mM and of mEGFP is 74 mM.¹⁸ The dissociation/association equilibrium between dimer (D) and monomers (M) is:



The corresponding equation for the dissociation constant is:

$$K_D = \frac{[M]^2}{[D]} \quad (\text{S3.2})$$

The concentration of EGFP monomers ($[M]$) and dimers ($[D]$) is related to the total concentration (m)EGFP molecules in C3Ms ($[(m)EGFP]_{total}$) according to:

$$[(m)EGFP]_{total} = [M] + 2[D] \quad (\text{S3.3})$$

Substituting Equation S3.3 into Equation S3.2 yields a quadratic equation. One of the solutions of that equation relates to the dimer concentration:

$$[D] = \frac{\left(\frac{1}{4}K_D + [(m)EGFP]_{total} \right) - \sqrt{\left(\frac{1}{4}K_D + [(m)EGFP]_{total} \right)^2 - [(m)EGFP]_{total}^2}}{2} \quad (\text{S3.4})$$

Considering a $[(m)EGFP]_{total}$ of 10 mM and the above-mentioned K_D values, this results in an EGFP dimer percentage of 93% and an mEGFP dimer percentage of 18%.

S3.5. Obtaining geometric information on the (m)EGFP molecules in C3Ms

We observed a minor decrease of the fluorescence lifetime of (m)EGFP upon encapsulation in C3Ms, which can be due to an increase of the local refractive index of the medium (n), because the refractive index squared is inversely proportional to the fluorescence lifetime of a fluorescent dye ($n^2 \propto \tau_f^{-1}$).^{46,47} The decrease in τ_f permits us to determine the refractive index of the protein-filled micelle as compared to the refractive index of water (1.33) and accounts to 1.41. However, as pointed out by Suhling and co-workers (2002)⁴⁶, it is a long-range method with a cut-off distance (at which the radiative rate constant becomes insensitive to refractive index) of about 4 μm for (m)EGFP. This would imply that not only the micellar interior, but also the micellar expanse and surrounding buffer would contribute to the refractive index. For further calculations, we will use $n = 1.41$, because this is the only indication we have for the refractive index in the C3Ms.

Table S3.1. Transfer rate constants and distances between (m)EGFP chromophores in C3Ms with different (m)EGFP/SBFP2 ratios. For the calculation of these parameters, we used a $\kappa^2 = 0.476$, $\Phi_0 = 0.60$, $n = 1.41$ and $J = 1.01 \times 10^{15} \text{ nm}^4 \text{ M}^{-1} \text{ cm}^{-1}$ resulting in a $R_0 = 43 \text{ \AA}$. Values in parentheses are the distances between EGFP dimers, calculated with $J = 2.03 \times 10^{15} \text{ nm}^4 \text{ M}^{-1} \text{ cm}^{-1}$ resulting in $R_0 = 48 \text{ \AA}$.

Sample	k_t (ns ⁻¹)	R (Å)
10% EGFP in C3Ms	0.06	60 (67)
20% EGFP in C3Ms	0.14	52 (58)
30% EGFP in C3Ms	0.30	46 (51)
40% EGFP in C3Ms	0.41	43 (49)
50% EGFP in C3Ms	0.53	41 (46)
10% mEGFP in C3Ms	0.10	55
20% mEGFP in C3Ms	0.16	51
30% mEGFP in C3Ms	0.40	44
40% mEGFP in C3Ms	0.59	41
50% mEGFP in C3Ms	0.62	41

The transfer correlation times, ϕ_1 , for the different ratios (m)EGFP/SBFP2 were obtained from the TRFA data and listed in Table 3.1. In case of homo-FRET the transfer correlation time, ϕ_1 , is the reciprocal of twice the transfer rate constant, k_t , or:

$$\phi_1 = \frac{1}{2k_t} \quad (\text{S3.5})$$

in which the factor of 2 indicates the reversibility of the FRET process. The transfer rate constants are collected in Table S3.1. The transfer rate constant, k_t , becomes larger at increasing concentrations of (m)EGFP in C3Ms. Since k_t is proportional to the FRET efficiency, encapsulated mEGFP might give more efficient homo-FRET than encapsulated EGFP.

Geometric information on the (m)EGFP molecules in C3Ms can be obtained from the transfer rate constant and the Förster equation:^{32,48}

$$k_t = \frac{1}{\tau_f} \left(\frac{R_0}{R} \right)^6 \quad (\text{S3.6})$$

where τ_f is the fluorescence lifetime of the donor without acceptor (2.4 ns for EGFP and 2.3 ns for mEGFP), R is the actual distance between donor and acceptor, and R_0 is the critical transfer distance or Förster distance. R_0 (in Å) can be obtained via the Förster equation (Equation S3.6), which requires knowledge about the orientation factor κ^2 , the quantum yield of donor fluorescence (without acceptor) Φ_0 , the refractive index n of the involved medium,

and the spectral overlap integral J :

$$R_0 = 0.2108(\kappa^2 \Phi_0 n^{-4} J)^{1/6} \quad (\text{S3.7})$$

In this case, we used a refractive index of $n = 1.41$, which is the best approximation for the environment of the EGFP molecules in the C3Ms. The solution in the C3Ms is more viscous than water and a corresponding orientation factor for randomized static transition dipoles should be used: $\kappa^2 = 0.476$.⁴⁹ Using these parameters, we calculated the Förster distance for a (m)EGFP FRET pair: $R_0 = 43 \text{ \AA}$ (Equation S3.7). Now it is possible to determine the average distance, R , between the chromophores of separate (m)EGFP molecules in C3Ms by using Equation S3.6; these calculated average distances are listed in Table S3.1. In line with the expectation, for increasing ratios (m)EGFP/SBFP2 shorter average distances between the (m)EGFP chromophores are found.

From the differences in the visible-near-UV CD spectra of EGFP free in solution and encapsulated in C3Ms, we conclude that the EGFP molecules are not randomly oriented, but probably form dimers in C3Ms. In that case, the Förster radius is different. Assuming that the dimerization in C3Ms takes place in a similar way as in the crystal structure, we can obtain the initial orientation factor from the structure of dimeric EGFP from *Aequorea victoria* (PDB entry 4N3D)⁵⁰ and the transition dipole moments for the EGFP chromophore.⁵¹ The orientation factor is quite high: $\kappa^2 = 1.86$ (Figure S3.5). The nearly parallel transition dipole moments would not lead to significant depolarization of fluorescence, thus EGFP homo-FRET will not be observed with TRFA. Depolarization of fluorescence with a specific transfer correlation time must then arise from homo-FRET between EGFP dimers. In a dimer, one EGFP molecule acts as donor and in the excited state it “sees” another dimer in close proximity consisting of two acceptors, making the effective molar extinction coefficient (and thus spectral overlap integral J) twice as large. The parameters in Equation S3.7 that remain the same are the refractive index ($n = 1.41$), the quantum yield Φ_0 and a random orientation factor $\kappa^2 = 0.476$. Taking the before mentioned changes into account, the Förster radius between two dimers would increase to 48 \AA . The average distance between the chromophores of two different dimers (they are proportional to R_0) are listed in Table S3.1 (values between parentheses).

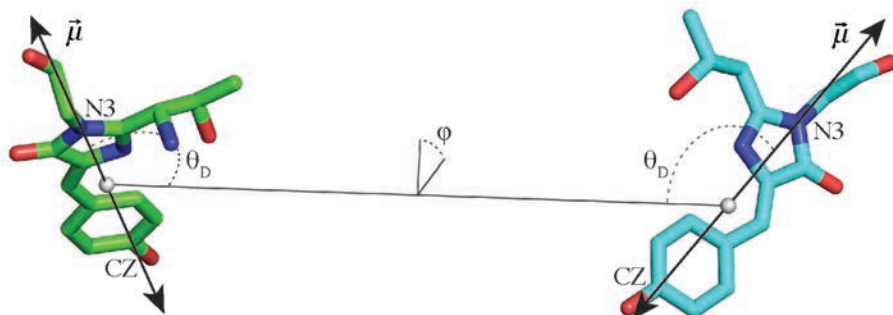
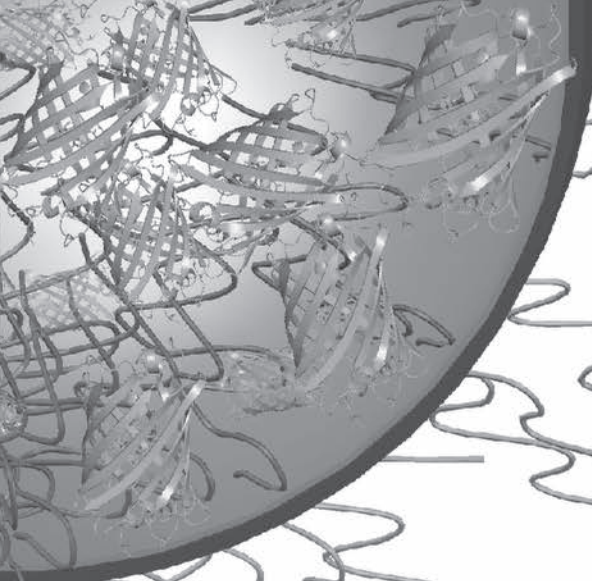


Figure S3.5. Illustration of the transition dipole moment, $\vec{\mu}$, of the EGFP chromophore (drawn through N3 and CZ of the chromophore, based on the model of Ansbacher et al. (2012)⁵¹) with the corresponding angles between two chromophores in an EGFP dimer (based on PDB entry 4N3D⁵⁰), which are used for the calculation of κ^2 . The equation for κ^2 is: $\kappa^2 = (\sin\theta_D \sin\theta_A \cos\phi - 2\cos\theta_D \cos\theta_A)^2$, with $\phi = 46.6^\circ$, $\theta_D = 135.6^\circ$ and $\theta_A = 180^\circ - \theta_D = 44.4^\circ$ for this EGFP dimer. This gives a κ^2 of 1.86 and a Förster radius, R_θ , of 48 Å.



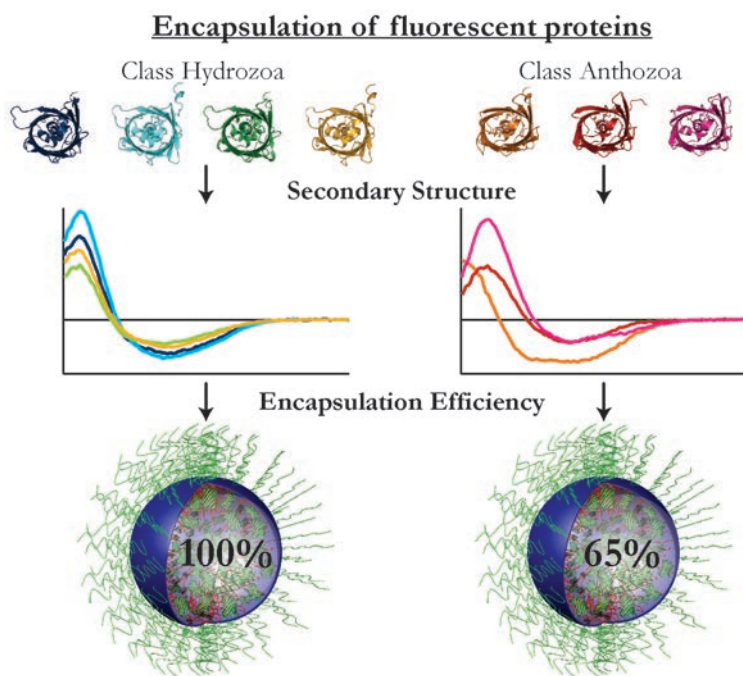
Chapter 4

Colorful packages: Encapsulation of fluorescent proteins in complex coacervate core micelles

Published as: A. Nolles, A. H. Westphal, J. M. Kleijn,
W. J. H. van Berkel, and J. W. Borst, *Int. J. Mol. Sci.*, **2017**, 18, 1557.

Abstract

Encapsulation of proteins can be beneficial for food and biomedical applications. To study their biophysical properties in complex coacervate core micelles (C3Ms), we previously encapsulated enhanced green fluorescent protein (EGFP) and its monomeric variant, mEGFP, with the cationic-neutral diblock copolymer poly(2-methyl-vinyl-pyridinium)_n-*b*-poly(ethylene-oxide)_m (P2MVP_n-*b*-PEO_m) as enveloping material. C3Ms with high packaging densities of fluorescent proteins (FPs) were obtained, resulting in a restricted orientational freedom of the protein molecules, influencing their structural and spectral properties. To address the generality of this behavior, we encapsulated seven FPs with P2MVP₄₁-*b*-PEO₂₀₅ and P2MVP₁₂₈-*b*-PEO₄₇₇. Dynamic light scattering and fluorescence correlation spectroscopy showed lower encapsulation efficiencies for members of the Anthozoa class (*an*FPs) than for Hydrozoa FPs derived from *Aequorea victoria* (*av*FPs). Far-UV CD spectra of the free FPs showed remarkable differences between *av*FPs and *an*FPs, caused by rounder barrel structures for *av*FPs and more elliptic ones for *an*FPs. These structural differences, along with the differences in charge distribution, might explain the variations in encapsulation efficiency between *av*FPs and *an*FPs. Furthermore, the *av*FPs remain monomeric in C3Ms with minor spectral and structural changes. In contrast, the encapsulation of *an*FPs gives rise to decreased quantum yields (monomeric Kusabira Orange 2 (mKO2) and Tag red fluorescent protein (TagRFP)) or to a p*K*_a shift of the chromophore (FP variant mCherry).



4.1. Introduction

Fluorescent proteins (FPs) are nowadays indispensable in life sciences.³⁻⁶ The discovery of FPs started in the early 1960s with studies on the identification of the glow of jellyfish from *Aequorea victoria* by Osamu Shimomura.⁹ The protein emitting the green light was called green fluorescent protein (GFP)¹² and its sequence was obtained in 1992 by Prasher.¹³ In the following years, a wide variety of GFP variants with different colors and improved brightness and stability were developed. However, there were no GFP variants with emission maxima above 527 nm.⁶ This limitation was overcome by cloning of GFP homologs from non-bioluminescent reef corals of the Anthozoa class.¹⁴⁻¹⁷ From this class, a palette of FPs became available emitting at longer wavelengths. Consequently, the number of applications of FPs has exploded, which is mainly because they can be genetically introduced into cells, tissues or whole organisms. This allows using FPs for multicolor imaging and for studying protein interactions.^{7,18,19} Besides using FPs as fusion tags and biosensors, they have also been used as model proteins in encapsulation studies.²⁰⁻²³

Encapsulation of proteins is of interest for food and biomedical applications, because it can protect and stabilize the encapsulated protein. Encapsulation of FPs allows the use of fluorescence techniques for the characterization of protein-containing micelles.²³

Previously, we reported on the encapsulation of enhanced green fluorescent protein (EGFP) and its monomeric variant (mEGFP) in complex coacervate core micelles (C3Ms) with the cationic-neutral diblock copolymer poly(2-methyl-vinyl-pyridinium)_n-*b*-poly(ethylene-oxide)_m (P2MVP_n-*b*-PEO_m) as enveloping material.^{23,24} The two GFP variants showed considerable differences in their spectral and structural properties upon encapsulation. Encapsulation into C3Ms promoted dimerization of EGFP but not of mEGFP, due to the difference in dissociation constant (K_D , 0.11 mM for EGFP and 74.0 mM for mEGFP)⁸. Dimerization of EGFP upon encapsulation in C3Ms results in a pK_a shift of its chromophore, leading to specific changes in the spectral and structural properties of EGFP.²⁴

The aim of the present study is to determine whether structural and spectral changes are common upon encapsulation of members of the visible fluorescent protein family. Therefore, we encapsulated a variety of fluorescent proteins covering the whole visible spectrum (Figure 4.1). We investigated seven differently colored FPs: four FPs derived from *Aequorea victoria* GFP (*av*FPs: strongly enhanced blue fluorescent protein 2 (SBFP2), mTurquoise2, mEGFP, and strongly enhanced yellow fluorescent protein 2 (SYFP2), from class Hydrozoa) and three FPs from class Anthozoa (*an*FPs: monomeric Kusabira Orange 2 (mKO2), Tag red fluorescent protein (TagRFP), and mCherry). The seven FPs originate from four different ancestors: one from the Hydrozoa class and three from the Anthozoa class. Even though these proteins have a comparable fold and function, the amino acid sequences vary between the different species (see Figure S4.1 and Table S4.1). The sequence identities among the *av*FPs are about 97%, whereas the *an*FPs show about 25% - 30% similarity to the *av*FPs. Amongst the *an*FPs, TagRFP and mCherry show a higher sequence identity (57%)

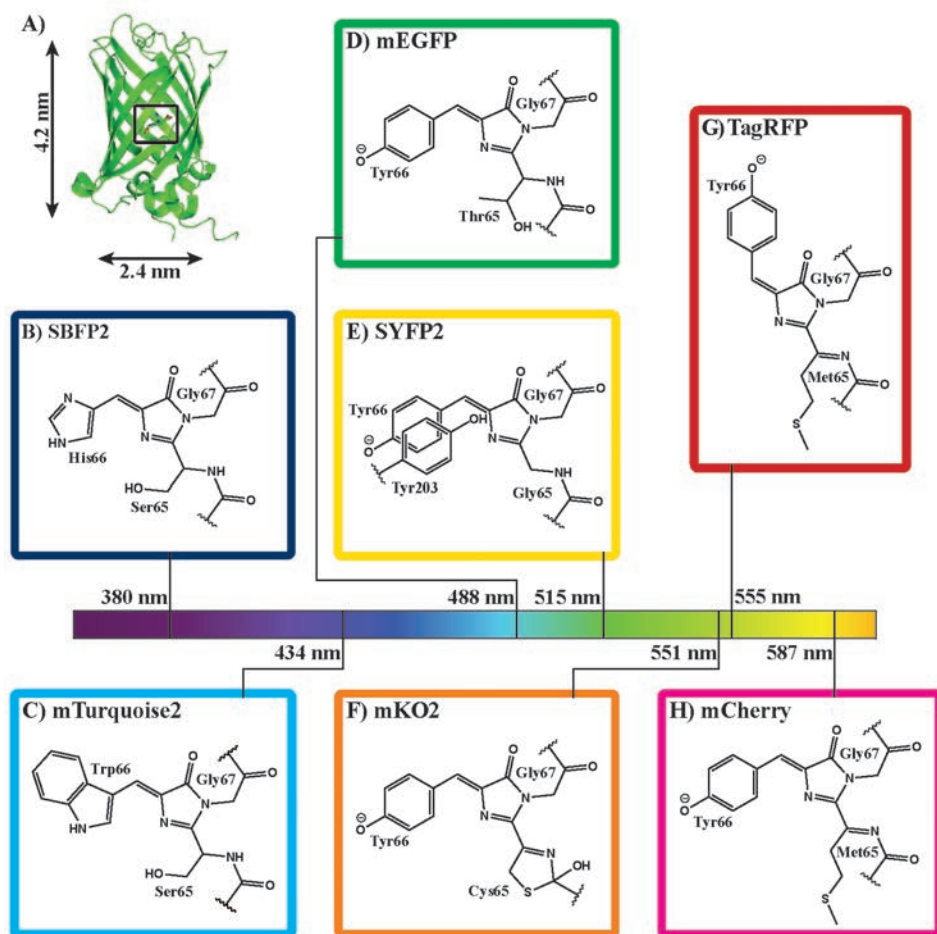


Figure 4.1. Chromophore properties of fluorescent proteins used in this research (A) Ribbon diagram of mEGFP with its chromophore in the center of the barrel (PDB entry 4EUL³⁰); (B) chromophore of SBFP2 made from Ser65, His66, and Gly67; (C) chromophore of mTurquoise2 made from Ser65, Trp66, and Gly67; (D) chromophore of mEGFP made from Thr65, Tyr66, and Gly67 in the anionic form; (E) chromophore of SYFP2 made from Gly65, Tyr66, and Gly67 in the anionic form with Tyr203 to extend the π -system; (F) chromophore of mKO2 made from Cys65, Tyr66, and Gly67 in the anionic form; (G) chromophore of TagRFP made from Met65, Tyr66, and Gly67 in the anionic form and in the *trans*-conformation and (H) chromophore of mCherry made from Met65, Tyr66 and Gly67 in the anionic form and in the *cis*-conformation. Absorption maxima are indicated on the spectral bar and fluorescence colors are indicated as box colors.

than mKO2 does with these two proteins (~48%). The seven FPs contain about 10% of strictly conserved residues (Figure S4.1). These residues are mainly located at the end of beta-strands and in loops, except for the strictly conserved Gly67, Asp95, Arg96, and Glu222 amino acid residues, which are involved in the formation of the chromophore.²⁵

Some general properties of FPs are critical for understanding their structural and spectral properties. All FPs have an approximate molar mass of 27 kDa, constituting a single polypeptide chain of about 230 amino acids. They all share a fold consisting of an 11-stranded β -barrel with a length of 4.2 nm and a diameter of 2.4 nm (Figure 4.1A). The barrel is wrapped around a single distorted helix, which contains three amino acid residues that create the fluorophore. The fluorophore is formed via cyclization, dehydration, and oxidation of the amino acid residues located at positions 65 to 67 (mEGFP numbering, Figure 4.1B to 4.1H). Depending on the pH of the solution, the chromophore can exist in differing protonation states, which influences the spectral properties of the FP. Furthermore, the fluorophore is comprised of a highly conjugated π -electron resonance system that together with its environment accounts for the spectroscopic and photophysical properties of an FP.

The spectroscopic features of the seven FPs will be presented according to their absorption maxima. We start with strongly enhanced blue fluorescent protein (SBFP2), which was obtained by the Y66H substitution in GFP (Figure 4.1B).²⁶ Turquoise FPs are obtained by a Y66W substitution in GFP (Figure 4.1C), which yields amongst others mTurquoise2.²⁷ mTurquoise2 is especially characterized by its long mono-exponential fluorescence lifetime ($\tau_f = 3.8$ ns), which makes it very suitable as a Förster resonance energy transfer (FRET) donor in conjunction with a yellow fluorescent protein as the acceptor. Originally, FPs are not monomeric, but this can be achieved with the A206K substitution, which is used in mEGFP.⁸ The GFP variants with emission maxima at the longest wavelengths are yellow FPs, obtained by a T203Y substitution in GFP, and in this research we used SYFP2 (Figure 4.1E).²⁸ This FP has a high molar extinction coefficient compared to other FPs ($\epsilon_{\text{SYFP2}} = 101\,000 \text{ M}^{-1} \text{ cm}^{-1}$, Table S4.2) making it a very suitable acceptor in FRET-pairs.²⁸

The chromophore structures of FPs from Anthozoa species generally have more extended π -systems, enabling higher excitation and emission wavelengths. Such a type of fluorophore is found in mKO2, which evolved from a fluorescent protein of the mushroom coral *Fungia concinna*, with a cysteine located at position 65 (mEGFP numbering, Figure 4.1F).^{15,29} mKO2 is very useful in multicolor imaging applications as it can be combined with cyan, green, yellow, and red FPs. A protein with an almost similar excitation maximum as mKO2 is TagRFP (Figure 4.1G), but this protein has been derived from the sea anemone *Entacmaea quadricolor*.¹⁶ TagRFP has an even more extended π -system than mKO2, because it has a methionine located at position 65 (mEGFP numbering, Figure 4.1G). Next to that, TagRFP is one of the few FPs bearing a *trans*-isomerized chromophore. A protein that also contains a methionine at position 65 (mEGFP numbering) is mCherry, one of the “mFruit” FPs derived from *Discosoma species*.^{1,2} mCherry shows a high photostability and its chromophore is rapidly formed (Figure 4.1H), which makes it very suitable as a FRET acceptor in combination with EGFP in fluorescence-lifetime imaging microscopy (FLIM) studies.³¹

In this research, we used the diblock copolymers P2MVP₄₁-*b*-PEO₂₀₅ and P2MVP₁₂₈-*b*-PEO₄₇₇ to form C3Ms in combination with the above-mentioned FPs. We characterized the C3Ms with dynamic light scattering (DLS) and fluorescence correlation spectroscopy (FCS), and explored the effects of packing on the FPs with circular dichroism (CD) and fluorescence spectral analysis. The experimental data, and in particular the observed encapsulation efficiencies, are discussed in relation to what is known about the structural features of the FPs.

4.2. Experimental section

4.2.1. Materials

Poly(2-vinyl-pyridinium)_n-*b*-poly(ethylene-oxide)_m (P2VP_n-*b*-PEO_m) with different chain lengths was quaternized: P2VP₄₁-*b*-PEO₂₀₅ (Polymer Source Inc., $M_w/M_n = 1.05$, $M_n = 13.3$ kg/mol) and P2VP₁₂₈-*b*-PEO₄₇₇ (Polymer Source Inc., $M_w/M_n = 1.10$, $M_n = 34.5$ kg/mol), following a procedure described elsewhere.²³ For P2MVP₄₁-*b*-PEO₂₀₅ ($M_n = 18.6$ kg/mol) and for P2MVP₁₂₈-*b*-PEO₄₇₇ ($M_n = 50.8$ kg/mol) a final degree of quaternization of approximately 80% and 87% was obtained, respectively. Stock solutions of P2MVP₄₁-*b*-PEO₂₀₅ (51 μM) and P2MVP₁₂₈-*b*-PEO₄₇₇ (50 μM) were prepared by dissolving the polymers in 10 mM borate buffer (pH 9.0) and stored at -20 °C. All solutions were filtered through 0.20 μm poly(ether-sulfone) membrane syringe filters (Advanced Microdevices Pvt. Ltd.). All other chemicals were from commercial sources and of the purest grade available.

4.2.2. Protein production

The cDNAs coding for mTurquoise2, SYFP2-His, and mCherry were cloned into the bacterial expression vector pTYB12 (New England Biolabs) to generate FP fusions with a chitin-binding domain and an intein.³²⁻³⁴ The cDNAs of SBFP2, mEGFP, mKO2, and TagRFP in pRSETb vectors were kindly provided by Dr. Joachim Goedhart, University of Amsterdam.²⁶⁻²⁸ For protein production, *E. coli* BL21 cells were used. Details on protein production and purification are described elsewhere.²⁴ FPs without the chitin-binding domain were acquired after on-column cleavage of mTurquoise2, SYFP2-His, and mCherry. The other FPs, *i.e.*, SBFP2, mEGFP, mKO2, and TagRFP still contained the His-tag after purification. Purified protein samples were stored in 10 mM borate buffer (pH 9.0) at -20 °C.

Protein concentrations were determined with a Pierce BCA protein assay (Pierce Biotechnology), using a bovine serum albumin standard as reference. The purity of the FPs was checked by SDS-PAGE.

4.2.3. Modeling

Homology models were built from existing crystal structures using SWISS-MODEL.³⁵⁻³⁸ Table 4.1 shows the proteins used in this paper and their corresponding PDBs. Table 4.2 shows the proteins used in this paper and their respective templates used for the homology modeling. The chromophores were placed in the model structure at the same position and orientation as the chromophore in the template structure. Pairwise sequence alignments of the FPs are listed in Figures S4.2 to S4.8. Because some N- and C-termini were missing in the created homology models (for SBFP2, mEGFP, and SYFP2), these termini were modeled manually using the PDB entry 3ZTF as a template. The A206K mutants were created by mutagenesis of Ala206 into Lys206 in PDB entries 4EUL and 3ZTF to construct mEGFP and mTurquoise2, respectively.

Table 4.1. PDB structures used for the proteins studied in this research listed with their corresponding figures, sequence identities (% ID) and references.

Protein	PDB Entry	Figure	% ID	Reference
mTurquoise2	3ZTF	S4.3	99.57	Goedhart, et al. [27]
mEGFP	4EUL	S4.4	99.56	Arpino, et al. [30]
TagRFP	3M22	S4.7	100.00	Subach, et al. [39]
mCherry	2H5Q	S4.8	100.00	Shu, et al. [2]

Table 4.2. Homology models built from PDB entry templates for the proteins studied in this research listed with their corresponding figures, sequence identities (% ID) and references.

Protein	PDB Entry	Figure	% ID	Reference
SBFP2	1BFP	S4.2	96.44	Wachter, et al. [40]
SYFP2	1MYW	S4.5	99.12	Rekas, et al. [41]
mKO2	2ZMU	S4.6	95.31	Kikuchi, et al. [42]

4.2.4. C3M preparation

Encapsulation of FPs with polymers was achieved by first diluting the FP stock solution in 10 mM borate buffer at pH 9.0 for SBFP2, mTurquoise2, mEGFP, SYFP2, mKO2, and mCherry; and at pH 10.0 for TagRFP to the desired concentration, followed by addition of the polymer. After mixing, samples were stored at room temperature for 24 h before measuring. All experiments were performed in 10 mM borate buffer at the encapsulation pH.

4.2.5. Dynamic light scattering (DLS)

DLS measurements were performed on an ALV instrument equipped with a 300 mW Cobolt Samba-300 DPSS laser operating at 660 nm and 100 mW, and static and dynamic enhancer fiber optics for an ALV/High QE APD (high quantum efficiency avalanche photo diode) single photon detector connected to an ALV5000/60X0 External Correlator (ALV-Laser Vertriebsgesellschaft m-b.H.). The detection angle, θ , was set at 90° and all measurement were performed at room temperature.

DLS measures fluctuations in scattered light intensities caused by the diffusion of particles. The diffusion time of particles is dependent on their size: proteins diffuse faster than the encapsulated proteins in C3Ms. Furthermore, larger particles scatter more light, because the scattered light intensity is proportional to R^6 , where R is the particle radius. The formation of more C3Ms leads to higher light intensities, which results in a maximum in the scattered light intensity versus composition plot (I vs F^+). The composition at the maximum in scattered light intensity is denoted as the preferred micellar composition (PMC). For determination of the PMC, 500 μ L solutions with different polymer/protein compositions were prepared. The protein concentration was kept constant at 1 μ M for each composition. The amount of P2MVP_{41-b}-PEO₂₀₅ or P2MVP_{128-b}-PEO₄₇₇ was varied to obtain the desired values of F^+ :

$$F^+ = \frac{[n_+]}{[n_+] + [n_-]} \quad (4.1)$$

where $[n_+] = c_+N_+$ refers to the total concentration of positively charged groups on the polymer and

$[n_-] = c_- N_-$ is the total concentration of negatively charged groups on the protein molecules. The number of charged groups on the diblock copolymer (N_+) taking the degree of quaternization into account, is +33.1 for P2MVP_{41-b}-PEO₂₀₅ and +112.0 for P2MVP_{128-b}-PEO₄₇₇, which is used to calculate $[n_+]$. The net charge of the proteins as a function of pH was calculated using the software package PROPKA 3.1.^{43,44} The charges of the native proteins at pH 9 or 10 (N_-) are listed in Table 4.4, which are used to calculate $[n_-]$.

4.2.5.1. DLS data analysis

DLS autocorrelation curves were generated from 10 intensity traces and averaged. The CUMULANT method^{45,46} was used to analyze the mean apparent hydrodynamic radius (R_h) as:

$$R_h = \frac{k_B T q^2}{6\pi\eta\Gamma} \quad (4.2)$$

where q is the scattering vector, k_B is the Boltzmann constant, T is the absolute temperature, η is the viscosity of the solvent, and Γ is the measured average decay rate of the correlation function. The CONTIN method^{47,48} is used to analyze the distribution of the radii of the C3Ms. The data were analyzed with the AfterALV program (AfterALV 1.0d, Dullware).

4.2.6. Fluorescence correlation spectroscopy (FCS)

FCS was performed on a Leica TCS SP8 X SMD system equipped with a 63x 1.20 NA water immersion objective with coverslip thickness correction collar. Samples with FPs were excited using a diode laser (emits at 440 nm) or a super continuum laser (emits a continuous spectrum from 470 to 670 nm). The lasers were set at a pulsed frequency of 40 MHz. The size-adjustable pinhole was set at 70 μm for all measurements. Fluorescence emission was detected using bandpass-adjustable spectral filters. In Table 4.3 the used laser lines and range of the spectral filters are given per fluorescent protein. Fluorescence was recorded via the internal hybrid detector, which was coupled to a PicoHarp 300 TCSPC module (PicoQuant). With this system, it was not possible to measure SBFP2, because its excitation maximum is below 440 nm.

Rhodamine 110 ($D = 4.3 \times 10^{-10} \text{ m}^2 \text{ s}^{-1}$) was used to calibrate the confocal volume of the setup. A diffusion time of 18 μs and a structural parameter (a , expressed as (ω_z/ω_{xy})) between 5 and 10 were obtained, resulting in a confocal volume of approximately 0.2 fL. Measurements were performed in a μ -Slide 8-wells chambered coverslip (Ibidi®).

Samples with concentrations of 1 μM FP were measured free in buffered solution as well as encapsulated with P2MVP_{41-b}-PEO₂₀₅ or P2MVP_{128-b}-PEO₄₇₇ at their respective PMCs. For each sample, five fluorescence intensity fluctuation traces of 30 s each were collected. All measurements were performed at room temperature.

Table 4.3. Settings for the FCS measurements per studied protein.

Protein	Laser line (nm)	Spectral filter (nm)
mTurquoise2	440	475 - 500
mEGFP	488	495 - 525
SYFP2	514	520 - 550
mKO2	550	650 - 600
TagRFP and mCherry	561	575 - 610



4.2.6.1. FCS data analysis

For the FCS data analysis, the FFS-data processor version 2.3 (Scientific Software Technologies Software Centre) was used.⁴⁹ The equation used to fit translational data, which includes triplet state, is as follows:⁵⁰

$$G(t) = 1 + \frac{1}{\langle N \rangle} \left(1 + \frac{F_{trip}}{1 - F_{trip}} \cdot e^{-t/T_{trip}} \right) \cdot \sum_{i=1}^n \frac{F_i}{(1 + t/\tau_{diff,i}) \cdot \sqrt{1 + (\omega_{xy}/\omega_z)^2} \cdot t/\tau_{diff,i}} \quad (4.3)$$

where $\langle N \rangle$ represents the average number of fluorescent particles, N , in the confocal volume. The exponential term describes the triplet state behavior of the molecule, in which F_{trip} is the fraction of molecules in the triplet state and T_{trip} is the average time a molecule resides in the triplet state. The last part of the equation describes the diffusion behavior of the molecules, where F_i is the fraction of species i , $\tau_{diff,i}$ is the diffusion time of species i , ω_{xy} and ω_z are the equatorial and axial radii of the detection volume, respectively. Equation 4.3 was used to obtain $\langle N \rangle$ for the different samples.

4.2.7. Steady-state fluorescence spectroscopy

Fluorescence excitation and emission spectra were measured using a Cary Eclipse spectrofluorimeter (Varian). Excitation and emission slits were set to yield bandwidths of 5 nm. All measurements were performed at 20 °C. Samples with concentrations of 1 μ M FP were measured free in buffered solution as well as encapsulated with P2MVP_{41-b}-PEO₂₀₅ or P2MVP_{128-b}-PEO₄₇₇ at their respective PMCs.

The relative quantum yields are calculated using the following equation:⁵¹

$$QY_{C3M} = \frac{QY_P \cdot FA_{C3M} \cdot A_P}{FA_P \cdot A_{C3M}} \quad (4.4)$$

where QY represents the quantum yield, FA the integrated area under the corrected emission spectrum, and A the absorbance at the excitation wavelength. The subscripts $C3M$ and P refer to the proteins in the C3Ms and the proteins free in solution, respectively.

4.2.8. Circular dichroism (CD)

CD experiments were performed on a JASCO J-715 spectropolarimeter with a Jasco PTC 348 WI temperature controller set at 20 °C. The far-UV CD spectra (195 - 260 nm) were obtained from samples in a 0.3 mL quartz cuvette with an optical path length of 1 mm. Thirty spectra, each recorded with a resolution of 1 nm, a scan speed of 50 nm/min and a response time of 1 s, were accumulated and averaged. Samples with concentrations of 2.5 μ M FP were measured free in buffered solution as well as encapsulated with P2MVP_{41-b}-PEO₂₀₅ or P2MVP_{128-b}-PEO₄₇₇ at their respective PMC. The polymers did not show any CD signal over the measured range, therefore, buffer blank spectra, obtained at identical conditions, were subtracted.

4.3. Results

In this work, we purified seven FPs using either the intein/chitin-binding-domain system (for mTurquoise2, SYFP2-His, and mCherry) or metal affinity chromatography (for SBFP2, mEGFP, mKO2, and TagRFP, see Section 4.2). The influence of the His-tag was tested by encapsulation of mTurquoise2 and of mTurquoise2-His (data not shown). We did not observe any differences in encapsulation properties between the two proteins; therefore, it is presumed that His-tags have no effects on our experiments using other FPs. The purified FPs have distinctive spectral properties. Figure 4.2 shows our recorded normalized fluorescence excitation and emission spectra of the FPs, which display maxima in agreement with those listed in literature (Table S4.2).

4.3.1. Fluorescent protein charge determination

Measurements on encapsulated FPs in C3Ms are commonly performed at the preferred micellar composition (PMC), which is the ratio between protein and polymer at which the highest concentration of micelles is obtained.^{23,24,52} The PMC is defined in terms of the total concentration of positively charged groups on the polymers and the net concentration of negative charges on the protein (Equation 4.1, Section 4.2.5). The positive charge on the polymers is fixed due to quaternization, but the charge of the proteins varies with pH. The amino acid residues on the protein surface determine to a great extent the net charge of the protein, which can be deduced from the protein's three-dimensional structure using the PROPKA software package.^{43,44} For four of the studied FPs (mTurquoise2, mEGFP, TagRFP, and mCherry), a crystal structure is available in the RCSB Protein Data Bank (Table 4.1).⁵³ For the three other FPs (SBFP2, SYFP2, and mKO2), a Blast search was performed to obtain the most suitable template, which was then used for building homology models (Table 4.2).

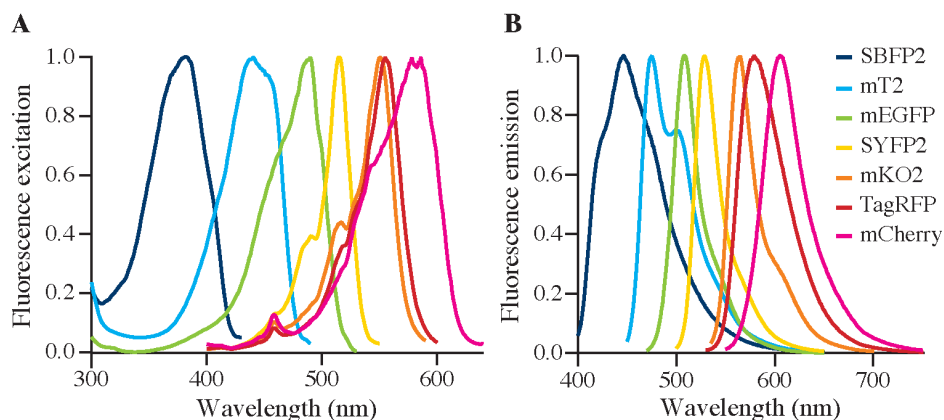


Figure 4.2. Normalized fluorescence (A) excitation and (B) emission spectra of SBFP2, mTurquoise2 (mT2), mEGFP, SYFP2, mKO2, TagRFP and mCherry.

Table 4.4. Results of PROPKA 3.1 analysis and preferred micellar composition (PMC) determination. The charge of the proteins was determined at pH 9, except for TagRFP (pH 10), with PROPKA 3.1.^{43,44} PMC (F^+) and hydrodynamic radii (with standard deviations) were determined with dynamic light scattering for all used fluorescent protein variants encapsulated using the two diblock copolymers.

FP variant	Charge	P2MVP ₄₁ - <i>b</i> -PEO ₂₀₅		P2MVP ₁₂₈ - <i>b</i> -PEO ₄₇₇	
		PMC (F^+)	Radius (nm)	PMC (F^+)	Radius (nm)
SBFP2	-8.96	0.75	38.3 ± 0.5	0.70	33.6 ± 0.2
mTurquoise2	-11.30	0.70	37.1 ± 1.0	0.70	33.9 ± 0.5
mEGFP	-9.87	0.70	30.4 ± 0.5	0.65	32.2 ± 0.2
SYFP2	-9.75	0.70	30.4 ± 0.4	0.60	35.2 ± 0.7
mKO2	-13.09	0.65	25.7 ± 0.5	0.60	28.3 ± 0.5
TagRFP ^a	-10.35	0.70	36.7 ± 5.0	0.65	33.3 ± 1.9
mCherry	-8.93	0.75	30.0 ± 0.8	0.75	35.1 ± 1.0

^a Values determined at pH 10.

The pI value for the four avFPs and for two anFPs (mKO2 and mCherry) is about 5.5, while TagRFP has a significantly higher pI value, 7.4 (Table S4.2). To achieve similar electrostatic interactions between the polymers and the different FPs, we encapsulated all FPs at the pH at which they have a net negative charge of about 10 unit charges. Thus, TagRFP was encapsulated at pH 10 and the other FPs at pH 9 (Table 4.4). At these conditions, all FPs are stable.⁵⁴

4.3.2. Preferred micellar composition (PMC)

The seven FPs were encapsulated using two diblock copolymers with different lengths (P2MVP₄₁-*b*-PEO₂₀₅ or P2MVP₁₂₈-*b*-PEO₄₇₇). As a start, dynamic light scattering (DLS) experiments were performed to determine the PMCs. The results of SBFP2 with P2MVP₄₁-*b*-PEO₂₀₅ and P2MVP₁₂₈-*b*-PEO₄₇₇ are shown in Figure 4.3. The highest concentration of micelles is found at the maximum of the scattered light intensity. For SBFP2, PMCs are found at F^+ values of 0.75 and 0.70 for P2MVP₄₁-*b*-PEO₂₀₅ and P2MVP₁₂₈-*b*-PEO₄₇₇, respectively (Figure 4.3 and Table 4.4). Similar DLS experiments were performed on the other six FPs with both diblock copolymers (Figure S4.9) and their respective PMCs are listed in Table 4.4. For all FPs and with both diblock copolymers, optimal F^+ values ranging between 0.60 and 0.75 were found. Samples with this optimal composition were used in all other spectroscopic analyses: fluorescence correlation spectroscopy (FCS), circular dichroism (CD), and steady-state fluorescence spectroscopy.

The fluctuations of the scattered light intensities were used to calculate the hydrodynamic radii of the C3Ms. For all seven FPs, the hydrodynamic radii of the C3Ms are quite constant over a relatively wide range of F^+ compositions ($0.40 < F^+ < 0.80$, Figures 4.3 and S4.9). In general, radii of the formed C3Ms vary between 30 and 38 nm, except for C3Ms formed with mKO2, which are somewhat smaller with radii of about 27 nm (Table 4.4).

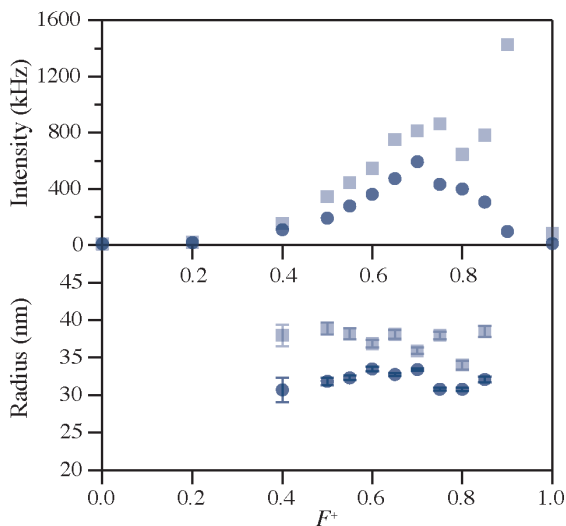


Figure 4.3. DLS results of micellar compositions of SBFP2 mixed with P2MVP₄₁-*b*-PEO₂₀₅ (light blue colored squares) or P2MVP₁₂₈-*b*-PEO₄₇₇ (dark blue colored dots). The protein concentration was kept constant at 1.0 μ M. Top graph shows scattered intensity as a function of the F^+ composition, and bottom graph shows the hydrodynamic radius as a function of the F^+ composition. Error bars reflect the distribution of radii in one experiment. DLS composition results of the six other fluorescent proteins are given in Figure S4.9.

4.3.3. Encapsulation efficiency

Next to DLS, FCS can be used for the determination of PMC values.²³ An advantage of FCS is that it gives, amongst other parameters, the average number of fluorescent particles in the confocal volume (N , Equation 4.3). In this study, the fluorescent particles observed are free FPs and C3Ms with multiple FPs encapsulated. We quantified the number of free FPs before addition of polymers (N_{before}) and of fluorescent particles after addition of polymers (N_{after}), and expressed the encapsulation efficiency per FP according to the following relation: $E_{\text{encap}} = 1 - (N_{\text{after}}/N_{\text{before}})$. The encapsulation efficiencies per FP are shown in Figure 4.4 and the corresponding graph with the number of fluorescent particles is shown in Figure S4.10. FCS was not performed on samples containing SBFP2 because no suitable excitation source for this FP was available on the used confocal microscope.

For all *an*FPs, the encapsulation efficiencies are almost 100% with both diblock copolymers, meaning that virtually all protein molecules are packed in C3Ms. However, we observed lower encapsulation efficiencies for *an*FPs (50% to 75%, Figure 4.4), which implicates that, for these FPs, more protein molecules remain free in solution (Figure S4.10).

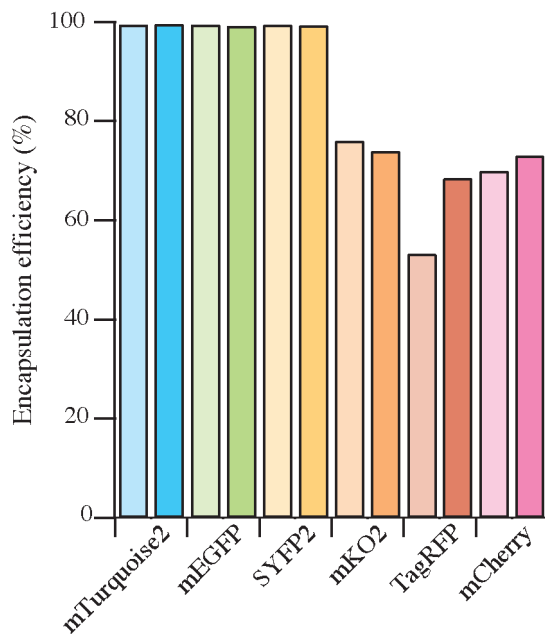


Figure 4.4. Encapsulation efficiencies of the different fluorescent proteins studied (except SBFP2) at their respective PMCs with P2MVP₄₁-*b*-PEO₂₀₅ (light colored bars) and P2MVP₁₂₈-*b*-PEO₄₇₇ (dark colored bars) determined using FCS. Efficiencies are calculated from the average number of fluorescent particles observed in the confocal volume (N in Equation 4.3 and Figure S4.10).

4.3.4. Fluorescence properties

Previously, we have shown that encapsulation of EGFP and mEGFP resulted in different spectral properties compared to that of the proteins free in solution.²⁴ The spectral properties of EGFP upon encapsulation change more than that of mEGFP, which is due to the pK_a shift of the chromophore of EGFP. To investigate if encapsulation changes the spectral properties of the FPs, absorption and fluorescence excitation and emission spectra for all FPs free in solution, as well as encapsulated in C3Ms were recorded (Figures 4.5 and S4.11).

We observed that encapsulation of the FPs leads to minor differences in their absorption and fluorescence properties and these are dependent on the kind of FP and the type of polymer used. Figure 4.6 shows that, for SBFP2, both the absorption and the fluorescence intensity increases upon encapsulation. Encapsulation of mTurquoise2, mEGFP, and SYFP2 resulted in a decrease of the fluorescence intensity, whereas the absorption remained the same. Both the absorption and fluorescence intensity decreases upon encapsulation of TagRFP. For mCherry, the fluorescence intensity increases and the absorption and excitation maxima become blue-shifted upon encapsulation (for spectra see Figure 4.5 and S4.11). The absorption and fluorescence results were combined in the determination of relative quantum yields of FPs encapsulated in C3Ms (Equation 4.4 and Table 4.5). Table 4.5 shows that the quantum yield of SBFP2 does not change, that of mCherry increases, and that of the other FPs decreases upon encapsulation.

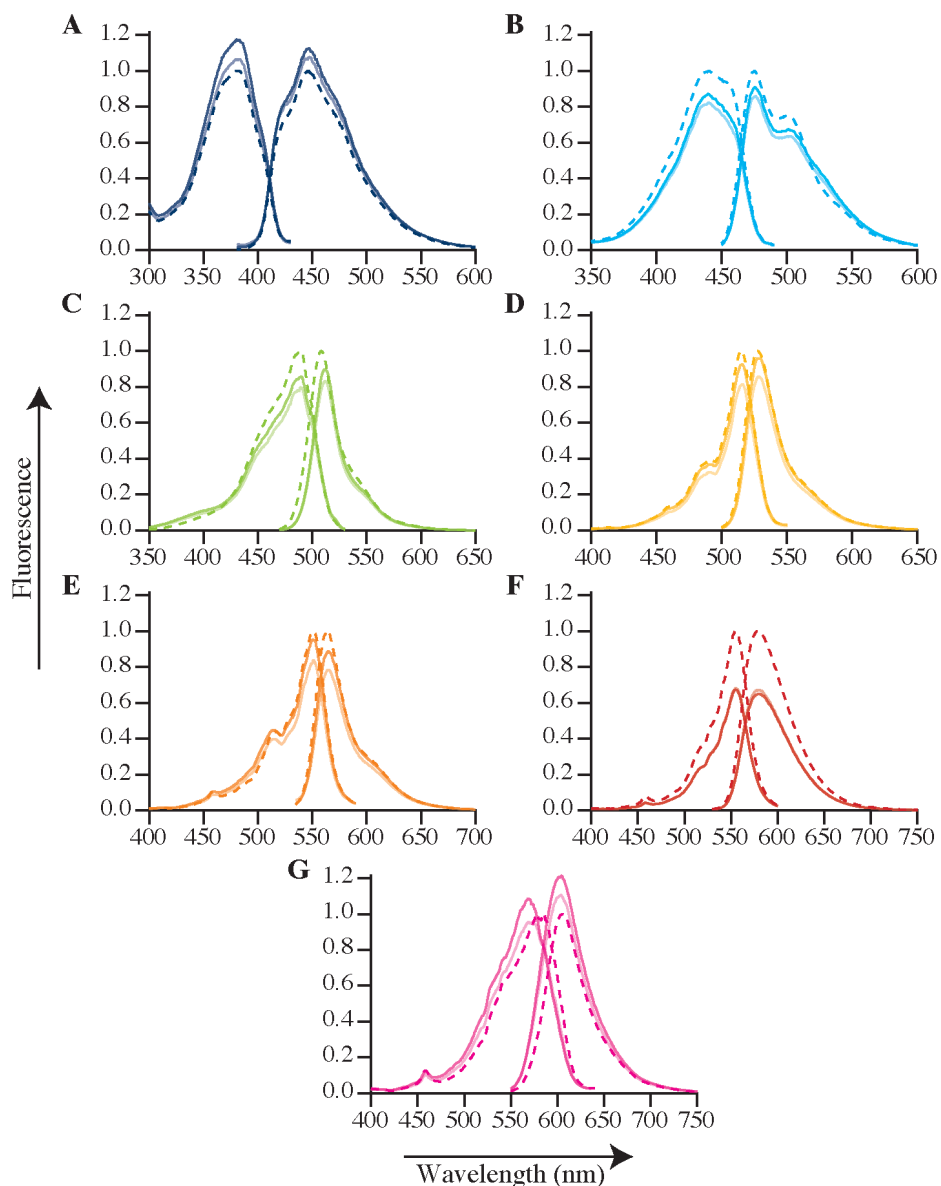


Figure 4.5. Fluorescence excitation and emission spectra of (A) SBFP2; (B) mTurquoise2; (C) mEGFP; (D) SYFP2; (E) mKO2; (F) TagRFP and (G) mCherry for protein free in solution (dashed lines) and encapsulated proteins in C3Ms at their respective PMCs with P2MVP₄₁-b-PEO₂₀₅ (solid light colored lines) and P2MVP₁₂₈-b-PEO₄₇₇ (solid dark colored lines). The spectra are normalized to those of the free proteins measured at identical conditions.

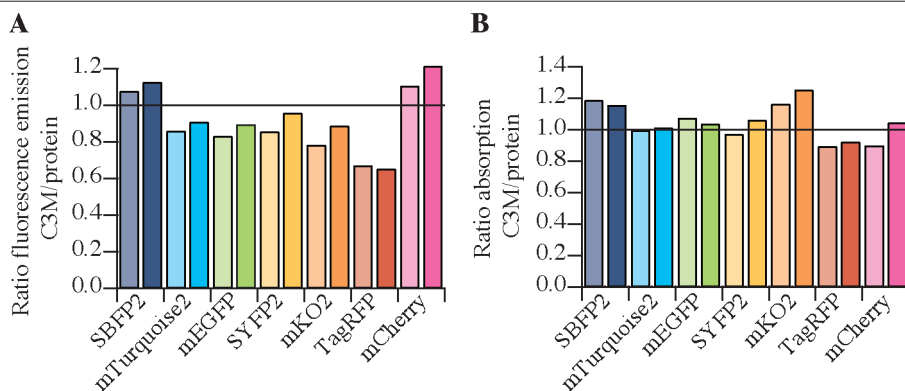


Figure 4.6. (A) Ratio of fluorescence emission and (B) ratio of absorption of encapsulated protein (C3M) to that of protein free in solution (values for mCherry are taken from the maxima). Ratios for all proteins were measured at the PMC with P2MVP_{41-b}-PEO₂₀₅ (light colored bars) and P2MVP_{128-b}-PEO₄₇₇ (dark colored bars). The corresponding fluorescence and absorption spectra are displayed in Figure 4.5 and S4.11, respectively.

To address if the observed spectral changes are due to a pH-related phenomenon, fluorescence excitation and emission spectra at different pH values were acquired of all FPs free in solution (Figure S4.12). SBFP2, mEGFP, SYFP2, and mKO2 have a pK_a of 5.5 - 6.0 and show a large decrease in their fluorescence intensity at pH 5. For the latter three proteins, this effect is caused by protonation of the phenolic oxygen of the chromophore (Figures 4.1D to 4.1F and S4.12C to S4.12E). mCherry shows a stronger susceptibility to changes in pH (Figure S4.12G): at increasing pH values (from pH 5 to 10), the spectra are blue-shifted and the fluorescence intensity increases. These changes resemble the changes observed upon encapsulation of mCherry.

The only two FPs showing no significant effect upon changes of pH are mTurquoise2 and TagRFP, which can be explained by their rather low pK_a values ($pK_a \sim 3.5$, see Figure S4.12F). It is therefore remarkable that the fluorescence intensity of TagRFP decreases about 40% upon encapsulation compared to the free protein (Figure 4.6A), even though the encapsulation efficiency is about 60% (Figure 4.4). This suggests that the fluorescence of TagRFP is highly affected upon encapsulation. In solution, TagRFP tends to dimerize with a K_D of 38.4 μM .¹¹ Assuming a protein concentration of about 10 mM in the C3Ms, this implies that TagRFP associates into dimers or tetramers inside C3Ms, which might cause the drastic decrease of quantum yield of the chromophore upon encapsulation.

Next to these differences between the FPs, we also observed an effect depending on the length of diblock copolymer used: if the fluorescence increases upon encapsulation, the increase is larger with the longer polymer (P2MVP_{128-b}-PEO₄₇₇) than with the shorter one (P2MVP_{41-b}-PEO₂₀₅). Conversely, if the fluorescence decreases upon encapsulation, the decrease is larger with the shorter polymer than with the longer one, except for TagRFP (Figure 4.6A). This dependency, however, is not observed in the absorption spectra (Figure 4.6B).

Table 4.5. Quantum yields of the encapsulated proteins in C3Ms with P2MVP₄₁-*b*-PEO₂₀₅ (C3M_P41) and P2MVP₁₂₈-*b*-PEO₄₇₇ (C3M_P128) compared to those of the proteins free in solution according to Equation 4.4.

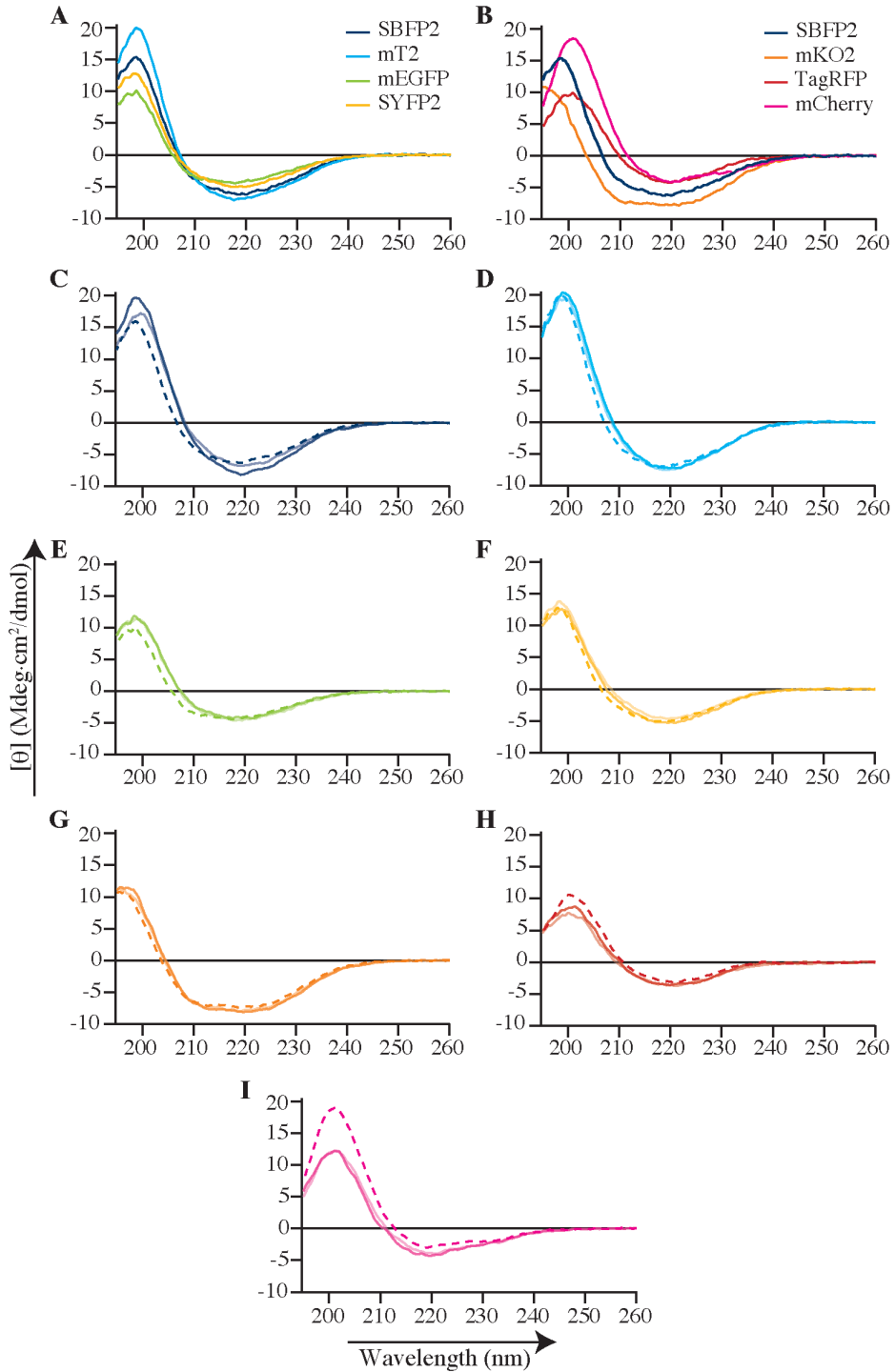
FP variant	Free protein	C3M_P41	C3M_P128
SBFP2	0.47	0.47	0.46
mTurquoise2	0.93	0.84	0.88
mEGFP	0.60	0.44	0.50
SYFP2	0.68	0.60	0.62
mKO2	0.62	0.41	0.45
TagRFP	0.48	0.33	0.25
mCherry	0.22	0.25	0.24

4.3.5. Secondary structure

To investigate whether the differences in encapsulation efficiencies are due to structural perturbations of the FPs, far-UV circular dichroism (CD) experiments were performed. Figure 4.7 shows CD spectra of all seven FPs free in solution and encapsulated with P2MVP₄₁-*b*-PEO₂₀₅ or with P2MVP₁₂₈-*b*-PEO₄₇₇. The CD spectra of the FPs are not affected by the increase in pH, as the CD spectra at pH 9.0 or 10.0 do not show any differences compared to those at pH 7.0 (data not shown). For all FPs, a negative mean residue ellipticity near 220 nm was observed, which is in good agreement with the prominent β -barrel architecture of these proteins (Figure 4.1A) and in line with previous observations.^{24,55} The spectrum of mKO2, however, resembles more a α -helical architecture with two negative peaks near 210 and 220 nm.^{56,57}

The CD spectra of the four *an*FPs free in solution are quite similar in shape (Figure 4.7A). The CD spectra of the *an*FPs are remarkably different compared to those of the *an*FPs (SBFP2 was taken as a representative reference, see Figure 4.7B). To our knowledge, these differences have not been reported before, and are further addressed in Section 4.4.2.

Upon encapsulation of the FPs, the CD spectra alter to a greater or lesser extent compared to that of the proteins free in solution, especially in the range where the spectra switch ellipticity (“zero crossing”, between 205 and 215 nm). For the encapsulated *an*FPs and for encapsulated mKO2, the zero crossing shifts to higher wavelength compared to that of the respective free FPs (Figures 4.7C to 4.7G). On the other hand, the zero crossings of encapsulated TagRFP and mCherry change to lower wavelengths compared to that of the free proteins (Figures 4.7H and 4.7I). In general, the zero crossings of all encapsulated FPs shift to ± 210 nm. Apart from the zero crossings, the changes upon encapsulation of mTurquoise2, SYFP2, and mKO2 are moderate. More pronounced deviations in CD spectra after encapsulation are observed for SBFP2, mEGFP, and TagRFP. The largest change, however, can be observed for mCherry, with a significant positive decrease and a negative increase in ellipticity around 200 and 220 nm, respectively (Figure 4.7I).



4.4. Discussion

Previously, we found that the encapsulation of EGFP in C3Ms stimulates protein dimerization and changes the spectral properties of the EGFP chromophore.²⁴ Because mEGFP mainly remains monomeric in the densely packed C3Ms, encapsulation of this protein hardly affects its spectral properties. In this work, we studied the encapsulation of four *av*FPs and three *an*FPs in C3Ms. All investigated FPs were successfully encapsulated using two diblock copolymers (P2MVP₄₁-*b*-PEO₂₀₅ and P2MVP₁₂₈-*b*-PEO₄₇₇) with F^+ values ranging between 0.60 and 0.80. For strong polyelectrolytes, stoichiometric C3M systems are formed at a F^+ value of 0.50.⁵⁸ Proteins, however, are weak polyelectrolytes and therefore their charge may change upon interaction with the diblock copolymer. Moreover, coacervation between polymer and protein does not necessarily arise from the overall charge of the protein, but rather from specific charge patches on the protein surface.⁵⁹ Both effects can even lead to coacervation between similarly charged proteins and polyelectrolytes.⁶⁰⁻⁶³

4.4.1. Encapsulation efficiency

The encapsulation efficiencies of *av*FPs (mEGFP, SBFP2, SYFP2 and mTurquoise2) were almost 100%, whereas those of *an*FPs (mKO2, TagRFP and mCherry) varied between 50% and 75%. This implicates that the interactions between the *av*FPs and the diblock copolymers to form C3Ms are less favorable. The formation of C3Ms requires an interaction between the FPs and the polymers, which can be dependent on the surface charge distribution and/or the shape of the protein. For the investigation of the presence of specific charge patches on the protein surface, we determined the surface potential distribution of the FPs on the acquired protein structures. For this, homology modeling was used to obtain the protein structures of SBFP2, SYFP2, and mKO2, next to the crystal structures of mTurquoise2, mEGFP, TagRFP, and mCherry. In Figure 4.8, the surface potentials of the FPs are visualized at the pH value at which they were encapsulated. All *av*FPs share a negative surface patch, as displayed on the side view at 90°, with an expansion to half of the molecule displayed in the side view at 180°. The amino acid residues with negative charge belonging to this patch are located on β -strands 1 and 2. The three *an*FPs do not contain a similar negative patch displayed on the side view at 90°, as observed for *av*FPs. Negative patches for mKO2 and TagRFP are mainly present in the side view at 0°. For TagRFP, the amino acid residues with negative charge are more distributed over the entire protein surface than for the other proteins. For mCherry, there is not a side entirely filled with negatively charged amino acid residues. It is key for the positively charged polyelectrolyte to bind to a local negative charge patch on the protein while minimizing the repulsive effect arising from the positively charged amino acid residues. Therefore, the interactions between the diblock copolymers and mKO2, TagRFP, and mCherry might not be optimal, thus affecting their encapsulation efficiencies.

Figure 4.7 (previous page). Comparison of the far-UV CD spectra of the free proteins (A) *av*FPs and (B) *an*FPs with SBFP2 as a reference representing the *av*FPs. Far-UV CD spectra of (C) SBFP2, (D) mTurquoise2, (E) mEGFP, (F) SYFP2, (G) mKO2, (H) TagRFP, and (I) mCherry free in solution (dashed line) and encapsulated with P2MVP₄₁-*b*-PEO₂₀₅ (solid light colored line) and P2MVP₁₂₈-*b*-PEO₄₇₇ (solid dark colored line). The corresponding high tension signals are shown in Figure S4.13.

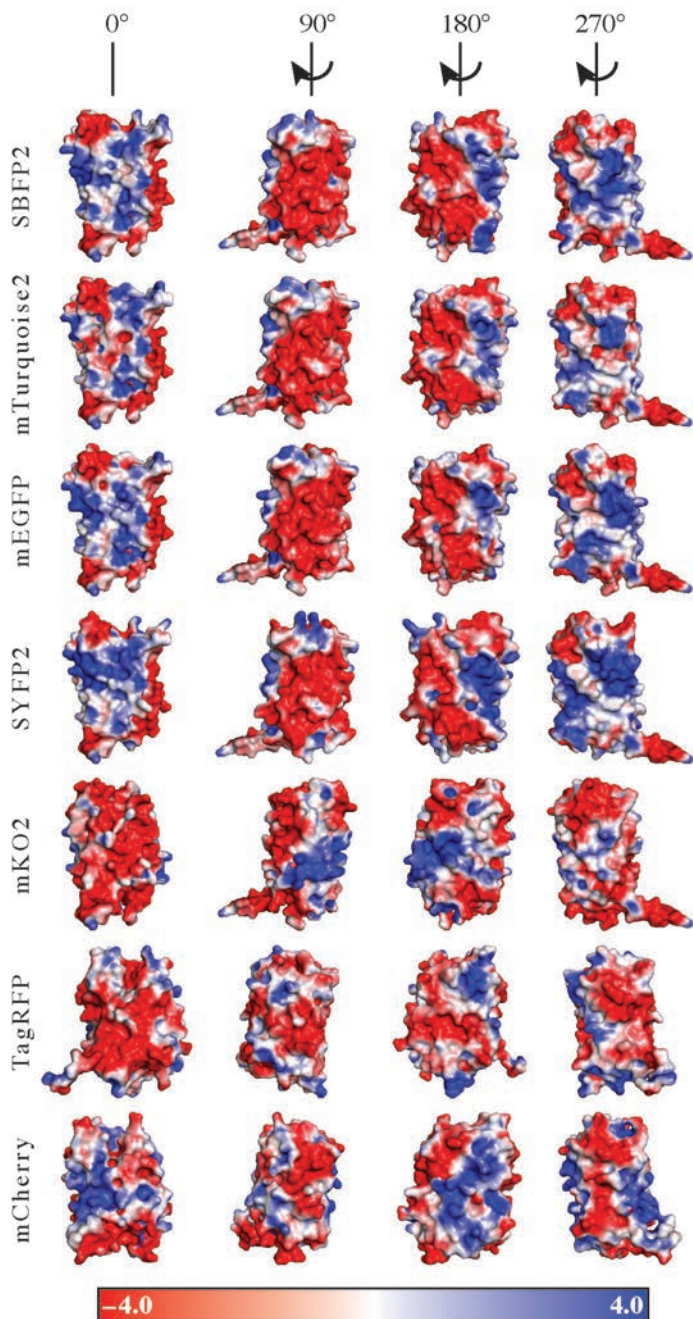


Figure 4.8. Comparison of the seven investigated proteins' electrostatic potentials (in $k_B T/e$) at the molecular surface in four different orientations: SBFP2, mTurquoise2, mEGFP, SYFP2, mKO2, TagRFP, and mCherry. Color surface overlay denotes electrostatic potential according to the scale shown: Red, negative potential; white, neutral; and blue, positive potential. Figure created by solution of the Poisson–Boltzmann equation using the default parameters of the PyMOL APBS (Adaptive Poisson–Boltzmann Solver) Tools plugin^{66,67} in MacPyMOL 1.4.⁶⁸

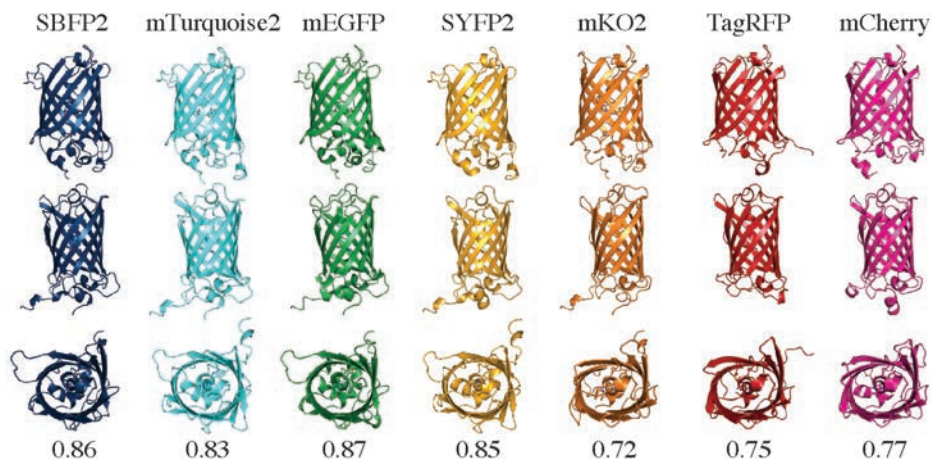


Figure 4.9. Ribbon structures of the seven FPs in three different orientations. At the top, the broad side; in the middle, the narrow side; and at the bottom, the “top” (the base containing both termini) of the proteins is shown. Numbers indicate the aspect ratio between the narrow and the broad side of the proteins.

4.4.2. Elliptical symmetry of FP barrels

During this study, we uncovered clear differences in the far-UV CD spectra between *av*FPs and *an*FPs free in solution (Figure 4.7B). It is well known that all FPs share a similar 11-stranded β -barrel fold (Figure 4.1A). However, it is hardly reported in the literature that the elliptical symmetry between *av*FPs and *an*FPs is diverse.⁶⁴ Figure 4.9 shows the ribbon structures of the studied FPs in three different orientations: the broad side, the narrow side, and the top. From the top views, it is clear that the barrels of the FPs are not completely round, but form elliptical cylinders. The *av*FPs are rounder than the *an*FPs, which is depicted by the difference in aspect ratio: ~ 0.85 for the *av*FPs and ~ 0.74 for the *an*FPs. Especially mKO2 is the most “squeezed” of the *an*FPs. We hypothesize that these differences are the cause for the observed differences in the far-UV CD spectra. Micsonai *et al.*, reported that CD spectra are influenced, among others, by degree of twist and distortion of the β -sheets.⁶⁵ The variance in the elliptical symmetry is another apparent difference between *av*FPs and *an*FPs, and could also be influencing their encapsulation efficiencies.

4.4.3. Biophysical properties of encapsulated proteins

Encapsulation of the *av*FPs hardly influenced their secondary structural properties and only minor changes in absorption and emission characteristics were observed. All *av*FPs bear the A206K mutation, which favors their monomeric state. This supports that the minor spectral changes observed are caused by the electrostatic interactions between the polymers and the protein surfaces of these FPs.

All *an*FPs are found as tetramers in their hosts.^{1,15,16} The *an*FPs used here are all modified to enhance their tendency to remain monomeric. In literature, this tendency is expressed in terms of dissociation constants and “monomeric quality” (see Table S4.2). Previously, we calculated the number of EGFP molecules present in a C3M to be around 450, yielding a local protein concentration of about 10 mM.^{23,24} Since the FPs used in this study form C3Ms with PMCs (~0.65) and radii (~34 nm) similar to EGFP-C3Ms, it is a reasonable assumption that the protein concentration in the various FP-C3Ms is about the same. Hence, we expect that mCherry with a monomeric quality of 95% remains mostly monomeric upon encapsulation. However, mKO2 and TagRFP with monomeric qualities of 68% and 58%, respectively, and a dissociation constant of 0.038 mM for TagRFP, will likely form oligomers in the C3Ms (Table S4.2). This oligomerization causes the large decrease in quantum yield of the encapsulated forms of mKO2 and TagRFP (Table 4.5).

For encapsulated mCherry, the absorption spectrum changes according to a pK_a shift of its chromophore (Figure S4.11). For EGFP it was proposed that the pK_a shift of its chromophore is caused by a reorientation of Glu222 due to the dimerization of EGFP in C3Ms.²⁴ For free mCherry, the equivalent Glu215 is also linked to the pH-dependent spectral shifts (Figure S4.12G).² If mCherry, however, remains monomeric in the C3Ms, the reorientation of Glu215 can only occur due to the interaction between protein and polymer.

4.4.4. Future research

We show that encapsulation of structurally similar FPs in C3Ms is dependent on the origin of the FPs and can give rise to different encapsulation efficiencies. Moreover, the spectral and structural perturbations observed are dependent on the kind of FP and the type of polymer used. In future research, we plan to investigate the stability and dynamics of encapsulated FPs. This can be accomplished by mixing two appropriate FPs using FRET as a readout. Some requirements should be considered choosing an optimal FP FRET-pair: first, use fluorescent proteins with similar encapsulation efficiencies. Second, use FPs that show minor changes in their absorption and fluorescence properties upon encapsulation into the C3Ms. Third, use the diblock copolymer which has the least effect on the fluorescence properties of the FPs. According to the present results, the ideal partners of an FRET-pair in C3Ms would be mTurquoise2 and SYFP2 in combination with P2MVP₁₂₈-*b*-PEO₄₇₇.

4.5. Conclusions

We have studied the encapsulation efficiency of SBFP2, mTurquoise2, mEGFP, SYFP2, mKO2, TagRFP, and mCherry and determined their spectral and structural properties as protein free in solution and upon encapsulation with P2MVP₄₁-*b*-PEO₂₀₅ or P2MVP₁₂₈-*b*-PEO₄₇₇. This revealed that *aw*FPs are almost 100% encapsulated, while *an*FPs show encapsulation efficiencies ranging between 50% and 75%. Upon encapsulation, all FPs show differences in spectral properties compared to their respective protein free in solution: the chromophores of SBFP2, mKO2, and mCherry are affected in their molar extinction coefficient and the chromophores of mTurquoise2, mEGFP, SYFP2, TagRFP, and mKO2 are affected in their fluorescence quantum yield. Only for mCherry, the changes in spectral properties upon encapsulation are similar to changes observed as a result of pH variation and are, therefore, related to a shift in the pK_a . Even though all FPs have an 11-stranded β -barrel fold, the CD spectra differ between *aw*FPs and *an*FPs. This is most likely due to a different shape of the cylinders between the two groups of FPs, where the β -barrel structures of *aw*FPs are almost round cylinders and that of *an*FPs elliptic ones. This variation in structure, together with the difference in charge distribution on FP surfaces, potentially causes the differences in encapsulation efficiency.

Acknowledgments

Financial support from the Graduate School VLAG (Wageningen, The Netherlands) is gratefully acknowledged. The fluorescence correlation spectroscopy experiments were performed on a multimode confocal microscope supported by a NWO Middelgroot Investment Grant (721.011.004; Jan Willem Borst). We thank Dr. Joachim Goedhart (University of Amsterdam, Amsterdam, The Netherlands) for providing us with pRSETb vectors containing SBFP2, mEGFP, mKO2, and TagRFP.

References

1. Shaner, N. C.; Campbell, R. E.; Steinbach, P. A.; Giepmans, B. N.; Palmer, A. E.; Tsien, R. Y., Improved monomeric red, orange and yellow fluorescent proteins derived from *Discosoma sp.* red fluorescent protein. *Nat. Biotechnol.* **2004**, *22*, (12), 1567-1572.
2. Shu, X.; Shaner, N. C.; Yarbrough, C. A.; Tsien, R. Y.; Remington, S. J., Novel chromophores and buried charges control color in mFruits. *Biochemistry* **2006**, *45*, (32), 9639-9647.
3. Miyawaki, A.; Niino, Y., Molecular spies for bioimaging - Fluorescent protein-based probes. *Mol. Cell* **2015**, *58*, (4), 632-643.
4. Enterina, J. R.; Wu, L.; Campbell, R. E., Emerging fluorescent protein technologies. *Curr. Opin. Chem. Biol.* **2015**, *27*, 10-17.
5. Zimmer, M., Green fluorescent protein (GFP): applications, structure, and related photophysical behavior. *Chem. Rev.* **2002**, *102*, (3), 759-781.
6. Tsien, R. Y., The green fluorescent protein. *Annu. Rev. Biochem.* **1998**, *67*, 509-544.
7. Cranfill, P. J.; Sell, B. R.; Baird, M. A.; Allen, J. R.; Lavagnino, Z.; de Gruiter, H. M.; Kremers, G. J.; Davidson, M. W.; Ustione, A.; Piston, D. W., Quantitative assessment of fluorescent proteins. *Nat. Methods* **2016**, *13*, (7), 557-562.
8. Zacharias, D. A.; Violin, J. D.; Newton, A. C.; Tsien, R. Y., Partitioning of lipid-modified monomeric GFPs into membrane microdomains of live cells. *Science* **2002**, *296*, (5569), 913-916.
9. Shimomura, O.; Johnson, F. H.; Saiga, Y., Extraction, purification and properties of aequorin, a bioluminescent protein from the luminous hydromedusa, *Aequorea*. *J. Cell. Comp. Physiol.* **1962**, *59*, 223-239.
10. von Stetten, D.; Noirclerc-Savoye, M.; Goedhart, J.; Gadella, T. W., Jr.; Royant, A., Structure of a fluorescent protein from *Aequorea victoria* bearing the obligate-monomer mutation A206K. *Acta Crystallogr., Sect. F: Struct. Biol. Cryst. Commun.* **2012**, *68*, (Pt 8), 878-882.
11. Han, L.; Zhao, Y.; Zhang, X.; Peng, J.; Xu, P.; Huan, S.; Zhang, M., RFP tags for labeling secretory pathway proteins. *Biochem. Biophys. Res. Commun.* **2014**, *447*, (3), 508-512.
12. Morise, H.; Shimomura, O.; Johnson, F. H.; Winant, J., Intermolecular energy transfer in the bioluminescent system of *Aequorea*. *Biochemistry* **1974**, *13*, (12), 2656-2662.
13. Prasher, D. C.; Eckenrode, V. K.; Ward, W. W.; Prendergast, F. G.; Cormier, M. J., Primary structure of the *Aequorea victoria* green-fluorescent protein. *Gene* **1992**, *111*, (2), 229-233.
14. Matz, M. V.; Fradkov, A. F.; Labas, Y. A.; Savitsky, A. P.; Zaraisky, A. G.; Markelov, M. L.; Lukyanov, S. A., Fluorescent proteins from nonbioluminescent *Anthozoa* species. *Nat. Biotechnol.* **1999**, *17*, (10), 969-973.
15. Karasawa, S.; Araki, T.; Nagai, T.; Mizuno, H.; Miyawaki, A., Cyan-emitting and orange-emitting fluorescent proteins as a donor/acceptor pair for fluorescence resonance energy transfer. *Biochem. J.* **2004**, *381*, (Pt 1), 307-312.
16. Merzlyak, E. M.; Goedhart, J.; Shcherbo, D.; Bulina, M. E.; Shcheglov, A. S.; Fradkov, A. F.; Gaintzeva, A.; Lukyanov, K. A.; Lukyanov, S.; Gadella, T. W. J.; Chudakov, D. M., Bright monomeric red fluorescent protein with an extended fluorescence lifetime. *Nat. Methods* **2007**, *4*, (7), 555-557.
17. Shcherbo, D.; Murphy, C. S.; Ermakova, G. V.; Solovieva, E. A.; Chepurnykh, T. V.; Shcheglov, A. S.; Verkhusha, V. V.; Pletnev, V. Z.; Hazelwood, K. L.; Roche, P. M.; Lukyanov, S.; Zaraisky, A. G.; Davidson, M. W.; Chudakov, D. M., Far-red fluorescent tags for protein imaging in living tissues. *Biochem. J.* **2009**, *418*, (3), 567-574.
18. Shcherbo, D.; Merzlyak, E. M.; Chepurnykh, T. V.; Fradkov, A. F.; Ermakova, G. V.; Solovieva, E. A.; Lukyanov, K. A.; Bogdanova, E. A.; Zaraisky, A. G.; Lukyanov, S.; Chudakov, D. M., Bright far-red fluorescent protein for whole-body imaging. *Nat. Methods* **2007**, *4*, (9), 741-746.
19. Chudakov, D. M.; Matz, M. V.; Lukyanov, S.; Lukyanov, K. A., Fluorescent proteins and their applications in imaging living cells and tissues. *Physiol. Rev.* **2010**, *90*, (3), 1103-1163.
20. Rhee, J. K.; Hovlid, M.; Fiedler, J. D.; Brown, S. D.; Manzenrieder, F.; Kitagishi, H.; Nycholat, C.; Paulson, J. C.; Finn, M. G., Colorful virus-like particles: fluorescent protein packaging by the Qbeta capsid. *Biomacromolecules* **2011**, *12*, (11), 3977-3981.
21. Seebeck, F. P.; Woycechowsky, K. J.; Zhuang, W.; Rabe, J. P.; Hilvert, D., A simple tagging system for protein encapsulation. *J. Am. Chem. Soc.* **2006**, *128*, (14), 4516-4517.
22. Minten, I. J.; Hendriks, L. J.; Nolte, R. J.; Cornelissen, J. J., Controlled encapsulation of multiple proteins in virus capsids. *J. Am. Chem. Soc.* **2009**, *131*, (49), 17771-17773.
23. Nolles, A.; Westphal, A. H.; de Hoop, J. A.; Fokkink, R. G.; Kleijn, J. M.; van Berkel, W. J. H.; Borst, J. W., Encapsulation of GFP in complex coacervate core micelles. *Biomacromolecules* **2015**, *16*, (5), 1542-1549.

24. Nolles, A.; van Dongen, N. J. E.; Westphal, A. H.; Visser, A. J. W. G.; Kleijn, J. M.; van Berkel, W. J. H.; Borst, J. W., Encapsulation into complex coacervate core micelles promotes EGFP dimerization. *Phys. Chem. Chem. Phys.* **2017**, *19*, (18), 11380-11389.
25. Sniegowski, J. A.; Phail, M. E.; Wachter, R. M., Maturation efficiency, trypsin sensitivity, and optical properties of Arg96, Glu222, and Gly67 variants of green fluorescent protein. *Biochem. Biophys. Res. Commun.* **2005**, *332*, (3), 657-663.
26. Kremers, G. J.; Goedhart, J.; van den Heuvel, D. J.; Gerritsen, H. C.; Gadella, T. W. J., Improved green and blue fluorescent proteins for expression in bacteria and mammalian cells. *Biochemistry* **2007**, *46*, (12), 3775-3783.
27. Goedhart, J.; von Stetten, D.; Noirclerc-Savoye, M.; Lelimousin, M.; Joosen, L.; Hink, M. A.; van Weeren, L.; Gadella, T. W. J.; Royant, A., Structure-guided evolution of cyan fluorescent proteins towards a quantum yield of 93%. *Nat. Commun.* **2012**, *3*, 751.
28. Kremers, G. J.; Goedhart, J.; van Munster, E. B.; Gadella, T. W. J., Cyan and yellow super fluorescent proteins with improved brightness, protein folding, and FRET Forster radius. *Biochemistry* **2006**, *45*, (21), 6570-6580.
29. Sakaue-Sawano, A.; Kurokawa, H.; Morimura, T.; Hanyu, A.; Hama, H.; Osawa, H.; Kashiwagi, S.; Fukami, K.; Miyata, T.; Miyoshi, H.; Imamura, T.; Ogawa, M.; Masai, H.; Miyawaki, A., Visualizing spatiotemporal dynamics of multicellular cell-cycle progression. *Cell* **2008**, *132*, (3), 487-498.
30. Arpino, J. A.; Rizkallah, P. J.; Jones, D. D., Crystal structure of enhanced green fluorescent protein to 1.35 Å resolution reveals alternative conformations for Glu222. *PLoS One* **2012**, *7*, (10), e47132.
31. Albertazzi, L.; Arosio, D.; Marchetti, L.; Ricci, F.; Beltram, F., Quantitative FRET analysis with the EGFP-mCherry fluorescent protein pair. *Photochem. Photobiol.* **2009**, *85*, (1), 287-297.
32. Chong, S.; Mersha, F. B.; Comb, D. G.; Scott, M. E.; Landry, D.; Vence, L. M.; Perler, F. B.; Benner, J.; Kucera, R. B.; Hirvonen, C. A.; Pelletier, J. J.; Paulus, H.; Xu, M. Q., Single-column purification of free recombinant proteins using a self-cleavable affinity tag derived from a protein splicing element. *Gene* **1997**, *192*, (2), 271-281.
33. Evans, T. C., Jr.; Xu, M. Q., Intein-mediated protein ligation: harnessing nature's escape artists. *Biopolymers* **1999**, *51*, (5), 333-342.
34. Xu, M. Q.; Paulus, H.; Chong, S., Fusions to self-splicing inteins for protein purification. *Methods Enzymol.* **2000**, *326*, 376-418.
35. Biasini, M.; Bienert, S.; Waterhouse, A.; Arnold, K.; Studer, G.; Schmidt, T.; Kiefer, F.; Gallo Cassarino, T.; Bertoni, M.; Bordoli, L.; Schwede, T., SWISS-MODEL: modelling protein tertiary and quaternary structure using evolutionary information. *Nucleic Acids Res.* **2014**, *42*, (Web Server issue), W252-258.
36. Arnold, K.; Bordoli, L.; Kopp, J.; Schwede, T., The SWISS-MODEL workspace: a web-based environment for protein structure homology modelling. *Bioinformatics* **2006**, *22*, (2), 195-201.
37. Kiefer, F.; Arnold, K.; Künzli, M.; Bordoli, L.; Schwede, T., The SWISS-MODEL Repository and associated resources. *Nucleic Acids Res.* **2009**, *37*, (Database issue), D387-392.
38. Guex, N.; Peitsch, M. C.; Schwede, T., Automated comparative protein structure modeling with SWISS-MODEL and Swiss-PdbViewer: a historical perspective. *Electrophoresis* **2009**, *30* Suppl 1, S162-173.
39. Subach, O. M.; Malashkevich, V. N.; Zencheck, W. D.; Morozova, K. S.; Piatkevich, K. D.; Almo, S. C.; Verkhusa, V. V., Structural characterization of acylimine-containing blue and red chromophores in mTagBFP and TagRFP fluorescent proteins. *Chem. Biol.* **2010**, *17*, (4), 333-341.
40. Wachter, R. M.; King, B. A.; Heim, R.; Kallio, K.; Tsiens, R. Y.; Boxer, S. G.; Remington, S. J., Crystal structure and photodynamic behavior of the blue emission variant Y66H/Y145F of green fluorescent protein. *Biochemistry* **1997**, *36*, (32), 9759-9765.
41. Rekas, A.; Alattia, J. R.; Nagai, T.; Miyawaki, A.; Ikura, M., Crystal structure of venus, a yellow fluorescent protein with improved maturation and reduced environmental sensitivity. *J. Biol. Chem.* **2002**, *277*, (52), 50573-50578.
42. Kikuchi, A.; Fukumura, E.; Karasawa, S.; Mizuno, H.; Miyawaki, A.; Shiro, Y., Structural characterization of a thiazoline-containing chromophore in an orange fluorescent protein, monomeric Kusabira Orange. *Biochemistry* **2008**, *47*, (44), 11573-11580.
43. Olsson, M. H.; Sondergaard, C. R.; Rostkowski, M.; Jensen, J. H., PROPKA3: Consistent treatment of internal and surface residues in empirical pKa predictions. *J. Chem. Theory Comput.* **2011**, *7*, (2), 525-537.
44. Rostkowski, M.; Olsson, M. H. M.; Sondergaard, C. R.; Jensen, J. H., Graphical analysis of pH-dependent properties of proteins predicted using PROPKA. *BMC Struct. Biol.* **2011**, *11*, 6.
45. Koppel, D. E., Analysis of macromolecular polydispersity in intensity correlation spectroscopy - method of cumulants. *J. Chem. Phys.* **1972**, *57*, (11), 4814-4820.



46. Berne, B. J.; Pecora, R., *Dynamic light scattering with application to chemistry, biology and physics*. Courier Dover: New York, NY, USA, 1976.
47. Provencher, S. W., Contin - a general-purpose constrained regularization program for inverting noisy linear algebraic and integral-equations. *Comput. Phys. Commun.* **1982**, 27, (3), 229-242.
48. Provencher, S. W., A constrained regularization method for inverting data represented by linear algebraic or integral equations. *Comput. Phys. Commun.* **1982**, 27, (3), 213-227.
49. Skakun, V. V.; Hink, M. A.; Digris, A. V.; Engel, R.; Novikov, E. G.; Apanasovich, V. V.; Visser, A. J. W. G., Global analysis of fluorescence fluctuation data. *Eur. Biophys. J.* **2005**, 34, (4), 323-334.
50. Skakun, V. V.; Engel, R.; Digris, A. V.; Borst, J. W.; Visser, A. J. W. G., Global analysis of autocorrelation functions and photon counting distributions. *Front. Biosci., Elite Ed.* **2011**, 3, 489-505.
51. Velapoldi, R. A.; Tonnesen, H. H., Corrected emission spectra and quantum yields for a series of fluorescent compounds in the visible spectral region. *J. Fluoresc.* **2004**, 14, (4), 465-472.
52. Lindhoud, S.; Norde, W.; Cohen Stuart, M. A., Reversibility and relaxation behavior of polyelectrolyte complex micelle formation. *J. Phys. Chem. B* **2009**, 113, (16), 5431-5439.
53. Berman, H. M.; Westbrook, J.; Feng, Z.; Gilliland, G.; Bhat, T. N.; Weissig, H.; Shindyalov, I. N.; Bourne, P. E., The Protein Data Bank. *Nucleic Acids Res.* **2000**, 28, (1), 235-242.
54. Haupts, U.; Maiti, S.; Schwille, P.; Webb, W. W., Dynamics of fluorescence fluctuations in green fluorescent protein observed by fluorescence correlation spectroscopy. *Proc. Natl. Acad. Sci. U. S. A.* **1998**, 95, (23), 13573-13578.
55. Visser, N. V.; Hink, M. A.; Borst, J. W.; van der Krogt, G. N. M.; Visser, A. J. W. G., Circular dichroism spectroscopy of fluorescent proteins. *FEBS Lett.* **2002**, 521, (1-3), 31-35.
56. Brahms, S.; Brahms, J., Determination of protein secondary structure in solution by vacuum ultraviolet circular dichroism. *J. Mol. Biol.* **1980**, 138, (2), 149-178.
57. Woody, R. W., Circular dichroism. *Methods Enzymol.* **1995**, 246, 34-71.
58. Voets, I. K.; de Keizer, A.; Cohen Stuart, M. A., Complex coacervate core micelles. *Adv. Colloid Interface Sci.* **2009**, 147-148, 300-318.
59. Blocher, W. C.; Perry, S. L., Complex coacervate-based materials for biomedicine. *WIREs Nanomed. Nanobiotechnol.* **2017**, 9, (4).
60. Kayitmazer, A. B.; Seyrek, E.; Dubin, P. L.; Staggemeier, B. A., Influence of chain stiffness on the interaction of polyelectrolytes with oppositely charged micelles and proteins. *J. Phys. Chem. B* **2003**, 107, (32), 8158-8165.
61. Cooper, C. L.; Goulding, A.; Kayitmazer, A. B.; Ulrich, S.; Stoll, S.; Turksen, S.; Yusa, S.; Kumar, A.; Dubin, P. L., Effects of polyelectrolyte chain stiffness, charge mobility, and charge sequences on binding to proteins and micelles. *Biomacromolecules* **2006**, 7, (4), 1025-1035.
62. Du, X.; Dubin, P. L.; Hoagland, D. A.; Sun, L., Protein-selective coacervation with hyaluronic acid. *Biomacromolecules* **2014**, 15, (3), 726-734.
63. de Vos, W. M.; Leermakers, F. A.; de Keizer, A.; Cohen Stuart, M. A.; Kleijn, J. M., Field theoretical analysis of driving forces for the uptake of proteins by like-charged polyelectrolyte brushes: effects of charge regulation and patchiness. *Langmuir* **2010**, 26, (1), 249-259.
64. Day, R. N.; Davidson, M. W., The fluorescent protein palette: tools for cellular imaging. *Chem. Soc. Rev.* **2009**, 38, (10), 2887-2892.
65. Miconai, A.; Wien, F.; Kernya, L.; Lee, Y. H.; Goto, Y.; Refregiers, M.; Kardos, J., Accurate secondary structure prediction and fold recognition for circular dichroism spectroscopy. *Proc. Natl. Acad. Sci. U. S. A.* **2015**, 112, (24), E3095-3103.
66. Dolinsky, T. J.; Czodrowski, P.; Li, H.; Nielsen, J. E.; Jensen, J. H.; Klebe, G.; Baker, N. A., PDB2PQR: expanding and upgrading automated preparation of biomolecular structures for molecular simulations. *Nucleic Acids Res.* **2007**, 35, (Web Server issue), W522-525.
67. Baker, N. A.; Sept, D.; Joseph, S.; Holst, M. J.; McCammon, J. A., Electrostatics of nanosystems: application to microtubules and the ribosome. *Proc. Natl. Acad. Sci. U. S. A.* **2001**, 98, (18), 10037-10041.
68. Schrödinger, L. *The MacPyMOL Molecular Graphics System, Version 1.4*, Schrödinger, LLC: New York, NY, USA, 2016.
69. Shealy, P.; Valafar, H., Multiple structure alignment with msTALI. *BMC Bioinf.* **2012**, 13, 105.
70. Robert, X.; Gouet, P., Deciphering key features in protein structures with the new ENDscript server. *Nucleic Acids Res.* **2014**, 42, (Web Server issue), W320-324.
71. Huang, X. Q.; Miller, W., A time-efficient, linear-space local similarity algorithm. *Adv. Appl. Math.* **1991**, 12, (3), 337-357.
72. Yang, T. T.; Cheng, L.; Kain, S. R., Optimized codon usage and chromophore mutations provide enhanced sensitivity with the green fluorescent protein. *Nucleic Acids Res.* **1996**, 24, (22), 4592-4593.

Supplementary information

S4.1. Sequence identities and multiple structural alignment of the FPs

Table S4.1. Sequence identity percentages (%) between pairs of FPs that have been studied. (mT2 = mTurquoise2)

FP variant	mEGFP	SBFP2	mT2	SYFP2	mKO2	TagRFP	mCherry
mEGFP	100	97.1	96.7	97.1	27.5	25.3	29.5
SBFP2	97.1	100	98.3	97.9	27.5	25.3	29.5
mTurquoise2	96.7	98.3	100	97.5	27.5	24.9	29.5
SYFP2	97.1	97.9	97.5	100	28.4	25.8	30.4
mKO2	27.5	27.5	27.5	28.4	100	47.1	48.5
TagRFP	25.3	25.3	24.9	25.8	47.1	100	56.9
mCherry	29.5	29.5	29.5	30.4	48.5	56.9	100

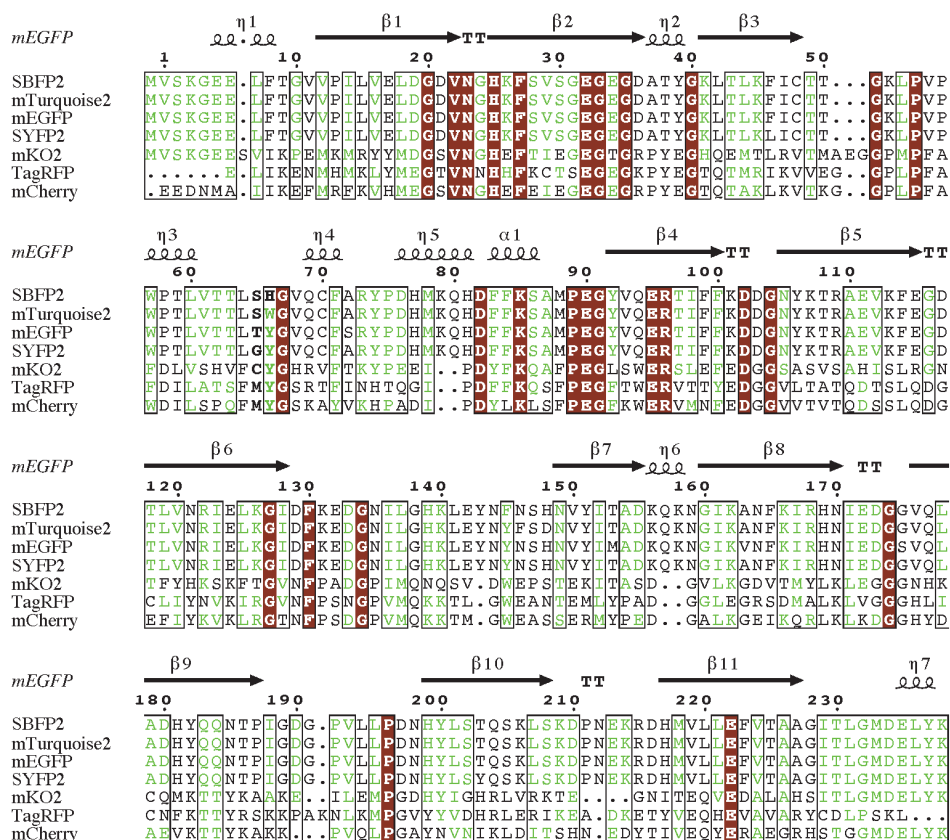


Figure S4.1. Multiple structural alignment of seven FPs that were studied. Protein structures were aligned using msTALI software.⁶⁹ The alignment was then manually adjusted and drawn using ESPrpt 3.0 software.⁷⁰ Strictly conserved amino acid residues are shown with brown background and similar amino acid residues are boxed and shown in green. The amino acid residues forming the chromophore are indicated in bold letters. Secondary structure elements derived from mEGFP (PDB entry 4EUL³⁰) are depicted as arrows (representing β -strands), coils (representing α - and 3^{10} -helices), and TT letters (representing turns). The numbering is based on that of mEGFP.

S4.2. Sequence alignment of all FPs with their PDB entries

```

          10      20      30      40      50      60
SBFP2  VSKGEELFTGVVPIILVELDGDVNGHKFSVSGEGEGDATYGKLTCLKFICTTGKLPVPWPTL
      .....
1BFP   MSKGEELFTGVVPIILVELDGDVNGHKFSVSGEGEGDATYGKLTCLKFICTTGKLPVPWPTL
          10      20      30      40      50      60

          70      80      90     100     110     120
SBFP2  VTTLSHGVQCFARYPDHMKQHDFFKSAMPEGYVQERTIFFKDDGNYKTRAEVKFEGDTLV
      .....
1BFP   VTTFSHGVQCFSRYPDHMKRHDFFKSAMPEGYVQERTIFFKDDGNYKTRAEVKFEGDTLV
          70      80      90     100     110     120

          130     140     150     160     170     180
SBFP2  NRIELKGIIDFKEDGNILGHKLEYNFNHNVYITADKQKNGIKANFKIRHNIEDGGVQLAD
      .....
1BFP   NRIELKGIIDFKEDGNILGHKLEYNFNHNVYIMADKQKNGIKVNFKIRHNIEDGVSQVLAD
          130     140     150     160     170     180

          190     200     210     220     230
SBFP2  HYQQNTPIGDGPVLLPDNHYLSTQSKLSKDPNEKRDHMLLEFVTAAGITLGMDELYK
      .....
1BFP   HYQQNTPIGDGPVLLPDNHYLSTQSALSKDPNEKRDHMLLEFVTAAGITLGMDELYK
          190     200     210     220     230
    
```

Figure S4.2. Pairwise sequence alignment of SBFP2 with the template 1BFP generated by lalign.⁷¹ The identical (double points) and similar (single point) residues are highlighted.

```

          10      20      30      40      50      60
mT2    MVSKGEELFTGVVPIILVELDGDVNGHKFSVSGEGEGDATYGKLTCLKFICTTGKLPVPWPTL
      .....
3ZTF   MVSKGEELFTGVVPIILVELDGDVNGHKFSVSGEGEGDATYGKLTCLKFICTTGKLPVPWPTL
          10      20      30      40      50      60

          70      80      90     100     110     120
mT2    LVTTLSWGVCQCFARYPDHMKQHDFFKSAMPEGYVQERTIFFKDDGNYKTRAEVKFEGDTL
      .....
3ZTF   LVTTLSWGVCQCFARYPDHMKQHDFFKSAMPEGYVQERTIFFKDDGNYKTRAEVKFEGDTL
          70      80      90     100     110     120

          130     140     150     160     170     180
mT2    VNRIELKGIIDFKEDGNILGHKLEYNFYSDNVYITADKQKNGIKANFKIRHNIEDGGVQLA
      .....
3ZTF   VNRIELKGIIDFKEDGNILGHKLEYNFYSDNVYITADKQKNGIKANFKIRHNIEDGGVQLA
          130     140     150     160     170     180

          190     200     210     220     230
mT2    DHYQQNTPIGDGPVLLPDNHYLSTQSKLSKDPNEKRDHMLLEFVTAAGITLGMDELYK
      .....
3ZTF   DHYQQNTPIGDGPVLLPDNHYLSTQSALSKDPNEKRDHMLLEFVTAAGITLGMDELYK
          190     200     210     220     230
    
```

Figure S4.3. Pairwise sequence alignment of mTurquoise2 (mT2) with the template 3ZTF generated by lalign.⁷¹ The identical (double points) and similar (single point) residues are highlighted.



```

      10      20      30      40      50      60
mEGFP  MVSKGEELFTGVVPIILVELDGDVNGHKFSVSGEGEGDATYGKLTTLKFICTTGKLPVPWPT
      .....
4EUL   MVSKGEELFTGVVPIILVELDGDVNGHKFSVSGEGEGDATYGKLTTLKFICTTGKLPVPWPT
      10      20      30      40      50      60

      70      80      90      100     110     120
mEGFP  LVTTLTYGVQCFSRYPDHMKQHDFFKSAMPEGYVQERTIFFKDDGNYKTRAEVKFEGDTL
      .....
4EUL   LVTTLTYGVQCFSRYPDHMKQHDFFKSAMPEGYVQERTIFFKDDGNYKTRAEVKFEGDTL
      70      80      90      100     110     120

      130     140     150     160     170     180
mEGFP  VNRIELKGIDFKEDGNILGHKLEYNYNShNVYIMADKQKNGIKVNFKIRHNIEDGSVQLA
      .....
4EUL   VNRIELKGIDFKEDGNILGHKLEYNYNShNVYIMADKQKNGIKVNFKIRHNIEDGSVQLA
      130     140     150     160     170     180

      190     200     210     220     230
mEGFP  DHYQQNTPIGDGPVLLPDNHYLSTQSKLSKDPNEKRDHMLLEFVTAAGITLGMDELYK
      .....
4EUL   DHYQQNTPIGDGPVLLPDNHYLSTQALSADPNEKRDHMLLEFVTAAGITLGMDELYK
      190     200     210     220     230

```

Figure S4.4. Pairwise sequence alignment of mEGFP with the template 4EUL generated by lalign.⁷¹ The identical (double points) and similar (single point) residues are highlighted.

```

      10      20      30      40      50      60
SYFP2  MVSKGEELFTGVVPIILVELDGDVNGHKFSVSGEGEGDATYGKLTTLKLICTTGKLPVPWPT
      .....
1MYW   MVSKGEELFTGVVPIILVELDGDVNGHKFSVSGEGEGDATYGKLTTLKLICTTGKLPVPWPT
      10      20      30      40      50      60

      70      80      90      100     110     120
SYFP2  LVTTLGYGVQCFARYPDHMKQHDFFKSAMPEGYVQERTIFFKDDGNYKTRAEVKFEGDTL
      .....
1MYW   LVTTLGYGLQCFARYPDHMKQHDFFKSAMPEGYVQERTIFFKDDGNYKTRAEVKFEGDTL
      70      80      90      100     110     120

      130     140     150     160     170     180
SYFP2  VNRIELKGIDFKEDGNILGHKLEYNYNShNVYITADKQKNGIKANFKIRHNIEDGGVQLA
      .....
1MYW   VNRIELKGIDFKEDGNILGHKLEYNYNShNVYITADKQKNGIKANFKIRHNIEDGGVQLA
      130     140     150     160     170     180

      190     200     210     220     230
SYFP2  DHYQQNTPIGDGPVLLPDNHYLSYQSKLSKDPNEKRDHMLLEFVTAAGITLGMDELYK
      .....
1MYW   DHYQQNTPIGDGPVLLPDNHYLSYQSALSADPNEKRDHMLLEFVTAAGITHGMDELYK
      190     200     210     220     230

```

Figure S4.5. Pairwise sequence alignment of SYFP2 with the template 1MYW generated by lalign.⁷¹ The identical (double points) and similar (single point) residues are highlighted.


```

      10      20      30      40      50      60
mKO2  SVIKPEMKMRYYMDGSGVNGHEFTIEEGTGRPYEGHQEMTLRVMTAEGGPMPPAFDLVSH
      .....
2ZMU  SVIKPEMKMRYYMDGSGVNGHEFTIEEGTGRPYEGHQEMTLRVMTAKGGPMPPAFDLVSH
      10      20      30      40      50      60

      70      80      90      100     110     120
mKO2  VFCYGHRVFTKYPEEIPDYFKQAFPEGLSWERSLEFEDGGSASVSAHISLRGNTFYHKS
      .....
2ZMU  VFCYGHRPFTKYPEEIPDYFKQAFPEGLSWERSLEFEDGGSASVSAHISLRGNTFYHKS
      70      80      90      100     110     120

      130     140     150     160     170     180
mKO2  FTGVNFPADGPIMQNQSVDEWEPSTEKITASDGVKGDVTMYLKLGGGNHCKQMKTTYKA
      .....
2ZMU  FTGVNFPADGPIMQNQSVDEWEPSTEKITASDGVKGDVTMYLKLGGGNHCKQFKTTYKA
      130     140     150     160     170     180

      190     200     210     220
mKO2  AKEILEMPGDHYIGHRLVRKTEGNITEQVEDALAH
      .....
2ZMU  AKKILKMPGSHYISHRLVRKTEGNITELVEDAVAHS
      190     200     210

```

Figure S4.6. Pairwise sequence alignment of mKO2 with the template 2ZMU generated by lalign.⁷¹ The identical (double points) and similar (single point) residues are highlighted.

```

      10      20      30      40      50      60
TagRFP MVSKGEELIKENMHMKLYMEGTVNHHFKCTSEGEKPYEGTQTMRIKVVGGPLPFAFD
      .....
3M22  MVSKGEELIKENMHMKLYMEGTVNHHFKCTSEGEKPYEGTQTMRIKVVGGPLPFAFD
      10      20      30      40      50      60

      70      80      90      100     110     120
TagRFP ILATSFMYGSRTFINHTQGIPDFFKQSFPEGFTWERVTTYEDGGVLTATQDTSLQDGLI
      .....
3M22  ILATSFMYGSRTFINHTQGIPDFFKQSFPEGFTWERVTTYEDGGVLTATQDTSLQDGLI
      70      80      90      100     110     120

      130     140     150     160     170     180
TagRFP YNVKIRGVNFPNPGVPMQKKTGLWEANTEMLYPADGGLEGRSDMALKLVGGGHLICNFKT
      .....
3M22  YNVKIRGVNFPNPGVPMQKKTGLWEANTEMLYPADGGLEGRSDMALKLVGGGHLICNFKT
      130     140     150     160     170     180

      190     200     210     220     230
TagRFP TYRSKPKAKNLKMPGVVYVDHRLERIKEADKETYVEQHEVAVARYCDLPSKLLYK
      .....
3M22  TYRSKPKAKNLKMPGVVYVDHRLERIKEADKETYVEQHEVAVARYCDLPSKLGHK
      190     200     210     220     230

```

Figure S4.7. Pairwise sequence alignment of TagRFP with the template 3M22 generated by lalign.⁷¹ The identical (double points) and similar (single point) residues are highlighted.



```

          10      20      30      40      50      60
mCherry  MVSKGEEDNMAI IKEFMRFKVHMEGSVNGHEFEIEGEGEGRPEYEGTQTAKLKVTKGGPLP
          .....
2H5Q     MVSKGEEDNMAI IKEFMRFKVHMEGSVNGHEFEIEGEGEGRPEYEGTQTAKLKVTKGGPLP
          10      20      30      40      50      60

          70      80      90      100     110     120
mCherry  FAWDILSPQFMYGSKAYVKHPADIPDYLKLSFPEGFKWERVMNFEDGGVVTVTQDSSLQD
          .....
2H5Q     FAWDILSPQFMYGSKAYVKHPADIPDYLKLSFPEGFKWERVMNFEDGGVVTVTQDSSLQD
          70      80      90      100     110     120

          130     140     150     160     170     180
mCherry  GEFYIKVKLRGTFNPSDGPVMQKKTMGWEASSERMPYEDGALKGEIKQRLKLDGGHYDA
          .....
2H5Q     GEFYIKVKLRGTFNPSDGPVMQKKTMGWEASSERMPYEDGALKGEIKQRLKLDGGHYDA
          130     140     150     160     170     180

          190     200     210     220     230
mCherry  EVKTTYKAKKPVQLPGAYNVNIKLDITSHNEDYTIVEQYERAEGRHSTGGMDELYK
          .....
2H5Q     EVKTTYKAKKPVQLPGAYNVNIKLDITSHNEDYTIVEQYERAEGRHSTGGMDELYK
          190     200     210     220     230

```

Figure S4.8. Pairwise sequence alignment of mCherry with the template 2H5Q generated by lalign.⁷¹ The identical (double points) and similar (single point) residues are highlighted.

S4.3. FP characteristics

Table S4.2 shows the characteristics of the studied FPs. Next to the standard characteristics, some specific features for this article are given, *i.e.*, charge, monomeric quality and dissociation constant. The net charge of the FPs at pH 9.0 or pH 10.0 is given, which were calculated using the software package PROPKA 3.1.^{43,44} The monomeric qualities of more than 40 FPs were determined by Cranfill, *et al.*⁷ For this, they fused FPs onto an endoplasmic reticulum (ER) membrane protein (CytERM). If the FP formed homo-oligomers due to high effective concentrations, the ER configured from a tubular network into an organized smooth ER whorl structure. The percentage of observed cells exhibiting an organized smooth ER whorl structure was related to the monomeric quality of the FPs. The dissociation constants were determined by sedimentation equilibrium analytical ultracentrifugation experiments. The A206K mutation introduced into yellow fluorescent protein (YFP) increased the dissociation constant from 0.11 to 74 mM.⁸ This mutation is present in SBFP2, mTurquoise2, mEGFP, and SYFP2, providing these proteins with dissociation constants of about 74 mM. Next to that, mTurquoise2 bears the N146F mutation resulting in an increased dissociation constant.¹⁰ The K_D of mKO2 is not determined so far. The dissociation constants of TagRFP and mCherry were investigated by Han, *et al.*¹¹ For TagRFP a K_D of 0.038 mM was found and the K_D of mCherry was beyond the limit of their instrument.

Table S4.2. Properties of the studied FPs.

FP variant	λ_{ex} (nm)	λ_{em} (nm)	EC ($\text{M}^{-1} \text{cm}^{-1}$)	QY	pK _a	pI	Charge ^c	Monomeric quality (%) ^e	K _p (mM)	Reference
SBFP2	380	446	34000	0.47	5.5	5.59	-8.96	nd	74.0 ^{f,g}	Kremers, <i>et al.</i> [26]
mTurquoise2	434	474	30000	0.93	3.1	5.29	-11.30	93.8	> 74.0 ^{f,g,h}	Goedhart, <i>et al.</i> [27]
mEGFP	488	507	56000	0.60	6.0	5.49	-9.87	98.1	74.0 ^{f,g}	Yang, <i>et al.</i> [72]
SYFP2	515	527	101000	0.68	6.0	5.62	-9.75	nd	74.0 ^{f,g}	Kremers, <i>et al.</i> [28]
mKO2	551	565	63800	0.62	5.5	5.48	-13.09	68.4	nd	Sakaue-Sawano, <i>et al.</i> [29]
TagRFP	555	584	100000	0.48	3.8	7.43	-10.35	57.7	0.038 ⁱ	Merzlyak, <i>et al.</i> [16]
mCherry	587	610	72000	0.22	4.5 ^a , 10.3 ^b	5.70	-8.93	95.0	> 0.050 ⁱ	Shaner, <i>et al.</i> [1]

^afrom Shaner, *et al.* [26]; ^bfrom Shu, *et al.* [27]; ^cCharge based on PROPKA 3.1 results, determined at their respective pH value used for the experiments;

^dValue determined at pH 10; ^efrom Cranfill, *et al.* [12]; ^ffrom Zachariás, *et al.* [20]; ^gValue based on the presence of the $\Delta 206\text{K}$ mutation; ^hfrom von Stetten, *et al.* [71];

ⁱfrom Han, *et al.* [53]; nd, not determined.

S4.4. Dynamic light scattering results

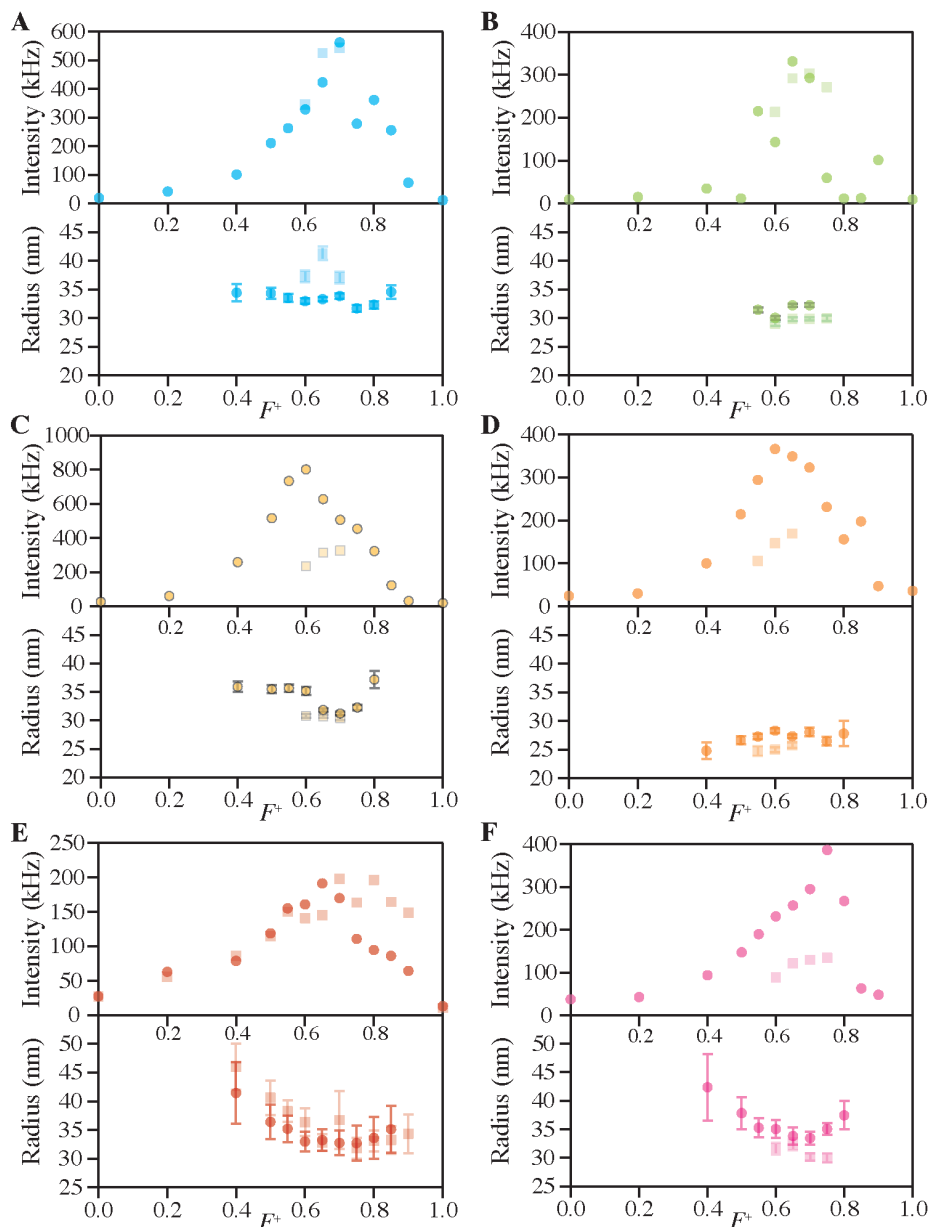


Figure S4.9. DLS composition results of (A) mTurquoise2, (B) mEGFP, (C) SYFP2, (D) mKO2, (E) TagRFP, and (F) mCherry with P2MVP₄₁-b-PEO₂₀₅ (light colored squares) and P2MVP₁₂₈-b-PEO₄₇₇ (dark colored dots) wherein the concentration of protein was kept constant. Top graphs show scattered intensity as a function of the F^+ composition, and bottom graphs show hydrodynamic radius as a function of the F^+ composition. Error bars show the distribution of radii in one experiment.

S4.5. Fluorescence correlation spectroscopy results

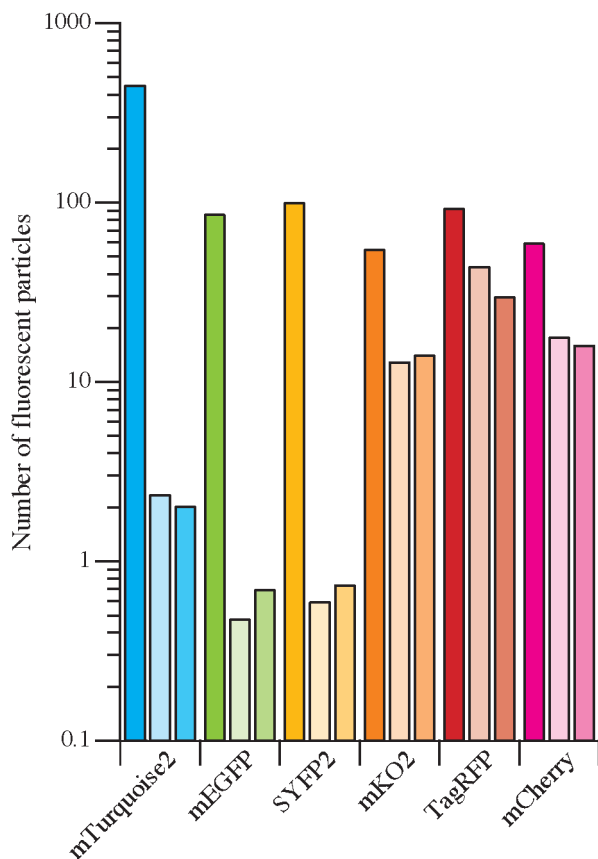


Figure S4.10. FCS results the number of fluorescent particles measured of all used FPs (except SBFP2) free in solution (darkest colored, left bars), and measured at the PMC with P2MVP₄₁-b-PEO₂₀₅ (light colored, middle bars) and P2MVP₁₂₈-b-PEO₄₇₇ (dark colored, right bars).



S4.6. Absorption spectral analysis

Absorption spectra were recorded on a Hewlett Packard 8453 diode array spectrophotometer in 10 mM borate buffer at pH 9.0 for SBFP2, mTurquoise2, mEGFP, SYFP2, mKO2, and mCherry and at pH 10.0 for TagRFP at 20°C. Spectrophotometer settings were controlled using the UV-Visible ChemStation software package (Hewlett Packard). Samples with concentrations of 1 μM FP were measured free in buffered solution as well as encapsulated with P2MVP₄₁-*b*-PEO₂₀₅ and P2MVP₁₂₈-*b*-PEO₄₇₇ at their respective PMCs.

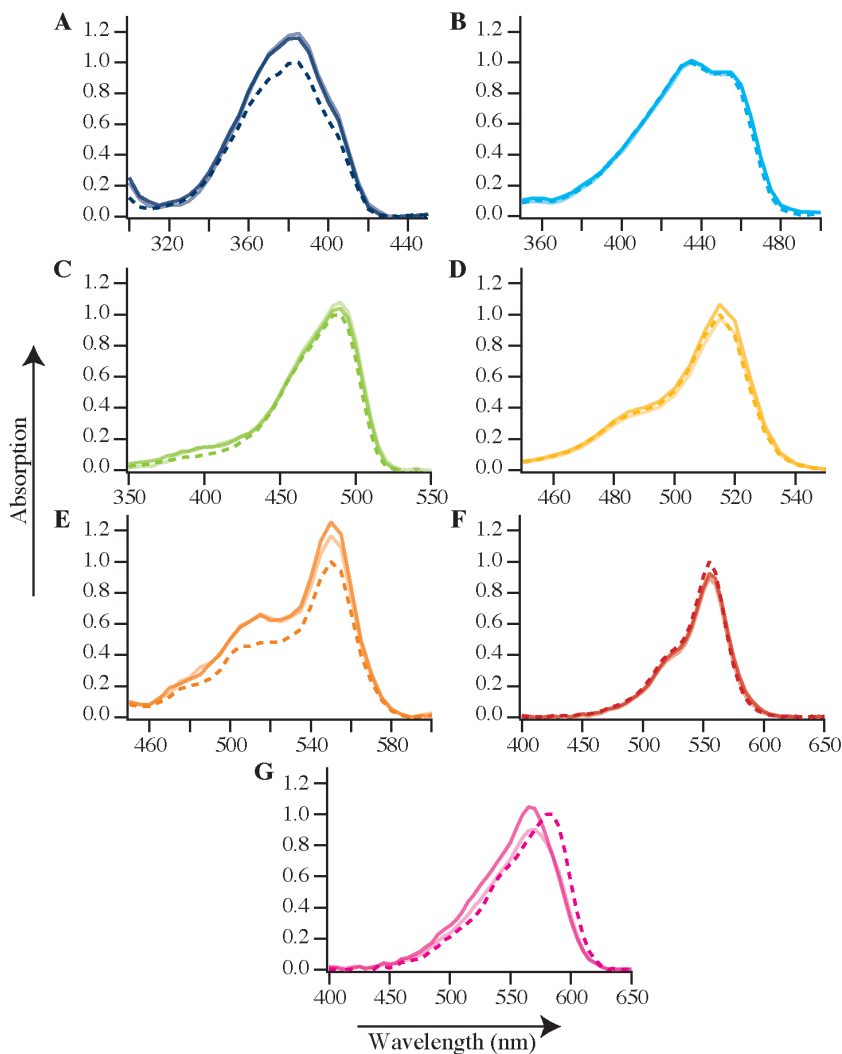


Figure S4.11. Normalized absorption spectra of (A) SBFP2, (B) mTurquoise2, (C) mEGFP, (D) SYFP2, (E) mKO2, (F) TagRFP, and (G) mCherry for proteins free in solution (dashed lines) and encapsulated proteins in C3Ms at their respective PMCs with P2MVP₄₁-*b*-PEO₂₀₅ (solid light colored line) and P2MVP₁₂₈-*b*-PEO₄₇₇ (solid dark colored line). The spectra are normalized to those of the free proteins.

S4.7. Steady-state fluorescence at different pH values

Fluorescence excitation and emission spectra were measured using a Cary Eclipse spectrofluorimeter (Varian). Excitation and emission slits were set to yield bandwidths of 5 nm. All measurements were performed at 20°C. A master buffer was used consisting of 20 mM sodium phosphate, 20 mM citric acid, 10 mM glycine, and 150 mM NaCl adjusted to the desired pH by addition of NaOH. Samples with concentrations of 1 μM FP at pH 5.2, 7.1, 9.0, and 10.0 were measured.

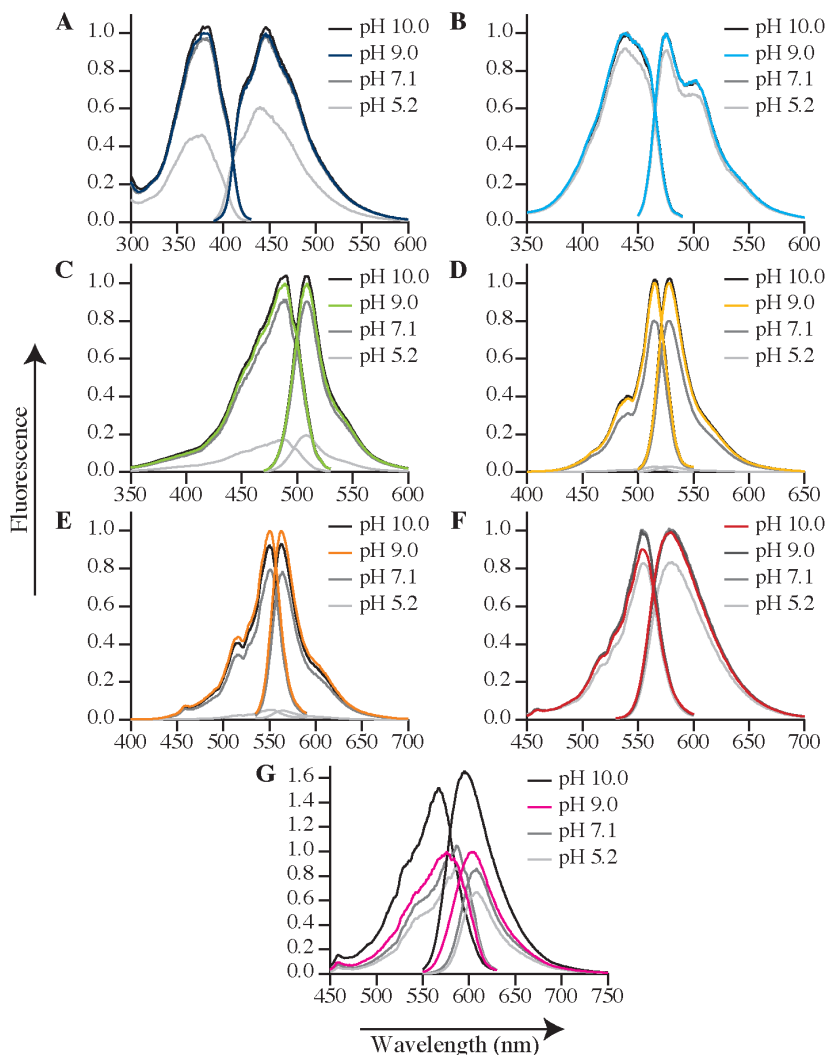


Figure S4.12. Normalized fluorescence excitation and emission spectra of (A) SBFP2, (B) mTurquoise2, (C) mEGFP, (D) SYFP2, (E) mKO2, (F) TagRFP, and (G) mCherry in solutions with different pH values. The spectra are colored according to the FP at the respective pH: pH 9.0 for SBFP2, mTurquoise2, mEGFP, SYFP2, mKO2, and mCherry and pH 10.0 for TagRFP. Spectra are normalized to the FPs at pH 9.0.

S4.8. High tension graphs related to the far-UV CD spectra

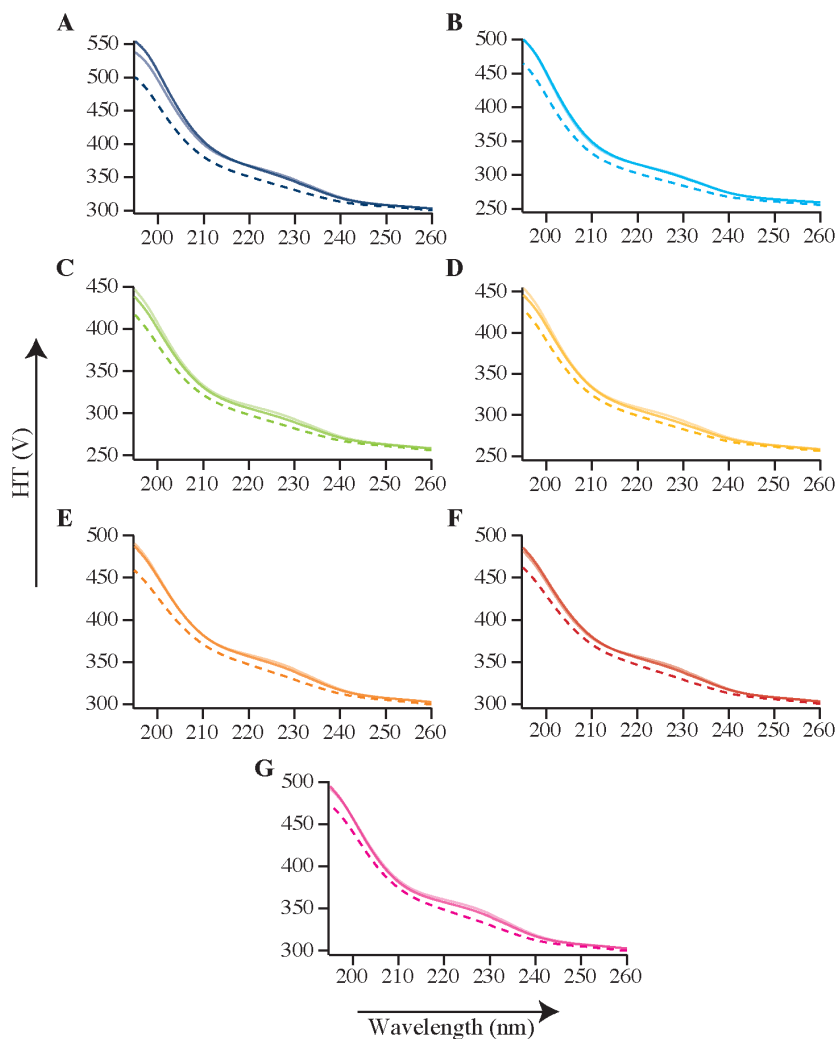
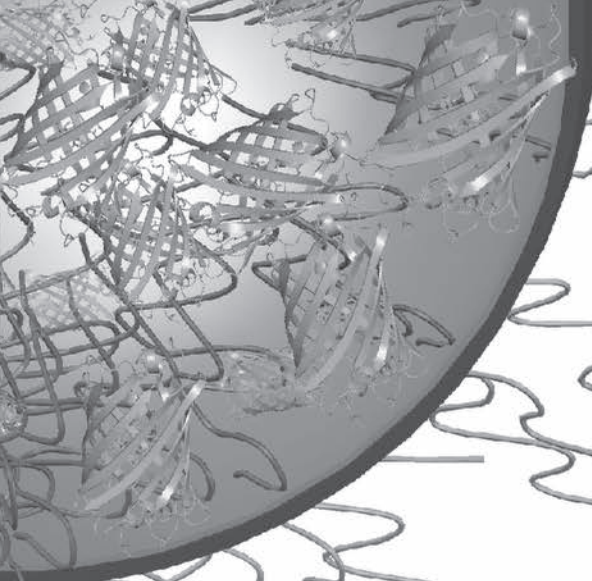


Figure S4.13. High tension (HT) signals of free FPs (dashed lines) and encapsulated with P2MVP₄₁-b-PEO₂₀₅ (solid light colored line) and P2MVP₁₂₈-b-PEO₄₇₇ (solid dark colored line) belonging to the far-UV CD spectra in Figure 4.6: (A) SBFP2, (B) mTurquoise2 (mT2), (C) mEGFP, (D) SYFP2, (E) mKO2, (F) TagRFP, and (G) mCherry, respectively.



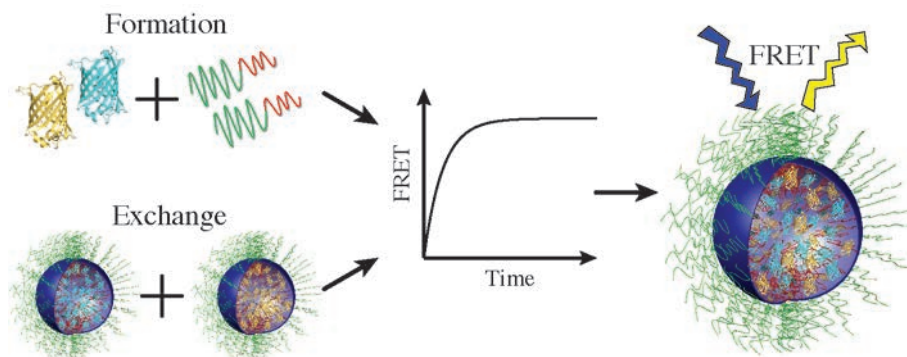
Chapter 5

FRET reveals formation and exchange dynamics of protein-containing complex coacervate core micelles

Submitted as: A. Nolles, E. Hooiveld, A. H. Westphal, W. J. H. van Berkel, J. M. Kleijn, and J. W. Borst.

Abstract

Encapsulation of proteins into complex coacervate core micelles (C3Ms) is of potential interest for a wide range of applications. To address the stability and dynamic properties of these polyelectrolyte complexes, combinations of cyan, yellow, and blue fluorescent proteins were encapsulated with the cationic-neutral diblock copolymer poly(2-methyl-vinyl-pyridinium)₁₂₈-*b*-poly(ethylene-oxide)₄₇₇. Förster resonance energy transfer (FRET) allowed us to determine the kinetics of C3M formation and of protein exchange between C3Ms. Both processes follow first-order kinetics with relaxation times of about 100 s at low ionic strength ($I = 2.5$ mM). Stability studies revealed that 50% of FRET was lost at $I = 20$ mM, pointing at disintegration of the C3Ms. Based on experimental and theoretical considerations, we propose that C3Ms relax to their final state by association and dissociation of near-neutral soluble protein-polymer complexes. To obtain protein-containing C3Ms suitable for applications it is necessary to improve the rigidity and salt stability of these complexes.



5.1. Introduction

Encapsulation of proteins is important in many applications, such as controlled delivery of functional ingredients in foods, medical formulations, industrial enzymatic processes, and storage of proteins. In all cases, it is required to achieve adequate encapsulation while keeping bioactivity or functionality intact. Micelles composed of polyelectrolyte complexes, so-called complex coacervates core micelles (C3Ms), are promising structures for protein protection, stabilization and controlled delivery.¹⁻⁶ They are simple to prepare by mixing protein solutions with oppositely charged diblock copolymer solutions at stoichiometric charge ratio.^{7,8} Micellar structures are then spontaneously formed and are small enough to remain in solution. The inner core of C3Ms has a high loading capacity; hundreds of protein molecules can be incorporated into one micelle.¹ The micellar core provides a relatively water-rich environment, thereby shielding protein molecules from the bulk solution while protein structure and functionality are preserved and any immune response is reduced. Since formation of C3Ms is driven by electrostatic interactions, contributed by coulombic attraction and entropic counter-ion release⁹⁻¹¹, pH and ionic strength strongly influence formation, dynamics and stability of these complexes.

While the structure and morphology of C3Ms have been the subject of many studies, stability and dynamical aspects of micelles and the exchange between individual C3Ms have been scarcely investigated. Back in 1998, Cohen Stuart and co-workers were the first to study the rate of formation of C3Ms, composed of poly((dimethylamino)ethyl-methacrylate)-*ω*-poly(glyceryl-methacrylate) (PDMAEMA-*ω*-PGMA) and poly(acrylic-acid)₁₅₈ (PAA₁₅₈), using dynamic light scattering.⁷ They found that micelle formation took place at time scales from 0.01 to 100 s depending on the ionic strength. Before equilibrium was reached, a relatively high transient turbidity was found, which they attributed to macroscopic phase separation (formation of transient large aggregates) at short timescales (< 1 ms) after which the dense phase rearranges into C3Ms. A corresponding molecular model was tested using self-consistent field theory.¹² Similar results were found by Hofs *et al.*,¹³ for C3Ms consisting of poly([4-(2-aminoethylthio)butylene]hydrochloride)₄₉-*b*-poly(ethylene-oxide)₂₁₂ (PAETB₄₉-*b*-PEO₂₁₂) and poly(acrylic-acid) (PAA) of various lengths. For formation of C3Ms from poly((methacryloyloxyethyl)trimethylammonium-chloride)₅₃₀ (PMOTAC₅₃₀) and poly(ethylene-oxide)₁₁₃-*b*-poly(methacrylic-acid)_{122 or 294} (PEO₁₁₃-*b*-PMAA_{122 or 294}) at an ionic strength of 10 mM, Holappa *et al.*,¹⁴ found two processes occurring on different time scales: a process with a kinetic coefficient of 0.0126 s⁻¹, which was attributed to ‘insertion and expulsion’ of single chains, and a slow process with a kinetic coefficient of 7.77 × 10⁻⁵ s⁻¹, which was attributed to ‘merging and splitting’ of C3Ms. The final equilibrium state of C3Ms was reached only after about 16 h. The authors discussed their findings in terms of a model that was introduced by Dormidontova¹⁵, describing micellization of polymeric surfactants (hydrophilic-hydrophobic block copolymers). Zhang *et al.*,¹⁶ also referred to this model for the formation of their C3Ms in deionized water composed of poly(ethylene-oxide)₁₁₃-*b*-poly(sodium-4-styrene-sulfonate)₄₇ (PEO₁₁₃-*b*-PSSNa₄₇) and poly(ethylene-oxide)₁₁₃-*b*-poly(quaternized-2-(dimethylamino)ethyl-methacrylate)₄₈ (PEO₁₁₃-*b*-PQDMA₄₈).

They observed a fast relaxation process (within 2.6 ms), which they related to an initial quasi-equilibrium complex formation. A slower process (within 0.4 s) was attributed to structural rearrangements leading to final equilibrium complexes and supposed to proceed through a micelle fusion-fission mechanism. Very long relaxation times were reported by Lindhoud *et al.*,⁴ for two protein containing three-component C3Ms, *i.e.*, PAA₄₂-*b*-PAAm₄₁₇/PDMAEMA₁₅₀/lysozyme (poly(acrylic-acid)₄₂-*b*-poly(acryl-amide)₄₁₇ and poly(N,N-dimethylaminoethyl-methacrylate)₁₅₀, respectively) and P2MVP₄₁-*b*-PEO₂₀₅/PAA₁₃₉/α-lactalbumin (poly(2-methyl-vinyl-pyridinium-iodide)₄₁-*b*-poly(ethylene-oxide)₂₀₅ and poly(acrylic-acid)₁₃₉, respectively), at low ionic strength. For lysozyme containing C3Ms a relaxation time of two days was found, while C3Ms containing α-lactalbumin did not reach equilibrium in their experiment of two weeks. Differences in relaxation behavior were explained from the diversity in molecular properties, in particular the nature of used polyelectrolytes: weak or strong. The authors pointed to the possible advantage of quenched systems in which over longer periods no rearrangements in micelles occur, so that proteins are really trapped and cannot leave them.

Understanding the dynamics and stability of C3Ms under different conditions is crucial for designing functional structures. Previously, we have studied encapsulation of a range of different fluorescent proteins (FPs).¹⁷ The results showed that mTurquoise2 (a cyan FP) and SYFP2 (strongly enhanced yellow fluorescent protein 2), both derived from *Aequorea victoria* green fluorescent protein (GFP), are the best candidates for Förster resonance energy transfer (FRET) studies regarding dynamics of C3Ms. Based on similar preferred micellar compositions (PMCs), C3M sizes, and encapsulation efficiencies, we concluded that these FPs are encapsulated in the same way and with the same affinity. Moreover, for both proteins, encapsulation in C3Ms resulted in only minor changes in fluorescence properties. Next to that, the mTurquoise2-SYFP2 combination is a good FRET pair, because of the high quantum yield of mTurquoise2 ($\Phi_{mTurquoise2} = 0.93$) and the high molar extinction coefficient of SYFP2 ($\epsilon_{SYFP2} = 101\,000\text{ M}^{-1}\text{ cm}^{-1}$).^{18,19} In addition to these two FPs, SBFP2 (strongly enhanced blue fluorescent protein 2, derived from *Aequorea victoria* GFP) was used as an invisible protein substitute to lower the fluorescence signal of interest while keeping the total protein concentration constant.¹⁷

In the present study, C3Ms were prepared from the above-mentioned FPs in combination with poly(2-methyl-vinyl-pyridinium)₁₂₈-*b*-poly(ethylene-oxide)₄₇₇ (P2MVP₁₂₈-*b*-PEO₄₇₇), because this diblock copolymer shows only little effect on the fluorescence properties of FPs upon encapsulation.¹⁷ FRET was used to study the kinetics of formation of C3Ms, the dynamics of protein exchange between these structures, and their salt stability. Based on our results, we propose a model to describe formation and relaxation of C3Ms. The obtained results allow us to develop strategies generating a tunable stability of micelles for different applications.

5.2. Experimental section

5.2.1. Materials

Poly(2-vinyl-pyridinium)₁₂₈-*b*-poly(ethylene-oxide)₄₇₇ (P2VP₁₂₈-*b*-PEO₄₇₇, PolymerSource, $M_w/M_n = 1.10$, $M_n = 34.5$ kg/mol) was quaternized following a procedure described elsewhere.¹ For P2MVP₁₂₈-*b*-PEO₄₇₇ ($M_n = 50.8$ kg/mol) a final degree of quaternization of approximately 87% was obtained. A stock solution of P2MVP₁₂₈-*b*-PEO₄₇₇ (50 μ M) was prepared by dissolving the polymer in 10 mM borate buffer (pH 9.0) and stored at -20°C . All solutions were filtered through 0.20 μ m poly(ether-sulfone) membrane syringe filters (Advanced Microdevices Pvt. Ltd.). All other chemicals were from commercial sources and of the purest grade available.

5.2.2. Protein production

The genes of mTurquoise2 and SYFP2-His were cloned into the bacterial expression vector pTYB12 (New England Biolabs Inc.) to generate FP fusions with a chitin-binding domain and an intein.²⁰⁻²² The cDNA of SBFP2 in a pRSETb vector was kindly provided by Dr. Joachim Goedhart, University of Amsterdam.²³ For protein production, *E. coli* BL21 cells were used. Details on protein production and purification are described elsewhere.² After on-column cleavage, mTurquoise2 and SYFP2-His were acquired without the chitin-binding domain. SBFP2 and SYFP2 still contained the His-tag after purification. Purified protein stock solutions of mTurquoise2 (21.7 μ M), SYFP2 (29.5 μ M), and SBFP2 (35.5 μ M) were stored in 10 mM borate buffer (pH 9.0) at 4°C .

Protein concentrations were determined with a Pierce BCA protein assay (Pierce Biotechnology), using a bovine serum albumin standard as reference. The purity of the fluorescent proteins was checked by SDS-PAGE.

5.2.3. Absorption and steady-state fluorescence spectroscopy

Absorption spectra of 1 μ M SBFP2, mTurquoise2, or SYFP2 in 10 mM borate buffer (pH 9.0) were recorded on a Hewlett Packard 8453 diode array spectrophotometer at 20°C . Spectrophotometer settings were controlled using the UV-Visible ChemStation software package (Hewlett Packard).

Steady-state fluorescence spectra were recorded on a Cary Eclipse spectrofluorimeter (Varian Inc.). Excitation and emission slits were set to yield bandwidths of 5 nm. Samples were measured in 1 mL quartz cuvettes with a path length of 1 cm. Fluorescence emission spectra of 1 μ M SBFP2, mTurquoise2, and SYFP2 in 10 mM borate buffer (pH 9.0) were separately measured at an excitation wavelength of 350 nm, 440 nm, and 490 nm, respectively. For the FRET experiments, fluorescence emission spectra were obtained using an excitation wavelength of 440 nm and emission was recorded between 450 nm and 600 nm. FRET ratios were determined from donor (475 nm) and acceptor channels (527 nm, Figure 5.1). All measurements and incubations prior to the measurements were performed at 20°C .

5.2.4. C3M preparations

In general, encapsulation of FPs with polymers into C3Ms was achieved by first diluting fluorescent protein stock solutions in 10 mM borate buffer (pH 9.0) to a final protein concentration of 1 μ M and FRET pair composition of 1:1 (mTurquoise2:SYFP2), followed by addition of polymer. C3Ms were prepared at a F^+ ratio of 0.70, which is the preferred micellar composition (PMC) at pH 9.0 of proteins

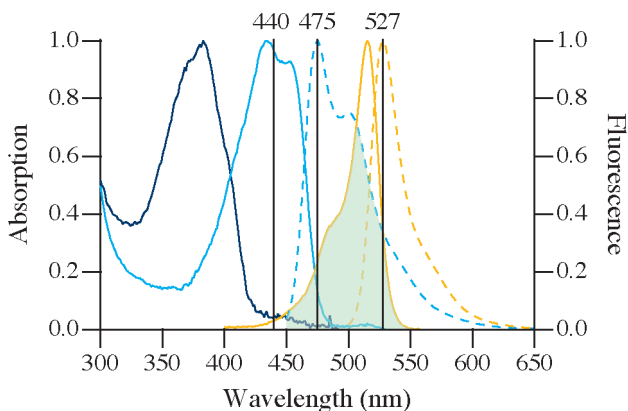


Figure 5.1. Normalized absorption (solid lines) and fluorescence emission (dashed lines) spectra of SBFP2 (blue line), mTurquoise2 (cyan lines), and SYFP2 (orange lines). The listed wavelengths at the top of the graph indicate from left to right: excitation wavelength of mTurquoise2 (donor excitation), emission wavelength of mTurquoise2 (donor channel), and emission wavelength of SYFP2 (acceptor channel). The green area indicates the spectral overlap between mTurquoise2 and SYFP2.

with diblock copolymer P2MVP₁₂₈-*b*-PEO₄₇₇.¹⁷ The PMC is expressed as $F^+ = [n_+]/([n_+] + [n_-])$ with $[n_+]$ and $[n_-]$ representing the total concentration of positively charged groups on the polymer and the net concentration of negative charges on the protein, respectively.

5.2.4.1. Equilibrium states of C3Ms with differing FRET pair amounts

Protein solutions with different amounts of FRET pair were obtained by varying the FRET pair/SBFP2 ratio between 0.1 and 1.0. C3Ms were formed by mixing the protein solution with an aliquot of a stock solution of P2MVP₁₂₈-*b*-PEO₄₇₇. The resulting solutions were left to equilibrate for 3 h prior to recording the fluorescence emission spectra.

5.2.4.2. Formation of C3Ms

A protein solution of 50% FRET pair was prepared (25% mTurquoise2, 25% SYFP2, and 50% SBFP2). To follow formation of C3Ms at the PMC, this equilibrated protein solution and an aliquot of a stock solution of P2MVP₁₂₈-*b*-PEO₄₇₇ were mixed rapidly in a quartz cuvette and placed in the fluorescence spectrophotometer sample compartment. Fluorescence emission spectra were recorded with a time interval of 30 s. The data set was fitted using IGOR Pro 6.11 (Wavemetrics).

5.2.4.3. Protein exchange between C3Ms

Two separate C3M solutions were prepared, one with mTurquoise2-C3Ms and one with SYFP2-C3Ms, both with varying amounts of SBFP2, so that after mixing the final FRET pair/SBFP2 ratios varied between 0.20 and 0.50. The solutions were left to equilibrate for 3 h prior to the measurement. To follow protein exchange between C3Ms equilibrated solutions of mTurquoise2-C3Ms and SYFP2-C3Ms with same SBFP2 amounts were mixed rapidly in a quartz cuvette and placed in the fluorescence spectrophotometer sample compartment. Fluorescence emission spectra were recorded with a time interval of 30 s. The data sets were fitted using global analysis with IGOR Pro 6.11.

5.2.4.4. Salt titration of C3Ms

To test salt stability of C3Ms, first, a solution of 50% FRET pair C3Ms was prepared at the PMC. Next, aliquots of a stock solution of NaCl were added to this solution in such a way that the NaCl concentration changed from 0 (initial) to 37.0 (final) mM, corresponding to an ionic strength change from 2.5 to 39.5 mM. To determine the dilution effect of the addition of NaCl, a control experiment was performed by adding corresponding volumes of 10 mM borate buffer (pH 9.0) to preformed 50% FRET pair C3Ms. Fluorescence emission spectra were recorded at the start of the experiment and after every addition of NaCl or buffer.

5.2.5. FRET data analysis

FRET is a spectroscopic phenomenon that is applied in different research disciplines to study (bio)molecular interactions.^{24,25} This phenomenon involves non-radiative energy transfer from a fluorescent donor to an acceptor and can only take place if the following three prerequisites are met: (1) overlap between donor fluorescence emission and acceptor excitation spectra, (2) distance between both fluorophores in the range of 1 - 10 nm, and (3) appropriate orientation of the dipole moments of both fluorophores. These three conditions determine the propensity of energy transfer, which is reported as FRET efficiency. Most fluorescent proteins emit in the visible spectrum and have overlapping spectra, and therefore are widely used for FRET experiments.^{26,27} The most effective combination for FRET is the pair formed by cyan (CFP) and yellow (YFP) fluorescent proteins.

C3Ms containing mTurquoise2 and SYFP2 display FRET, which is demonstrated in Figure 5.2 (red solid line) showing that fluorescence emission of SYFP2 takes place upon excitation of mTurquoise2 (excitation at 440 nm, Figure 5.1). Furthermore, steady-state fluorescence data in Figure 5.2 shows that in FRET experiments cross-talk of mTurquoise2, *i.e.*, fluorescence emission of donor at 527 nm, and direct excitation of SYFP2 at 440 nm occur. Both contributions were taken into account for calculation of the overall FRET ratio. The FRET ratio between mTurquoise2 and SYFP2 is expressed as:

$$F_{FRET} = f_{D_{ex}}^{A_{em}} / f_{D_{ex}}^{D_{em}} \quad (5.1)$$

with $f_{D_{ex}}^{A_{em}}$ the measured fluorescence intensity in the acceptor channel upon donor excitation, which is corrected for spectral cross-talk and direct excitation of acceptor, and $f_{D_{ex}}^{D_{em}}$ the measured fluorescence intensity in the donor channel after donor excitation, which is corrected for detection efficiencies of the dyes.²⁸ Both corrected parameters are also used to calculate the FRET efficiency, E :

$$E = f_{D_{ex}}^{A_{em}} / (f_{D_{ex}}^{D_{em}} + f_{D_{ex}}^{A_{em}}) \quad (5.2)$$

The average apparent inter-molecular distance, R , is related to the FRET efficiency via:

$$R = R_0 \sqrt[6]{(1/E) - 1} \quad (5.3)$$

with R_0 the Förster radius, which is calculated using

$$R_0 = 0.211 (\kappa^2 n^{-4} \Phi_D J(\lambda))^{1/6} \quad (5.4)$$

and

$$J(\lambda) = \int_0^{\infty} f_D(\lambda) \epsilon_A(\lambda) \lambda^4 d\lambda \quad (5.5)$$

where Φ_D is the donor quantum yield in absence of an acceptor ($\Phi_{mTurquoise2} = 0.93$), n is the refractive index of the intervening solution ($n = 1.41$)², and κ^2 is the orientation factor describing the relative

orientation of the transition dipoles of donor and acceptor ($\kappa^2 = 2/3$). The overlap integral, J , is a function of the wavelength, λ , and is calculated using $f_D(\lambda)$ and $\epsilon_A(\lambda)$ as the wavelength-dependent emission spectrum of donor and the wavelength-dependent molar extinction coefficient of acceptor ($\epsilon_{\text{SYFP2}} = 101\,000 \text{ M}^{-1} \text{ cm}^{-1}$), respectively.

5.3. Results

5.3.1. FRET efficiency in C3Ms with varying FRET pair concentrations

Figure 5.2 shows fluorescence emission spectra of equimolar amounts of mTurquoise2 and SYFP2 free in solution as well as encapsulated in C3Ms upon excitation at 440 nm. Encapsulating mTurquoise2 and SYFP2 together in C3Ms yields a strong reduction of donor fluorescence intensity and sensitized emission of SYFP2. In these experiments, concentrations of fluorescent proteins are the same and from the reduction of fluorescence intensity of mTurquoise2 a FRET efficiency of about 90% was estimated.

To determine the FRET efficiency at different FRET pair concentrations in C3Ms, SBFP2 was used to change the FRET pair amount in a C3M by replacing both mTurquoise2 and SYFP2, while keeping the final protein concentration constant. Figure 5.3A shows fluorescence emission spectra for different FRET pair amounts in C3Ms. Clearly, a FRET pair amount of 10% already shows energy transfer in C3Ms between mTurquoise2 and SYFP2. At increasing FRET pair amounts the donor fluorescence intensity further decreases and the acceptor fluorescence intensity increases. The related FRET ratio (Equation 5.1) increases in an almost linear fashion at increasing FRET pair amounts (Figure S5.1A). The corresponding FRET efficiency (Equation 5.2) follows an asymptotic curve reaching a maximum of ~ 0.90 for a FRET pair amount of 100% (Figure 5.3B). Conversely, the average apparent inter-molecular distance (Equation 5.3) between mTurquoise2 and SYFP2 decreases from 67 Å at 10% FRET pair to about 40 Å at 100% FRET pair (Figure S5.1B).

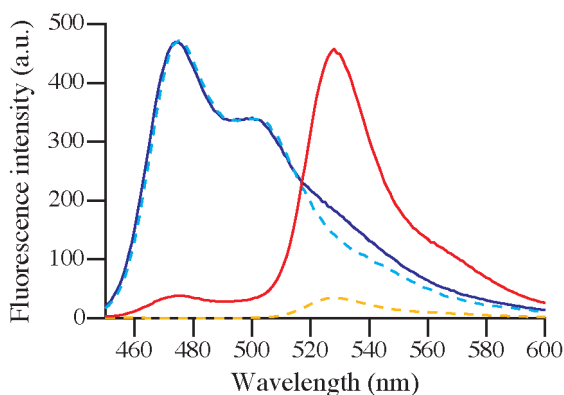


Figure 5.2. Steady-state fluorescence emission spectra of mixed C3Ms containing mTurquoise2 and SYFP2 (red solid line), and of mixed mTurquoise2 and SYFP2 free in solution (blue solid line), of mTurquoise2 in C3Ms (cyan dashed line), and of SYFP2 in C3Ms (orange dashed line). Proteins are at equimolar concentrations and excited at 440 nm.

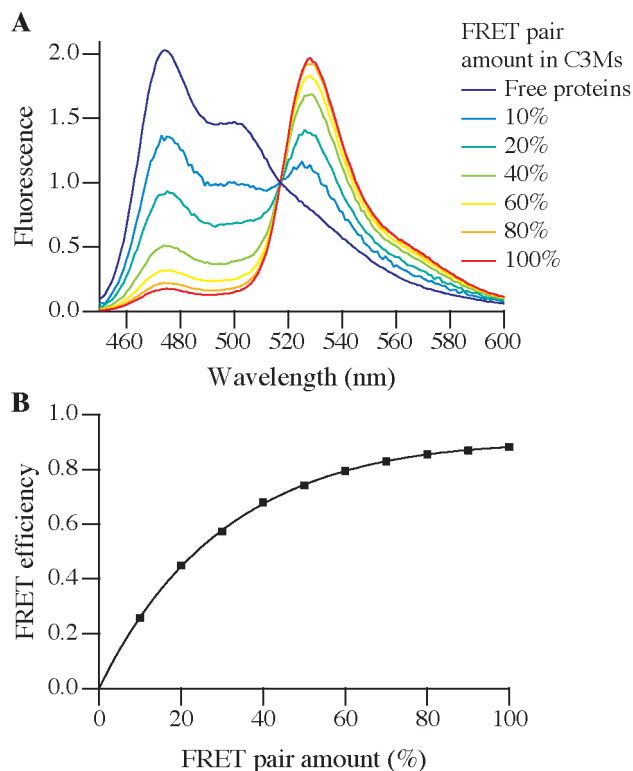


Figure 5.3. FRET properties of the FRET pair mTurquoise2 and SYFP2 in C3Ms at different FRET pair amounts (10% to 100%: FRET pair/SBFP2 ratio). (A) Fluorescence emission spectra at different FRET pair amounts (normalized at 517 nm). (B) FRET efficiency as a function of the FRET pair amount. The solid line is a guide to the eye.

The correlation of the FRET ratio with FRET pair content in C3Ms demonstrates that all three proteins have similar interactions with the diblock copolymer. Furthermore, the average apparent inter-molecular distance in micelles of 40 Å for 100% FRET pair suggests that the protein molecules do not stick to each other in C3Ms, because the minimal theoretical distance between FPs is about 24 Å.^{29,30} Moreover, the tendency of the three FPs to either homo- or heterodimerize is reduced compared to wild-type GFP due to the presence of the A206K mutation in the used FPs.³¹

5.3.2. Kinetics of micellization

To measure kinetics of C3M formation, we monitored changes in FRET by measuring fluorescence intensities of mTurquoise2 and SYFP2 as a function of time. Figure 5.4 shows the time dependence of the FRET ratio upon mixing solutions of proteins and polymer at a FRET pair amount of 50%. Upon mixing, the FRET ratio increases, indicating formation of C3Ms. After about 600 s a plateau is reached with a similar FRET ratio as found for equilibrated C3Ms with a FRET pair amount of 50% (FRET ratio ~2.5, Figure S5.1A). The

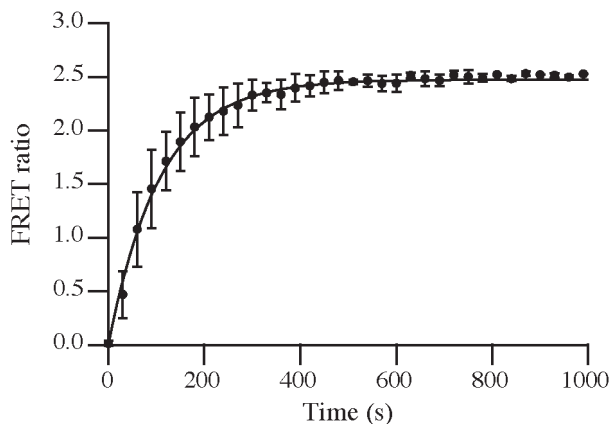


Figure 5.4. FRET ratio (527nm/475nm) as a function of time following the mixing of a P2MVP₁₂₈-*b*-PEO₄₇₇ solution with the protein solution. The solid line is the curve obtained using Equation 5.6, with $F_{eq} = 2.47$ and $k = 9 \times 10^{-3} \text{ s}^{-1}$. Error bars represent the spread of the data ($n = 2$).

time course of the FRET ratio was fitted using various equations corresponding to different reaction orders (Figure S5.2). Only the plot of the natural logarithm of the concentration of mTurquoise2 molecules that are not involved in FRET against time ($\ln[\text{mTurquoise2}]$ vs t) shows a linear behavior, confirming first-order kinetics. Consequently, time dependent change of the FRET ratio ($F(t)$) was fitted to:

$$F_t = F_{eq} (1 - e^{-kt}) \quad (5.6)$$

where F_{eq} is the FRET ratio at equilibrium and k the kinetic coefficient. The parameters obtained from the fit are a kinetic coefficient (first-order rate constant), k , of $9 \times 10^{-3} \pm 1 \times 10^{-3} \text{ s}^{-1}$ and a final FRET ratio, F_{eq} , of 2.47 ± 0.02 ($n = 2$). Thus, the relaxation time of formation of C3Ms is about 100 s.

5.3.3. Protein exchange between preformed C3Ms

To determine dynamics of protein exchange between C3Ms, we monitored changes in FRET after mixing C3Ms containing SYFP2 with C3Ms containing mTurquoise2 at different final FRET pair amounts (Figure 5.5). Immediately upon mixing of the micelle solutions, the FRET ratio increases, indicating exchange of FPs between C3Ms. Within a couple of hundreds of seconds a plateau is reached with similar FRET ratios as the corresponding equilibrated C3Ms (0.8 - 2.3, Figure S5.1A). The data were globally fitted according to first-order reaction kinetics (Equation 5.6, Figure S5.3). The obtained kinetic coefficient, k , is $10 \times 10^{-3} \pm 1 \times 10^{-3} \text{ s}^{-1}$ and the final FRET ratios, F_{eq} , are listed in Table 5.1. The relaxation time for C3Ms to reach their equilibrium compositions is also about 100 s.

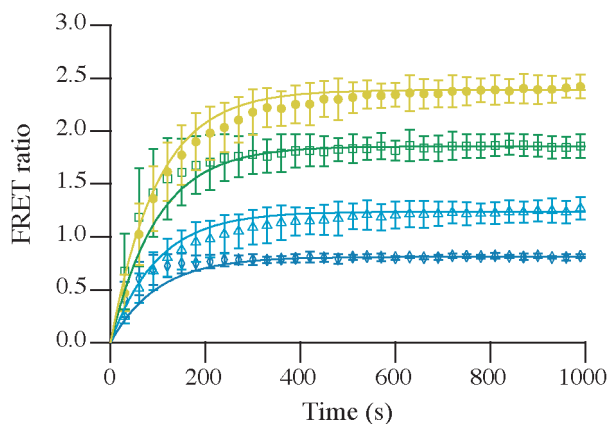


Figure 5.5. FRET ratio (527nm/475nm) as a function of time following exchange of SYFP2-C3Ms with mTurquoise2-C3Ms at different final FRET pair amounts: 50% (yellow solid dots), 40% (green open squares), 30% (cyan open triangles), and 20% (blue open diamonds). The solid lines are the curves obtained using Equation 5.6, with $k = 10 \times 10^{-3} \text{ s}^{-1}$ and $F_{eq} = 2.39$ for 50%, $F_{eq} = 1.86$ for 40%, $F_{eq} = 1.24$ for 30%, and $F_{eq} = 0.81$ for 20%. Error bars represent the standard deviation ($n = 4$).

Table 5.1. Final FRET ratios of protein exchange of C3Ms determined from the increase of the FRET ratio at different FRET pair amounts, with a kinetic coefficient of $10 \times 10^{-3} \pm 1 \times 10^{-3} \text{ s}^{-1}$. Standard deviations are based on multiple measurements ($n = 4$).

FRET pair amount	F_{eq}
20%	0.81 ± 0.01
30%	1.24 ± 0.01
40%	1.86 ± 0.02
50%	2.39 ± 0.02

5.3.4. Salt stability of C3Ms

It is well known that ionic strength is a parameter that strongly affects complexation of oppositely charged polyelectrolytes. We therefore investigated the influence of salt (NaCl) concentration on the stability of C3Ms. Figure 5.6A shows the dependency of the normalized fluorescence intensity of C3Ms on ionic strength (I), taking into account both buffer and added salt. It can be seen that donor fluorescence intensity increases and acceptor fluorescence intensity decreases with increasing ionic strength. Sodium chloride screens the electrostatic interaction between proteins and polymers and as a result a 50% decrease in FRET was observed at an ionic strength of 20 mM (Figure 5.6B).

The apparent stability, defined as the change in Gibbs energy ($\Delta G_{association}$) of association of C3Ms, was calculated over a range of ionic strengths using Equation 5.7:

$$\Delta G_{association} = -RT \ln K \quad (5.7)$$

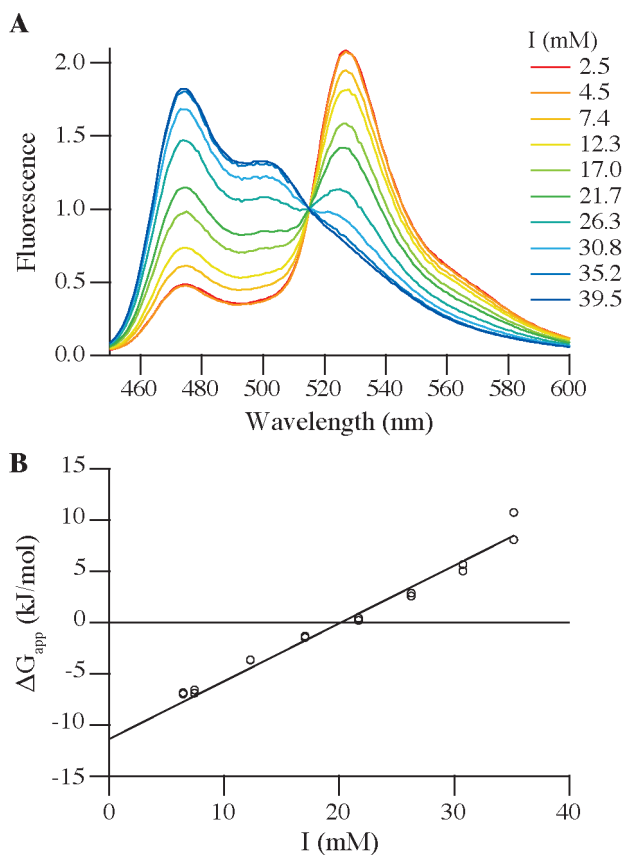


Figure 5.6. Salt stability of C3Ms. (A) Steady-state fluorescence emission spectra (normalized at 517 nm) at different ionic strengths. (B) Apparent Gibbs energy of association of C3Ms as a function of ionic strength.

where R is the gas constant and T is the absolute temperature (in K). K is the salt stability constant defined as the ratio between the concentrations of FPs involved in FRET and FPs not involved in FRET, measured for donor and acceptor separately ($n = 3$). The corresponding results are shown in Figure 5.6B. Extrapolation of these data to 2.5 mM ionic strength leads to an apparent stability of C3Ms of -10.0 kJ/mol or $-4.1 k_B T$ (with k_B the Boltzmann constant). We will come back to the meaning of this change in Gibbs energy in the discussion section.

5.4. Discussion

Based on our kinetic results, we propose a model for the formation and relaxation of FP-containing C3Ms, in line with commonly accepted two-state models for formation of simple surfactant micelles.³²⁻³⁴ This model implies that immediately after mixing of protein and diblock copolymer solutions, electrically neutral protein-polymer complexes are formed.

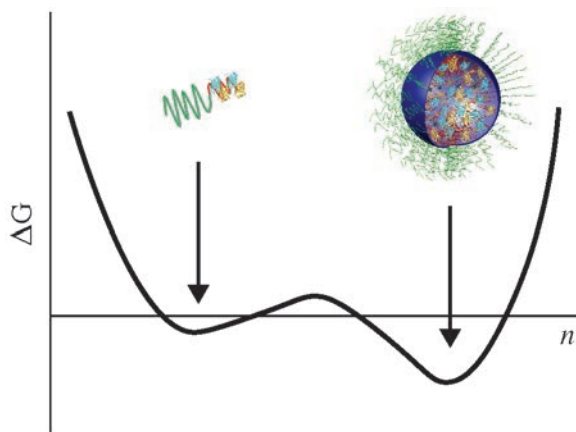


Figure 5.7. Schematic representation of the Gibbs energy of C3M formation as a function of aggregation number n . The curve shows two minima: one at low aggregation number corresponding to SCs and one at the optimum aggregation size for C3Ms.

Such a process is comparable to the fast formation of large intermediate aggregates as found for PAA-containing C3Ms.^{7,9} Since for our systems we never observed a high light scattering intermediate, we assume the presence of small soluble protein-polymer complexes (SCs). Above a certain concentration SCs start to aggregate, forming complex coacervate microphases that grow spontaneously. While for simple oppositely charged polyelectrolytes this growth proceeds until two macroscopic phases are formed, here growth is limited by the hydrophilic neutral chains of the diblock copolymer, which remain in the polymer-poor phase. Since growth occurs in three dimensions, the volume of the microphases increases stronger than their surface area, hence the available area per neutral chain decreases, driving the chains together. Repulsion between these chains stops the growth of the complex coacervate cores, yielding defined sizes of the micelles.^{8,32}

The formation of C3Ms should have two minima in the Gibbs energy, *i.e.*, one at low aggregation number and one at the optimum aggregation size (Figure 5.7). These minima correspond to the two states in the model: SCs and C3Ms. The maximum between these two states is the nucleation barrier for aggregation of SCs (or dissociation of C3Ms) and is caused by two opposite contributions: the negative ‘volume’ contribution due to attraction between oppositely charged polyelectrolyte chains and protein molecules and a positive ‘surface’ contribution due to the surface tension between the complex coacervate phase and the solution. However, because this surface tension is quite low,³⁵ this surface contribution is small compared to the contribution due to aggregation of SCs.

Linking this theory to our experimental results yield a proposed model for formation of C3Ms, which is summarized in Figure 5.8. Upon mixing of protein and diblock copolymer solutions first a rapid formation of SCs occurs; the second step is a slower process in which C3Ms relax to their final equilibrium state due to association and dissociation of SCs to and from the micelles.

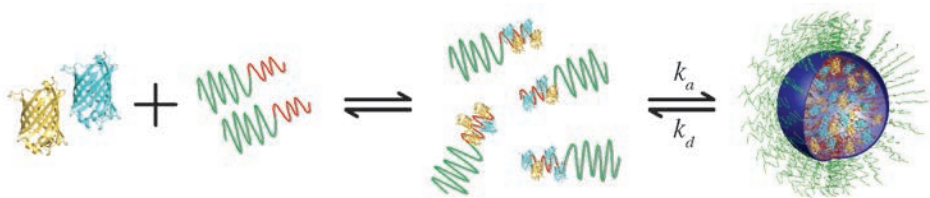


Figure 5.8. Schematic representation of C3M formation. Upon mixing of protein and diblock copolymer solutions a rapid formation of SCs occurs. These SCs are assumed to be near neutral protein-polymer complexes. Subsequently, formation of C3Ms is a slower process in which SCs continuously associate to and dissociate from C3Ms, with the corresponding rate constants k_a and k_d , respectively.

It is reasonable to assume that formation of SCs is diffusion controlled. This implies that this process would be on the micro- to millisecond time scale,¹⁶ which is way too fast to be monitored by our FRET measurements. This would mean that not the formation of SCs, but the increase in the volume of core material (complex coacervate microphases) is reflected by the FRET ratio as a function of time after mixing protein and polymer solutions.

In the C3M mixing experiments, changes in FRET reflect gradual exchange of core material. Actually, this process is not that different from the relaxation process observed in formation of C3Ms and is depicted in Figure 5.9: after mixing of the two types of equilibrated C3Ms, further association and dissociation of SCs occur allowing C3Ms to relax to their final equilibrium composition. This explains why we observed similar kinetic coefficients and relaxation times of about 100 s for formation of C3Ms and for exchange of proteins between them. An alternative mechanism for exchange of proteins and relaxation of micelles by “fusion and fission” is less likely,¹⁴⁻¹⁶ because the neutral hydrophilic PEO units form a dense stabilizing corona preventing the merging of C3Ms.

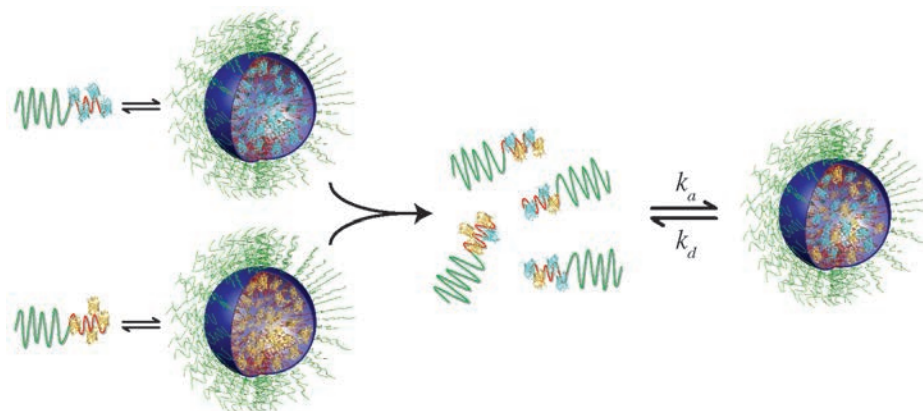


Figure 5.9. Schematic representation of protein exchange between C3Ms. Upon mixing of equilibrated C3Ms with their corresponding SCs, the SCs become mixed. These mixed SCs associate and dissociate with the C3Ms with rate constants k_a and k_d , respectively, resulting in a population of mixed C3Ms.

The rate at which SCs associate with (growing) C3Ms, r_a , is proportional to the concentrations of SCs and of C3Ms:

$$r_a = k_a [\text{SC}] \cdot [\text{C3M}] \quad (5.8)$$

in which k_a is the association rate constant (Figures 5.8 and 5.9) and $[\text{SC}]$ and $[\text{C3M}]$ denote molar concentrations of SCs and C3Ms, respectively. Our FRET measurements of C3M formation and exchange between C3Ms convincingly revealed first-order kinetics, and therefore, either $[\text{SC}]$ or $[\text{C3M}]$ should be constant at the time scale of the experiment. For that reason, Equation 5.8 would represent *pseudo* first-order kinetics. We can rule out that $[\text{SC}]$ would be constant, because the increase in FRET is due to conversion of SCs into complex coacervate microphases (Figures 5.8 and 5.9), resulting in a decrease of $[\text{SC}]$ during the measurements. Consequently, $[\text{C3M}]$ should be constant to explain the order of the reaction. This is only possible if during the FRET measurements nucleation of new micelles does not happen anymore and only micelle growth takes place.

The dissociation rate, r_d , of SCs from C3Ms is proportional to the concentration of C3Ms and the average number of SCs, n , that the C3Ms contain:

$$r_d = k_d \cdot n [\text{C3M}] \quad (5.9)$$

in which k_d is the dissociation rate constant (Figures 5.8 and 5.9). Thus, the net change in the concentration of SCs in time can be expressed as:

$$-\frac{d[\text{SC}]}{dt} = k_a [\text{SC}] \cdot [\text{C3M}] - k_d \cdot n [\text{C3M}] = (k_a [\text{SC}] - k_d n) \cdot [\text{C3M}] \quad (5.10)$$

At equilibrium, $-d[\text{SC}]/dt$ is zero, n is constant and Equation 5.10 reduces to:

$$[\text{SC}]_{eq} = k_d n / k_a \quad (5.11)$$

This implies that in the final state and provided that the concentrations of protein and polymer are high enough to form micelles, the concentration of SCs is independent of the total concentration of protein and polymer. The concentration of SCs at equilibrium approximately corresponds to the critical micelle concentration (CMC), which we have expressed previously in terms of the ‘free’ protein concentration.¹ For large aggregation numbers, n , the CMC is related to the Gibbs energy of micellization³⁶:

$$\Delta G_{micellization} = RT \ln(\text{CMC}) \quad (5.12)$$

with R the universal gas constant and T the absolute temperature. For simplicity, we assume that soluble complexes correspond to one polymer chain (number of charged groups is about +112) with on average 10 - 11 protein molecules (net charge is about -10) resulting in more or less electrically neutral moieties. With a CMC of 18 nM (which corresponds to 100 nM protein at a PMC of 0.65¹), the Gibbs energy equals to -44 kJ/mol or $-18 k_B T$ at an ionic strength of 2.5 mM. This is the free energy gain if a SC associates with a C3M.

The decrease in FRET during the salt titration reflects an increase in the average distance between mTurquoise2 and SYFP2. This is probably due to the disintegration of the micellar cores or swelling of the C3Ms, because salt screens the attractive electrostatic interaction between the protein molecules and the charged block of the polymer, thereby lowering the entropic contribution of counter-ion release to the stability. We assume that electrostatic interactions play a role particularly in the formation of SCs, because formation of C3Ms results from assembly of these near-neutral entities. Therefore, addition of salt would especially affect the stability of SCs and the Gibbs energy, $\Delta G_{\text{association}}$ (Equation 5.8), obtained from the salt titration would reflect this stability. Together with the Gibbs energy of the insertion of a SC in the micelle, $\Delta G_{\text{micellization}}$ (Equation 5.13), a rough estimate of the overall Gibbs energy of formation of a C3M is:

$$\Delta G_{\text{C3M}} = n(\Delta G_{\text{association}} + \Delta G_{\text{micellization}}) \quad (5.13)$$

with n the aggregation number of SCs in a C3M. Taking the aggregation number equal to the amount of diblock copolymers per C3M, *i.e.*, $n \approx 40$,¹ this yields a value for ΔG_{C3M} of about -2160 kJ/mol or $-880 k_B T/\text{micelle}$ (at 2.5 mM ionic strength).

Although the overall stability of C3Ms thus seems to be quite high, their structure is highly dynamic and SCs with proteins are easily dissociated from and re-associated with C3Ms, resulting in a rapid exchange of proteins between the micelle core and bulk solution. This has a huge impact on the practical applicability of C3Ms as protein carriers: the protein molecules reside part of the time outside the C3Ms and thus are unprotected. In addition, half of the micelles dissociate already at an ionic strength of 20 mM, which makes these systems inapplicable under, for example, physiological conditions.

To improve the stability and reduce dynamics of C3Ms several options exist. For example, one could choose to add an additional homopolymer to obtain three-component C3Ms; as shown by Lindhoud *et al.*,⁴ such C3Ms can have very long relaxation times. The cause for this phenomenon is not clear, however, and a disadvantage is that much less protein molecules per micelle can be accommodated. Alternatively, one could modify the protein, as has been done by Obermeyer *et al.*,³⁷ who increased the net charge of several proteins by converting positively charged lysine residues to negatively charged residues. These negatively charged proteins were encapsulated with strong polycations resulting in improved stability of the micelles to increased ionic strength as the net charge on the protein increased. In view of our findings a very effective option to trap proteins would be to cross-link the charged blocks of the diblock copolymers in the C3M cores, by using, for example, amide bonds.^{38,39} By doing so, it is not possible for proteins to leave micelles in the form of almost neutral SCs and the energy barrier to escape on their own will be much higher. An additional advantage of this approach is that the proteins do not need to be modified.

5.5. Conclusion

In this paper, the formation of protein-containing C3Ms, the protein exchange between them and their salt stability have been studied using FRET. Energy transfer was followed between mTurquoise2 and SYFP2, which come in close proximity of each other in C3Ms upon mixing with the diblock copolymer P2MVP₁₂₈-*b*-PEO₄₇₇. At an ionic strength of about 20 mM, FRET in such a micellar solution reduces to 50% of its initial value, due to weakening of the electrostatic interactions between polymers and proteins. Both formation of C3Ms and of protein exchange between C3Ms follow first-order kinetics with a relaxation time of about 100 s, implying that the structures are dynamic. The similarity between both processes can be explained by a two-state model in which equilibration of C3Ms to their final size and composition involves association and dissociation of SCs. Based on the salt stability results, the proposed model, and assuming that a SC comprises one diblock copolymer molecule and about 10 protein molecules, we estimate the overall Gibbs energy of C3M formation to be $-880 k_B T/\text{micelle}$.

Acknowledgments

Financial support from the Graduate School VLAG (Wageningen, The Netherlands) is gratefully acknowledged. We thank Dr. Joachim Goedhart (University of Amsterdam, Amsterdam, The Netherlands) for providing us with the pRSETb vector containing SBFP2 and Prof. Frans Leermakers (Wageningen University & Research, Wageningen, The Netherlands) for fruitful discussions.

References

1. Nolles, A.; Westphal, A. H.; de Hoop, J. A.; Fokkink, R. G.; Kleijn, J. M.; van Berkel, W. J. H.; Borst, J. W., Encapsulation of GFP in complex coacervate core micelles. *Biomacromolecules* **2015**, *16*, (5), 1542-1549.
2. Nolles, A.; van Dongen, N. J. E.; Westphal, A. H.; Visser, A. J. W. G.; Kleijn, J. M.; van Berkel, W. J. H.; Borst, J. W., Encapsulation into complex coacervate core micelles promotes EGFP dimerization. *Phys. Chem. Chem. Phys.* **2017**, *19*, (18), 11380-11389.
3. Lindhoud, S.; de Vries, R.; Norde, W.; Cohen Stuart, M. A., Structure and stability of complex coacervate core micelles with lysozyme. *Biomacromolecules* **2007**, *8*, (7), 2219-2227.
4. Lindhoud, S.; Norde, W.; Cohen Stuart, M. A., Reversibility and relaxation behavior of polyelectrolyte complex micelle formation. *J. Phys. Chem. B* **2009**, *113*, (16), 5431-5439.
5. Harada, A.; Kataoka, K., Pronounced activity of enzymes through the incorporation into the core of polyion complex micelles made from charged block copolymers. *J. Control. Release* **2001**, *72*, (1-3), 85-91.
6. Yuan, X. F.; Yamasaki, Y.; Harada, A.; Kataoka, K., Characterization of stable lysozyme-entrapped polyion complex (PIC) micelles with crosslinked core by glutaraldehyde. *Polymer* **2005**, *46*, (18), 7749-7758.
7. Cohen Stuart, M. A.; Besseling, N. A. M.; Fokkink, R. G., Formation of micelles with complex coacervate cores. *Langmuir* **1998**, *14*, (24), 6846-6849.
8. Voets, I. K.; de Keizer, A.; Cohen Stuart, M. A., Complex coacervate core micelles. *Adv. Colloid Interface Sci.* **2009**, *147-148*, 300-318.
9. Hof, B.; Voets, I. K.; de Keizer, A.; Cohen Stuart, M. A., Comparison of complex coacervate core micelles from two diblock copolymers or a single diblock copolymer with a polyelectrolyte. *Phys. Chem. Chem. Phys.* **2006**, *8*, (36), 4242-4251.
10. de Vries, R.; Cohen Stuart, M. A., Theory and simulations of macroion complexation. *Curr. Opin. Colloid Interface Sci.* **2006**, *11*, (5), 295-301.
11. Kriz, J.; Dybal, J.; Dautzenberg, H., Cooperative interactions of unlike macromolecules: 3. NMR and theoretical study of the electrostatic coupling of sodium polyphosphates with diallyl(dimethyl) ammonium chloride-acrylamide copolymers. *J. Phys. Chem. A* **2001**, *105*, (31), 7486-7493.
12. Besseling, N. A. M.; Cohen Stuart, M. A., Self-consistent field theory for the nucleation of micelles. *J. Chem. Phys.* **1999**, *110*, (11), 5432-5436.
13. Hof, B.; de Keizer, A.; Cohen Stuart, M. A., On the stability of (highly aggregated) polyelectrolyte complexes containing a charged-block-neutral diblock copolymer. *J. Phys. Chem. B* **2007**, *111*, (20), 5621-5627.
14. Holappa, S.; Kantonen, L.; Andersson, T.; Winnik, F.; Tenhu, H., Overcharging of polyelectrolyte complexes by the guest polyelectrolyte studied by fluorescence spectroscopy. *Langmuir* **2005**, *21*, (24), 11431-11438.
15. Dormidontova, E. E., Micellization kinetics in block copolymer solutions: Scaling model. *Macromolecules* **1999**, *32*, (22), 7630-7644.
16. Zhang, J.; Chen, S.; Zhu, Z.; Liu, S., Stopped-flow kinetic studies of the formation and disintegration of polyion complex micelles in aqueous solution. *Phys. Chem. Chem. Phys.* **2014**, *16*, (1), 117-127.
17. Nolles, A.; Westphal, A. H.; Kleijn, J. M.; van Berkel, W. J. H.; Borst, J. W., Colorful packages: Encapsulation of fluorescent proteins in complex coacervate core micelles. *Int. J. Mol. Sci.* **2017**, *18*, (7), 1557.
18. Goedhart, J.; von Stetten, D.; Noirclerc-Savoye, M.; Lelimosin, M.; Joosen, L.; Hink, M. A.; van Weeren, L.; Gadella, T. W. J.; Royant, A., Structure-guided evolution of cyan fluorescent proteins towards a quantum yield of 93%. *Nat. Commun.* **2012**, *3*, 751.
19. Kremers, G. J.; Goedhart, J.; van Munster, E. B.; Gadella, T. W. J., Cyan and yellow super fluorescent proteins with improved brightness, protein folding, and FRET Förster radius. *Biochemistry* **2006**, *45*, (21), 6570-6580.
20. Chong, S.; Mersha, F. B.; Comb, D. G.; Scott, M. E.; Landry, D.; Vence, L. M.; Perler, F. B.; Benner, J.; Kucera, R. B.; Hirvonen, C. A.; Pelletier, J. J.; Paulus, H.; Xu, M. Q., Single-column purification of free recombinant proteins using a self-cleavable affinity tag derived from a protein splicing element. *Gene* **1997**, *192*, (2), 271-281.
21. Evans, T. C., Jr.; Xu, M. Q., Intein-mediated protein ligation: harnessing nature's escape artists. *Biopolymers* **1999**, *51*, (5), 333-342.
22. Xu, M. Q.; Paulus, H.; Chong, S., Fusions to self-splicing inteins for protein purification. *Methods Enzymol.* **2000**, *326*, 376-418.

23. Kremers, G. J.; Goedhart, J.; van den Heuvel, D. J.; Gerritsen, H. C.; Gadella, T. W. J., Improved green and blue fluorescent proteins for expression in bacteria and mammalian cells. *Biochemistry* **2007**, *46*, (12), 3775-3783.
24. Förster, T., Zwischenmolekulare energiewanderung und fluoreszenz. *Ann. Phys.* **1948**, *437*, 55-75.
25. Stryer, L., Fluorescence energy transfer as a spectroscopic ruler. *Annu. Rev. Biochem.* **1978**, *47*, 819-846.
26. Zhang, J.; Campbell, R. E.; Ting, A. Y.; Tsien, R. Y., Creating new fluorescent probes for cell biology. *Nat. Rev. Mol. Cell. Biol.* **2002**, *3*, (12), 906-918.
27. Piston, D. W.; Kremers, G. J., Fluorescent protein FRET: the good, the bad and the ugly. *Trends Biochem. Sci.* **2007**, *32*, (9), 407-414.
28. Hohlbein, J.; Craggs, T. D.; Cordes, T., Alternating-laser excitation: single-molecule FRET and beyond. *Chem. Soc. Rev.* **2014**, *43*, (4), 1156-1171.
29. Ormö, M.; Cubitt, A. B.; Kallio, K.; Gross, L. A.; Tsien, R. Y.; Remington, S. J., Crystal structure of the *Aequorea victoria* green fluorescent protein. *Science* **1996**, *273*, (5280), 1392-1395.
30. Yang, F.; Moss, L. G.; Phillips, G. N. J., The molecular structure of green fluorescent protein. *Nat. Biotechnol.* **1996**, *14*, (10), 1246-1251.
31. Zacharias, D. A.; Violin, J. D.; Newton, A. C.; Tsien, R. Y., Partitioning of lipid-modified monomeric GFPs into membrane microdomains of live cells. *Science* **2002**, *296*, (5569), 913-916.
32. Sams, P. J.; Wyn-Jones, E.; Rassing, J., A new model describing the kinetics of micelle formation from chemical relaxation studies. *Chem. Phys. Lett.* **1972**, *13*, (3), 233-236.
33. Laughlin, R. G., *The aqueous phase behavior of surfactants*. Academic Press: London, 1994.
34. Leermakers, F. A. M.; Eriksson, J. C.; Lyklema, J., Association colloids and their equilibrium modelling. In *Fundamentals of interface and colloid science: soft colloids*, Lyklema, J., Ed. Academic press: Amsterdam, 2005; Vol. 5.
35. Spruijt, E.; Sprakel, J.; Cohen Stuart, M. A.; van der Gucht, J., Interfacial tension between a complex coacervate phase and its coexisting aqueous phase. *Soft Matter* **2010**, *6*, (1), 172-178.
36. Phillips, J. N., The energetics of micelle formation. *Trans. Faraday Soc.* **1955**, *51*, (4), 561-569.
37. Obermeyer, A. C.; Mills, C. E.; Dong, X. H.; Flores, R. J.; Olsen, B. D., Complex coacervation of supercharged proteins with polyelectrolytes. *Soft Matter* **2016**, *12*, (15), 3570-3581.
38. Bourouina, N.; Cohen Stuart, M. A.; Kleijn, J. M., Complex coacervate core micelles as diffusional nanoprobes. *Soft Matter* **2014**, *10*, (2), 320-331.
39. Kim, J. O.; Ramasamy, T.; Yong, C. S.; Nukolova, N. V.; Bronich, T. K.; Kabanov, A. V., Cross-linked polymeric micelles based on block ionomer complexes. *Mendeleev Commun.* **2013**, *23*, (4), 179-186.

Supplementary information

S5.1. FRET ratio and average distance of mTurquoise2 and SYFP2 in C3Ms

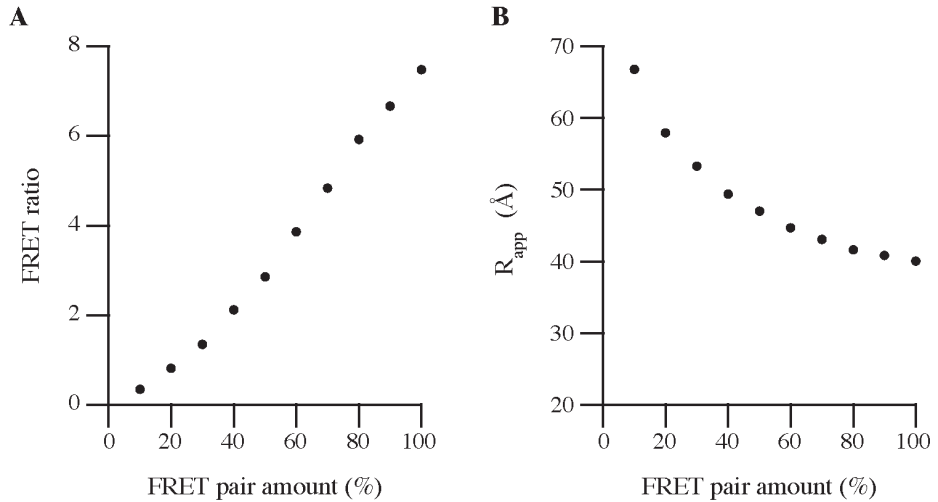


Figure S5.1. FRET ratios of and average distances between mTurquoise2 and SYFP2 in C3Ms at different FRET pair amounts (10% to 100%: FRET pair/SBFP2 ratio). (A) FRET ratio (527 nm/475 nm) and (B) apparent inter-molecular distance (R_{app}) as a function of the FRET pair amount.

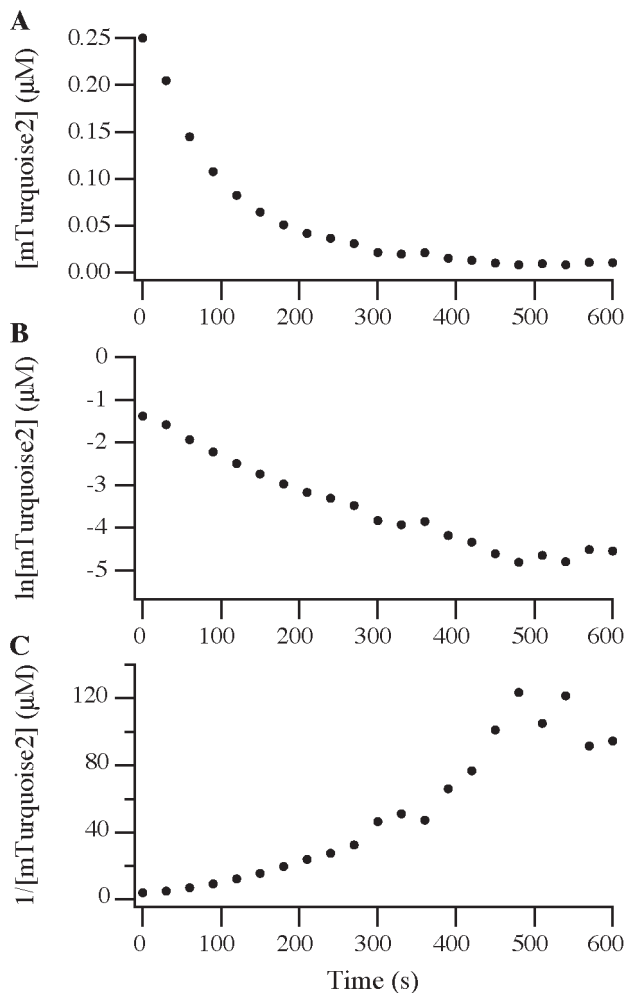
S5.2. Time course of the FRET ratio of C₃M formation at different reaction orders

Figure S5.2. Time course of the FRET ratio using various equations corresponding to different reaction orders: (A) zero, (B) first, and (C) second order kinetics of formation of C₃M with [mTurquoise2] the concentration of mTurquoise2 molecules that are not involved in FRET.

S5.3. Time course of the FRET ratio of protein exchange at different reaction orders

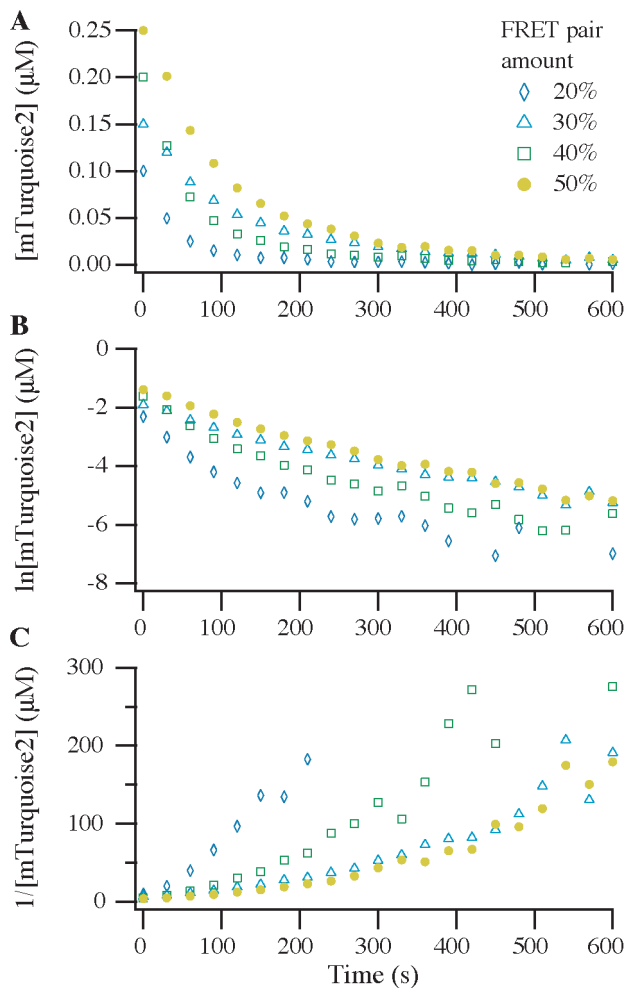
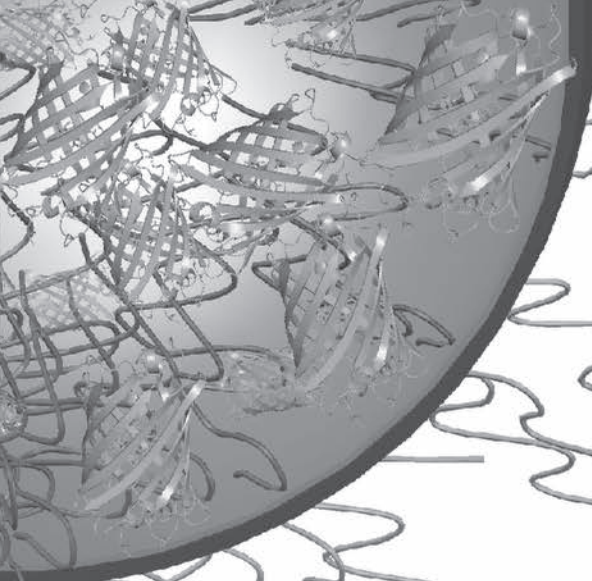


Figure S5.3. Time course of the FRET ratio using various equations corresponding to different reaction orders: (A) zero, (B) first, and (C) second order kinetics of protein exchange between preformed C3Ms with [mTurquoise2] the concentration of mTurquoise2 molecules that are not involved in FRET.





Chapter 6

General discussion

This thesis explores the encapsulation of fluorescent proteins (FPs) into complex coacervate core micelles (C3Ms) and features the impact of this encapsulation on the biophysical properties of the FPs. In total eight different FPs were investigated originating from two different classes (Hydrozoa: SBFP2, mTurquoise2, EGFP, mEGFP, and SYFP2; and Anthozoa: mKO2, mCherry, and TagRFP), thereby covering the whole visible spectrum. As enveloping material the diblock copolymer poly(2-methyl-vinyl-pyridinium)_n-*b*-poly(ethylene-oxide)_m (P2MVP_n-*b*-PEO_m) of two different lengths (P2MVP₄₁-*b*-PEO₂₀₅ and P2MVP₁₂₈-*b*-PEO₄₇₇) was used. The research was focused on the formation, composition, dynamics, and stability of the FP-containing C3Ms, but it also gave us insights into the structural and spectral properties of the encapsulated FPs. In this chapter, we start with practical aspects regarding the formation and detection of FPs in solution and explain the advantages of using the detection techniques to study the structure and dynamics of protein-containing C3Ms. Next, the effects of encapsulation on the fluorescent proteins are discussed. Subsequently, our findings are placed in perspective with regard to the applicability of protein-containing C3Ms in biotechnology and controlled release. Finally, directions for future research are provided.

6.1. Formation and detection of FPs and advantages of the detection techniques to study C3Ms

Protein-containing C3Ms can easily be prepared by mixing solutions of charged proteins and diblock copolymers, containing an oppositely charged block and a neutral hydrophilic block. The driving force for micelle formation is the Coulomb interaction between charged groups on protein and polymer and the entropic gain due to counter ion release. For correct determination of the system's composition at which most C3Ms are formed (the preferred micellar composition, PMC), amongst others, the concentration of the components is a critical parameter. The concentration of a FP can be determined using its molar extinction coefficient in the visible region. However, it should be noted that determination of the correct FP concentration might suffer from incomplete maturation of the chromophore, which is in particular true for red FP variants.^{1,2} This causes an underestimation of the protein concentration from the absorption intensity of the solution, therefore, a general protein assay was used for the fluorescent protein concentrations (Sections 2.2.2, 3.2.2, and 4.2.2).

By using FPs, it was possible to study many different properties of protein-containing C3Ms with fluorescence techniques, next to more conventional techniques like dynamic light scattering (DLS). Using FPs as model proteins for encapsulation studies is advantageous, because they can easily be obtained in pure form and they are intrinsically fluorescent, which avoids the use of external fluorescent labels. Such rather bulky hydrophobic labels can have a significant effect on the interaction between protein and polymer, thereby influencing the structure and stability of C3Ms. In addition, quantitative labeling of proteins requires quite some extra effort in terms of time and money.³

DLS is commonly used to study the size and stability of C3Ms; hence, it was also used in this study. The advantage of DLS is that the investigated structures do not need to be fluorescent, but quantification of the number of encapsulated FPs and C3M formation and dynamics is not possible. For these latter properties, fluorescence techniques like fluorescence correlation spectroscopy (FCS) and steady-state fluorescence spectroscopy have been used in the present study. FCS is a single molecule technique that was used to determine the sizes of C3Ms and the number of encapsulated FPs with their corresponding encapsulation efficiency. A disadvantage of FCS is that it can only be applied if the concentration of the fluorescent particles is low. Therefore, in our FCS measurements we partly substituted the FPs by non-fluorescent variants to characterize the C3Ms. With steady-state fluorescence spectroscopy, it was possible to study Förster resonance energy transfer (FRET), thereby following the formation of FP-containing C3Ms and the exchange of proteins between the micelles.

6.2. Fluorescent proteins as encapsulated biomolecules

Encapsulation of FPs resulted in several changes in their spectral properties. In short, it was found that the β -barrel structure of some FPs was affected by the protein-polymer interaction. In addition, it was observed that EGFP has the tendency to dimerize inside C3Ms. For the other Hydrozoa FPs this tendency is reduced due to the presence of the A206K substitution.⁴ For the Anthozoa FPs it was concluded that they di- or tetramerize inside the C3Ms (Section 4.4.3). Below, the changes in spectroscopic properties upon FP encapsulation are further discussed.

We observed that encapsulation of the FPs leads to minor changes in their absorption and fluorescence properties depending on the kind of FP and the length of polymer used. To better understand these differences, the chromophore environments were investigated (Figure 6.1, Tables 4.1 and 4.2). All FPs contain the conserved amino acid residues Glu222 and Arg96 (EGFP numbering, Figures 1.4C, S4.1, and 6.1). The side chain of Glu222 adopts different conformations that seem to be related to its protonation state and to its orientation related to the chromophore (Figure 6.1). It should be noted that circular dichroism (CD) revealed a difference between the Hydrozoa FPs and the Anthozoa FPs, which we could relate to a more elliptic β -barrel shape for the Anthozoa FPs than for the Hydrozoa FPs.

SBFP2. For SBFP2 we observed an increase in absorption and fluorescence intensities upon encapsulation (Figures 4.5A, 4.6, and S4.4A), resulting in similar fluorescence quantum yields for free and encapsulated protein (Table 4.5). Relating this to the far-UV CD spectra, which indicate a change in the β -barrel structure (Figure 4.7C), the interactions of the chromophore with its environment alter upon encapsulation of SBFP2. In free SBFP2, the hydrogen bonds of His66 with its surroundings are rather long (3.1 - 3.4, Figure 6.1A). These distances might be decreased upon encapsulation of SBFP2, thereby increasing the rigidity of the chromophore in its environment and thus increasing its molar extinction coefficient.⁵

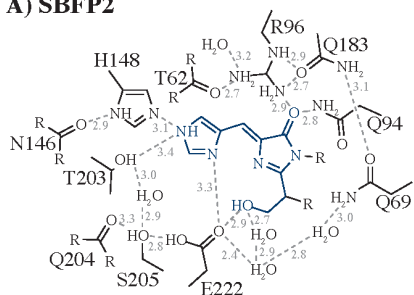
mTurquoise2. The quantum yield of mTurquoise2 is very high (93%) and with a pK_a of 3.1 the chromophore of mTurquoise2 is barely susceptible to changes in pH (Table S4.2 and Figure S4.5B). Both aspects are probably due to the highly stabilizing van der Waals interactions of Val61, Phe146, and Ile167 with the chromophore (Figure 6.1B).⁶ Upon encapsulation of mTurquoise2, its molar extinction coefficient does not change, but its quantum yield decreases slightly from 93% to ~86% (Figure 4.6 and Table 4.6). This may be caused by a subtle change in the β -barrel structure, which is seen in the far-UV CD spectra (Figure 4.7D), thereby weakening some of the interactions between the chromophore and its environment. In **Chapter 5** mTurquoise2 was used in the FRET study, because its relatively high quantum yield makes it a perfect donor molecule.

EGFP and mEGFP. In **Chapter 3** we extensively discussed the differences observed between encapsulated mEGFP and EGFP. Normally, the chromophore of (m)EGFP is deprotonated (Figure 6.1C), resulting in a fluorescence excitation maximum at 490 nm and fluorescence emission maximum at 509 nm. Upon encapsulation of EGFP, however, an additional absorption peak at 395 nm was observed together with a decrease of the absorption at 490 nm (Figure 3.2). Comparing the encapsulation of EGFP with that of mEGFP and together with time-resolved fluorescence anisotropy, it was concluded that EGFP dimerizes in C3Ms. Consequently, this dimerization leads to reorientation of Glu222 resulting in a pK_a shift of the chromophore (Figures 6.1C and 3.5). A conformational rearrangement of Glu222 does not take place in mEGFP, because it remains mainly monomeric in C3Ms.

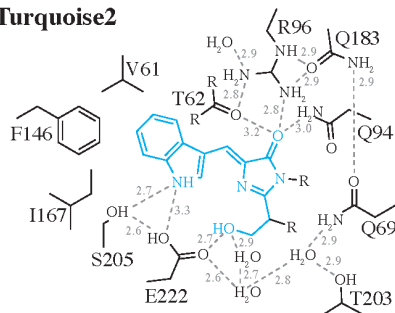
SYFP2. Upon encapsulation of SYFP2 the β -barrel structure of this protein also slightly changes (Figure 4.7F), causing a minor decrease in fluorescence quantum yield (from 68% to ~61%, Table 4.5). However, the molar extinction coefficient of SYFP2 is hardly affected (Figure 4.6). Its chromophore is stabilized due to the coplanar π - π contacts between the hydroxyphenyl group of the chromophore and the side chain of Tyr203 (Figure 6.1D),⁷ which stabilizes the interactions of the chromophore with amino acid residues of the β -barrel resulting in unchanged absorption and emission spectra upon encapsulation of SYFP2. Therefore, we used SYFP2 as an acceptor molecule in the FRET study described in **Chapter 5**.

mKO2. Looking at the chromophore environment of mKO2 (Figure 6.1E), it seems that there are not many direct interactions between the chromophore and the amino acid residues surrounding it. Nevertheless, just like for the other fluorescent proteins, Arg94 forms hydrogen bonds with the carbonyl oxygen of Tyr66 in mKO2. Furthermore, the hydroxyphenyl group of the chromophore forms coplanar π - π contacts with the side chain of His197.⁸ Next to a water molecule, also Ser145 forms a hydrogen bond with the phenolate of the chromophore (Figure 6.1E).⁸ Encapsulation of mKO2 causes on the one hand an increase in its molar extinction coefficient and on the other hand a decrease in its fluorescence quantum yield (Figures 4.5, 4.6, and S4.4 and Table 4.5). Based on these results and a monomeric quality of 68% (Table S4.2), we propose that mKO2 dimerizes inside C3Ms. If mKO2 forms a dimer or tetramer like DsRed,⁹ the dimer and/or tetramer interfaces are at the side of the protein where the main residues reside that interact with the chromophore. It is likely that this causes the change in the chromophore environment upon encapsulation of mKO2.

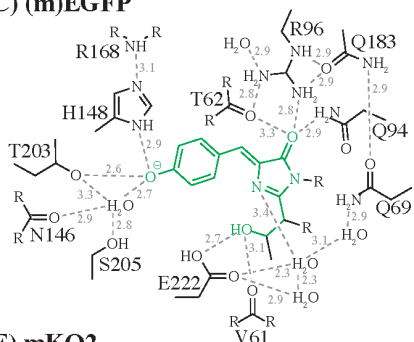
A) SBFP2



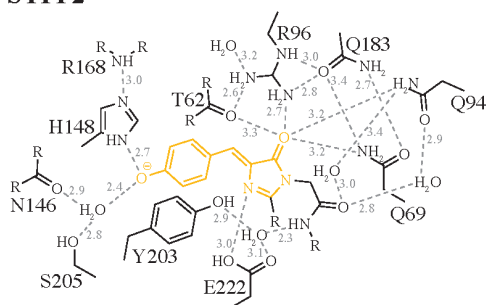
B) mTurquoise2



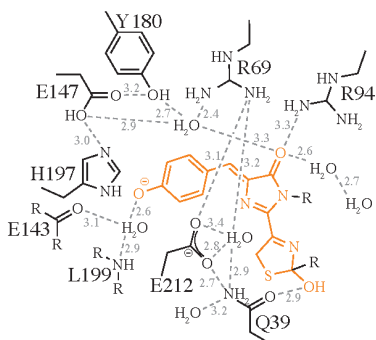
C) (m)EGFP



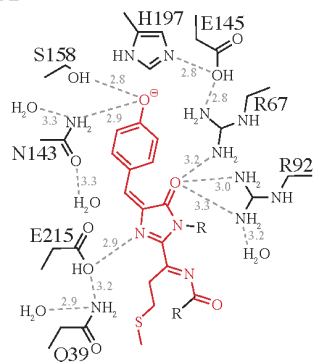
D) SYFP2



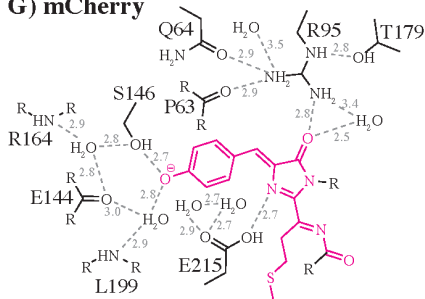
E) mKO2



F) TagRFP



G) mCherry



TagRFP. TagRFP is the only FP in this series with the chromophore in the *trans*-conformation (Figure 4.1G). However, this conformation does not specifically lead to interactions with other amino acid residues in the β -barrel compared to the other FPs. Next to that, the hydroxyphenyl group of the chromophore is, like in mKO2, stabilized via coplanar π - π contacts with the side chain of His197 (Figure 6.1F).¹⁰ With a pK_a of 3.8 the chromophore of TagRFP is relatively insensitive to changes in pH (Table S4.2), which we also observed in Figure S4.5F. Furthermore, upon encapsulation the far-UV CD spectrum of TagRFP slightly changes in the zero crossing just like the other FPs. All these characteristics make it remarkable that the fluorescence intensity decreases about 40% upon encapsulation of TagRFP compared to that of the free protein (Figure 4.6A). TagRFP is a weak monomer, with a monomeric quality of 57.5% and a K_D of 38.4 μ M (Table S4.2). Thereby considering that the protein concentration in the C3Ms is about 10 mM, we conclude that TagRFP dimerizes or even tetramerizes inside the C3Ms and this may explain the drastic decrease of its fluorescence quantum yield.

mCherry. The chromophore of mCherry is very susceptible to changes in pH, which is due to Glu215 as titratable group (Figure 6.1G),¹¹ resulting in a blue shift of the fluorescence spectra with increasing pH (Figure S4.5G). Upon encapsulation of mCherry, we observe a similar blue shift in both the absorption and fluorescence spectra. Encapsulation even slightly increases the fluorescence quantum yield of mCherry (Table 4.5). Therefore, these spectral changes must be initiated by a modification in conformation of Glu215, which is caused by the change in the β -barrel structure of mCherry upon encapsulation (Figure 4.7). So, just like for EGFP, the pK_a of the chromophore of mCherry shifts upon encapsulation due to the conformation of Glu215, which also may be caused by the di- or tetramerization of mCherry.

Overall, although FPs are considered to be very robust, encapsulation of them revealed some interesting structural changes. Besides from changes in the local environment of the chromophores, association of protein molecules in dimers or tetramers occurs for EGFP and the Anthozoa FPs, *i.e.*, mKO2, TagRFP, and mCherry. Such oligomerization phenomena should be considered in protein-protein interaction studies when using these FPs in FRET pairs, because the induced spectral difference may influence the FRET efficiency.

Figure 6.1 (previous page). H-bond network around the chromophores of (A) SBFP2, (B) mTurquoise2, (C) EGFP and mEGFP, (D) SYFP2, (E) mKO2, (F) TagRFP, and (G) mCherry based on the PDB entries listed in Tables 4.1 and 4.2. The chromophores are colored in line with the actual colors of the fluorescent proteins. Hydrogen bonds are drawn as gray dashed lines and have the indicated lengths in \AA . The cut-off for the hydrogen bond distance is set to ~ 3.4 \AA . Val61, Phe146, and Ile167 of mTurquoise2 stabilize the chromophore by van der Waals interactions.⁶ For SYFP2, Tyr203 is oriented parallel to the phenol ring of the chromophore, resulting in a π - π stacking interaction with the chromophore. In mKO2 and TagRFP, His197 is situated parallel to the phenol ring of the chromophore, resulting in a π - π stacking interaction with the chromophore.

6.3. Challenges for the practical application of C3Ms as protein carriers

In many applications it is important to protect proteins from adverse environmental conditions (see **Chapter 1**). When C3Ms are used for this purpose, they should remain intact and protect their protein content upon changes in concentration, pH and ionic strength, and against attack from proteases and the immune system. This also implies that they do not exchange their protein content for other proteins. On the other hand, some of these features can be used to trigger the release of content from the micelles, depending on the specific application and the site of action. However, as described in **Chapter 5**, the investigated FP-containing C3Ms are only stable under a restricted set of conditions and the same is expected for other protein-containing C3Ms.

The formation of C3Ms is based on electrostatic interactions between polymers and proteins, as explained in **Chapter 1**. The charged block of the diblock copolymer used in our study is a strong polyelectrolyte, while proteins in general are weak, ampholytic polyelectrolytes. The used FPs have a pI of around 5.5, which means that at neutral pH their net charge is negative, and therefore neutral-cationic diblock copolymers were used for their encapsulation. To have sufficient charges on the proteins to form complexes with the polymers¹², it was chosen to work with a net negative protein charge of around 10. Consequently, it was required to work at pH 9 for most FPs and even at pH 10 for TagRFP (**Chapter 4**). This high pH has no influence on the function and stability of the fluorescent proteins. However, it shows that the pI of the protein relative to the pH of application of protein-containing C3Ms is crucial. For food and pharmaceutical applications it should be realized that most foods are acidic, having a pH lower than 7,¹³ while body fluids are near neutral pH (~7.4) and the pH in the stomach is highly acidic. Bringing our FP-containing C3Ms into these fluids would mean that the charge on the protein decreases, which results in disintegration of the micelles. Thus, for a successful application in food or pharma, C3Ms should be designed in such a way that they stay intact until they reach the site of delivery.

For the encapsulation of enzymes, and especially for nanoreactors, finding optimal conditions might even be more complicated. On the one hand enzymes require a pH value for a sufficient charge on their surface to be encapsulated and on the other hand they have a pH range in which they are active. In many cases these pH values do not match, so the enzymes need additional interaction(s) with the polymer to keep the C3Ms intact while using the optimum pH for their activity.

Next to the pH, which influences the amount of charges on the proteins, salt can also disrupt the micelles by screening the charges on the protein and polymers and by diminishing the entropic gain from counter ion release. In the present study, the C3Ms have been prepared at low ionic strength, in a 10 mM borate buffer with an ionic strength of 2.5 mM. In **Chapter 5** we show that the micelles disintegrate already at an ionic strength of 20 mM. This would mean that under physiological conditions (corresponding to an ionic strength of about 150 mM), no C3Ms remain in solution. Furthermore, the rather fast exchange dynamics of the C3Ms, as shown in **Chapter 5**, makes them sensitive to dilution and unwanted protein exchange with for example blood proteins.

Nevertheless, there are many advantages of using C3Ms as protein carriers, as explained in detail in **Chapter 1**. Preparation is simple and the preparation conditions are favorable for proteins, as no organic solvents are required, which can disrupt the protein's function. The core of the C3Ms is highly hydrated, keeping the protein intact and easily accessible for ligands and substrates. Next to that, the micellar core can accommodate many protein molecules (~500). Finally, it is important to mention that the C3Ms have an ideal size for optimal uptake and bioavailability in the body (10 - 100 nm).¹⁴

6.4. Towards application of C3Ms as protein carriers and delivery systems

The issues mentioned in the section before show that improvements are needed to make protein-containing C3Ms suitable for application. To this end, one may add extra ingredients to the C3Ms, modify the protein or the diblock copolymer, or use combinations of these methods. Modification of the protein may involve either increasing its charge or adding functional groups to better interact with the polymer. Modification of the polymer may include adding a functional group or group of molecules to improve the interaction with the protein or to cross-link the micellar core.

First, addition of extra components to the C3Ms may add to their stability. For example, Lindhoud *et al.*, encapsulated proteins together with a homopolymer with the same charge sign and an oppositely charged diblock copolymer.^{12,15,16} The addition of the homopolymer increased the salt stability and the amount of enzymes in the core could be controlled. A serious drawback of this approach, however, is that only a few protein molecules per micelle can be stored.

Changing amino acid residues in a protein occurs via editing its gene. In this way, for example, positive amino acid residues on the surface can be changed into negative residues, or a sequence of residues can be added to one of the protein's termini. Increasing the charge on the protein's surface, either by replacing amino acid residues¹⁷ or modifying lysine residues to negatively charged residues¹⁸, only modestly enhances the stability of the protein-containing C3Ms. For example, the salt concentration at which protein-containing C3Ms micelles disintegrated, was increased from 18 mM to 48 mM by modifying lysine residues on the RNase A protein's surface to a net charge of -14.2.¹⁸ Alternatively, addition of a highly charged amino acid sequence to a protein via gene editing or bioconjugation may be more effectively. This strategy has already been used for the encapsulation of proteins in virus capsids and vesicles.^{19,20} Addition of such an extra stretch of amino acid residues did not alter the structure and function of the proteins. Next to that, in these systems the encapsulation was very specific, because the added sequence interacts specifically to a sequence modified on the side of the enveloping material. For example, a deca-arginine tag was added to the protein to interact with a set of glutamates in the capsids²¹, and a coiled-coil sequence was added to the protein to interact with another coiled-coil sequence attached to the capsid that together form stable dimers.^{22,23}

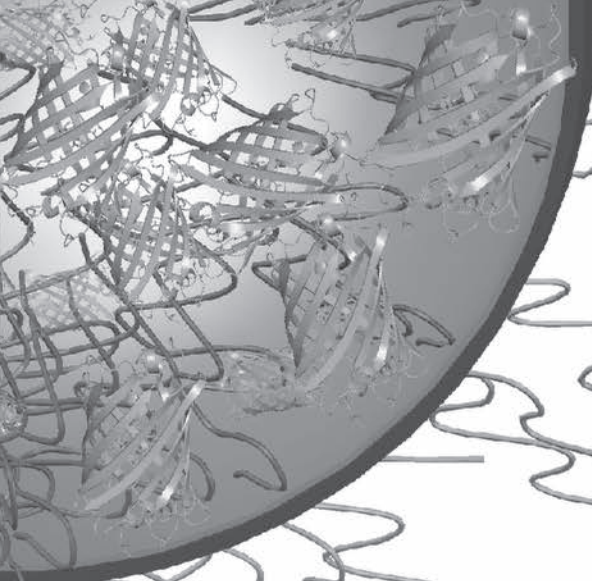
To use the latter type of interactions in C3Ms would also require a modification of the polymer, so there is another type of interaction between protein and polymer in addition to the electrostatic interaction. Another possibility is to modify the polymer in such a way that the polymers in the corona or core of the micelles can be cross-linked without changing the protein. From the results and the model proposed in **Chapter 5** it follows that this cross-linking would make it very difficult for the proteins to leave the micelles, because dissociation of small, near neutral polymer-protein complexes would be no longer possible. Different ways of polymer cross-linking exist with the involvement of various functional groups on the polymers and/or bifunctional cross-linkers.^{24,25} Cross-linking has already been proven to enhance the stability of drug-, polynucleotide- and protein-containing polyion complex micelles compared to non-cross-linked ones.²⁴ Biodegradable or reversible cross-links in turn can be used to trigger the release of the cargo at the target site, leading to specific drug delivery and a reduction of side effects.^{26,27}

In this thesis, we showed the successful encapsulation of about 500 EGFP molecules in a C3M using diblock copolymers. This high amount of FPs per C3M led to dimerization of EGFP, resulting in a pK_a shift of its chromophore. By using seven other FPs, the effect of encapsulation on the structure and spectral properties of these proteins was systematically investigated. Hydrozoa FPs were more efficiently encapsulated than Anthozoa FPs, and the latter proteins were subject to di- or tetramerization in C3Ms. Finally, fast exchange dynamics of C3Ms were detected using FRET. Combining the insights obtained during this PhD project with sophisticated protein engineering and bioconjugation procedures, may lead in the near future to C3M-based protein nanoparticles that can be used for food and pharmaceutical applications.

References

- Maeder, C. I.; Hink, M. A.; Kinkhabwala, A.; Mayr, R.; Bastiaens, P. I.; Knop, M., Spatial regulation of Fus3 MAP kinase activity through a reaction-diffusion mechanism in yeast pheromone signalling. *Nat. Cell Biol.* **2007**, *9*, (11), 1319-1326.
- Hink, M. A., Fluorescence correlation spectroscopy. In *Advanced fluorescence microscopy. Methods in molecular biology (methods and protocols)*, Verwee, P., Ed. Humana Press: New York, NY, 2015; Vol. 1251.
- Rachel, N. M.; Toulouse, J. L.; Pelletier, J. N., Transglutaminase-catalyzed bioconjugation using one-pot metal-free bioorthogonal chemistry. *Bioconjugate Chem.* **2017**, *28*, (10), 2518-2523.
- Zacharias, D. A.; Violin, J. D.; Newton, A. C.; Tsien, R. Y., Partitioning of lipid-modified monomeric GFPs into membrane microdomains of live cells. *Science* **2002**, *296*, (5569), 913-916.
- Megley, C. M.; Dickson, L. A.; Maddalo, S. L.; Chandler, G. J.; Zimmer, M., Photophysics and dihedral freedom of the chromophore in yellow, blue, and green fluorescent protein. *J. Phys. Chem. B* **2009**, *113*, (1), 302-308.
- Goedhart, J.; von Stetten, D.; Noirclerc-Savoye, M.; Lelimousin, M.; Joosen, L.; Hink, M. A.; van Weeren, L.; Gadella, T. W. J.; Royant, A., Structure-guided evolution of cyan fluorescent proteins towards a quantum yield of 93%. *Nat. Commun.* **2012**, *3*, 751.
- Rekas, A.; Alattia, J. R.; Nagai, T.; Miyawaki, A.; Ikura, M., Crystal structure of venus, a yellow fluorescent protein with improved maturation and reduced environmental sensitivity. *J. Biol. Chem.* **2002**, *277*, (52), 50573-50578.
- Kikuchi, A.; Fukumura, E.; Karasawa, S.; Mizuno, H.; Miyawaki, A.; Shiro, Y., Structural characterization of a thiazoline-containing chromophore in an orange fluorescent protein, monomeric Kusabira Orange. *Biochemistry* **2008**, *47*, (44), 11573-11580.
- Yarbrough, D.; Wachter, R. M.; Kallio, K.; Matz, M. V.; Remington, S. J., Refined crystal structure of DsRed, a red fluorescent protein from coral, at 2.0-Å resolution. *Proc. Natl. Acad. Sci. U. S. A.* **2001**, *98*, (2), 462-467.
- Subach, O. M.; Malashkevich, V. N.; Zencheck, W. D.; Morozova, K. S.; Piatkevich, K. D.; Almo, S. C.; Verkhusa, V. V., Structural characterization of acylimine-containing blue and red chromophores in mTagBFP and TagRFP fluorescent proteins. *Chem. Biol.* **2010**, *17*, (4), 333-341.
- Shu, X.; Shaner, N. C.; Yarbrough, C. A.; Tsien, R. Y.; Remington, S. J., Novel chromophores and buried charges control color in mFruits. *Biochemistry* **2006**, *45*, (32), 9639-9647.
- Lindhoud, S.; Norde, W.; Cohen Stuart, M. A., Reversibility and relaxation behavior of polyelectrolyte complex micelle formation. *J. Phys. Chem. B* **2009**, *113*, (16), 5431-5439.
- Food-info (1999). [Online]. Available: <http://www.food-info.net>. (Accessed: 28 Oct 2017)
- Zhao, M.; Zhou, J.; Su, C.; Niu, L.; Liang, D.; Li, B., Complexation behavior of oppositely charged polyelectrolytes: Effect of charge distribution. *J. Chem. Phys.* **2015**, *142*, (20), 204902.
- Lindhoud, S.; de Vries, R.; Norde, W.; Cohen Stuart, M. A., Structure and stability of complex coacervate core micelles with lysozyme. *Biomacromolecules* **2007**, *8*, (7), 2219-2227.
- Lindhoud, S.; Norde, W.; Cohen Stuart, M. A., Effects of polyelectrolyte complex micelles and their components on the enzymatic activity of lipase. *Langmuir* **2010**, *26*, (12), 9802-9808.
- Lam, C. N.; Yao, H.; Olsen, B. D., The effect of protein electrostatic interactions on globular protein-polymer block copolymer self-assembly. *Biomacromolecules* **2016**, *17*, (9), 2820-2829.
- Obermeyer, A. C.; Mills, C. E.; Dong, X. H.; Flores, R. J.; Olsen, B. D., Complex coacervation of supercharged proteins with polyelectrolytes. *Soft Matter* **2016**, *12*, (15), 3570-3581.
- de la Escosura, A.; Nolte, R. J. M.; Cornelissen, J. J. L. M., Viruses and protein cages as nanocontainers and nanoreactors. *Journal of Materials Chemistry* **2009**, *19*, (16), 2274.
- Park, W. M.; Champion, J. A., Thermally triggered self-assembly of folded proteins into vesicles. *J. Am. Chem. Soc.* **2014**, *136*, (52), 17906-17909.
- Seebeck, F. P.; Woycechowsky, K. J.; Zhuang, W.; Rabe, J. P.; Hilvert, D., A simple tagging system for protein encapsulation. *J. Am. Chem. Soc.* **2006**, *128*, (14), 4516-4517.
- Minten, I. J.; Hendriks, L. J.; Nolte, R. J.; Cornelissen, J. J., Controlled encapsulation of multiple proteins in virus capsids. *J. Am. Chem. Soc.* **2009**, *131*, (49), 17771-17773.
- Minten, I. J.; Nolte, R. J. M.; Cornelissen, J. J. L. M., Complex assembly behavior during the encapsulation of green fluorescent protein analogs in virus derived protein capsules. *Macromol. Biosci.* **2010**, *10*, (5), 539-545.
- Kim, J. O.; Ramasamy, T.; Yong, C. S.; Nukolova, N. V.; Bronich, T. K.; Kabanov, A. V., Cross-linked polymeric micelles based on block ionomer complexes. *Mendeleev Commun.* **2013**, *23*, (4), 179-186.

25. Elsabahy, M.; Wooley, K. L., Design of polymeric nanoparticles for biomedical delivery applications. *Chem. Soc. Rev.* **2012**, 41, (7), 2545-2561.
26. Sahay, G.; Kim, J. O.; Kabanov, A. V.; Bronich, T. K., The exploitation of differential endocytic pathways in normal and tumor cells in the selective targeting of nanoparticulate chemotherapeutic agents. *Biomaterials* **2010**, 31, (5), 923-933.
27. Lee, Y.; Kataoka, K., Biosignal-sensitive polyion complex micelles for the delivery of biopharmaceuticals. *Soft Matter* **2009**, 5, (20), 3810-3817.



Chapter 7

English summary

Nederlandse samenvatting

Fryske gearfetting

Summary

During this PhD-project the composition, formation, dynamics, and stability of complex coacervate core micelles (C3Ms) containing fluorescent proteins have been explored. The project started with encapsulation of enhanced green fluorescent protein (EGFP) in C3Ms and the characterization of these micelles using dynamic light scattering (DLS) and fluorescence correlation spectroscopy (FCS). The potential of these two techniques for the C3M research is analyzed in **Chapter 2**. Subsequently, the consequences of encapsulation on the structure and spectral properties of EGFP were investigated (**Chapter 3**). In **Chapter 4** fluorescent proteins (FPs) from different classes (Hydrozoa and Anthozoa), covering the whole visible spectrum, were encapsulated in C3Ms. In **Chapter 5**, C3M dynamics were investigated by using two selected FPs. Finally, in **Chapter 6**, the results of this project are placed into perspective with respect to their implications for the application of protein-containing C3Ms in biotechnology and medicine. Furthermore, directions for future research are discussed. Below the main findings are outlined per chapter.

Protein-containing complex coacervate core micelles

In **Chapter 1** the background of this research is introduced. In general, for applications of proteins in industry and in food and medical applications, encapsulation is important to protect these proteins from environmental conditions. C3Ms are promising structures to protect proteins, since they are prepared in aqueous solution, they have a high loading capacity and their core contains a considerable amount of water, which is beneficial to preserve the proteins' structure and functionality. However, details on the composition and dynamics of protein-containing C3Ms were still largely unknown. In this thesis, C3Ms are formed using cationic-neutral diblock copolymers and negatively charged fluorescent proteins. The driving forces for the formation of these C3Ms are attractive Coulomb interactions and the entropy gain due to counter-ion release. The resulting complexes consist of a corona containing the neutral water-soluble block and a core comprising the complex of protein and cationic block of the diblock copolymer.

Encapsulation of EGFP

The PhD project started with the encapsulation of EGFP in C3Ms with two different lengths of the diblock copolymer poly(2-methyl-vinyl-pyridinium)_n-*b*-poly(ethylene-oxide)_m (P2MVP_n-*b*-PEO_m): P2MVP₄₁-*b*-PEO₂₀₅ and P2MVP₁₂₈-*b*-PEO₄₇₇, as described in **Chapter 2**. First the optimal ratio between protein and polymer, at which most C3Ms were formed (the preferred micellar composition, PMC), was investigated with DLS. C3Ms with a hydrodynamic radius of about 33 nm were formed with a PMC at $F^+ = 0.65$ (F^+ is the concentration of positive charges on the polymers divided by the total sum of charges on the polymers and protein molecules) for both lengths of diblock copolymer. Comparable measurements were performed with FCS, which yielded similar results. Further investigation of EGFP in C3Ms was performed with FCS, because this technique is more sensitive than DLS and it gives an additional parameter, *i.e.*, the average number of fluorescent particles in the confocal volume.

C3Ms at the PMC were prepared at a relative high concentration and then diluted to find the critical micelle concentration (CMC), which is the lowest concentration at which C3Ms are formed. This CMC was found at a concentration of 100 nM EGFP with both lengths of diblock copolymer. To determine the amount of EGFP molecules encapsulated in C3Ms, the fluorescence intensity of free EGFP was related to the fluorescence intensity of C3Ms containing EGFP. For this it was necessary to decrease the fluorescence signal of C3Ms containing EGFP by replacing EGFP with a non-absorbing and non-fluorescent EGFP variant, called darkGFP. It was found that about 450 EGFP molecules are encapsulated in one C3M for P2MVP₄₁-*b*-PEO₂₀₅ and 530 EGFP molecules for P2MVP₁₂₈-*b*-PEO₄₇₇. During this last experiment, it appeared that the fluorescence excitation and emission spectra of encapsulated EGFP differed from that of free EGFP.

EGFP dimerizes in C3Ms

In **Chapter 3** the fluorescence spectral properties of encapsulated EGFP were further investigated. It was known that free EGFP has the tendency to dimerize, and therefore, the characteristics of encapsulated EGFP were compared with those of encapsulated mEGFP, a monomeric variant of EGFP. The difference between these two proteins is an A206K substitution in mEGFP. This substitution increases the dimer dissociation constant from 0.11 mM for EGFP to approximately 74 mM for mEGFP. First, the spectral properties were compared for both proteins encapsulated in C3Ms with P2MVP₄₁-*b*-PEO₂₀₅. The results revealed a significant change in the absorption and fluorescence spectra of EGFP compared to its free form and both free and encapsulated mEGFP, which all show fluorescence excitation maxima at 490 nm and fluorescence emission maxima at 509 nm. However, the spectra of encapsulated EGFP showed an additional absorption peak at 395 nm, which was of special interest to us. This peak is similar to the absorption peak at 395 nm of wild-type GFP, which is due to the protonation of the chromophore. Consequently, protonation of the chromophores of EGFP and mEGFP was examined by pH titrations, which resulted into similar features in absorption and fluorescence spectra. In addition, the structural characteristics of the β -barrel and chromophore were examined with circular dichroism (CD). Upon encapsulation of both proteins their far-UV CD spectra showed minor changes compared to that of both free proteins. The most striking difference, however, was found in the visible-near-UV CD spectra of the chromophores, which pointed to a structural change of the encapsulated EGFP chromophore. Finally, Förster resonance energy transfer (FRET) between encapsulated protein molecules, more precisely homo-FRET, was probed with time-resolved fluorescence anisotropy (TRFA). For this experiment, the average distance between the (m)EGFP molecules in C3Ms was increased by using SBFP2 as invisible protein substitute thereby keeping the total protein concentration in C3Ms constant. The TRFA data showed faster transfer correlation times with increasing amounts of (m)EGFP molecules in the C3Ms, confirming the presence of homo-FRET in C3Ms for both proteins. Furthermore, it was found that encapsulated mEGFP gave lower transfer correlation times than encapsulated EGFP. Based on these results we concluded that EGFP dimerizes in C3Ms and mEGFP mainly remains monomeric. The dimerization of EGFP probably

causes a reorientation of Glu222 in the chromophore environment resulting in a pK_a shift of the chromophore. After release of EGFP from the C3Ms at high ionic strength the characteristics of free EGFP in solution are fully restored.

Encapsulation of FPs covering the whole visible spectrum

In **Chapter 4** the research was extended with the encapsulation of other FPs from different species, covering the whole visible spectrum: SBFP2 (blue FP), mTurquoise2 (cyan FP), mEGFP (green FP), and SYFP2 (yellow FP) from class Hydrozoa (*av*FPs) and mKO2 (orange FP), TagRFP (red FP), and mCherry (red FP) from class Anthozoa (*an*FPs). To be able to encapsulate the proteins in C3Ms with the same diblock copolymers as used before, the net charge of all FPs was calculated and the pH at which they have a sufficiently negative charge was determined. All FPs were encapsulated with both P2MVP₄₁-*b*-PEO₂₀₅ and P2MVP₁₂₈-*b*-PEO₄₇₇ at pH 9.0, except for TagRFP, which was encapsulated at pH 10.0. With DLS, F^+ PMC values between 0.60 and 0.75 were found. The corresponding radii of C3Ms varied between 30 and 38 nm, except for mKO2 for which radii of about 27 nm was found. Subsequently, with FCS the encapsulation efficiencies of all FPs were determined. For all *av*FPs, it was found that almost all protein molecules were packed in C3Ms, thus resulting in almost 100% encapsulation efficiencies. Lower encapsulation efficiencies, however, were found for *an*FPs, of which only 50% to 75% of the protein molecules were encapsulated. The study was continued with characterizing the spectral and structural properties of the encapsulated FPs. The spectral characterization revealed minor changes for the *av*FPs and major changes in fluorescence quantum yield for mKO2 and TagRFP, and a pK_a shift of the chromophore of mCherry. For all FPs the CD spectral properties alter to a greater or lesser extent upon encapsulation. It should be noted that also for the free proteins, the CD spectra of the *an*FPs are different from that of the *av*FPs. This can be explained from the ribbon structures of the studied FPs: the β -barrel exhibits a more elliptic cylinder for the *an*FPs than for the *av*FPs. Other differences between the two classes of proteins concern the charge distribution on their surface and the tendency to remain monomeric. All these differences probably contribute to the variations in encapsulation efficiency between *av*FPs and *an*FPs.

Formation, dynamics, and stability of C3Ms

In **Chapter 5**, the dynamics of C3Ms were investigated using two FPs that form a good FRET pair, as concluded from the analysis in **Chapter 4**. These FPs, mTurquoise2 and SYFP2, were encapsulated with P2MVP₁₂₈-*b*-PEO₄₇₇. Also in this study, SBFP2 was used as an invisible protein substitute to lower the fluorescence signal while keeping the total protein concentration constant. Encapsulation of mTurquoise2 and SYFP2 together in a C3M yielded a strong reduction of donor fluorescence intensity and sensitized emission of acceptor upon donor excitation. FRET depended on the amount of FRET pair present in C3Ms, which was illustrated by an asymptotic curve for the FRET efficiency with a maximum of 0.90. From this FRET efficiency, a minimal distance of 40 Å at a 100% FRET pair amount was calculated. Furthermore, FRET was also used to follow C3M formation in time and protein exchange between C3Ms. Both processes were found to follow first-order

kinetics with relaxation times of about 100 s at an ionic strength of 2.5 mM. The salt stability of the C3Ms was also investigated. Titration with sodium chloride revealed that 50% of FRET was lost at $I = 20$ mM, pointing at disintegration of the C3Ms. Based on the kinetic results, a two-state model was proposed for the formation and relaxation of FP-containing C3Ms. This model involved the formation of soluble complexes consisting of probably one diblock copolymer and about 10 associated protein molecules. For the formation of C3Ms and protein exchange between them, it is hypothesized that these soluble complexes associate and dissociate with the micelles until their equilibrium size and composition is reached. From the kinetic experiments and the salt stability, the Gibbs energy of formation of a C3M is estimated to be about $-880 k_B T/\text{micelle}$ at an ionic strength of 2.5 mM.

General discussion

Finally, we discuss in **Chapter 6** how the encapsulation influences the fluorescent proteins, how the interactions between proteins and polymers influence the stability of the C3Ms, and how the results from this research contribute to the development of protein-containing C3Ms that are suitable for applications. For the latter, C3Ms are needed that have improved rigidity and salt stability. Promising strategies that have been developed can be adapted, *e.g.*, adding functional groups to the protein or using cross-linking methods between polymers alone or between polymers and proteins.

Nederlandse samenvatting

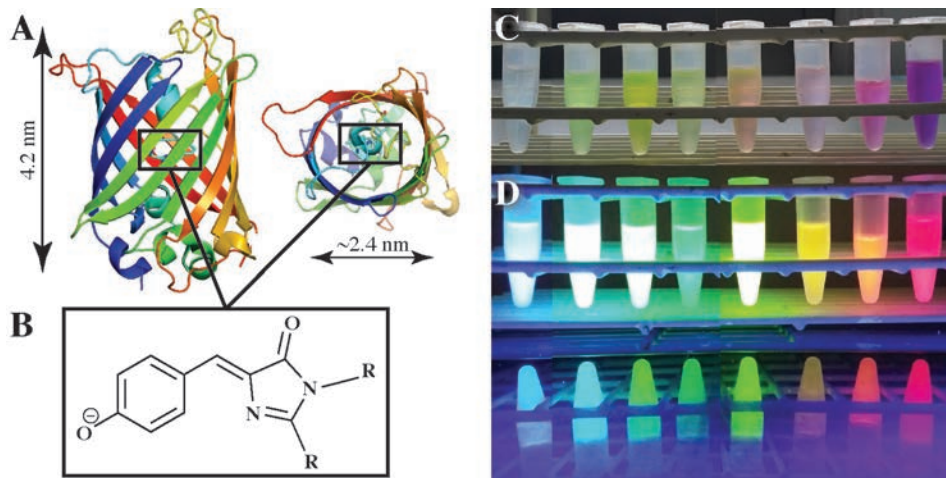
Eiwitten, of proteïnen, zijn de bouwstenen van het leven en zijn de meest voorkomende biomacromoleculen in alle levende organismen. Daarnaast worden eiwitten op veel verschillende manieren gebruikt, bijvoorbeeld als therapeutisch middel, als toevoeging aan voedingsmiddelen, of in industriële processen. In al deze en andere toepassingen zou het van belang kunnen zijn om eiwitten te beschermen tegen hun omgeving om hun functie te behouden. Bijvoorbeeld therapeutische eiwitten die toegediend worden aan het lichaam moeten worden beschermd tegen maag- of andere lichaamssappen en/of het immuunsysteem. Daarom is het belangrijk om strategieën te vinden om eiwitten te beschermen op zo'n manier dat hun belangrijkste kenmerken behouden blijven en dat ze op de gewenste plek gebruikt kunnen worden.

Eiwitten

Een eiwit is opgebouwd uit een keten van verschillende aminozuren. In totaal zijn er 20 verschillende aminozuren en deze hebben uiteenlopende eigenschappen: sommigen houden niet van water (hydrofoob) en anderen juist wel (hydrofiel); de hydrofiele aminozuren kunnen geladen zijn. De keten van aminozuren wordt ook wel een polypeptideketen genoemd. Afhankelijk van de volgorde van de aminozuren vouwt de polypeptideketen zich op een bepaalde manier en de uiteindelijke driedimensionale vorm zorgt ervoor dat een eiwit functioneel kan zijn. Veelvoorkomende functies van eiwitten zijn: het geven van vorm en stevigheid aan een cel (zoals collageen), het verzorgen van de communicatie in en tussen cellen (zoals hormonen), het beschermen van het lichaam (zoals antilichamen), en het katalyseren van biochemische reacties (zoals enzymen).

Fluorescente eiwitten

De eiwitten die in dit onderzoek zijn gebruikt, zijn speciale kleurrijke eiwitten, namelijk fluorescente eiwitten. Deze eiwitten komen van nature voor in sommige soorten kwallen (klasse Hydrozoa) en koralen (klasse Anthozoa), zoals weergegeven op de omslag van dit proefschrift. Ze hebben de vorm van een cilinder die 4.2 nanometer hoog en ongeveer 2.4 nanometer breed is (Figuur 7.1A). (1 nanometer is 0.000001 millimeter.) In het midden van deze cilinder bevindt zich een zogenaamde chromofoor die voor de kleur van het eiwit zorgt (Figuur 7.1B). Dit chromofoor ziet er in de verschillende fluorescente eiwitten net iets anders uit en heeft net iets andere interacties met zijn omgeving, waardoor de eiwitten verschillende kleuren hebben (Figuur 7.1C en 7.1D). In daglicht zien we alleen de kleur van de eiwitten (absorptie, Figuur 7.1C), terwijl met ultraviolet (UV) licht de fluorescentie van de eiwitten duidelijk te zien is (Figuur 7.1D). Bij fluorescentie wordt het kortgolvlige UV-licht omgezet in kleuren met langere golflengten (zoals geel en rood). Door de fluorescente eigenschappen van deze eiwitten zijn ze met bepaalde technieken goed te volgen. Dat is de reden dat ze in dit onderzoek zijn gebruikt.



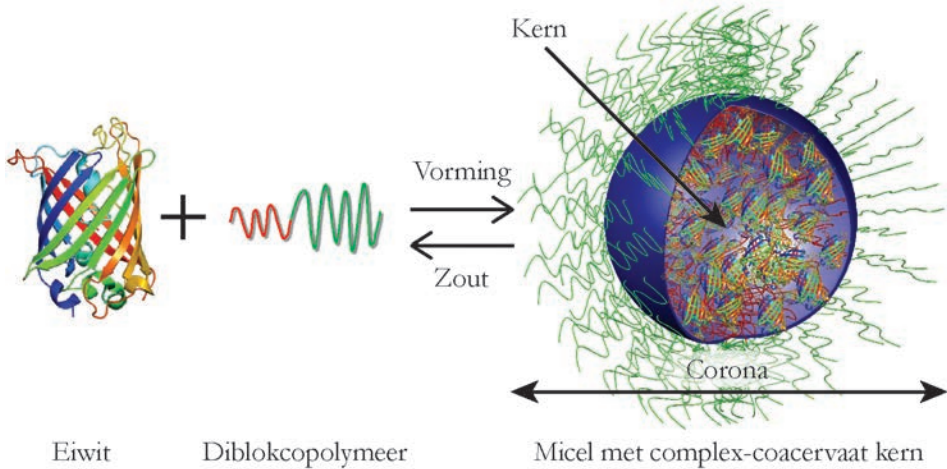
Figuur 7.1. Eigenschappen van de fluorescente eiwitten die zijn gebruikt in dit proefschrift. (A) De vorm van de eiwitten en (B) de chromofor die de kleur bepaalt van de eiwitten. De fluorescente eiwitten in (C) normaal licht en (D) UV-licht.

Inpakken van fluorescente eiwitten

Er zijn al verschillende methodes onderzocht en gebruikt om eiwitten in te pakken. Een manier die nog niet zoveel onderzocht is, is het gebruik van zogenaamde micellen met complex-coacervaat kernen (micel in het kort). Zo'n micel ontstaat wanneer tenminste twee soorten macromoleculen die tegengesteld geladen zijn, gemengd worden. Een van deze moleculen is compleet geladen en het andere soort molecuul moet behalve een geladen stuk ook een ongeladen deel bevatten dat goed in water oplost; dit wordt een diblokcopolymeer genoemd. De fluorescente eiwitten zijn negatief geladen, waardoor we voor het inpakken gebruik hebben gemaakt van een diblokcopolymeer dat een positief geladen deel heeft. Wanneer oplossingen van deze twee moleculen worden gemengd, ontstaan de micellen door de aantrekkingskracht tussen de negatieve en positieve ladingen. Hierdoor komen de eiwitten en het positief geladen deel van de diblokcopolymeren als een complex terecht in de kern van de micellen. De ongeladen gedeelten van de diblokcopolymeren bevinden zich aan de buitenkant van de micellen die zo een corona vormen en op deze manier de micellen in oplossing houden (zie Figuur 7.2).

Micellen met fluorescente eiwitten

Het inpakken van de fluorescente eiwitten met de diblokcopolymeren leidt tot de vorming van zeer kleine bolletjes met een straal van ongeveer 33 nanometer (dat is zo'n 1000 keer kleiner dan de dikte van een mensenhaar). Om deze deeltjes, de micellen, te kunnen bekijken heb je speciale technieken nodig die uitgebreid beschreven staan in **Hoofdstuk 1**. Met een aantal van deze technieken zijn de samenstelling en de grootte van de micellen bestudeerd in **Hoofdstukken 2 en 4**. We vonden bijvoorbeeld dat er zo'n 500 fluorescente eiwitten in één micel zitten. Zoals hierboven vermeld, hebben we gebruik gemaakt van fluorescente eiwitten



Figuur 7.2. De verschillende componenten van een micel met een complex-coacervaat kern, dat wil zeggen een kern die bestaat uit een complex van tegengesteld geladen moleculen. Bij de vorming van de micel gaat de reactie naar rechts en bij het toevoegen van zout gaat de reactie naar links.

afkomstig van twee verschillende groepen, Hydrozoa en Anthozoa. Het bleek dat de vijf fluorescente eiwitten afkomstig van klasse Hydrozoa allemaal goed werden ingepakt (voor zo'n 100%) en dat de drie afkomstig van klasse Anthozoa minder goed werden ingepakt (voor zo'n 50% tot 75%). Wij vermoeden dat deze afwijking te maken heeft met het verschil van de vorm van de eiwitten tussen de twee groepen: de Anthozoa-eiwitten zijn elliptischer dan de Hydrozoa-eiwitten, want de Anthozoa-eiwitten zijn breder dan 2.4 nanometer. Daarnaast is de ladingsverdeling op het oppervlak van de eiwitten anders: bij de Hydrozoa-eiwitten zit aan één kant van het oppervlak van de eiwitten veel negatieve ladingen, terwijl bij de Anthozoa-eiwitten de negatieve ladingen meer gelijkmatig verdeeld zijn over het gehele oppervlak van het eiwit.

De gevolgen van inpakken

Naast het bestuderen van een micel in zijn geheel, hebben we ook gekeken naar de kenmerken van de ingepakte eiwitten, dit hebben we onderzocht in **Hoofdstukken 3 en 4**. De ingepakte eiwitten blijken te veranderen van vorm en in hun fluorescente eigenschappen ten opzichte van de eiwitten vrij in oplossing. De hoeveelheid fluorescente eiwitten in de kern van een micel blijkt van invloed te zijn op de mate waarin de eiwitmoleculen aan elkaar plakken (associëren). Vrij in oplossing zijn eiwitmoleculen niet geassocieerd en daardoor zijn ze als monomeer aanwezig. Als ze ingepakt worden komen ze echter zo dicht bij elkaar dat, afhankelijk van het type, een deel van de eiwitmoleculen associeert, waardoor ze ook als dimeer (twee eiwitmoleculen aan elkaar) of tetrameer (vier eiwitmoleculen aan elkaar) in de kern aanwezig zijn.

Zowel de mate van associatie als de vorm van de fluorescente eiwitten is van invloed op de fluorescente eigenschappen. Echter, de interactie tussen het eiwit en het diblokcopolymeer heeft ook effect op deze eigenschappen. Dit werd duidelijk uit de metingen aan fluorescente eiwitvarianten die monomeer bleven in de kern van de micellen.

In het kort hebben we uit het onderzoek beschreven in de **Hoofdstukken 2, 3 en 4** de volgende conclusies kunnen trekken:

- fluorescente eiwitten afkomstig van klasse Hydrozoa worden beter ingepakt dan die van klasse Anthozoa;
- de fluorescente eigenschappen van de ingepakte eiwitten worden minder beïnvloed door het langere diblokcopolymeer;
- zowel associatie van de eiwitten in de micellen als de interactie met het diblokcopolymeer leidt tot veranderingen in structuur en fluorescente eigenschappen van de eiwitten;
- de eigenschappen van de cyaan- en geelgekleurde eiwitten worden het minst beïnvloed door het inpakken.

Dynamiek van micellen

In Hoofdstuk 5 is de dynamiek van de micellen onderzocht. Dat wil zeggen dat de snelheid van de vorming van de micellen, de uitwisseling van eiwitmoleculen tussen micellen onderling, en de stabiliteit van de micellen in aanwezigheid van verschillende hoeveelheden zout is gemeten. Hieruit bleek dat de vorming van de micellen en de volledige uitwisseling van eiwitmoleculen tussen micellen onderling even snel gebeurt; beide processen duren zo'n 100 seconden. De aantrekkingskracht tussen tegengesteld geladen deeltjes neemt af als de zoutconcentratie toeneemt en dat geldt ook voor de kracht tussen de eiwitten en de diblokcopolymeren. De zoutconcentratie van menselijk bloed is 150 millimolair natriumchloride (keukenzout). De onderzochte micellen vallen echter al uit elkaar bij 20 millimolair natriumchloride, dus ze zijn niet goed bestand tegen zout (zie Figuur 7.2).

Conclusie

Dit proefschrift geeft nieuwe inzichten in het inpakken van eiwitten met geladen diblokcopolymeren in micellen met een complex-coacervaat kern. De samenstelling, grootte en dynamische eigenschappen van de micellen en de gevolgen van inpakken op de eiwitten zijn onderzocht. De resultaten zijn bediscussieerd in **Hoofdstuk 6** in relatie tot de praktische toepassing van het inpakken van eiwitten in de micellen. Daarnaast hebben we ook mogelijke verbeteringen aangedragen. Het is vooral nodig dat de micellen stabiel worden gemaakt, waardoor ze onder andere bestand zijn tegen een hogere zoutconcentratie en minder snel onderling eiwitten uitwisselen.

Fryske gearfetting

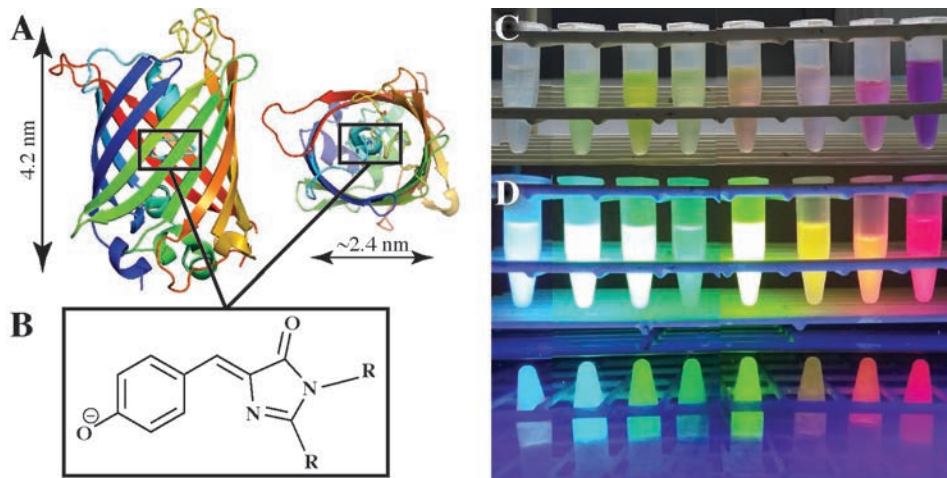
Aaiwiten, of proteïnen, binne de boustiennen fan it libben en binne de meast foarkommende biomakromolekulen yn alle libbene organismen. Dêrneist wurde aaiwiten op in soad ferskate wizen brûkt, bygelyks as terapeutysk middel, as tafoeging oan libbensmiddels, of yn yndustriële prosessen. Yn al dy en oare tapassingen soe it fan belang wêze kinne om aaiwiten te beskermjen tsjin harren omjouwing om harren funksje te behâlden. Bygelyks terapeutyske aaiwiten dy't yn it liif brocht wurde, moatte beskermje wurde tsjin mage- en oare lichemssoppen en/of it ymmúnstysteem. Dêrom is it wichtich om strategyen te finen om aaiwiten te beskermjen op sa'n wize dat harren wichtichste eigenskippen behâlden bliuwe en dat se op it goede plak brûkt wurde kinne.

Aaiwiten

In aaiwyt is opboud út in keten fan ferskate aminosuieren. Yn totaal binne der 20 ferskate aminosuieren en dy ha inoar ûntrinnende eigenskippen: guon hâlde net fan wetter (hydrofoob) en oaren just wol (hydrofyl); de hydrofile aminosuieren kinne laden wêze. De keten fan aminosuieren wurdt ek wol in polypeptideketen neamd. Ofhinklik fan de folchoarder fan de aminosuieren teart de polypeptideketen him op in bepaalde manier. De úteinlike trijediminsjonale foarm soarget derfoar dat in aaiwyt funksjoneel wêze kin. In protte foarkommende funksjes fan aaiwiten binne: it jaan fan foarm en stevigens oan in sel (lykas kollageen), it fersoargjen fan de kommunikaasje yn en tusken sellen (lykas hormoanen), it beskermjen fan it liif (lykas antylichems), en it katalysearjen fan biogemyske reaksjes (lykas ensimen).

Fluoressinte aaiwiten

De aaiwiten dy't foar dit ûndersyk brûkt binne, binne spesjale kleurige aaiwiten, nammentlik fluoressinte aaiwiten. Dy aaiwiten komme fan natuere foar yn guon soarten kwallen (klasse Hydrozoa) en koralen (klasse Anthozoa), lykas werjûn op it omslach fan dit proefskrift. Se ha de foarm fan in silinder dy't 4.2 nanometer heech en likernôch 2.4 nanometer breed is (Figuer 7.3A). (1 nanometer is 0.000001 milimeter.) Yn 'e midden fan dy silinder sit in saneamde gromofoar dy't foar de kleur fan it aaiwyt soarget (Figuer 7.3B). Dat gromofoar sjocht der yn de ferskate fluoressinte aaiwiten krekt wat oars út en hat krekt wat oare ynteraksjes mei syn omjouwing, wêrtroch't de aaiwiten ferskate kleuren ha (Figuer 7.3C en 7.3D). Yn deiljocht sjogge wy allinnich de kleur fan it aaiwyt (absorpsje, Figuer 7.3C), wylst mei ultrafiolet (UF) ljocht de fluoressinsje fan de aaiwiten dúdlik te sjen is (Figuer 7.3D). By fluoressinsje wurdt it koartweagjende UF-ljocht omset yn kleuren mei in langere weachlingte (lykas giel en read). Troch de fluoressinte eigenskippen fan dy aaiwiten binne se mei guon techniken goed te folgjen. Dat is de reden dat se yn dit ûndersyk brûkt binne.



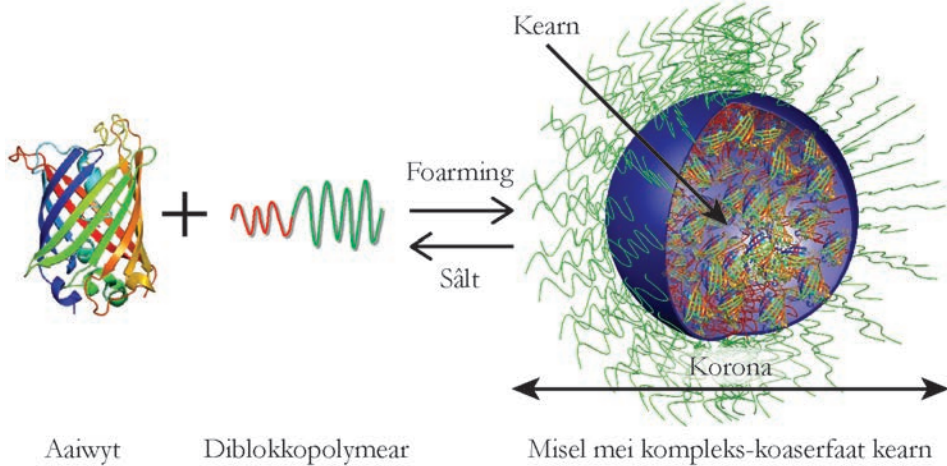
Figuer 7.3. Eigenskippen fan de fluoressinte aaiwiten dy't brûkt binne yn dit proefskrift. (A) De foarm fan de aaiwiten en (B) de gromfoar dy't de kleur bepaalt fan de aaiwiten. De fluoressinte aaiwiten yn (C) deiljocht en (D) UF-ljocht.

Ynpakken fan fluoressinte aaiwiten

Der binne al in tal ferskillende metoaden ûndersocht en brûkt om aaiwiten yn te pakken. Ien manier dy't noch net safolle ûndersocht is, is it brûken fan saneamde misellen mei kompleks-koaserfaat kearnen (misel yn it koart). Sa'n misel ûntstiet wannear't teminsten twa soarten makromolekulen dy't tsjinoersteld laden binne, mingd wurde. Ien fan dy molekule is kompleet laden en it oare soart molekule moat neist in laden stik ek in ûnladen diel befetsje dat goed yn wetter oplost; dat wurdt in diblokkopolymeer neamd. De fluoressinte aaiwiten binne negatyf laden, wêrtroch't wy foar it ynpakken gebrûk makke ha fan in diblokkopolymeer dat in posityf laden diel hat. Wannear't oplossingen fan dy twa molekule mingd wurde, ûntstean de misellen troch de oanlûkingskrêft tusken de negative en positive ladingen. Dêrtroch komme de aaiwiten en it posityf laden diel fan de diblokkopolymearen as in kompleks telâne yn de kearn fan de misellen. De ûnladen dielen fan de diblokkopolymearen befine harren oan de bûtenkant fan de misellen dy't sa in korona foarmje en op dy manier de misellen yn oplossing hâlde (sjoch Figuer 7.4).

Misellen mei fluoressinte aaiwiten

It ynpakken fan de fluoressinte aaiwiten mei de diblokkopolymearen liedt ta de foarming fan tige lytse boltsjes mei in striel fan likernôch 33 nanometer (dat is sa'n 1000 kear lytser as de tsjokte fan in minskehier). Om dy dieltsjes, de misellen, besjen te kinnen hat men spesjale techniken nedich dy't wijdweidich beskreaun stean yn **Haadstik 1**. Mei in tal fan dy techniken binne de gearstalling en de grutte fan de misellen bestudearre yn **Haadstikken 2 en 4**. Wy fûnen bygelyks dat der sa'n 500 fluoressinte aaiwiten yn ien misel sitte. Lykas hjirboppe beskreaun, ha wy gebrûk makke fan fluoressinte aaiwiten ôfkomstich fan twa ferskillende groepen, Hydrozoa en Anthozoa. It die bliken dat de fiif fluoressinte aaiwiten ôfkomstich



Figuer 7.4. De ferskate komponinten fan in misel mei in kompleks-koaserfaat kearn, dat wol sizze in kearn dy't bestiet út in kompleks fan tsjinoersteld laden molekulen. By de foarming fan de misel giet de reaksje nei rjochts en by it tafoegjen fan sâlt giet de reaksje nei links.

fan klasse Hydrozoa allegearre goed ynpakt wurde (foar sa'n 100%) en dat de trije ôfkomstich fan klasse Anthozoa minder goed ynpakt wurde (foar sa'n 50% oant 75%). Wy tinke dat dy ôfwiking te meitsjen hat mei it ferskil fan de foarm fan de aaiwiten tusken de twa groepen: de Anthozoa-aaiwiten binne elliptysker as de Hydrozo-aaiwiten, want de Anthozoa-aaiwiten binne breder as 2.4 nanometer. Dêrneist is de ladingsferdieling op it oerflak fan de aaiwiten oars: by de Hydrozoa-aaiwiten sit oan ien kant fan it oerflak in soad negative ladingen, wylst by de Anthozoa-aaiwiten de negative ladingen mear lykmjittich ferdield binne oer it hiele oerflak fan it aaiwyt.

De gefolgen fan ynpakken

Njonken it bestudearjen fan in misel yn syn gehiel, ha wy ek sjoen nei skaaimerken fan de ynpakte aaiwiten, dat ha wy ûndersocht yn **Haadstikken 3 en 4**. De ynpakte aaiwiten wize út te feroarjen fan foarm en yn harren fluoressinte eigenskippen oangeande de aaiwiten frij yn oplossing. It tal fluoressinte aaiwiten yn de kearn fan in misel blykt fan ynfloed te wêzen op de mjitte wêryn't de aaiwytmolekulen oan inoar plakke (assosjearje). Frij yn oplossing binne aaiwytmolekulen net assosjearre en dêrtroch binne se as monomear oanwêzich. As se ynpakt wurde komme se lykwols sa ticht byinoar dat, ôfhinklik fan it type, in part fan de aaiwytmolekulen assosjearret, wêrtroch't se ek as dimear (twa aaiwytmolekulen oan inoar) of tetramear (fjouwer aaiwytmolekulen oan inoar) yn de kearn oanwêzich binne.

Sawol de mjitte fan assosjaasje as de foarm fan de fluoressinte aaiwiten is fan ynfloed op de fluoressinte eigenskippen. Lykwols, de ynteraksje tusken it aaiwyt en it diblokkopolymear hat ek effekt op dy eigenskippen. Dat waard dúdlik út de mjittingen oan fluoressinte aaiwytvarianten dy't monomear bleaunen yn de kearn fan de misellen.

Yn it koart, út it ûndersyk beskreaun yn de **Haadstikken 2, 3 en 4** ha wy de folgjende konklúzjes lûke kinnen:

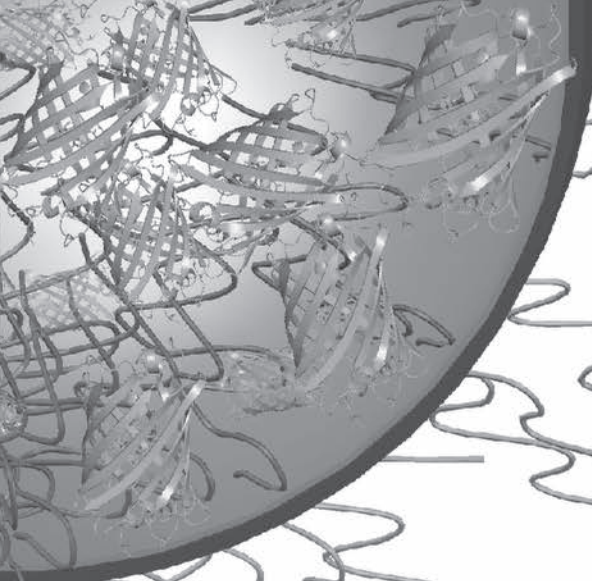
- fluoressinte aaiwiten ôfkomstich fan klasse Hydrozoa wurde better ynpakt as dy fan klasse Anthozoa;
- de fluoressinte eigenskippen fan de ynpakte aaiwiten wurde minder beynfloede troch it langere diblokkopolymear;
- sawol assosjaasje fan de aaiwiten yn de misellen as de ynteraksje mei it diblokkopolymear liedt ta feroaringen yn struktuer en fluoressinte eigenskippen fan de aaiwiten;
- de eigenskippen fan de syaan- en gielkleure aaiwiten wurde it minst beynfloede troch it ynpakken.

Dynamyk fan misellen

Yn **Haadstik 5** is de dynamyk fan de misellen ûndersocht. Dat wol sizze dat de faasje fan de foarming fan de misellen, de útwikseling fan aaiwytmolekulen tusken misellen ûnderinoar, en de stabiliteit fan de misellen yn oanwêzigens fan ferskate hoemannichten sâlt mjitten is. Dêr die út bliken dat de foarming fan de misellen en de folsleine útwikseling fan aaiwytmolekulen tusken misellen ûnderinoar like rap bart; beide prosessen duorje sa'n 100 sekonden. De oanlúkingskrêft tusken tsjinsteld laden dieltsjes nimt ôf as de sâltkonsintraasje tanimt en dat jildt ek foar de krêft tusken de aaiwiten en de diblokkopolymearen. De sâltkonsintraasje fan minsklik bloed is 150 milimolêr natriumgloride (keukensâlt). De ûndersochte misellen falle lykwols al út inoar by 20 milimolêr natriumgloride, dus se binne net sa goed bestân tsjin sâlt (sjoch Figuer 7.2).

Konklúzje

Dit proefskrift jout nije ynsichten yn it ynpakken fan aaiwiten mei laden diblokkopolymearen yn misellen mei in kompleks-koaserfaat kearn. De gearstalling, grutte en dynamyske eigenskippen fan de misellen en de gefolgen fan ynpakken op de aaiwiten binne ûndersocht. De resultaten binne bediskusjearre yn **Haadstuk 6** yn relaasje ta de praktyske tapassing fan it ynpakken fan aaiwiten yn de misellen. Dêrneist ha wy ek mooglike ferbetteringen oanfierd. It is foaral nedich dat de misellen stabiler makke wurde, wêrtroch't se ûnder oare bestân binne tsjin in hegere sâltkonsintraasje en minder gau ûnderinoar aaiwiten útwikselje.



About the author

Dankwoord

Curriculum Vitae

List of publications

Overview of completed training activities

Dankwoord

Hier is dan eindelijk mijn proefschrift! Bedankt dat je mijn thesis hebt opengeslagen en nu dit dankwoord aan het lezen bent. De totstandkoming ervan heeft nogal wat voeten in de aarde gehad. Dankzij de mensen op deze pagina's is het mij gelukt de tijd van mijn PhD goed door te komen.

Allereerst mijn co-promotors en promotor, Jan Willem, Mieke en Willem: bedankt dat jullie mij deze PhD-positie hebben gegeven. Jan Willem, bij jou stond de deur altijd open. Ik heb er misschien niet al te veel gebruik van gemaakt, maar ik heb vaak moeten aankloppen in verband met problemen met de microscoop. Hopelijk heb je hem nu werkend en krijg je er niet weer zoveel problemen mee. Bedankt dat je mijn dagelijkse begeleider was. Mieke, we hebben elkaar wat minder gezien, omdat ik de keuze had gemaakt om mijn PhD vooral bij biochemie door te brengen. Dankjewel dat je één keer in de twee weken naar biochemie kwam om te discussiëren over de voortgang van mijn onderzoek. Willem, we weten dat je van kleur houdt, hopelijk heb ik hierbij het kleurrijkste proefschrift gefabriceerd. Alle drie bedankt voor alle feedback op de artikelen, ook al was ik er niet altijd even blij mee, maar toch hadden jullie vaak gelijk en werd het verhaal er beter van. Ik, de perfectionist, had het alleen graag zelf al zo goed op willen schrijven. ;-)

Tijdens mijn onderzoek ben ik geholpen door vier fantastische studenten, waarvan drie als co-auteur op mijn artikelen staan. Jaap, Koen, Nienke en Ellard, heel erg bedankt dat jullie aan mijn onderzoek hebben gewerkt.

Gudrun en Joseline, fijn dat jullie mijn paranimfen willen zijn. Joseline, dank dat je het zo lang met mij hebt weten uit te houden als kantoormaatje in het Transitorium en dat je ons goed verzorgd hebt met de hoeveelheid fruit die je elke week weer meebracht. Gudrun, thanks for being my officemate in Helix and for the amount of chocolates you always brought. Meiden, bedankt voor alle feedback en hulp bij mijn tekstuele en figuratieve problemen en dat ik die ook gevraagd (en ongevraagd) terug mocht geven. Ook bedankt voor de momenten dat we even samen konden klagen over alle sores van de PhD!

Also thanks to the rest of the Enzymes@Work group: Adrie, Carlo, Mieke, Tom and Caroline. Adrie, Caroline, Mieke and Tom, thanks for being officemates in Helix.

Adrie en Remco, bedankt voor jullie hulp met de FCS- en DLS-technieken en alle andere problemen in het lab. Adrie, dankjewel voor de vele discussies die we hebben gevoerd over mijn onderzoek, dat je mij vaak hebt geholpen met mijn FCS-experimenten en altijd een helpende hand hebt geboden in het lab. Remco, dank voor je hulp als ik weer net iets meer of anders bij een DLS-experiment wilde doen.

Danny en Lisette, bedankt voor het delen van het lab in het Transitorium.

Laura, Mara, Anita en Josie, jullie zijn de mensen op de achtergrond, maar oh zo belangrijk voor een PhD'er. Bedankt dat jullie alles draaiende hebben gehouden en zorgden dat alles geregeld werd.

I also want to thank the rest of Biochemistry, you have made the past years very relaxing with many activities, like the PhD-trip, WE-days, gaming nights and dinners at Gudrun's. Next to that, thanks for appreciating my cakes and consuming them. During the after-party it will probably be the last time you can have a taste of them, so enjoy!

The people at PCC also need thanks, even though I haven't seen many of you. It was fun to go with you to California. Sabine, thanks for organizing the major part of the PhD-trip and being my roommate. Thanks to those that made the teaching more fun, especially Merve for the talks about our cats and my cakes. Frans bedankt voor jouw input via de discussies die je vooral met Mieke hebt gehad. Anton bedankt voor het helpen met de DSC-experimenten. Thanks to the people making the conferences bearable. If you feel I should appreciate you, thanks for being there, even though I did not mention your name!

Mede-Moleculairen, ik ben de laatste op het podium, nu is iedereen PhD af. Bas, Henriëtte, Joseline, Leonie en Mieke, bedankt voor de gedeelde studiejaren, vervolgens de PhD-klaaggroep en nu door naar het echte 'volwassen' leven.

Familie Blonk en familie Boer bedankt voor alle gesprekken, diners, koffie en spelletjesavonden die we al vele jaren delen. Fijn dat ik ook in de zware tijden van het doen van mijn PhD welkom was bij jullie. Hopelijk kan ik jullie weer gaan verslaan met verschillende spelletjes nu ik meer ontspannen ben. Familie Blonk bedankt voor alle oppasuurtjes op Djoeke.

Bobo, het begon met jouw positieve verwelcoming van mij tijdens de volleybalavonden. Nu hebben we goede gesprekken bij een warme kop koffie en wat lekkers; fijn dat alles ter sprake mag komen en dat er zoveel respect voor elkaar is. Bedankt dat je de fotograaf bent op mijn promotie.

Jasper, Malte en Maël, bedankt voor de ontspannende spelletjesavonden van het afgelopen jaar.

Jonathan, dankjewel voor jouw vriendschap en alle leuke activiteiten die we hebben ondernomen. Daarnaast heb je na een paar woorden van mij over mijn onderzoek er een schitterende omslag van gemaakt, geweldig!

Gon, Sophie en Laura, bedankt voor alle broodnodige ontspanningen van mijn zeer gestreste lijf. Gon, dankjewel dat je mij ook geholpen hebt met de Nederlandse teksten voor mijn proefschrift.

Mem, Heit & Johanna en Roelof & Ymie, dankjewol foar alle steun op de eftergrûn. It wie in pittich karwei om dit foar inoar te krijen en ik wie grif net altyd even gesellich. Dankjewol foar alle aktiviteiten en spultsjes om my efkes út myn bobbel te heljen.

Leave Djoeke, do wachtest eltse dei wer op myn komst. Bedankt foar al dyn leafde, waarmte, oankrûpers en gekkichheden. Tegearre sille wy it nije aventoer temjitte!

Curriculum Vitae

Antsje Nolles was born on November the 27nd 1986 in Groningen, the Netherlands, and raised in Hemrik. After finishing her secondary education (VWO) at Het Drachtster Lyceum in Drachten in 2006, she started her Bachelor in Molecular Life Sciences at Wageningen University, which allowed her to pursue some of her broad interests in science. She received her BSc in 2010 and started her Master in Molecular Life Sciences with a specialization in Biomedical Research. Her major thesis was on the Baculovirus PIF proteins in the group of Prof. Van Oers at the Laboratory of Virology at Wageningen University. For her internship, she went to Amsterdam to study the effects of radiation, Herceptin, and doxorubicin on heart cells in the group of Dr Stewart at the Netherlands Cancer Institute. Antsje finished her MSc with a minor in the group of Prof. De Vries at the Laboratory of Biochemistry at Wageningen University. There she investigated the mobility of BRI1 and SERK3 in *Arabidopsis* roots by fluorescence recovery after photobleaching, which resulted in a publication in PLoS ONE. Antsje received her MSc degree in January 2012 and started in February as a PhD candidate of both Physical Chemistry and Soft Matter and the Laboratory of Biochemistry, at Wageningen University & Research. Next to the production of this thesis, her PhD also provided the inspiration for baking rainbow cakes.



List of publications

This Thesis

Nolles, A.; Westphal, A.H.; de Hoop, J.A.; Fokkink, R.G.; Kleijn, J.M.; van Berkel, W.J.H.; Borst, J.W., Encapsulation of GFP in complex coacervate core micelles. *Biomacromolecules* **2015**, 16, (5), 1542-1549, DOI: 10.1021/acs.biomac.5b00092.

Nolles, A.; van Dongen, N.J.E.; Westphal, A.H.; Visser, A.J.W.G.; Kleijn, J.M.; van Berkel, W.J.H.; Borst, J.W., Encapsulation into complex coacervate core micelles promotes EGFP dimerization. *Phys. Chem. Chem. Phys.* **2017**, 19, (18), 11380-11389, DOI: 10.1039/c7cp00755h.

Nolles, A.; Westphal, A.H.; Kleijn, J.M.; van Berkel, W.J.H.; Borst, J.W., Colorful packages: Encapsulation of fluorescent proteins in complex coacervate core micelles. *Int. J. Mol. Sci.* **2017**, 18, (7), 1557, DOI: 10.3390/ijms18071557.

Nolles, A.; Hooiveld, E.; Westphal, A.H.; van Berkel, W.J.H.; Kleijn, J.M.; Borst, J.W., FRET reveals formation and exchange dynamics of protein-containing complex coacervate core micelles. (*submitted*)

Other work

Hutten, S.J.; Hamers, D.S.; aan den Toorn, M.; van Esse, G.W.; Nolles, A.; Bücherl, C.A.; de Vries, S.; Hohlbein, J.; Borst, J.W., Visualization of BRI1 and SERK3/BAK1 nanoclusters in Arabidopsis roots. *PLoS ONE* **2017**, 12, (1), e0169905, DOI: 10.1371/journal.pone.0169905

Overview of completed training activities



Discipline specific activities

Courses

FEBS	Wageningen (NL)	2012
3DM - Bio-Product	Nijmegen (NL)	2012
Biorefinery for Biomolecules*	Wageningen (NL)	2015

Conferences and meetings

FOM @ Veldhoven	Veldhoven (NL)	2012
NWO CW @ Veldhoven*	Veldhoven (NL)	2012
Dutch Polymer Days*	Lunteren (NL)	2013
AcademicExpo, BCF Careerevent*,#	Amsterdam (NL)	2013
Nanoscopy Netherlands	Amsterdam (NL)	2014
Dutch Polymer Days	Lunteren (NL)	2014
PicoQuant Workshop*	Berlin (DE)	2014
Mini-Symposium 'Pack and Go' #	Wageningen (NL)	2015
Dutch Polymer Days#	Lunteren (NL)	2015
FCS in Polymer Science Workshop#	Aachen (DE)	2015
CHAINS - chemistry as innovating science#	Veldhoven (NL)	2015
DutchBiophysics#	Veldhoven (NL)	2016

General courses

VLAG PhD week	Baarlo (NL)	2012
Techniques for writing and presenting a scientific paper	Wageningen (NL)	2013
Scientific writing	Wageningen (NL)	2014
Efficient writing strategies	Wageningen (NL)	2014
Brain training	Wageningen (NL)	2015
Career orientation	Wageningen (NL)	2016
Scientific artwork with Photoshop and Illustrator	Wageningen (NL)	2016
Adobe InDesign essential training	Wageningen (NL)	2016
Last stretch of the PhD program	Wageningen (NL)	2016

Optional activities

Preparation of research proposal	Wageningen (NL)	2012
PCC PhD trip#	USA	2013
BIC PhD trip#	UK	2013
PCC group meetings and colloquia	Wageningen (NL)	
BIC group meetings and colloquia	Wageningen (NL)	

*poster presentation, #oral presentation

The research described in this thesis was performed at the Laboratory of Biochemistry, Wageningen University & Research, and Physical Chemistry and Soft Matter, Wageningen University & Research, and was financially supported by VLAG (Advanced studies in Food Technology, Agrobiotechnology, Nutrition and Health Sciences), the Netherlands.

Financial support from Physical Chemistry and Soft Matter, Wageningen University & Research, and the Laboratory of Biochemistry, Wageningen University & Research, for printing this thesis is gratefully acknowledged.

Cover design by Jonathan Both

C3M design by Roelof Nolles

Layout by Antsje Nolles

Printed by GVO drukkers & vormgevers, Ede, the Netherlands

Antsje Nolles, February 2018

